TECHNICAL ASSESSMENT OF STRUCTURAL DEFORMATION AND SEISMICITY AT YUCCA MOUNTAIN, NEVADA

Prepared for

U.S. Nuclear Regulatory Commission
Contract NRC–02–97–009

Prepared by

D.J. Waiting
R. Chen
J.G. Crider
W.M. Dunne
R.W. Fedors
D.A. Ferrill
M.B. Gray
B.E. Hill
P.C. La Femina
H.L. McKague
A.P. Morris
D.W. Sims
J.A. Stamatakos

Center for Nuclear Waste Regulatory Analyses
San Antonio, Texas

September 2001

TABLE OF CONTENTS

TABLE OF CONTENTS (continued)

TABLE OF CONTENTS (continued)

TABLE OF CONTENTS (continued)

FIGURES

FIGURES (continued)

FIGURES (continued)

TABLES

ACKNOWLEDGMENTS

This report was prepared to document work performed by the Center for Nuclear Waste Regulatory Analyses (CNWRA) for the U.S. Nuclear Regulatory Commission (NRC) under contract No. NRC–02–97–009. The studies and analyses reported here were performed on behalf of the NRC Office of Nuclear Material Safety and Safeguards, Division of Waste Management. The report is an independent product of the CNWRA and does not necessarily reflect the views or regulatory position of the NRC.

The authors would like to thank Rebecca Emmot for her dedication to report preparation and Lee Selvey and Arturo Ramos for their assistance in the report preparation. We also thank Drs. David Pickett and John Russell for their reviews, and James Pryor and Cathy Cudd for their editorial reviews, all of which greatly improved the final report.

QUALITY OF DATA, ANALYSES, AND CODE DEVELOPMENT

Data: CNWRA-generated data contained in this report meet quality assurance requirements described in the CNWRA Quality Assurance Manual. Sources for other data should be consulted for determining the level of quality of those data.

Analyses and Codes: The software 3DSTRESS™ Version 1.3 was used for analyses presented in this report. 3DSTRESS™ Version 1.3 fulfills the CNWRA Technical Operating Procedures (TOP–018), Development and Control of Scientific and Engineering Software. Acquired commercial software EZ-FRISK™ Version 4.4 was also used for analyses provided in this report. EZ-FRISK™ Version 4.4 is also controlled under TOP–018 requirements. The rose diagrams of fracture data were made using the software StereoNet© Version 3.0, which is a commercially available plotting software. The software is under TOP–018 control. Similarly, maps of the fracture pavements at Yucca Mountain, Yucca Mountain geology, and regional Yucca Mountain features were generated by the software ArcView GIS© Versions 3.1 or 3.2a, which are commercially available software programs. ArcView GIS© Versions 3.1 and 3.2a are Geographic Information System mapping software and are under TOP–018 control.

1 INTRODUCTION

Yucca Mountain lies within the central Basin and Range Province of the North American Cordillera [e.g., Figure 1 in Wernicke (1992), page 554]. The region is characterized by complex interactions of strike-slip and extensional deformation, active since the beginning of the Cenozoic (65 Ma). The region remains tectonically active as indicated by numerous Quaternary faults (including evidence for Holocene activity), historic seismicity (including the 1992 Little Skull Mountain earthquake activity), and volcanism.

The NRC staff determined that the seismotectonic activities that may significantly affect the future (10,000 to 100,000 years or more) performance of a repository at Yucca Mountain can be identified and assessed adequately by existing methods, models, and codes. With prudent projections of changes of processes and conditions and analyses of uncertainties attendant on performance of engineered and natural systems, forward-modeled concepts of seismotectonic hazards and their effects can be reasonably applied to the analysis of risk.

This report is a revision of Structural Deformation and Seismicity Issue Resolution Status Report (Revision 3.0). However, in fiscal year 2001, evaluation of the U.S. Department of Energy (DOE) program for all key technical issues under acceptance criteria and review methods is now documented in the Integrated Issue Resolution Status Report. This letter report, renamed Technical Assessment of Structural Deformation and Seismicity at Yucca Mountain, Nevada, contains the technical and scientific bases that support the structural deformation and seismicity issue resolution process.

The technical work described in this document meets three NRC performance goals: (i) increasing public confidence, (ii) increasing the efficiency of NRC activities, and (iii) providing the technical basis necessary for NRC to make decisions that are effective and realistic. This documentation of the work performed for the Structural Deformation and Seismicity Key Technical Issue clearly demonstrates the sound science on which NRC decisions are based. The effect of documentation is to provide the public with a basis for increased confidence. It also provides a basis for decreasing regulatory burden by decreasing technical uncertainties, thereby documenting realism in NRC activities and decisions.

2 FAULTING

Previously, the general concept of faulting in the Structural Deformation and Seismicity Issue Resolution Status Report was subdivided into two components: (i) Type I faults and (ii) fault displacement hazards. Type I faults and fault displacement are generally investigated by deterministic methods. Type I faults are now considered in this report under seismic source characterization (Section 3.2). The state-of-the-art procedure for determining fault displacement hazards is by probabilistic analysis.

2.1 Fault Displacement Hazard

The objective of fault displacement analyses is to evaluate the potential hazards of an intersection of an active fault with vital components of the repository system, especially waste packages and other engineered components of the repository system. For this evaluation of faulting, both principal (including sympathetic) and secondary (or distributed) faulting must be considered (as defined in dePolo, et al., 1991). Principal faulting refers to displacement along the main fault zone responsible for the release of seismic energy (i.e., an earthquake). At Yucca Mountain, principal faulting is assumed to occur only on primary faults, mainly block-bounding faults. In contrast, secondary or distributed faulting is defined as rupture of smaller faults that occurs in response to the rupture in the vicinity (e.g., hanging wall and footwall) of the principal fault. These two subsets of faults are not mutually exclusive. Faults capable of principal rupture themselves can undergo secondary faulting in response to faulting on another primary fault. Because principal and secondary faults pose a potential risk to repository performance, both types must be considered by the DOE in its evaluation of external events in the site recommendation report and license application.

The simplest approach for the evaluations of principal faulting, and one that was used predominantly before 1998 for siting of nuclear reactors and other critical facilities, is a deterministic analysis. In that approach, capable faults as defined in 10 CFR Part 100, Appendix A are avoided by adequate setback distances. This approach may not be appropriate for Yucca Mountain (Coppersmith, 1996) because of the different performance requirements between a reactor and the repository. The proposed repository is too extensive to reasonably expect that virtually all faults of concern will fall outside its boundaries.

Methods similar to those developed for probabilistic seismic hazard analysis have been developed to evaluate fault displacement hazards, especially for principal faults for which detailed paleoseismic data are available. These methods construct individual fault displacement hazard curves, analogous to probabilistic seismic hazard analysis curves, for each principal fault (Youngs and Coppersmith, 1985; CRWMS M&O, 1998).

Few techniques, however, exist to evaluate the probability of secondary faulting (e.g., Coppersmith and Youngs, 1992). Because of the complexity of fault analyses, the DOE experts made assumptions and developed estimates of the future behavior of faults based on a variety of data and models (CRWMS M&O, 1998). The staff are currently evaluating the DOE assumptions and projections by examining the completeness, quality, consistency, and appropriate consideration of uncertainty. Further, this evaluation includes assessment of deterministic and probabilistic analyses of principal fault displacement, as well as integration of these analyses with structural and tectonic models used to assess secondary faulting. Fault

displacement hazard in postclosure performance assessment is treated as a disruptive event or series of events (as in features, events, and processes) that has a probability of occurrence derived from a geologic analysis of its recurrence rate. The critical aspect of the staff's current review is the significance of faulting (if any) to overall repository performance during the postclosure period. Review of the faulting hazard with respect to preclosure regulations will be addressed separately in later documents, including review of DOE Topical Report #3.

2.2 Faulting at Yucca Mountain

Evaluation and analyses of the faulting hazard require an understanding of the fault geometries and faulting history at Yucca Mountain. Yucca Mountain consists of a thick accumulation of volcanic tuff deposited on an irregular surface of eroded and deformed Paleozoic and Precambrian basement composed of highly faulted and folded sedimentary and metasedimentary rocks. These tuffs were erupted from a series of Middle to Late Miocene (15 to 9 million years ago) calderas that collectively form what has been defined as the southwestern Nevada volcanic field [see Sawyer, et al. (1994) for the most recent regional stratigraphy of the Miocene volcanic rocks in the Yucca Mountain region]. Rocks of the Paintbrush Group, principally Tiva Canyon Tuff (12.7 million years ago), make up the main surface exposures of Yucca Mountain (Figure 2-1), while the repository horizon is within the Topopah Springs Tuff (12.8 million years ago). The Paintbrush Group tuffs rest on a sequence of older tuffs, including the Prow Pass and Bullfrog Members of the Crater Flat Group. Younger tuffs related to the Timber Mountain Group are locally exposed at Yucca Mountain in topographic lows between large block-bounding faults. This observation, along with evidence for growth faults in the Paintbrush rocks in Solitario Canyon (e.g., Carr, 1990; Day, et al., 1998b), suggests that faulting and tuff deposition were synchronous at Yucca Mountain. Trenching studies of the Solitario, Paintbrush Canyon, and Bow Ridge faults also show sufficient evidence for multiple faulting events in the Quaternary (Sections 4.6 and 4.7 in U.S. Geological Survey, 1996). Thus, it appears that faulting has been active throughout the geologic history of Yucca Mountain, although present-day rates are significantly lower than in the late Miocene, when volcanic rocks at Yucca Mountain were first deposited.

The majority of faults at Yucca Mountain are either north-trending normal faults or northwest-trending, dextral strike-slip faults. The larger faults in these two orientations bound the fault blocks that underlie Yucca Mountain. These two sets of faults are interpreted to be contemporaneous, based on mutual terminations and secondary structures between them, such as pull-apart basins (Day, et al., 1998a,b). Some northwest-trending faults are dominantly normal faults, accommodating extension in relay ramps between overlapping normal faults (Ferrill, et al., 1999a). Only four reverse faults with north-south or northeast-southwest strikes have been identified, but they are potentially key features for constraining the kinematic history of the region (Day, et al., 1998a) and for identifying infiltration pathways (Levy, et al., 1997). Much of the detailed fieldwork to study faults in the central block focused on the Ghost Dance and Sundance faults, which are close to the subsurface trace of the Exploratory Studies Facility (Spengler, et al., 1994; Potter, et al., 1996).

Yucca Mountain consists of a sequence of north- to north-northeast-trending, fault-bound ridges crossed by occasional northwest-trending, dextral strike-slip faults. Faults dip almost uniformly to the west and separate blocks of gentle to moderate east-dipping tuff strata. From north to south, both fault displacement and dip of bedding increase and, thus, indicate progressively

Miocene Volcanic Section
Yucca Mountain, Nevada

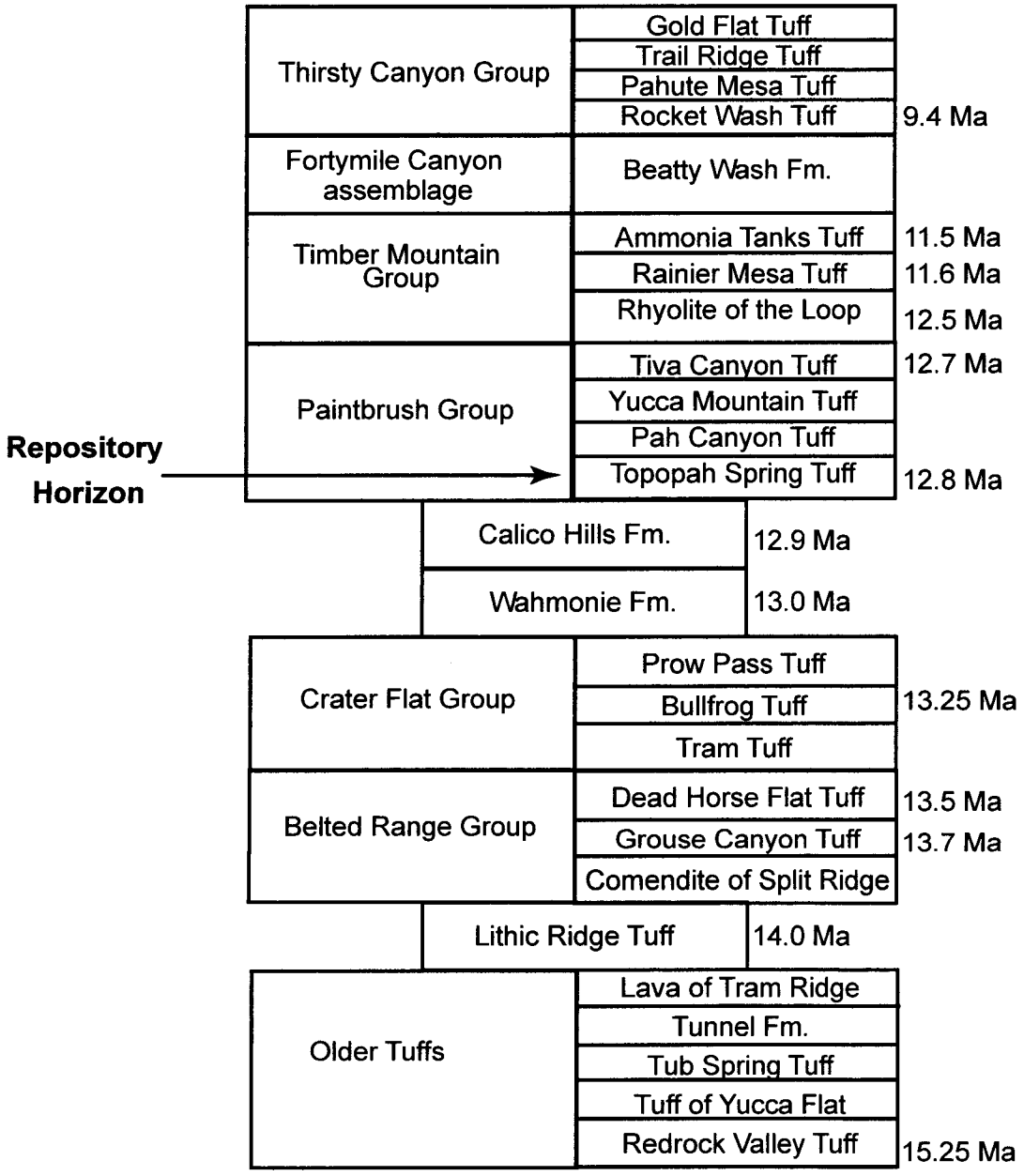

Figure 2-1. Summary Chart of the Miocene Volcanic Stratigraphy at Yucca Mountain (Derived from Sawyer, et al., 1994)

greater extension of the Crater Flat basin southward (Scott, 1990). This pattern is most profound on the west flank of Yucca Mountain, which is defined by a series of left-stepping and north-trending *en echelon* faults. The southward increase in fault offset is coupled with greater block rotation, both horizontal and vertical (Scott, 1990). Work by the U.S. Geological Survey suggests that this pattern of faulting, along with rotated paleomagnetic direction in the tuffs, resulted from a discrete period of extension followed by a discrete period of dextral shear, akin to an oroclinal bending model (Hudson, et al., 1994; Minor, et al., 1997).

More recent reanalyses of these data suggest an alternative explanation. The north-to-south displacement gradient and rotation of fault blocks are a result of increased rollover deformation in the hanging wall above a listric Bare Mountain fault (Section 5.1.2; Ferrill, et al., 1996b; Ferrill and Morris, 1997; Stamatakos and Ferrill, 1998; Morris and Ferrill, 1999).

An *en echelon* pattern of faulting is best expressed along the western edge of Yucca Crest and the fault line escarpment that follows the west-dipping Solitario Canyon, Iron Ridge, and Stagecoach Road faults (i.e., Simonds, et al., 1995). The geometry of faults and ridges defines a scallop trend composed of linear, north-trending fault segments connected by discrete curvilinear northwest-trending fault segments. For example, the ends of the northwest-trending curvilinear Iron Ridge fault bend to the northwest near its overlap with both the Stagecoach Road and Solitario Canyon faults. Yucca Mountain also contains numerous swarms of small northwest-trending faults that connect the large north-trending faults. One example is at West Ridge, which is cut by numerous small faults that connect segments of the Windy Wash and Fatigue Wash faults. This geometry strongly suggests that the entire Yucca Mountain fault system is an *en echelon* branching fault system (Ferrill, et al., 1999a), in which faulting on the large block-bounding fault triggers relatively widespread, but predictable, secondary faulting on connecting and linking faults. Linkage of the *en echelon* system is either by lateral propagation of curved fault tips or formation of connecting faults that breach the relay ramps (Figure 1 in Ferrill, et al., 1999a; Peacock and Sanderson, 1994; Trudgill and Cartwright, 1994). More importantly, from this interpretation of *en echelon* faulting, it follows that locally developed faults and fractures were produced by local variations of the stress field (Section 4.1; also see modeling by Crider and Pollard, 1998) rather than dramatic swings of the regional extension direction (Throckmorton and Verbeek, 1995). The amount, orientation, and degree of faulting directly depend on the relative position of the rock within the *en echelon* fault system, either in relay ramps that connect overlapping *en echelon* fault segments or in the hanging wall or footwall blocks of the block-bounding faults.

2.3 Faulting Models from Tectonic Models

As discussed in Section 5.1 and summarized in Appendix C of NRC (1999a), numerous tectonic models have been proposed to explain the structural evolution of Yucca Mountain. Faults at Yucca Mountain, for example, have been interpreted as the result of (i) hanging wall deformation related to normal fault motion on a listric Bare Mountain fault (Ferrill, et al., 1996b), (ii) hanging wall deformation above a regional low-angle detachment system (Scott, 1990; Hamilton, 1988), (iii) deformation on the margin of a pull-apart basin (Fridrich, 1999), (iv) listric faulting from a transtensional nappe deforming above the Amargosa Desert strike-slip shear system (Schweickert and Lahren, 1997), and (v) domino-style block deformation related to extension of an elastic-viscous Crater Flat graben (Janssen, 1995). These tectonic models can be used to estimate future fault activity at Yucca Mountain. For example, because a regional

detachment system of the kind envisioned by Scott (1990) is considered to have been truncated by more recent uplift of Bare Mountain, faulting at Yucca Mountain is presumed to be relatively inactive. Alternatively, active strike-slip motion along the Amargosa Desert fault is assumed to include relatively active faulting at Yucca Mountain.

In addition, the style (strike-slip or dip slip) of faulting in the alternative tectonic models is important to evaluations of faulting data from the paleoseismic investigations. In trenches, typically only the vertical component of separation can be deduced from offset stratigraphic marker beds. If the style of faulting is dominantly dip slip, then actual fault displacements, at least for the strand of the fault exposed in the trench, can be deduced from the paleoseismic data. In contrast, strike-slip separation is not readily apparent in trenches. If this style of faulting dominates, then the trenching data may grossly underestimate actual fault activity.

2.4 Deformation Mechanisms, Fault Zone Architecture, and Fault Width

Accurate models of faulting and the effects of faulting on repository performance (both direct fault disruption of waste packages and other engineered components or the effects of faults and faulting on groundwater flow) require a detailed description and understanding of faults at the repository horizon level. Detailed analyses of faults and fault zones in the Exploratory Studies Facility and Enhanced Characterization of the Repository Block were initiated by staff in 1998, mainly to refine models of faulting used in performance assessments codes. In the course of the investigations, it became apparent that results of the Exploratory Studies Facility fault studies also bear on questions of the thermochronology of Yucca Mountain, infiltration, and groundwater flow. The following discussion highlights the findings of the Exploratory Studies Facility fault-zone study.

Fault-zone deformation in the upper crust produces a wide variety of textures that affect the overall characteristics of fault zones. Idealized faults consist of two textural zones: fault core and a damage zone (Sibson, 1977; Caine, et al., 1996; Seront, et al., 1998). The fault-zone core is a zone of relatively high strain and accommodates most of the fault displacement by flow in gouge, cataclasite, breccia, or mylonite. The surrounding damage zone is less deformed, accommodates less displacement, and may contain subsidiary structures such as joints, fractures, and minor faults [i.e., Stillwater fault, Dixie Valley, Nevada (Seront, et al., 1998)] (Figure 2-2).

Deformation mechanisms govern the behavior of fault zones and their present-day geometric and textural morphologies. At Yucca Mountain, the protolith (undeformed volcanic tuff) has undergone brittle deformation by cataclasis at shallow levels in the upper crust. Changes in deformation mechanisms change and increase fault displacement. Changes in the availability of fluids in the fault zone, mineral transformations, and syndeformational mineralization affect the rheology of the fault zone. Both factors can cause the active parts of the faults to widen or narrow with increasing displacement. Two end-member possibilities exist. Deformation produces fault rocks that inhibit further slip in the fault core, such that additional fault displacement causes the protolith to fracture and the damage zone to widen with time (i.e., strain harden). The fault rocks become progressively easier to deform, such that deformation is localized within a narrow portion of the fault zone (i.e., strain localization or strain softening in the fault core). In strain softening, the intensely deformed fault core now accommodates all the deformation, and there is no further increase in fault-zone width.

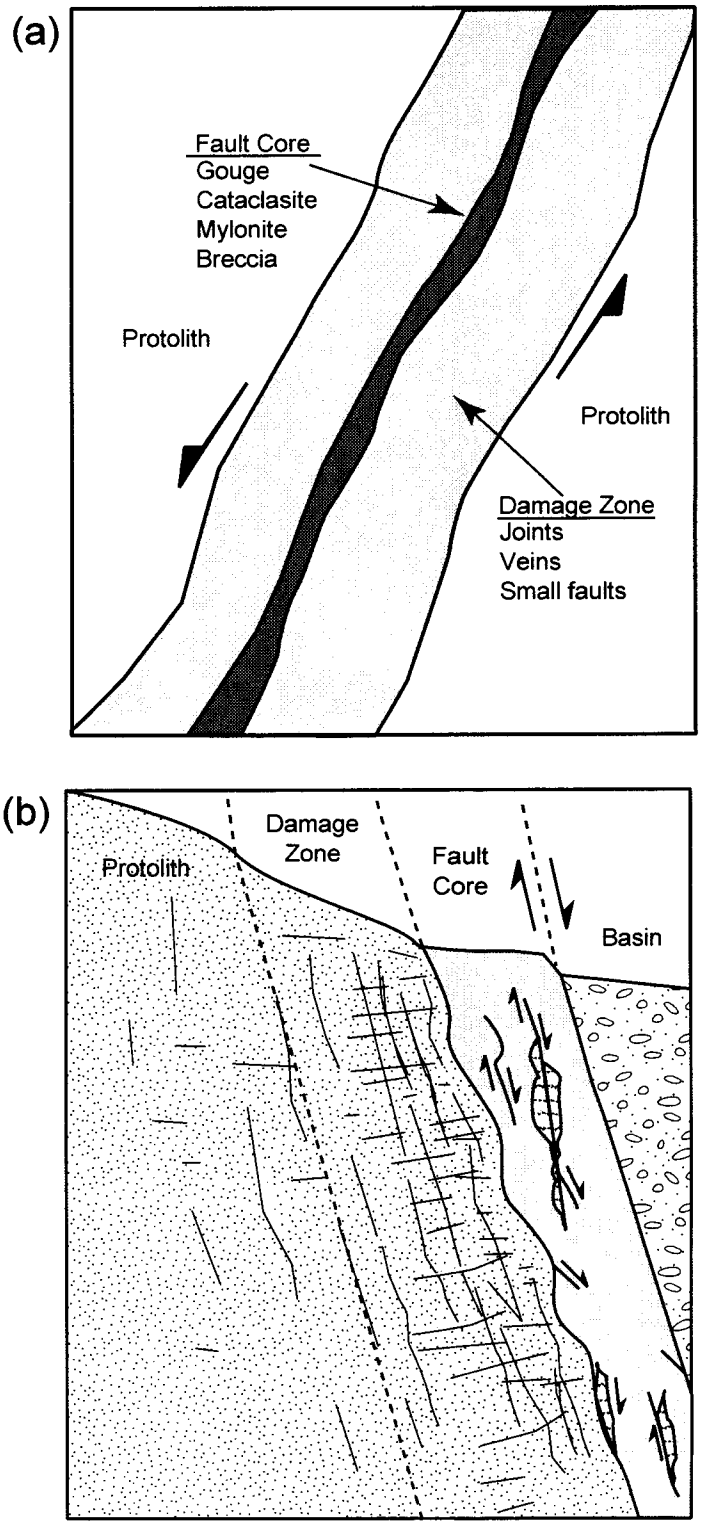

Figure 2-2. Definition of Fault Zone Characteristics: Diagrams Show Conceptual Model of Fault Zone Indicating (a) the Fault Core and Surrounding Damage Zone and (b) the Stillwater Fault in Dixie Valley, Nevada (Seront, et al., 1998)

Investigations of faulting at Yucca Mountain, especially studies of faults exposed in the Exploratory Studies Facility, reveal that all these deformation processes and related features are present (Gray, et al., 1998, 1999). Based on detailed field and microscope analyses of the Exploratory Studies Facility faults, four broadly defined fault zone morphologies (Figure 2-3) are recognized. Classes A, B, C, and D (Gray, et al., 1999) are associated with faults of increasing displacement from a few centimeters to more than 100 m. Class A faults have displacements from a few centimeters to a meter and have thin (<2 cm) fault cores and little or no damage zone. Class B faults generally have displacements of 1 cm to several meters and have moderately narrow (2 to 20 cm) fault cores with a poorly developed damage zone. As much as 65 percent of the Class B fault rocks are composed of coarsely crystalline secondary calcite. Class C faults have moderately wide (20 to 100 cm), well-developed fault cores consisting of multiple-generation breccia and cataclasite. The cores are surrounded by broad (1 to 10 m) damage zones. Little secondary mineralization is associated with Class C faults. Class D faults have wide fault cores (>1 m wide) characterized by smectitic fault gouge with composite foliation and bounded by a partially opalized zone of breccia and cataclasite. Broad, highly fractured damage zones tens of meters wide flank the fault cores.

Classes A, C, and D may be genetically linked, having experienced progressive grain size reduction with increased fault displacement. Class A faults accommodated deformation by Mohr-Coulomb fracturing and cataclastic flow. As grain size was reduced with increased displacement, the fault core underwent strain hardening, and the fault zone widened to form a Class C fault zone morphology. Further displacement, such as that associated with Class D faults, promoted alteration of volcanic rocks to smectite in part of the fault core. The smectite weakened the fault core, localizing most of the subsequent displacement to a narrow zone of foliated smectitic gouge.

In contrast, Class B faults appear to be unique and not readily interpreted as part of the progression outlined previously. Most Class B faults tend to strike northwest-southeast compared to the north-south strikes of Class A, C, and D faults. Class B faults are heavily mineralized, while Classes A, C, and D tend to contain only minor secondary minerals, mainly calcite. Class B calcite forms a crystalline matrix that supports relatively intact wall rock fragments. This observation and the poorly developed damage zone suggest that little cataclasis beyond initial brecciation preceded calcite mineralization in these fault rocks. Most calcite is synkinematic and contains two-phase fluid inclusions. Detailed universal stage analyses of calcite crystals from one fault zone confirm the presence of thick mechanical twins, indicative of deformation at elevated temperatures (Ferrill, 1991, 1998; Burkhard, 1993). The fault rocks also contain veins partially filled with postkinematic calcite. Poikilotopic texture incorporates both synkinematic and postkinematic calcite, suggesting that Class B fault breccias underwent postkinematic recrystallization. The evidence from Class B faults suggests that fault displacement was principally accommodated by crystal-plastic deformation and intercrystalline frictional sliding of calcite since the earliest stages of fault movement. The wall rock clasts suspended in the calcite matrix underwent rigid body rotation during flow of the calcite matrix. Frictional sliding along the fault core/damage zone boundaries also accommodated some displacement. These deformation mechanisms and the contrast in mechanical strength between calcite and the surrounding protolith are not conducive to strain hardening in the fault core at the minor displacements associated with Class B faults.

A critical observation is that fault zones of Classes C and D appear to narrow with depth from the surface to their subsurface exposures in the Exploratory Studies Facility and the Enhanced

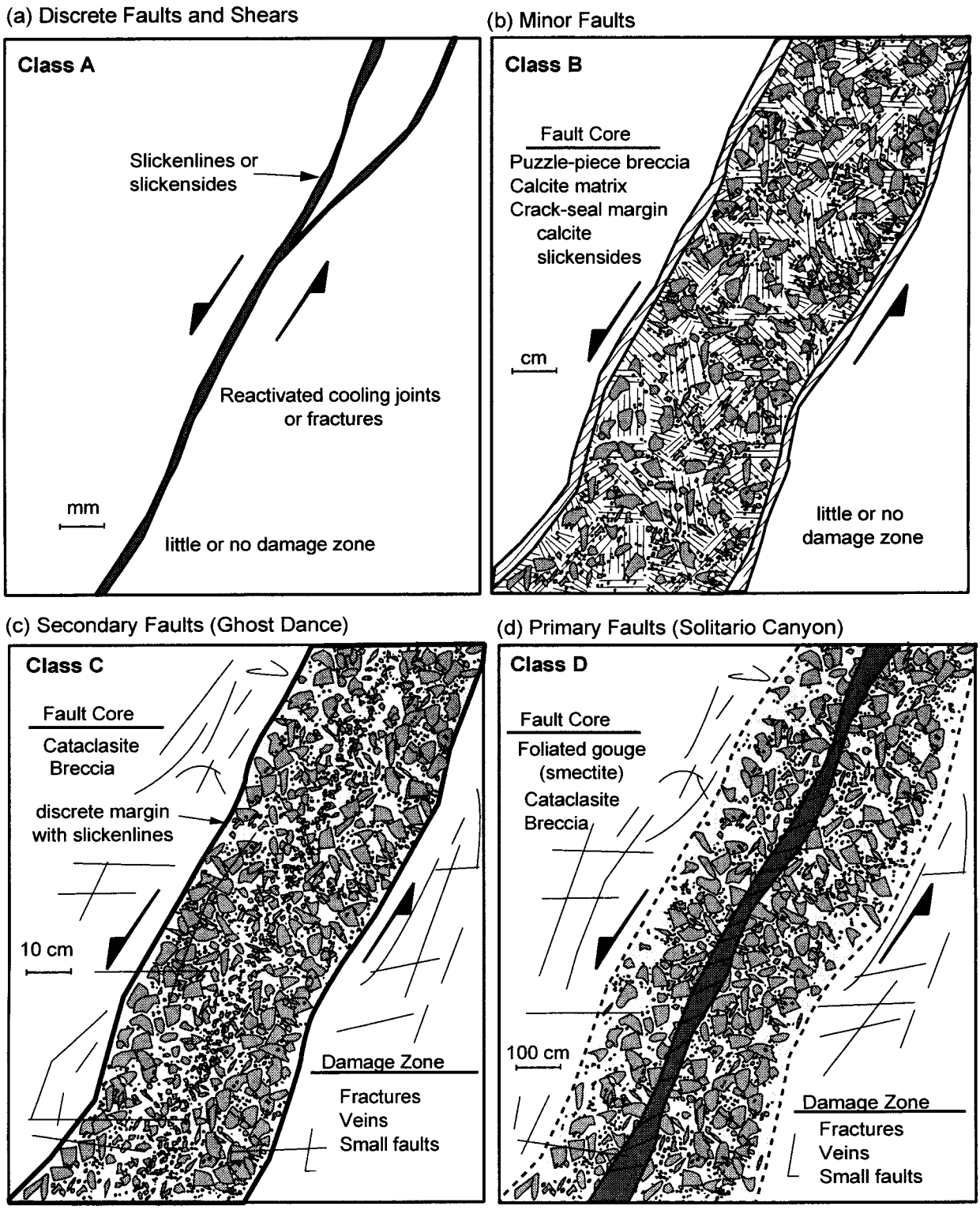

Figure 2-3. Types of Fault Zones Observed from the Exploratory Studies Facility at Yucca Mountain. The Four Fault Zones were Identified from Detailed Field and Laboratory Studies of Fault Zone Deformation (Gray, et al., 1998).

Characterization of the Repository Block. Wide fault zones at the surface, such as the exposure of the Ghost Dance fault zone at the UZ–7A drill pad that is more than 10 m wide, narrow to 1 m or less in exposures in the Exploratory Studies Facility. The exact cause of this observed change in fault width is not known and is currently being investigated by ongoing structural deformation and seismicity studies. Changes in fault width probably reflect differences in fault orientation and environmental conditions of faulting, including confining stress, lithology, and water content.

2.5 Recurrence Relationships of Faulting

Recurrence relationships of faulting are generally derived from paleoseismic data of faults exposed in alluvial trenches. The objective of the trenching studies is to find datable stratigraphic markers offset by the fault and, from the age and amount of offset, determine the recurrence relationship for the fault. Recurrence data for faults are then used in conjunction with regional seismicity parameters such as frequency of earthquakes to develop probabilistic fault displacement hazard curves for each fault of interest. The curves are derived from two different approaches, defined as the faulting-occurrence and magnitude-occurrence models (Cornell and Toro in Hunter and Mann, 1990). These methodologies, as applied in the DOE probabilistic seismic hazard analysis (CRWMS M&O, 1998), have been referred to as the displacement approach and earthquake approach. The first approach uses fault-specific data, such as cumulative displacement, fault length, paleoseismic data from trenches, and historic seismicity. The second approach relates the frequency of the fault's slip events to the frequency of earthquakes on the seismic sources defined in the seismic source models developed for the corresponding seismic hazard analysis.

There are numerous potential sources of uncertainty associated with interpretations of fault slip histories from trenching studies (Figure 2-4) (Ferrill, et al., 1996b). The underlying difficulty is that observations about faulting and seismicity are made from surface features, but the causative seismic rupture typically initiates on faults in the Basin and Range at depths of 5 to 15 km. Potential sources of uncertainty include: (i) distributed faulting, in which the trench captures only a fractional component of the total slip; (ii) blind faulting, in which the offset is restricted to the fault below the surface and, thus, no surface data are available for study; (iii) oblique or horizontal slip, in which the trench offset records only a small component of actual displacement; (iv) inaccurate age estimates of the marker beds; and (v) variability of slip from event to event and along the strike of the fault. In general, the effects of these uncertainties are to minimize estimates of fault slip and fault activity. Fault slip rates based only on fault throw or the possibility of an overlooked active fault within the Yucca Mountain region clearly lead to an underestimation of deformation rate [cf. 0.06-mm/yr slip rate on the Bare Mountain fault of Stamatakos, et al. (1997a) with the 0.01 mm/yr slip rate of Klinger and Anderson (1994)]. Thus, accurate probabilistic fault displacement analyses need to account for these uncertainties.

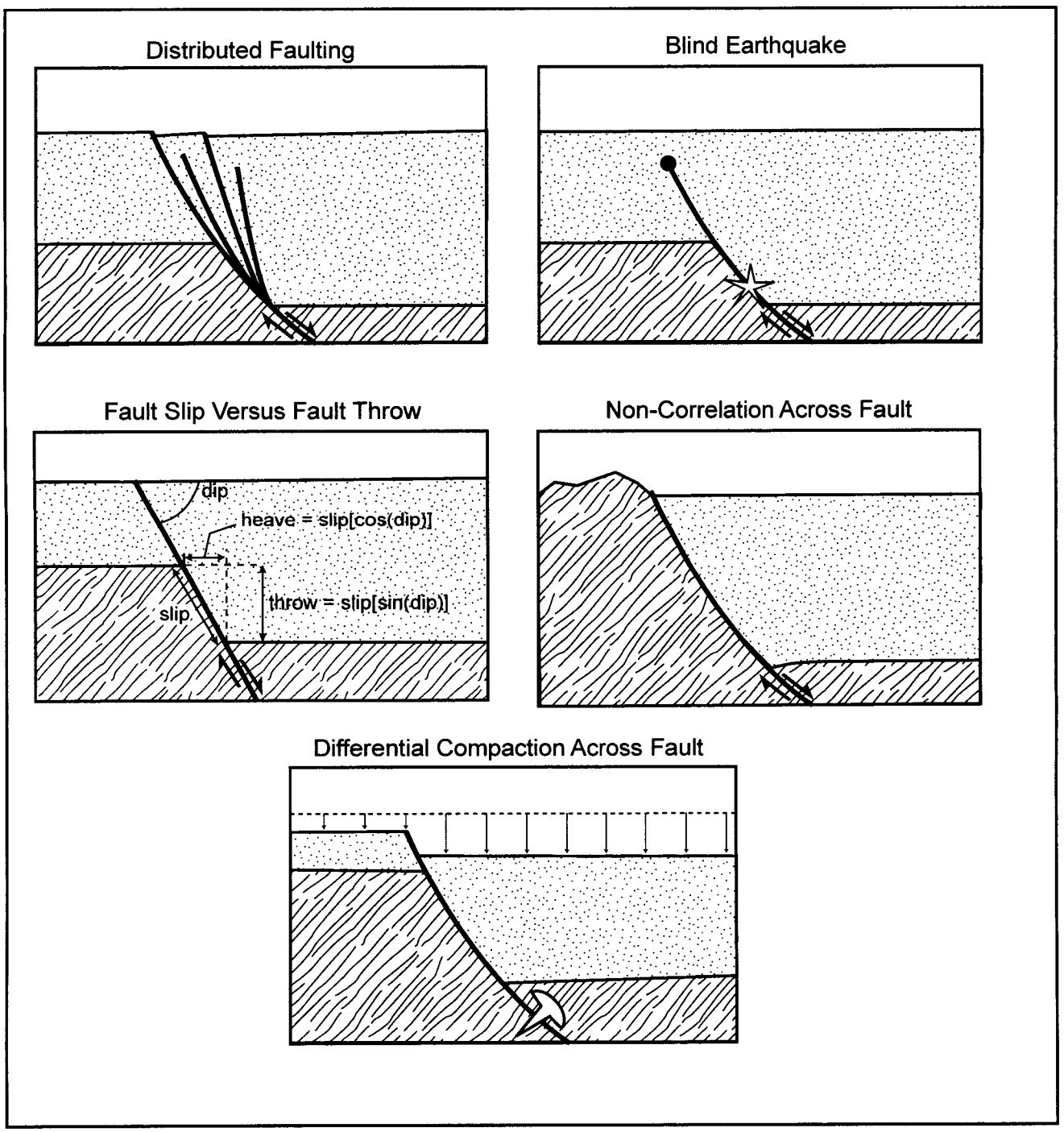

Figure 2-4. Potential Sources of Uncertainty in Fault-trenching Analyses of Paleoseismicity (after Ferrill, et al., 1996b)

3 SEISMICITY

In general, two approaches are considered acceptable by the staff to evaluate seismic hazards. These approaches are based on deterministic and probabilistic methodologies. Until January 1997, deterministic methodology has been the traditional evaluation of seismic hazards for construction and operation of nuclear facilities. Siting, review, and acceptance criteria for these facilities are embedded in many existing NRC documents, such as 10 CFR Part 100, Appendix A and Sections 2.5.1, Basic Geologic and Seismic Information; 2.5.2, Vibratory Ground Motion; and 2.5.3, Surface Faulting, of the NRC Standard Review Plan outlined in NUREG–0800 (NRC, 1997a).

Although the deterministic approach has worked reasonably well for the past three decades, it has been criticized as overly conservative. Moreover, the deterministic approach does not explicitly account for uncertainties in geological or seismological parameters. Probability methods have been developed to better quantify uncertainty in seismological parameters. Expert elicitations have been used to bound parameter ranges in the absence of complete information from data analysis or site characterization.

3.1 Seismic Hazard

For postclosure performance, the seismic hazard curve is an important input parameter for assessment of rockfall in the emplacement drifts that result from earthquake-induced ground shaking. The probabilistic seismic hazard analysis methodology has been identified by the NRC in 10 CFR 100.23 as an appropriate approach to address uncertainties associated with ground motion and fault displacement. The DOE has outlined the methodology it intends to use for a probabilistic seismic hazard analysis in DOE Topical Report #1 (DOE, 1997). This approach has been accepted in principle by the NRC[1]. The methodologies recommended in Budnitz, et al. (1997) also offer acceptable approaches for evaluating the probabilistic seismic hazard at Yucca Mountain.

The probabilistic seismic hazard analysis methodology was first described by Cornell (1968). Detailed descriptions are also given in Reiter (1990), McGuire and Arabasz (1990), and Budnitz, et al. (1997). The basic approach consists of four steps: (i) identification of seismic source, (ii) characterization of earthquake recurrence, (iii) estimation of vibratory ground motion attenuation from the sources to the site, and (iv) calculation of the seismic hazard (Figure 3-1).

3.2 Seismic Source Characterization

A seismic source is a portion of the Earth's crust that has relatively uniform seismicity characteristics (including earthquake potential) and is distinct from that of its neighbors. Sources can be either fault or areal sources. Within a seismic source, the probability of earthquake occurrence and the size of the maximum magnitude are generally considered to be invariant. Characterization of the tectonic setting and identification of seismic sources are based on regional and site geological and geophysical data, historical and instrumental

[1]Bell, M.J. "Issue Resolution Status Report on Methodology to Assess Fault Displacement and Vibratory Ground Motion Hazard at Yucca Mountain, Nevada." Letter (July 25) to S.J. Brocoum, DOE. Washington, DC: NRC, 1996.

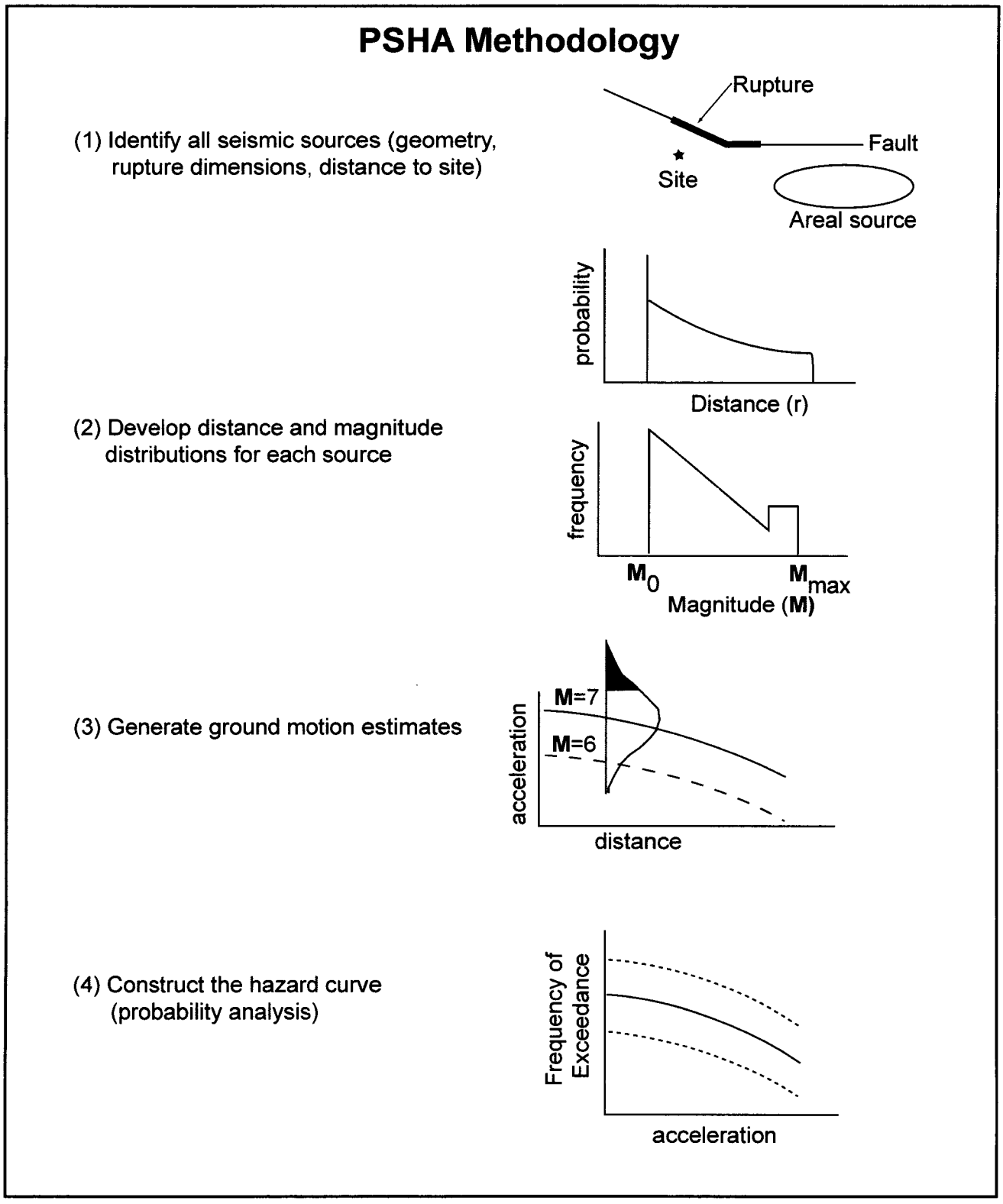

Figure 3-1. Schematic Diagram Illustrating the Four Basic Steps of a Probabilistic Seismic Hazard Analysis (after McGuire and Arabasz, 1990)

seismicity data, regional stress field, and geological investigations of prehistoric earthquakes (NRC, 1997b).

Aspects of seismic sources (Reiter, 1990) to consider in seismic hazard analysis are

- Earthquake potential of identified geological structures.
- Earthquake potential of tectonic zones (i.e., regions of uniform earthquake characteristics).
- Uncertainties associated with seismic source geometry (e.g., fault dip, width, segmentation, and depth of seismogenic crust).
- Uncertainties in recurrence and recurrence models with regard to individual faults, clustered fault activity, or regional recurrence models.
- Appropriate alternatives that allow incorporation of uncertainties about the geology and tectonic conditions into the overall calculation of the seismic hazard.

3.2.1 Historical Seismicity

Historical seismicity comprises earthquakes derived from the written record of the effect of earthquakes on civilization or direct instrumental records of earthquakes from seismographs. In the United States, a complete record extends back only to around 1960, when seismic recording networks were installed throughout most of the continental areas of North America. The record of prior earthquakes was mainly from anecdotal evidence of earthquake damage. The critical aspects that need to be considered in the development of an accurate historical record are the (i) record completeness; (ii) validity of the anecdotal evidence; (iii) conversion to a common intensity or magnitude scale; (iv) reliability of the earthquake data, especially location, time, and size; and (v) declustering to separate the fore-shocks, aftershocks, and human-induced shocks from the primary earthquakes.

Aspects of the seismic record to consider in seismic hazard analysis include

- Coordinates of the epicenter
- Focus depth
- Time of event
- Highest intensity
- Magnitude (with appropriate designation of magnitude type)
- Seismic moment
- Distance to the site
- Strong motion recordings
- Co-seismic deformation (i.e., landslides, liquefaction, or fracturing)
- Surface rupture information

For the southern Great Basin, including Yucca Mountain, there are about a dozen earthquake catalogs that cover the period between 1812 and the present. Catalogs of historical data include those from the California Institute of Technology, California Division of Mines and

Geology, Geological Society of America, National Earthquake Information Center, U.S. Geological Survey, University of California at Berkeley, University of Nevada at Reno, University of Northern Arizona, and University of Utah. Ferrill, et al. (1996b) presents a summary of the historical seismic data based on the Preliminary Determination of Epicenter Catalog compiled by the National Earthquake Information Center.

3.2.2 Paleoseismic Evidence for Past Earthquakes

The principal tool for the evaluation of prehistoric earthquakes is the study of paleoseismology. Paleoseismologists combined geologic skills of tectonic geomorphology and Quaternary geochronology to reconstruct the record of large earthquakes (e.g., McCalpin, 1996). The methodology is especially suited for the arid climate of southern Nevada, because erosion rates are sufficiently slow to allow prehistoric earthquake landforms to be preserved.

Once landforms are recognized as being potentially formed from prehistoric earthquakes, they are often trenched for detailed examination. Fault-trenching studies provide the main source of data to constrain the paleoseismic record. In trenching studies, sites are selected across fault offsets that juxtapose datable sedimentary units (often soil horizons). Based on the offset pattern of sedimentary units and their corresponding ages, a history of earthquakes at the trenching site can be reconstructed. Dating techniques generally confine the measurements to the Quaternary, especially the late Quaternary (~last 125,000 years). As discussed in Section 2.5, there are numerous potential sources of uncertainty associated with trenching data.

3.2.3 Fault Sources

Fault sources are geologic faults that show evidence of recent geologic seismicity. Faults can be identified from a number of geologic and geophysical data including exposed fault surfaces or fault zones with gouge or slickenlines, juxtaposed dissimilar geologic units or truncation of geologic units, topographic markers such as scarps or triangular facets, alignments of groundwater springs or volcanic features, geophysical potential-field anomalies, or alignment of earthquake hypocenters.

Definitions of what constitutes recent activity vary in the literature and regulation. NRC regulation CFR 100, Appendix A defines capable faults as those that show movement at or near the ground surface at least once within the last 35,000 years and several times within the last 500,000 years. In California, active faults are those that show evidence for Holocene (last 10,000 years) activity. In the Basin and Range, an active fault is considered to be one with movement within the late Quaternary (last ~125,000 years) or even the Quaternary (last 2 million years), mainly because the recurrence time for many large faults is approximately 10^4 to 10^5 years. Because of regulatory period of concern (10,000 years) and the long recurrence interval between most large Basin and Range earthquakes, fault sources in the Yucca Mountain probabilistic seismic hazard analysis should include all faults with evidence of movement in the last 2 million years. These criteria are consistent with NRC guidance given in the identification of Type I faults (see Section 3.2.3.4).

3.2.3.1 Location and Geometry of Fault Sources

Locations and geometries of fault sources are critical to evaluations of their contribution to the seismic hazard at Yucca Mountain. Locations of faults are primarily derived from detailed geologic mapping or from interpretations of geophysical data, especially gravity and magnetic anomalies, and seismic imaging. For faults relatively close to Yucca Mountain (within approximately 30 km), the down-dip geometry is also important because it controls estimates of the site-to-source distance. Because earthquake magnitudes depend on fault rupture area, the dip of the fault and the down-dip extent of the fault (depth of the seismogenic crust) are also critical to the seismic hazards analysis.

Classical structural models for the Basin and Range envision a simple horst and graben framework in which range-front faults are planar and extend to the base of the transition between the brittle and ductile crust 15 to 20 km below the surface (e.g., Stewart, 1978). More recent work has shown that many normal faults are not planar but instead have curved or listric shapes. The faults sole into detachments that may or may not coincide with the brittle-ductile transition in the crust (e.g., Wernicke, 1981). Sections 2.3 and 5.3 provide a more detailed discussion of these interpretations.

The end-member Basin and Range models result in different fault characteristics, namely fault segment length, down-dip width, fault dip and change in fault dip, and mechanical and kinematic relationships of individual faults to the tectonic framework. In the horst and graben model, fault systems are regarded as mechanically and kinematically independent. Earthquakes are isolated along individual faults without significant interaction among other faults in the region. In contrast, the detachment models predict a controlling fault under the basin. In this case the controlling fault would be the Bare Mountain fault. Slip along the Bare Mountain fault could trigger opposing slip on faults in the Yucca Mountain region in order to accommodate extension and rollover of the hanging wall into the Bare Mountain fault.

The implication of the detachment model is that antithetic faults in the hanging wall may not cut the entire thickness of the seismogenic crust. Depending on how strain is distributed in the hanging wall (Dula, 1990; Ferrill and Morris, 1997), faults in Crater Flat or at Yucca Mountain could terminate at depths as shallow as several kilometers, greatly reducing their potential to produce large earthquakes.

The relative difference of the seismic potential of the Bare Mountain fault in these end-member models is less clear, especially along the shallowly dipping listric portion of the fault. Earthquakes on detachment faults are rarely observed. Several alternative interpretations have been suggested to explain this lack of earthquakes on detachment faults. Mechanical analysis of listric normal faults suggests that deformation on listric faults is bimodal (Ofoegbu and Ferrill, 1998). Along the steeply dipping portions of the fault, deformation is accommodated by active (seismic) slip, which produces large earthquakes. Along the shallowly dipping portions of the fault, deformation is instead accommodated by aseismic creep. In contrast, Wernicke (1995) argued that because detachment faults are much more efficient at facilitating crustal extension than steep faults, they are capable of large, albeit infrequent, earthquakes with recurrence rates one tenth to one hundredth of their moderately to steeply dipping counterparts. The lack of observed earthquakes on detachment faults may simply reflect the short period of observation (~the last 100 years) compared to the average recurrence interval for Basin and Range faults.

3.2.3.2 Maximum Magnitude Earthquake of Fault Sources

Estimates of maximum magnitude earthquake (M_{max}) define the upper bound of the distribution of earthquakes capable for each fault source. There are two approaches to determining maximum magnitude: historical seismicity and empirical scaling relationships in which M_{max} is derived as a function of the physical dimensions of fault rupture. In the Basin and Range, M_{max} estimates derived from the historical record are deemed unreliable because of the short length of the historical record compared to the long recurrence intervals for most faults. Commonly, M_{max} is estimated from rupture length, rupture area, or displacement per event (e.g., Slemmons, 1977; Bonilla, et al., 1984; Wells and Coppersmith, 1994). In probabilistic seismic hazard analysis, the final M_{max} values are presented as distributions that reflect uncertainties in the estimates of fault rupture.

3.2.3.3 Recurrence Relationships of Fault Sources

Earthquake recurrence relationships show the annual frequency of all earthquakes up to the maximum earthquake for each seismic source. These relationships are derived from earthquake catalogs, paleoseismicity, and geological information. Typically, magnitude-recurrence models range between end-member exponential (Gutenberg and Richter, 1954) and characteristic (Schwartz and Coppersmith, 1984) models.

Aspects of earthquake recurrence (e.g., Reiter, 1990) to consider in seismic hazard analysis are

- Activity rate (or *a* value)
- Slope of the regression (or *b* value)
- Lower bound and upper bound earthquake magnitudes
- Shape of the recurrence curve (characteristic, logarithmic, or hybrid)
- Potential for clustered activity

3.2.3.4 Type I Faults

Faults in and around Yucca Mountain have been identified and investigated by (i) geologic mapping of surface exposures and underground openings (Day, et al., 1998b); (ii) geophysical methods, including gravity, magnetics, electromagnetics, seismic reflection, and hypocenter mapping (Langenheim, et al., 1991; Brocher, et al., 1993, 1996, 1998; Oliver and Fox, 1993; Harmsen, 1994; Ponce and Oliver, 1995; Majer, et al., 1997; Connor, et al., 1997); and (iii) borehole imaging and core logging (Carr, 1992). Insights into faults and faulting in and around Yucca Mountain have been gained from (i) three-dimensional geologic framework models and balanced cross sections (Young, et al., 1992a,b; Stirewalt and Henderson, 1995; Ferrill, et al., 1996b), (ii) tectonic modeling (Ferrill, et al., 1996b), (iii) numerical analyses of dynamic processes (Ofoegbu and Ferrill, 1998), and (iv) analog modeling (Rahe, et al., 1997; Sims, et al., 1999).

Type I faults are defined as faults or fault zones subject to displacement and of sufficient length and location that they (i) may affect repository design and performance of structures, systems, and components important to safety, containment, or waste isolation, and (ii) may provide significant input to models used in the design or assessment of waste isolation

(McConnell, et al., 1992). The concept of Type I faults (McConnell, et al., 1992) in this letter report applies only to those faults that can directly affect the geologic repository design or performance by ground motion or direct fault slip during the period of performance.

The definition of Type I faults applies only to faults that are both known and mapped. Faults that are blind or buried, hypothesized in tectonic models, or whose existence is otherwise inferred from geologic, geophysical, seismological, or analog data, are not considered Type I faults because useful attributes, such as their location, extent, age of last movement, or geometry are not known. However, such faults may be considered in probabilistic seismic hazard analysis and performance assessment. Type I faults are features that must be identified and investigated to determine the fault displacement hazard at the site.

There are six characteristics of faulting and seismicity used to evaluate Type I faults, following McConnell, et al. (1992) and McKague, et al. (1996).

1. **Faulting Component:** That region around Yucca Mountain in which faulting and seismicity could impact the site. Current estimates place this as a circular area with radius 100 km, centered on Yucca Mountain.

2. **Maximum Fault Trace Length:** The maximum possible rupture length of a fault, usually the full mapped trace length. This length is used to estimate the maximum magnitude earthquake.

3. **Geologic Age of Last Movement:** Faults with known or suspected movement in the last 2 million years are considered potential Type I faults.

4. **Maximum Earthquake:** The largest earthquake that a fault can potentially generate, usually based on scaling relationships that relate magnitude to the fault's rupture dimensions (i.e., length, width, area, or displacement) (Wells and Coppersmith, 1994).

5. **Closest Approach of Fault to Repository:** The shortest distance from the site to the fault trace. This distance is used to determine the attenuation of the seismic energy from the earthquake as it travels to the site.

6. **Peak Acceleration:** Peak ground motion that is produced at the site from earthquakes on potential Type I faults.

Results of the analysis of McKague, et al. (1996) reveal 78 Type I faults in the Yucca Mountain region (see Tables B-1, B-2, and B-4 of Appendix B in NRC, 1999a). The U.S. Geological Survey (1996, Table 11-1) tabulated 100 faults in the Yucca Mountain region, but these were not specifically classified as Type I faults. Of those faults tabulated by the U.S. Geological Survey, 69 were categorized as relevant or potentially relevant (Tables B-1 and B-2 in NRC, 1999a). U.S. Geological Survey (1996) uses the terms relevant for faults that have documented Quaternary displacement and the earthquake generated on the fault could produce 84th percentile peak acceleration greater than or equal to 0.1 g, and potentially relevant for faults that are considered subject to displacement on the basis of potential structural association with seismicity. The staff assumes these faults to be equivalent to Type I faults. Type I faults and relevant or potentially relevant faults are compiled in Tables B-1, B-2,

B-3, and B-4 of Appendix B (NRC, 1999a). The compilations relied on essentially the same data sources (Simonds, et al., 1995; Faulds, et al., 1994; Frizzell and Shulters, 1990; Scott and Bonk, 1984; Piety, 1995; and Nakata, et al., 1982), and studies assumed moment magnitude scales as a function of fault trace length according to Wells and Coppersmith (1994).

3.2.4 Areal Sources

Areal sources, also referred to as area sources or seismotectonic provinces, are areas of uniform seismic potential. Although according to geologic theory, all earthquakes are initiated by rapid displacement along a fault, many historical earthquakes cannot be tied directly to known faults. Most often, the causative faults are only located at depth and lack surface exposure. In the eastern United States, many of the causative faults are buried deep in the crust and cannot be easily identified. Low-angle faults that terminate in cores of folds are also difficult to identify accurately. For example, the 1994 Northridge earthquake ruptured a previously unknown low-angle thrust fault that terminated in the core of the Pico anticline (e.g., U.S. Geological Survey, 1995). To a lesser degree, mislocation of small earthquakes or misinterpretation of the geometry of fault zone at depth also contributes to the uncertainty of defining fault sources.

3.2.4.1 Location and Geometry of Areal Sources

To account for these uncertainties in seismic hazard analyses, areal sources are drawn to represent a region of homogeneous earthquake potential and distinct earthquake potential from the neighboring areal sources. The areal sources are recognized as an abstraction of the probabilistic seismic hazard analysis and not representative of a physical characteristic of the Earth. The boundaries of areal sources are drawn to define areas with relatively uniform seismicity and maximum magnitude, generally defined by the historic seismic record, although they may also be defined from changes in tectonic setting or simply along geologic boundaries. To further account for uncertainties in the areal source zone definitions, several alternative configurations can be developed and incorporated in the probabilistic seismic hazard analysis, each with its own weight or credibility. In Budnitz, et al. (1997), three types of areal source zones are defined: (i) concentration zones—concentrated zones of well-located instrumental seismicity; (ii) regional zones—spatial changes in the distribution, concentration, or density of seismicity; and (iii) background zones—regional changes in the structural style or tectonic history.

3.2.4.2 Maximum Magnitude Earthquake of Areal Sources

Characterizing M_{max} for areal sources is more uncertain than for fault sources because the physical dimensions of the faults that constrain earthquake sources are largely unknown. The primary tool is the historical seismic record aided by analogies to other seismic sources (Budnitz, et al., 1997). For the Basin and Range, the historical record may be too brief to ensure that the maximum magnitude earthquake was captured by the instrumental record. Thus, analogs to other regions provide the best way to estimate M_{max}. A critical question in the characterization of M_{max} in areal sources is the size of the maximum background earthquake—the largest earthquake that could reasonably occur without identifiable surface rupture. In the Basin and Range, there are several important historical earthquakes, each without surface rupture, that constrain the maximum background earthquake, including the

1986 **M**6.2 Chalfant Valley earthquake (Lienkaemper, et al., 1997) and the 1925 **M**6.6 Clarkston Valley earthquake (Doser and Smith, 1989).

3.2.4.3 Recurrence Relationships of Areal Sources

Recurrence relationships for areal sources are derived in a similar way as those for fault sources. Because of the lack of information about fault dimensions, however, development of recurrence relationships for areal sources relies more heavily on the historical earthquake record. Thus, the accuracy of the historical catalog is critical to development of reliable recurrence relationships for the areal sources. Unlike the fault sources, most recurrence relationships for areal sources assume an exponential or Gutenberg and Richter (1954) relationship. This assumption is based on the premise that the large sources (greater than **M**6.5) cause surface rupture and thus are already accounted for by the fault sources in the characteristic model.

As summarized by Budnitz, et al. (1997), areal source zone recurrence models can be developed by plotting the mean frequencies for each magnitude bin, along with associated uncertainties. A curve is then fit to the resulting distribution. Maximum likelihood methods (e.g., Weichert, 1980) are used for curve-fitting because these methods account for the decreasing number of earthquakes in each magnitude bin. From the resulting best-fit curve, the *a* (intercept) and *b* (slope) values can be obtained. If the seismicity is considered uniform throughout the areal source, then single values for *a* and *b* are used (maximum smoothing). For more detailed analyses, the *a* and *b* values can be varied within each zone, giving rise to varying recurrence parameters (see Section 4.3.5 of Budnitz, et al., 1997).

3.2.3 Vibratory Ground Motion

Ground motion attenuation models describe the relation among earthquake magnitude, distance from source to the site, and vibratory ground motion at the site. According to Budnitz, et al. (1997), ground motion should be characterized by two basic approaches: (i) a spectrum of the natural logarithm of the ground motion parameter determined as a function of magnitude and distance at multiple frequencies and (ii) the standard deviation of the natural logarithm of the ground motion parameter. The standard deviation could be a function of magnitude, distance, and frequency level, as applicable. Ground motion should be characterized for both horizontal and vertical field-free ground motion response spectra at the ground surface and repository depth.

Aspects of ground motion attenuation to consider in seismic hazard analysis are (Reiter, 1990)

- Seismic source properties (e.g., focal mechanism, depth, directivity, or magnitude saturation effects).
- Wave propagation between source and site.
- Peak ground motion and the response spectrum.
- Empirical or theoretical factors controlling the near-field region (typically within 10 km of the site).

- Site-response models, especially surface-to-subsurface attenuation and amplification and deamplification characteristics.

Ideally, ground motions from earthquakes in the Basin and Range should be used to develop attenuation relations for Yucca Mountain. However, strong motion data recorded from earthquakes in the Basin and Range were too sparse to adequately constrain an empirical attenuation model for Yucca Mountain. Therefore, empirical attenuation models from the western United States were used to develop an attenuation model for Yucca Mountain. Significant differences may exist in the seismic source, source effects (extensional versus compressional regimes and normal versus strike-slip faulting), path effects (differences in regional crustal structure), or site effects (differences in the shallow site properties) between Yucca Mountain and the western United States. Therefore, estimations of the ground motion attenuation needs to account for those differences when estimating the expected ground motion from earthquakes at Yucca Mountain.

3.2.4 Calculation of Seismic Hazard

Probabilistic seismic hazard analysis is a powerful tool for incorporating uncertainties associated with identifying and characterizing seismic sources and ground shaking. The probabilistic seismic hazard analysis will lead to identifying the ground motion hazard levels that will be used as the basis for development of seismic design basis input for Yucca Mountain.

Aspects of hazard calculations and presentation are

- Probabilistic seismic hazard analysis structure (National Research Council, 1988).
- Uncertainties, both aleatory and epistemic (Budnitz, et al., 1997).
- Probabilistic seismic hazard analysis calculation and results, both total hazard with fractiles and uniform hazard spectrum (Budnitz, et al., 1997).
- Deaggregation of results (Bernreuter, et al., 1998).

3.2.5 Seismic Hazard of Bare Mountain Fault

The Bare Mountain fault has been identified as an important source of seismicity and one that would contribute to the total seismic hazard at the proposed geologic repository at Yucca Mountain. The level of seismic ground motion produced by Bare Mountain at the proposed Yucca Mountain repository is determined by its geometric and kinematic characteristics. To evaluate the uncertainties and importance of the geometric and kinematic characteristics of the Bare Mountain fault, a sensitivity study was conducted. The sensitivity of ground motion level at the proposed Yucca Mountain repository to the maximum magnitude, dip angle, and slip rate of Bare Mountain was evaluated using probabilistic seismic hazard analysis software EZ-FRISK™ Version 4.4 produced by Risk Engineering, Inc. Table 3-1 gives the input parameters for twelve cases analyzed (Figure 3-2). Maximum magnitudes were estimated from two variations of fault surface extension (trace length or surface rupture) using the empirical relationships given by Wells and Coppersmith (1994). The surface extension of Bare Mountain fault was assumed to be 40 km in the first set of cases (labeled BML in Table 3-1) and 20 km in the second set of

Table 3-1. Sensitivity of Fault Geometry and Fault Slip Rate on the Seismic Hazard of the Bare Mountain Fault				
Cases	**Extension (km)**	**Maximum Magnitude**	**Dip Angle (degree)**	**Slip Rate (mm/yr)**
BML_1a	40	6.94	60	0.01
BML_1b				0.10
BML_1c				1.00
BML_2a			70 to 40 (at 7.5 km)	0.01
BML_2b				0.10
BML_2c				1.00
BML_3a			70 to 10 (at 10 km)	0.01
BML_3b				0.10
BML_3c				1.00
BMS_1a	20	6.59	60	0.01
BMS_1b				0.10
BMS_1c				1.00
BMS_2a			70 to 40 (at 7.5 km)	0.01
BMS_2b				0.10
BMS_2c				1.00
BMS_3a			70 to 10 (at 10 km)	0.01
BMS_3b				0.10
BMS_3c				1.00

cases (labeled BMS in Table 3-1). This difference led to 0.35**M** difference in M_{max}. Two variations of dip angle were considered: (i) a constant dip angle of 60° (planar fault) and (ii) a dip angle changing from the initial value of 70° to a shallow depth of 10° at 7.5 km depth (a listric fault). Three slip rates were considered for each set of geometric data, slip rate estimates from Global Positioning System data (1.0 mm/yr, Wernicke, et al., 1998), geological rates over the last 1 million years (0.1 mm/yr, Stamatakos, et al., 1997a), and trenching results (0.01 mm/yr, Klinger and Anderson, 1994).

Analysis of the results (Figure 3-2) shows that seismic hazard is most sensitive to slip rate. Increasing slip rate by one order of magnitude increases the annual frequency of exceedance of the same peak ground acceleration by one order of magnitude. At the frequency of

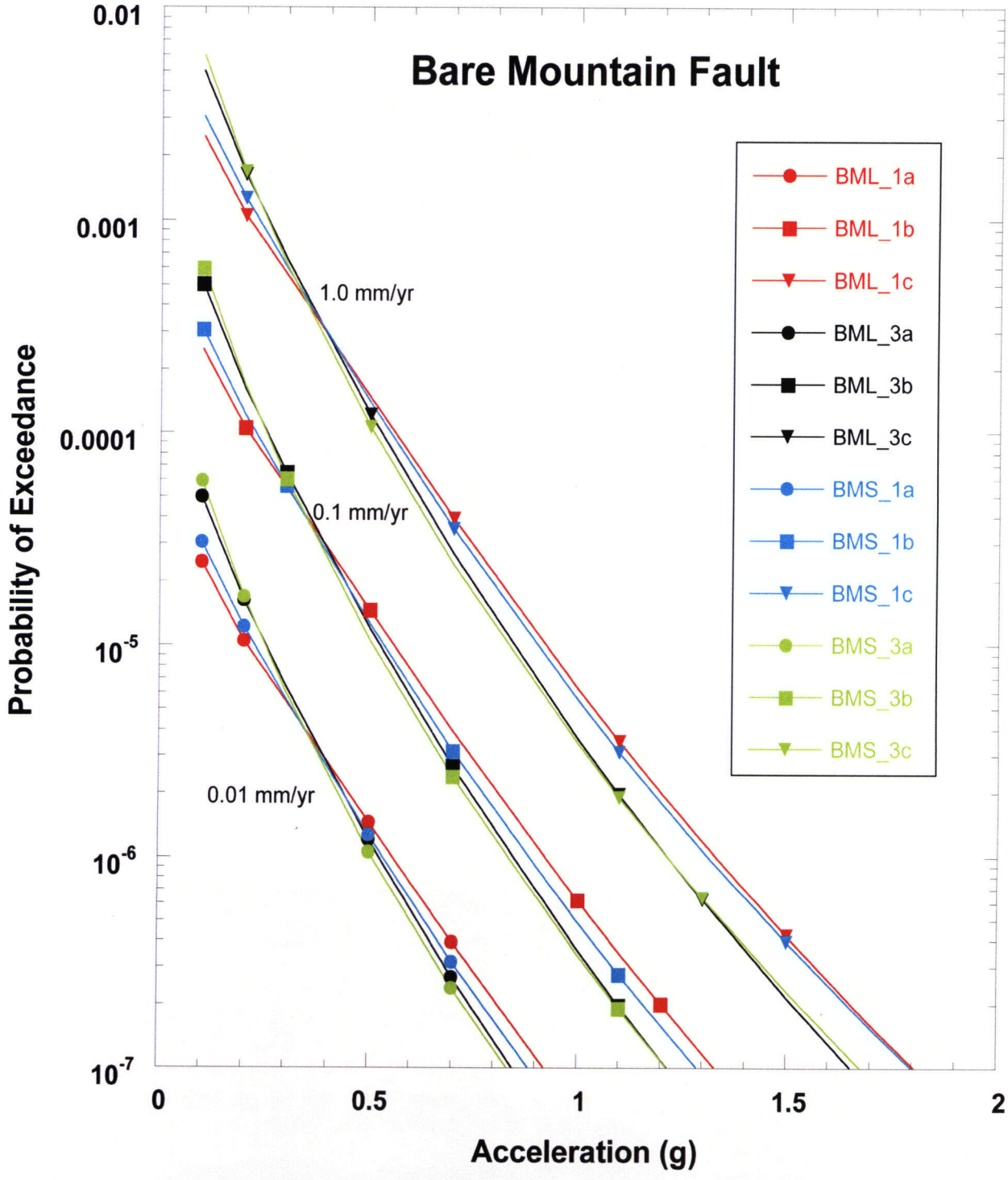

Figure 3-2. Seismic Hazard Results for the Bare Mountain Fault Based on Alternative Assumptions of Fault Geometry and Fault Activity. The 12 Cases are Defined in Table 3-1.

exceedance of 10^{-5} (return period of 100,000 years), increasing slip rate by one order of magnitude increases the peak ground acceleration by about 0.35 g. Computed seismic hazard is much less sensitive to geometric parameters. An increase in the length of the fault by twofold only slightly increases the long return period ground motions and decreases short return period ground motions. This change is expected because the longer fault generates larger but more infrequent earthquakes. Changing the fault geometry from planar to listric also decreases the short return period ground motion and increases long return period ground motions. As with a longer fault, the listric geometry is capable of larger magnitude but less frequent earthquakes.

These sensitivity results were based on analyses using the attenuation equation proposed by Abrahamson and Silva (1997) rather than the entire suite of Yucca Mountain attenuation equations. The Abrahamson and Silva (1997) equation is one of the proponent attenuation relations used by the probabilistic seismic hazard analysis expert elicitation to develop the ground motion equations for the Yucca Mountain probabilistic seismic hazard analysis (CRWMS M&O, 1998).

4 FRACTURING AND STRUCTURAL FRAMEWORK OF THE GEOLOGIC SETTING

Fracturing of the volcanic rocks at Yucca Mountain started when volcanic ash was deposited about 11 to 13 million years ago to produce the Paintbrush Tuffs. The first fractures were probably cooling joints. This type of fracturing ceased soon after deposition and cooling. Within the Yucca Mountain region, there is ample evidence that faulting was occurring contemporaneously with the deposition of the volcanic tuffs (Monsen, et al., 1990; Scott, 1990; Day, et al., 1998a), such that tectonic joints may have begun to form early in the history of the tuffs. Cooling joints and tectonic and unloading joints constitute the naturally occurring joint system. Tectonic and unloading joints continue to form to the present. Human-induced fractures in drifts at Yucca Mountain formed by excavation methods are discussed in the Repository Design and Thermal-Mechanical Effects Issue Resolution Status Report (NRC, 2000). Faults are another prominent feature of the structural framework at Yucca Mountain. Small faults and shear joints (up to meters in length and of small displacement) grade upward in scale to large features (hundreds of meters, in the case of joints, and tens of kilometers in the case of faults). Together, the complete system of joints and the small-to-large (block-bounding) faults constitute the structural framework of Yucca Mountain.

4.1 Fracture Models

Fracture models are depictions of a hierarchy of types and sizes of individual rock fractures that includes faults and joints. Faults and joints generally occur in patterns that reflect the physical properties of the tuff and the local stresses at the time of fracturing or faulting. Therefore, the fracture pattern and general characteristics (certain geometric and mechanical properties) of fractures may be estimated in volumes of rock hidden from view or otherwise lie just beyond the drill bit or tunnel boring machine disk-cutter. Estimates, ranges of estimates, or models of fractures not directly observed are made by processes of interpolation between fractures, or projection of fractures from their observed traces, providing that the rockmass properties, the primary and secondary fault properties, and the aspects of the fracture history are known. The better constrained such knowledge is of existing fractures, the better the fracture property estimates or fracture models are likely to be. Viable fracture models are those considered reasonable estimators of the unseen structural framework of Yucca Mountain.

Fracturing at Yucca Mountain has been the subject of numerous focused investigations. Key elements of fracture characterizations are listed next with associated topical references to highlight selected data and interpretations considered by staff as most pertinent to the evaluation of fracturing processes at Yucca Mountain and resulting implications for repository performance. Many of these studies have recently been integrated and summarized in the DOE Yucca Mountain Site Description (CRWMS M&O, 2000a).

4.1.1 Regional and Local Stratigraphic Elements

Stratigraphic elements to consider in fracture models are

- Age of host geologic units, especially with respect to timing of fracture formation events (Sawyer, et al., 1994; Buesch, et al., 1996; Day, et al., 1998b).

- Host rock types (igneous rocks, lithified sedimentary strata, and unlithified sediments) in the saturated zone and the unsaturated zone at Yucca Mountain, including lateral

and vertical lithologic variations, such as degree of welding, lithophysal development, alteration, and pumice content of tuff (Sweetkind, et al., 1997a,b) that could potentially affect fracturing.

- Host rock types in the Proterozoic and Paleozoic units of the subregional saturated zone, with particular emphasis on solubility features of Paleozoic carbonate units potentially related to karstic flow systems.

4.1.1.1 Regional, Subregional, and Local Structural and Tectonic Elements

Regional and subregional structural and tectonic elements to consider in fracture models are

- Evolution of regional stress field (Zoback, et al., 1981; Minor, 1995; Minor, et al., 1997; Ferrill, et al., 1996b; Morris, et al., 1996).

- Contemporary stress field (Stock, et al., 1985, 1986; Stock and Healy, 1988; Zoback, 1992; Zoback, et al., 1992; Wittmeyer and Ferrill, 1994; Wittmeyer, et al., 1994; Barton, et al., 1995; Ferrill, et al., 1994, 1995a, 1996b; Morris, et al., 1996; also cf. Engelder, 1993; Wesnousky and Jones, 1994).

- Geologic maps (Swadley and Parrish, 1988; Frizzell and Shulters, 1990; Scott and Bonk, 1984; Faulds, et al., 1994; Day, et al., 1998b; Scott, 1990; Piety, 1995; Simonds, et al., 1995).

- Structural cross sections (Scott and Bonk, 1984; Scott, 1990; Young, et al., 1992a,b, 1993; Ferrill, et al., 1996b; Ofoegbu and Ferrill, 1995, 1996, 1998; Day, et al., 1998b).

- Structural and tectonic setting including known and interpreted regional and subregional scale structural features such as faults and folds, with emphasis on structural features (both emergent and buried) in Crater Flat (including the Bare Mountain fault), Yucca Mountain, Jackass Flat, and Amargosa Valley (Snyder and Carr, 1982; Swadley, et al., 1984; Reheis, 1988; Scott, 1990; Young, et al., 1992b; Ferrill, et al., 1995b, 1996a,b,c, 1999a,b; Menges, et al., 1995; Stamatakos, et al., 1997b; Ofoegbu and Ferrill, 1998; Stamatakos and Ferrill, 1998).

- Geophysical data to constrain fault-related deformation (Brocher, et al., 1998; Majer, et al., 1997).

- Geodetic strain measurements (Gilmore, 1992; Savage, et al., 1994; Ferrill, et al., 1996b; Bennett, et al., 1997; Wernicke, et al., 1998).

- Long-term strain and deformation estimates, including geologically derived strain and fault displacement estimates and paleoseismic (trenching) studies (Ferrill, et al., 1996a,b; Stamatakos, et al., 1997b).

- Local stress field including lithostatic, tectonic, topographic, and excavation-related stresses and fluid pressure and effects on permeability (Wittmeyer and Ferrill, 1994;

Wittmeyer, et al., 1994; Barton, et al., 1995; Morris, et al., 1996; Finkbeiner, et al., 1997; Ferrill, et al., 1999b).

- Fracture and fault characteristics at Yucca Mountain, resulting from surface studies such as pavement mapping, outcrop investigations, subsurface studies such as borehole analyses, Exploratory Studies Facility mapping, and scanline studies (Barton and Hsieh, 1989; Carr, 1992; Stuckless, et al., 1992; Barton, et al., 1993; Carlos, et al., 1993; Lin, et al., 1993; Barton, et al., 1995; Chekuri, et al., 1995; Throckmorton and Verbeek, 1995; Sweetkind, et al., 1995a,b, 1996, 1997a,b; Sweetkind and Williams-Stroud, 1995a,b, 1996; Paces, et al., 1996; Piety, 1995; Potter, et al., 1996; Anna, 1997; Anna and Wallman, 1997; DOE, 1998).

- Three-dimensional geometry of Yucca Mountain faults and fault blocks, intersection relationships of faults, and patterns of fault displacements (e.g., vertical and lateral gradients) (Scott, 1990; Stamatakos and Ferrill, 1998; also Gay and Ortlepp, 1979; Allan, 1989; Higgs, et al., 1991; Peacock and Sanderson, 1991, 1994; Scholz, et al., 1993; Dawers and Anders, 1995; Willemse, et al., 1996; Zhang and Sanderson, 1996; Davies, et al., 1997; Ferrill and Morris, 1997; Willemse, 1997; Yielding, et al., 1997; Alexander and Handschy, 1998; Ferrill, et al., 1998, 1999a,b; Morris and Ferrill, 1999).

- Partitioning of regional and subregional strain (Ferrill and Dunne, 1989; Dunne and Ferrill, 1995) among mechanisms such as seismic and aseismic slip on large faults (Pezzopane, 1996; Ferrill, et al., 1996a, 1999a; Stamatakos, et al., 1997a; Ofoegbu and Ferrill, 1998), dilation and slip on fractures (Ferrill, et al., 1999b), small faults (Lienkaemper, et al., 1997), bedding-parallel foliations and layering (Morris, et al., 1996; Ferrill and Morris, 1997; Ferrill, et al., 1998), elastic deformation, and dike intrusion (Wernicke, et al., 1998; Connor, et al., 1999).

- Hydrologic features associated with structural features such as faults or fracture zones (Hill, et al., 1995; also Mozley and Goodwin, 1995; Fridrich, et al., 1994; Bredehoeft, 1997; Ferrill, et al., 1999b).

4.1.1.2 Topographic Elements

Local topographic elements to consider in fracture models are

- Morphology of topographic surface (Henderson, et al., 1996).

- Geometric relationship of topographic surface with respect to layering, foliations, and structural features (important for surficial and mass-wasting processes).

4.1.2 Hydrologic, Geochemical, and Pneumatic Elements

Hydrologic, geochemical, and pneumatic elements to consider in fracture models are

- Observations, measurements, and models of infiltration and subsurface flow processes (Montazer and Wilson, 1984; Barton, et al., 1993; Flint and Flint, 1995; Flint, et al.,

1996a; Stothoff, et al., 1997; also Ritzi and Andolsek, 1992; Mayer and Sharp, 1998; Ferrill, et al., 1999b).

- Cl-36 measurements in the Exploratory Studies Facility (Levy, et al., 1997).
- Air and seepage permeability measurements (Wang, et al., 1997, 1998).
- Water table elevation data and their relationship to fracture systems (Czarnecki, et al., 1997).
- Saturated zone tracer test and pump test results (Geldon, et al., 1997; Ferrill, et al., 1999b).

4.2 Summary of Yucca Mountain Fractures

Fractures are surfaces along which rocks or minerals have broken and lost cohesion (Twiss and Moores, 1992). Extension fractures (Mode I fractures) are characterized by motion perpendicular to the fracture walls. Shear fractures (Mode II and III fractures) are characterized by motion parallel to the fracture surface. Mode II shear fractures are distinguished by motion perpendicular to the edge of the fracture, whereas sliding on Mode III shear fractures is parallel to the edge of the fracture. Fractures that display very small displacement normal to their surfaces and little or no displacement parallel to their surfaces are called joints. Joints may originate in any of the above fracture modes. Fractures that have opened perpendicular to the fracture walls and that are filled with a mineral are termed filled (or partially filled) fractures or veins.

A fault is a surface or thin tabular zone along which opposing sides have moved in a direction parallel to the surface or zone, across which, the displacement parallel to the zone is appreciably greater than the thickness of the zone, and in which, the deformation is greater than outside the zone (Twiss and Moores, 1992; Groshong, 1988). Fault zones commonly consist of a fault core within which most of the displacement is accommodated and a fault damage zone that consists of a network of subsidiary structures that bound the fault core (Caine, et al., 1996). In porous rocks, fault cores commonly have lower permeability than the protolith because of grain size reduction and mineral precipitation. Fault damage zones commonly have enhanced permeability because of fracturing and faulting. Fault core and fault damage zone development is variable from fault to fault and along an individual fault (Caine, et al., 1996).

Joints in the central repository block at Yucca Mountain may be divided by age and genesis into three groups: oldest cooling joints, tectonic joints of intermediate age, and youngest unloading joints (Barton and Larsen, 1985; Barton and Hsieh, 1989; Barton, et al., 1993; Sweetkind, et al., 1995a,b; Throckmorton and Verbeek, 1995; Sweetkind and Williams-Stroud, 1996). Eight joint sets have been identified between these origins and ages, but no analyzed exposure contains all eight sets. Cooling joints are distinguishable because they (i) locally have degassing-related tubular structures (Barton, et al., 1984), (ii) do not cut lithophysae, (iii) have a smooth planar appearance, (iv) have surface areas in excess of 100 m^2, and (v) predate other joints (based on abutting relationships). Tectonic joints are distinguishable from cooling joints because they (i) lack tubular structures, (ii) cut lithophysae, (iii) are not normally as smooth, (iv) commonly are

smaller, and (v) in many cases, abut against cooling joints. Some tectonic joints, however, cut across cooling joints, which suggests that either the cooling joints were mineral-filled at the time of tectonic joint propagation or that the crossing tectonic joints originated as shear fractures. Thus, some cooling joints were not voids that blocked propagation of tectonic joints. Finally, unloading joints are subhorizontal, near surface, rough and curviplanar, and generally terminate against cooling and tectonic joints.

Cooling joints form during thermoelastic contraction resulting from heat loss after deposition of the welded tuffs. During heat loss in the thick cooling units, isotherms are not arranged in a blanket-like manner parallel to the unit boundaries. Instead, some fluid circulation occurs, creating thermal plumes and sinks that would have locally affected joint intensity and orientation. Typically, igneous cooling joints form polygonal patterns in situations where the minimum and maximum horizontal stresses are near equal, and the rocks are not free to expand laterally, which is the fixed-grip situation (Engelder and Fischer, 1996). Yet, the cooling joints in the welded tuffs of the Paintbrush Group are orthogonal (Sweetkind and Williams-Stroud, 1996) with two joint sets subnormal to layering and one parallel to layering. This deviation from typical geometry may be controlled by lateral thickness variations, paleotopography, differential compaction, tectonic stresses, and horizontal stresses that were significantly anisotropic. The setting was not fixed-grip but rather one of regional east-west extension during the Miocene (Zoback, et al., 1981; Scott, 1990; Wernicke, 1992; Ferrill, et al., 1996b; Morris, et al., 1996; Day, et al., 1998b). Thus, cooling joints at Yucca Mountain formed in a local stress field that was probably produced by a combination of sources, including thermoelastic cooling stresses, topographic stresses, lateral thickness variations, differential compaction, remote regional stress field, and stress perturbations around active faults (Engelder, 1993).

Tectonic joint development did not necessarily postdate cessation of cooling joint formation by an extended period because the oldest tectonic joints (T1) (Sweetkind and Williams-Stroud, 1995a) strike north-south, are subnormal to layers, and are attributed to the east-west horizontal extension during the Miocene. The next youngest joint set, northwest-trending joints (T2), would appear to require a regional stress field where minimum principal stress was oriented northeast-southwest. This stress-field geometry is undocumented by other geological features, and the existence of this set is not strongly supported (Sweetkind and Williams-Stroud, 1995a). T3 joints strike northeast-southwest and are related to the recent regional stress field where the minimum principal stress trends northwest (Sweetkind, et al., 1995b). The youngest tectonic joints are east-west-trending joints (T4), which have a problematic tectonic origin as no regional stress field has been identified to account for north-south extension. As a result, Throckmorton and Verbeek (1995) and Sweetkind and Williams-Stroud (1995b) attributed fractures of this set to an unspecified surficial unloading event. A possible tectonic rather than unloading origin for some T4 fractures would be as secondary structures accommodating north-south extension in the regions between two overlapping normal faults that strike north-south (Trudgill and Cartwright, 1994; Peacock and Sanderson, 1994; Ferrill, et al., 1999a). Late subhorizontal joints with significant surface roughness and curviplanar form are attributed to erosional unloading (Sweetkind and Williams-Stroud, 1995a,b).

When the origin of a fracture or joint is known, important attributes of that fracture and others related to it may be assumed because certain characteristics have been correlated to origin (e.g., low surface roughness and long length are associated with cooling joints; cooling joints,

when identified, are expected to be largely confined to the particular rock unit in which it occurs). Therefore, an adequate investigation and explanation of the mechanisms for fracture generation that include development of the various origins of joints at Yucca Mountain (i.e., cooling joints, tectonic joints, unloading joints, and construction-induced joints) consistent with evolution of the applicable regional and local stress field, should be attempted by the DOE to help constrain interpolation between and extrapolation beyond locally-exposed fractures and faults that are abstracted into process level and performance assessment models.

Overall fracture intensity in the Paintbrush Group nonwelded tuffs is lower than in the overlying and underlying welded Tiva Canyon and Topopah Spring Tuffs, respectively. In addition, fractures are poorly connected within and between the nonwelded tuff layers (Rousseau, et al., 1996; Sweetkind, et al., 1996, 1997a,b). Extension fractures in the nonwelded tuffs typically terminate at lithologic breaks. Faults, which typically originate as shear fractures capable of fracturing across discontinuities, have been considered to be structural pathways though the nonwelded tuffs. However, these faults may act as flow barriers, depending on the fault zone deformation mechanisms.

4.3 Clustering of Fractures at Yucca Mountain

One important morphological aspect of the joint sets, which was first noted during pavement studies by Barton, et al. (1993), is that joints do not have uniform spacing (Figure 4-1). Instead, some joints are closely spaced in swarms or clusters. The clusters are separated by large distances in excess of 10 m, where joint spacing is in excess of 1 m. Development of joint clusters clearly demonstrates that deformation in the rock was heterogeneously distributed in the rock during fracture formation. One type of cluster geometry is best exemplified by the joints in the hanging wall of the Ghost Dance fault (Sweetkind and Williams-Stroud, 1995a). Surface mapping around the north-south striking Ghost Dance fault has identified a 50-m-wide zone of highly fractured rock in the hanging wall of the fault (Sweetkind and Williams-Stroud, 1995a,b). North-south striking joints and north northwest-south southeast striking joints are intensely developed with spacings of a few centimeters at distances up to 50 m from the main fault trace, which also strikes north-south. The deformation concentrator here appears to be partitioning of a small portion of the east-west regional extension into hanging wall deformation by joint formation, perhaps, in a dilational quadrant during fault displacement. The width of hanging wall fault-damage zones is smaller in the Exploratory Studies Facility than at the surface. Fault footwalls typically show little or no increase in fracturing near faults (Sweetkind, et al., 1997a,b).

Another type of cluster geometry is closely spaced cooling joints (Barton, et al., 1993). Detailed mapping of large joints (lengths >2m) in the upper lithophysal unit of the Tiva Canyon Tuff on Live Yucca Ridge shows that cooling joints tend to be clustered into swarms that trend northeast and northwest (Section 4.4). Swarm spacings are on the order of 30 to 100 m. Cooling joint swarms consist of extensive planar smooth fractures occurring in sets of three to eight fractures, with joint spacings of about 25 cm and trace lengths typically 10 m. Individual cooling joint trace lengths exceed 25 m in some cases. Swarms span the entire thickness of the upper lithophysal unit of the Tiva Canyon Tuff, and have observed lengths that exceed 100 m. True lateral extents of swarms remain unconstrained. Why cooling joints would be heterogeneously distributed in space and form orthogonal sets rather than columnar arrays is

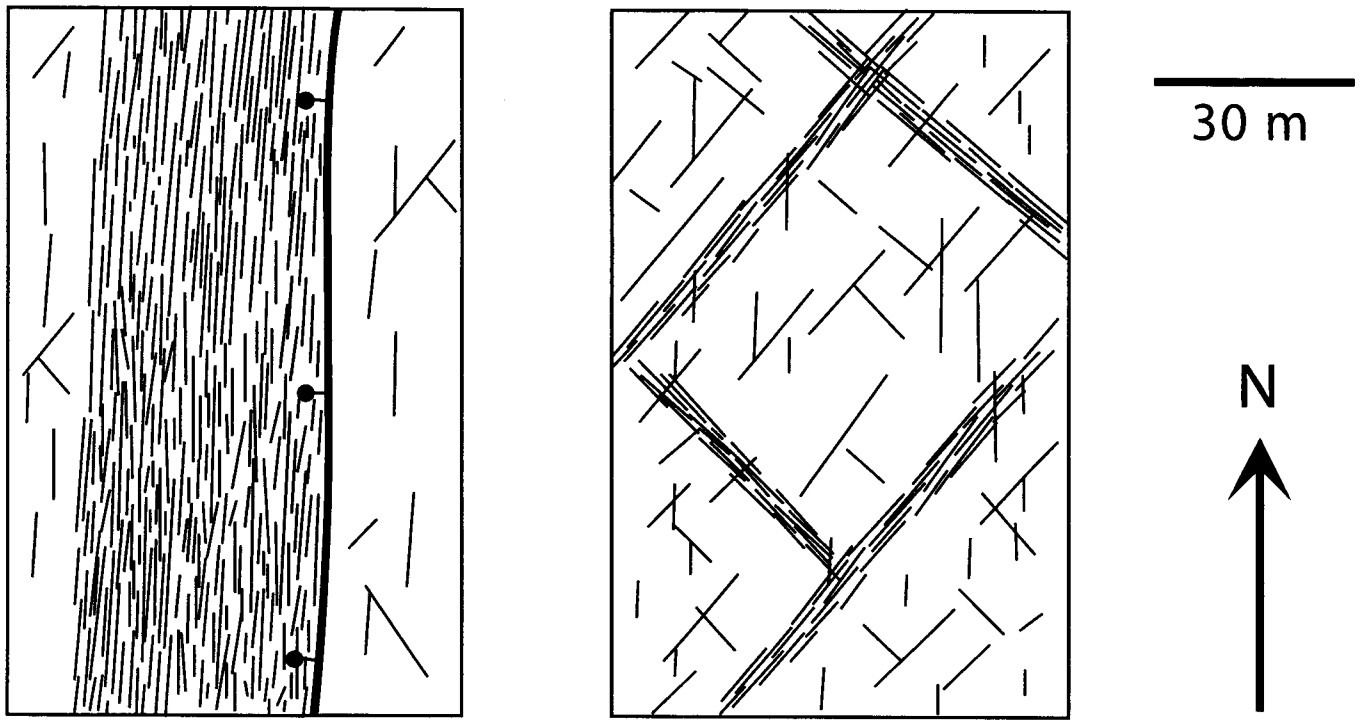

Figure 4-1. Schematic Illustrations of Joints at Yucca Mountain. The Diagrams Show (a) Fault Related Joint Swarms and (b) Cooling Joint Swarms at Yucca Mountain. Solid Lines are Fracture Traces, and Bold Line is a Fault with Blackened Circle on Hanging Wall. Both (a) and (b) are Plan Views.

not well understood, it may be a function of thermal gradients and topographic- and fault-related effects on the local stress field during cooling.

The presence of clusters may indicate that the majority of cooling joints were mineralized early (e.g., by vapor phase minerals). Otherwise, these large fractures would be expected to generate significant stress shadows up to meters away. These shadows would prevent nearby initiation of new joints, so joint spacings should be on the order of meters and not tens of centimeters. The spacings at a scale of tens of centimeters would either be achieved by mineralizing the joints, preventing them from acting as voids with associated stress shadows, or by increasing the driving stress for joint formation due to increased regional extension.

4.4 Orthogonal Jointing During Coeval Igneous Degassing and Normal Faulting, Yucca Mountain, Nevada

4.4.1 Orthogonal Joints at Yucca Mountain

The origin of an orthogonal fracture system in the Tiva Canyon Tuff at Yucca Mountain, Nevada, is an important consideration because this joint system is a prominent component of the groundwater infiltration pathways through the moderately welded tuff into the repository (Winograd, 1971; Flint and Flint, 1995; Flint, et al., 1996a,b). Joint fractures with morphologies similar to those exposed at the surface of Yucca Mountain are also found within the mountain as documented by data collected from the Exploratory Studies Facility and Enhanced Characterization of the Repository Block tunnels (Mongano, et al., 1999; CRWMS M&O, 2000b). These joints represent potential weaknesses that could strongly influence stability of designed excavations such as underground waste emplacement drifts. A better understanding of the geometry and origin of these joints provides a basis for better estimating repository performance.

Existing field data (e.g., Morgan, 1984; Barton, et al., 1984, 1993; Barton and Larsen, 1985; Sweetkind, et al., 1995a,b; Throckmorton and Verbeek, 1995), newly gathered field fracture data employing a Global Positioning System/Geographic Information System approach, new observations of field relationships between joints and volcanogenic features, and numerical modeling of stress field perturbation during active faulting were used to analyze the origin of this joint system. The fracture system is intriguing because: (i) the two sets comprising the system are orthogonal, (ii) both fracture sets are clearly associated with tuff degassing, and (iii) neither set is perpendicular to the direction of regional extension at the time of formation. Thus, the fractures formed as a system of joints during tuff cooling in response to additional stress components that not only perturbed the regional stress field, but also triggered a 90° rotation of horizontal stress directions, to produce both sets of the orthogonal system.

4.4.2 Development of Orthogonal Joint Systems

Orthogonal systems of two vertical joints sets are common (Ver Steeg, 1942; Eyal and Reches, 1983; Hancock 1985; Stauffer and Gendzwill, 1987; Dunne and North, 1990; Rawnsley, et al., 1992; Martel, 1994; Caputo, 1995; Olson, 1996; Fabbri, et al., 2001). Understanding their origin is problematic because the orthogonal geometry of the two sets requires at least one 90° change in local principal stress directions during system formation, so that each set of opening-mode fractures forms normal to the minimum principal compressive stress.

Specifically, the minimum horizontal stress direction (S_h) changes by 90° or switches with the direction of maximum horizontal stress (S_H). Three types of mechanism have been proposed for orthogonal joint systems (Lachenbruch, 1962; Stauffer and Gendzwill, 1987; Dunne and North, 1990; Caputo, 1995; Olson, 1996): (i) reorienting due to small stress fluctuations between two near-equal horizontal principal stresses ($S_h \approx S_H$), (ii) regional stress rotation by 90°, and (iii) local stress switching at the scale of individual joints. None of these mechanisms can be applied universally. Switching two nearly equal horizontal principal stresses is an intuitively simple scenario, but two nearly equal principal stresses can produce oriented orthogonal systems, random orthogonal systems, or nonorthogonal systems (Lachenbruch, 1962; Pollard and Aydin, 1988). Difficulties with regional rotations are that some workers (Martel, 1994) believe this scale of behavior to be unlikely, and that the mechanism is plausibly limited to only one switch, while abutting relationships in some orthogonal joint systems suggest multiple episodes of stress reorientation (Hancock, 1985; Stauffer and Gendzwill, 1987; Dunne and North, 1990; Caputo, 1995). For local switching, while initial analysis indicated only limited potential (Martel, 1994), recent numerical modeling has shown that local stress switching could occur as a consequence of close spacing in layer-bounded joints (Bai, et al., 2001). Thus, both regional and local-scale switching mechanisms may account for the formation of orthogonal joint systems.

At Yucca Mountain, the mechanism and scale triggering switching of horizontal stress directions needs to be identified because the distribution of orthogonal joint systems is controlled in part by local stress switching. Yet, the identity of this mechanism is intertwined in determining the cause or causes of the driving stress for joint formation. A variety of volcanogenic and tectonic sources exist for driving stress, given that (i) the region was actively extending, (ii) 12.7 to 12.8 million years ago a large silicic volcanic eruption had just occurred, (iii) the host tuff was still cooling, probably with differential temperature gradients through the deposit, (iv) it may have been compacting differentially, and (v) normal faults near Yucca Mountain could have been moving at that time. Considering their relative roles during joint formation is necessary to understanding the local swapping mechanism that controls the distribution of orthogonal joint systems.

4.4.3 Regional Geology

4.4.3.1 Tectonic Setting

The orthogonal joint system of interest is located in the welded ignimbrite deposit of the Miocene Tiva Canyon Tuff that was emplaced across the location of the present Yucca Mountain in southwestern Nevada at 12.7 million years ago (Figure 4-2a). Yucca Mountain consists of a thick accumulation of gently east-dipping Miocene volcanic tuff layers cut by an array of major north-trending, west-dipping normal faults, such as the Solitario Canyon, Bow Ridge, and Paintbrush Canyon faults, and northwest-trending dextral strike-slip faults (Scott and Bonk 1984; Day, et al. 1998a,b). These faults coevally accommodated active crustal extension within the central Basin and Range Province through the Cenozoic to the present day (Scott, 1990; Wernicke, 1992; Axen, et al., 1993; Morris, et al., 1996; Day, et al., 1998a).

While this period of tectonic activity includes the time of Tiva Canyon volcanism, data supporting fault displacements coeval with volcanism and cooling are limited. The Solitario Canyon fault has several splay faults that exhibit decreasing displacement upward to fault tips

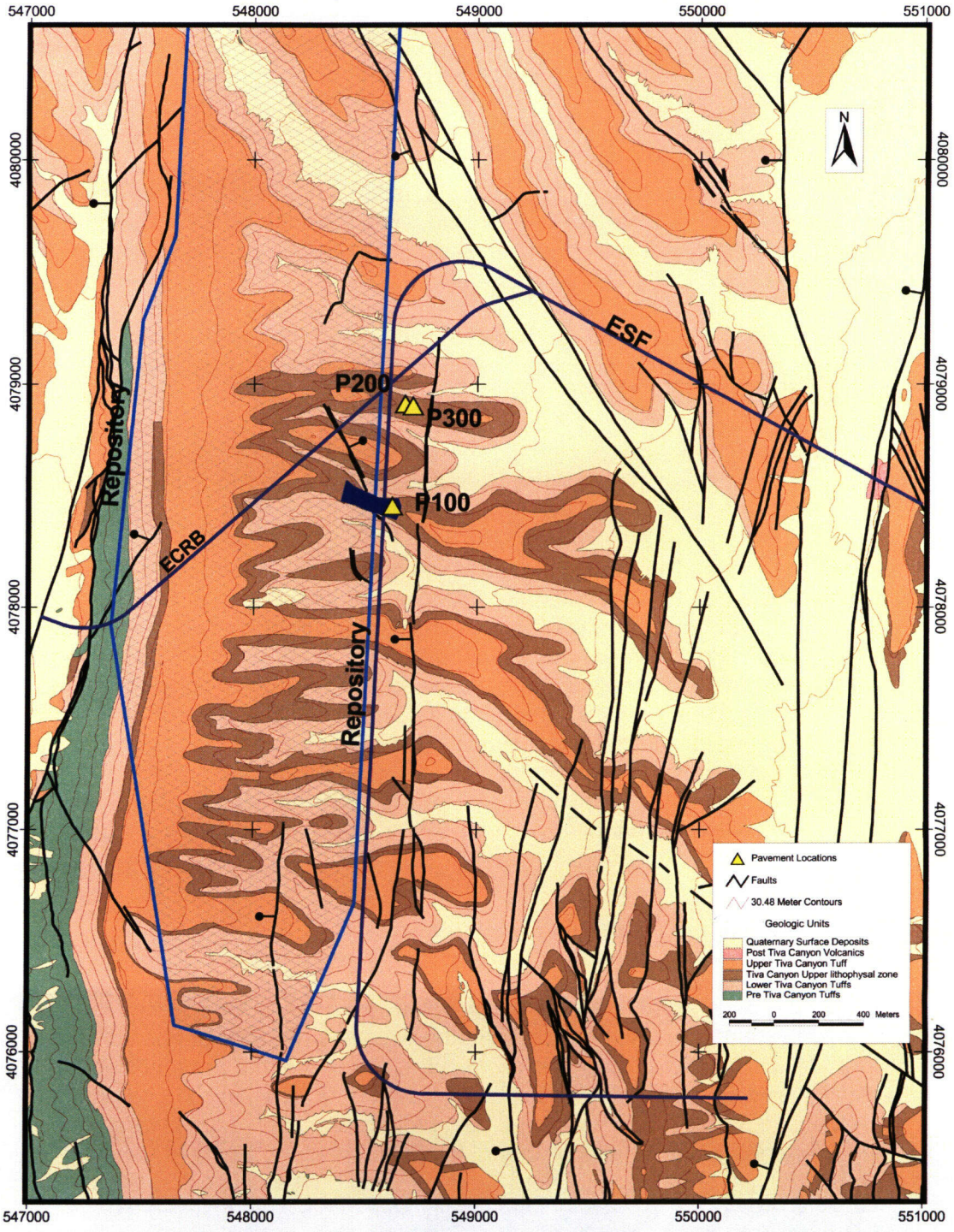

Figure 4-2. Regional Image and Local Map of Yucca Mountain. (a) Geologic Map of Yucca Mountain, Nevada. Map is Based on Geologic Mapping of Day, et al. (1998b) and Shows Proposed Repository Outline, Topographic Contours, Distribution of Tiva Canyon Tuff, Exploratory Studies Facility, Enhanced Characterization of the Repository Block, and Locations of Pavements 100, 200, and 300; and the Live Yucca Ridge Fracture Study Area.

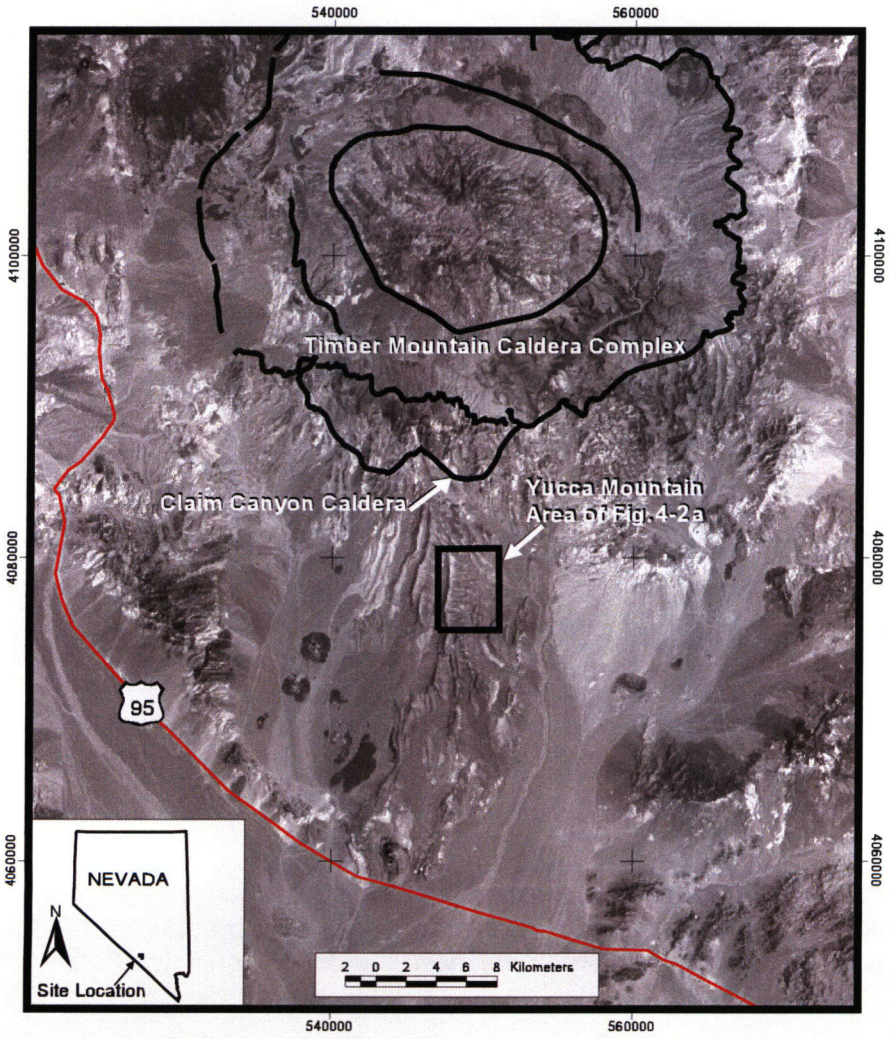

Figure 4-2 (continued). (b) Regional Map Showing Location of Yucca Mountain with Respect to the Caldera Complexes to the North

in the Tiva Canyon Tuff (Day, et al., 1998a), which are interpreted to result from growth faulting before and perhaps during deposition of the Tiva Canyon Tuff (Day, et al., 1998a). Based on unpublished subsurface thickness data, Fridrich (1999) concluded that some of the major north-trending faults in the Yucca Mountain region were active between 13.1 and 12.7 million years ago, which includes the eruption time for the Tiva Canyon Tuff. Finally, significant normal fault displacements occurred during the million years after deposition of the Tiva Canyon Tuff based on growth-faulting depositional geometries for the overlying 11.6 million years old Rainer Mesa Tuff (e.g., Christiansen, et al., 1977; Sawyer, et al., 1994; Monsen, et al., 1992; Day, et al., 1998a; Fridrich, 1999).

4.4.3.2 Volcanic Setting

The Tiva Canyon Tuff of the Paintbrush Group is a sequence of pyroclastic flow and minor ash fall deposits that most likely erupted from the Claim Canyon caldera, which is partially preserved on the southern edge of the younger Timber Mountain caldera complex (Figures 4-2b, 4-3) (Byers, et al., 1976; Buesch, et al., 1996). The Tiva Canyon Tuff consists mostly of moderately to densely welded ignimbrite deposits with devitrification, welding, and vapor-phase alteration features that resulted from the eruption of at least 1,000 km^3 of compositionally zoned rhyolitic magma at 12.7±0.03 million years ago (Byers, et al., 1976; Sawyer, et al., 1994). The approximately 100-m-thick Tiva Canyon Tuff has two lithostratigraphic members: a thin, crystal-rich upper and a thick, crystal-poor lower member (Buesch, et al., 1996). These members formed a single cooling unit (Rosenbaum, 1986). This study was conducted within the 20-m-thick upper lithophysal zone of the lower crystal-poor member (Buesch, et al., 1996).

Variations in underlying topography and depositional thickness affect the cooling behavior of ignimbrite deposits, and potentially their fracture development. The base of the Tiva Canyon Tuff is poorly exposed, so pre-emplacement topography is difficult to identify. Also, the top of the Tiva Canyon Tuff is eroded, obscuring its thickness variations. Still, Fridrich (1999) used surface outcrops and subsurface data to contour the thickness of underlying tuffs from the Paintbrush Group, which may indicate the location of depocenters for the younger Tiva Canyon. Assuming that tuff tops were flat after deposition, Fridrich interpreted the data to identify a northwest-trending basin directly north of the study area where the underlying Topopah Springs Tuff thickens 50 m into the depocenter. Also, the small-volume Yucca Mountain and Pah Canyon Tuffs, which are immediately underneath the Tiva Canyon Tuff, have lateral thickness variations that suggest deposition across irregular topography with a northwest-trending paleobasin and a gentle topographic high that limited tuff deposition immediately to the south (e.g., Day, et al., 1998b; Fridrich, 1999).

4.4.3.3 Ignimbrite Cooling Processes

Ignimbrites analogous to the Tiva Canyon Tuff are commonly emplaced at temperatures within 100 °C of magmatic temperatures, because little cooling occurs during flow except near the basal and upper contacts of the unit (Banks and Hoblitt, 1981; Bursik and Woods, 1996). The Tiva Canyon Tuff likely had a pre-eruption temperature around 700 °C (Lipman and Friedman, 1975). Uniform paleomagnetic directions indicate emplacement temperatures above a Curie temperature between 580 and 640 °C, and show that any rheomorphic deformation occurred above the Curie temperature (Rosenbaum, 1986, 1993).

GROUP	FORMATION	AGE
Timber Mountain Group	Rainier Mesa Tuff	11.6 Ma
Paintbrush Canyon Group	Bedded Tuff	
	Tiva Canyon Tuff	12.7 Ma
	Yucca Mountain Tuff	
	Pah Canyon Tuff	
	Topopah Spring Tuff	12.8 Ma
	Calico Hills Formation	12.9 Ma
Crater Flat Group	Prow Pass Tuff	
	Bullfrog Tuff	13.25 Ma
	Tram Tuff	>13.5 Ma

Figure 4-3. Stratigraphic Table for the Tuffs of the Paintbrush Group and the Overlying and Underlying Tuff Units

Degassing occurs rapidly and soon after ignimbrite emplacement at a rate largely controlled by variations in permeability (Miller, 1990; Riehle, et al., 1995). Gas pressures initially exceed lithostatic in the upper third of an ignimbrite (Riehle, et al., 1995). Trapped gas can form lithophysal cavities through matrix expansion or other gas-escape structures along pathways to the surface. Gas pressures likely fall below lithostatic within one month after emplacement (Riehle, et al., 1995). Gases continue to evolve from the volcanic glass through crystallization of anhydrous minerals (e.g., Smith, 1960), triggering vapor-phase crystallization for matrix porosity greater than 20 percent (Sheridan, 1970; Ragan and Sheridan, 1972). Subsequent devitrification and vapor-phase alteration continues to temperatures as low as 240 °C, which were probably reached several years after emplacement for the upper third of the Tiva Canyon Tuff (Lofgren, 1971; Riehle, et al., 1995).

The timing of joint development can be evaluated using features related to post-depositional cooling of the ignimbrite deposit. Earliest formed joints would be associated with gas escape structures such as fumaroles, which occur with noticeable alteration mineralization (e.g., Sheridan, 1970; Hildreth, 1983; Keith, 1991). Inflationary structures such as lithophysae also form in the earliest stage of degassing. Compaction and welding continue for time periods on the order of 1 to 10 years (Friedman, et al., 1963; Riehle, 1973; Bierwirth, 1982, cited in Cas and Wright, 1987; Riehle, et al., 1995). Ductile deformation features associated with joint formation would form during this time interval. Devitrification and vapor-phase mineralization likely continue after compaction ceases, but probably also cease about a century after emplacement (e.g., Keith, 1991; Riehle, et al., 1995). Finally, joints may form through cooling-induced contraction of the tuff to ambient temperatures (e.g., DeGraff and Aydin, 1987), which can occur more than a century after deposition without associated mineralization or alteration.

4.4.4 Joint Geometry and Origin

4.4.4.1 Previous Work

Since being identified as a potential site for the permanent disposal of high-level waste, Yucca Mountain has been a focus of fracture analysis. Fractures have been investigated at the surface (e.g., Morgan, 1984; Barton, et al., 1984, 1983; Barton and Larsen, 1985; Sweetkind, et al., 1995a; Throckmorton and Verbeek, 1995), in new tunnels (e.g., Albin, et al., 1997; Eatman, et al., 1997; Mongano, et al., 1999), and in wells (e.g., Carr, 1992). The early surface analyses used the then-novel approach of clearing pavements of about 200 to 250 m^2 (Figure 4-4) to investigate fractures as two-dimensional networks (e.g., Barton, et al., 1993) rather than relying on scanline or anecdotal station data (Hancock, 1985; La Pointe and Hudson, 1985). The tunnel work combined a rigorously collected line survey (scanline) that sampled 15 fracture attributes with a periphery map of the tunnel walls. It is the largest and most thorough data set of fractures at Yucca Mountain (CRWMS M&O, 2000b and references therein). The tunnel samples almost the entire Paintbrush Group, whereas surface data are mostly from the Tiva Canyon Tuff, which dominates the outcrop of Yucca Mountain.

The consensus of the surface investigations is that the natural joints at Yucca Mountain have three origins with distinct relative ages based on abutting relationships (Hancock, 1985; Sweetkind and Williams-Stroud, 1996). Volcanic cooling joints are oldest, largest, most planar and are mostly ornamented by tube structures (Barton, et al., 1984; Sweetkind and

(a)

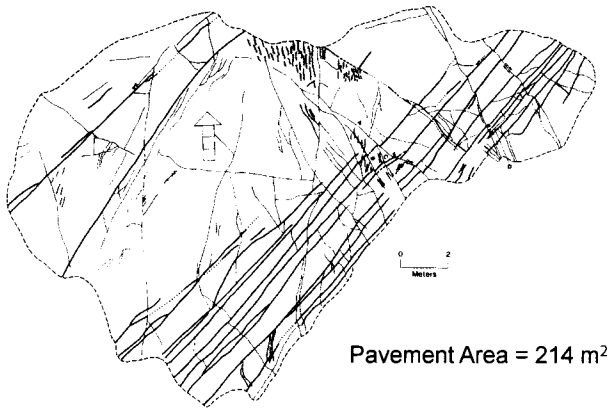

Pavement Area = 214 m^2

(b)

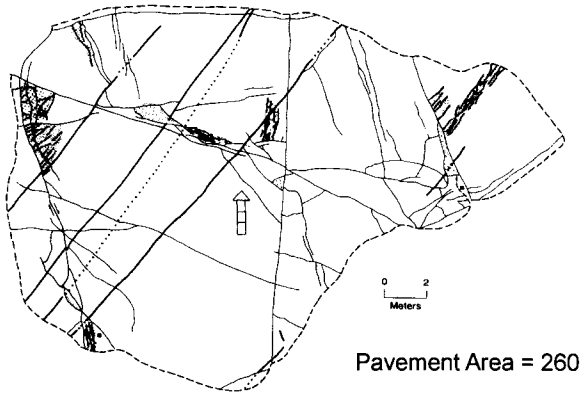

Pavement Area = 260 m^2

(c)

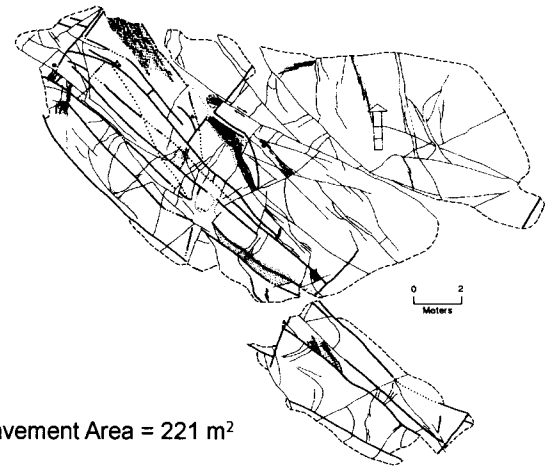

Pavement Area = 221 m^2

Figure 4-4. Fracture Trace Maps for Cleared Pavements in Upper Lithophysal Zone of the Crystal-Poor Member of the Tiva Canyon Tuff (After Barton, et al., 1993). (a) Pavement 100, (b) Pavement 200, (c) Pavement 300 (Modified from Barton, et al., 1993). Pavement Locations in Figure 4-2a.

Williams-Stroud, 1996) (Figures 4-5a,b,c, 4-6). Next, tectonic joints abut against cooling joints, are planar to curviplanar, are larger when fewer older cooling joints are present, and are smooth to rough. Unloading joints abut all other joints, are youngest, have hackly irregular surfaces, and are typically subparallel to the ground surface.

The cooling joints as defined by previous workers are the focus of this study. Because the origin of these joints is questioned here, the descriptive term tube-bearing refers to these fractures. Across much of Yucca Mountain, these joints occur in two subvertical orthogonal sets that are normal to flow foliation with a locally developed set parallel to flow layering. In the central block of Yucca Mountain, the orthogonal sets are typically northeast-trending (Figures 4-4a, 4-5c, 4-7) and northwest-trending (Figures 4-4c, 4-5d, 4-7). The relative age of the two orthogonal sets is not well constrained, as only a few abutting relationships are found (Figure 4-5d).

When considering the geometry of the orthogonal system at the scale of Yucca Mountain, some workers suggest that the two sets form a rectilinear pattern of joint swarms with swarm widths of 3 to 5 m and spacings of 150 to 200 m, based on anecdotal field observations (Barton, et al., 1993). The present study attempts to resolve the importance of the orthogonal sets of tube-bearing joints in the overall fracture network by considering their orientations over areas of thousands of square meters as opposed to hundreds of square meters.

4.4.4.2 Timing Relations Between Tube-Bearing Joints and Volcanogenic Features

Tube-bearing joints at Yucca Mountain have two characteristics that are interpreted to indicate that joint formation preceded lithophysae formation. First, tube-bearing joints do not intersect lithophysae, although lithophysae with decimeters diameters are common (Figure 4-5a,c,d). If joint propagation occurred in the presence of lithophysae, intersections and terminations with lithophysae should occur (Barton, et al., 1993; Buesch, et al., 1996), partially because some joints should have also propagated toward existing lithophysae, in response to local stress perturbations around the expanding void (Kirsch, 1898; Lachenbruch, 1962). Second, some joint walls within about a centimeter of lithophysae show outward deformation by lithophysal inflation, so the walls are older.

Tube-bearing joints also have two features that the authors interpret to indicate that joint formation preceded tube formation. First, some tubes wrap through joint intersections, which indicates that these intersections are older. Second, tubes are found only on joint faces.The millimeter-to-centimeter diameter tubes form anastomosing networks, which isolate areas of joint planes (Figure 4-5b,d,e). Area edges match across tube walls, indicating the tubes dilated joint faces during their formation. A retrodeformation to remove the effects of tube formation (Figure 4-5e) shows that tubes produced at least 15-percent vertical dilation of the joint face, accompanied by a few degrees of local rotation for some areas. This magnitude of vertical dilation is consistent with vertical expansion in the host unit of 16 to 22 percent due to lithophysal formation described by Barton, et al. (1993) (Figure 4-6). Thus, the tubes, which were degassing structures (Barton, et al., 1993), were coeval with lithophysae formation. Because the tube-bearing joints are older than the lithophysae and the tubes, and gas pressure must exceed lithostatic for their inflation, the timeframe for their formation bounds the timing of joint development in a lithophysae-free host. Thus, joint formation likely occurred within a month of tuff emplacement (Riehle, et al., 1995).

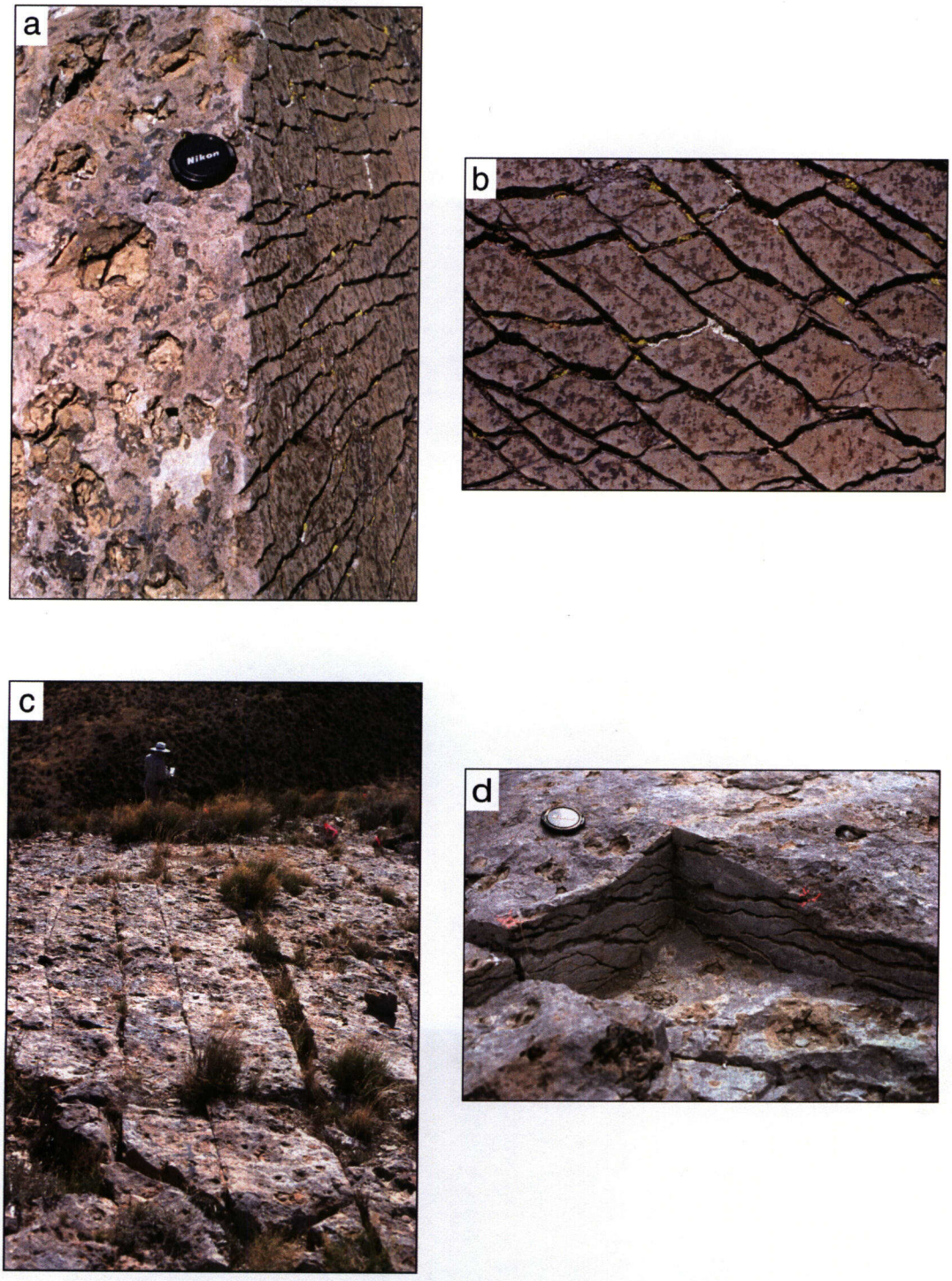

Figure 4-5. Photographs of Fractures in Upper Lithophysal Unit of the Tiva Canyon Tuff. (a) Smooth Cooling Joint with Tubular Structures Defines One Face of Loose Block (Right Side of Photo), and Later Joint with Rougher Surface Morphology Cuts Lithophysae (Left Side of Photo); (b) Tubular Structures on Cooling Joint Surface Shown in (a); (c) Cooling Joint Swarm on Pavement 100 (View Toward the Southwest); and (d) Intersection of Two Cooling Joints on Pavement 100.

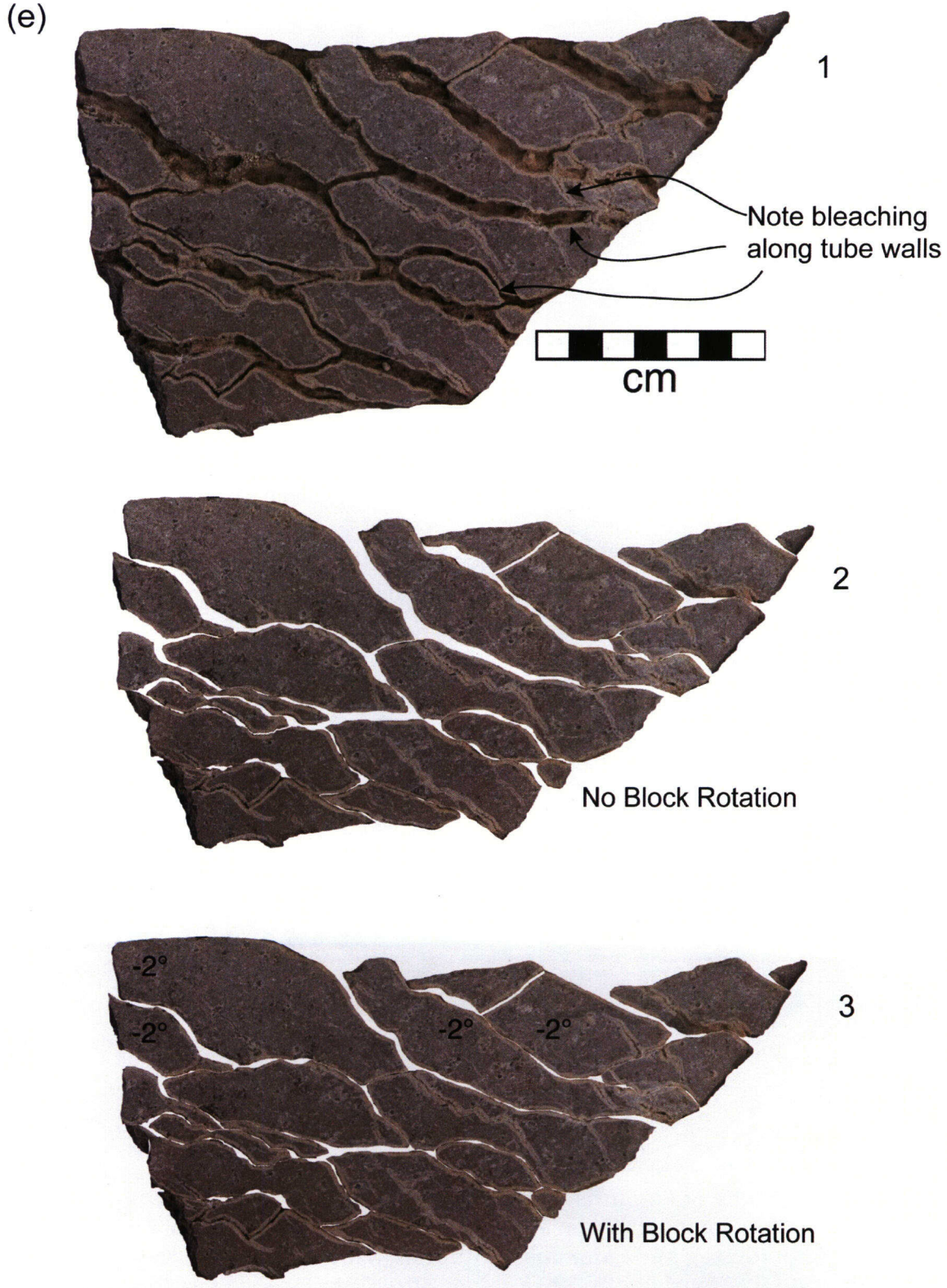

Figure 4-5 (continued). (e) Retrodeformation of Tubes by Matching Sides to Show Volume Increase During Tube Formation

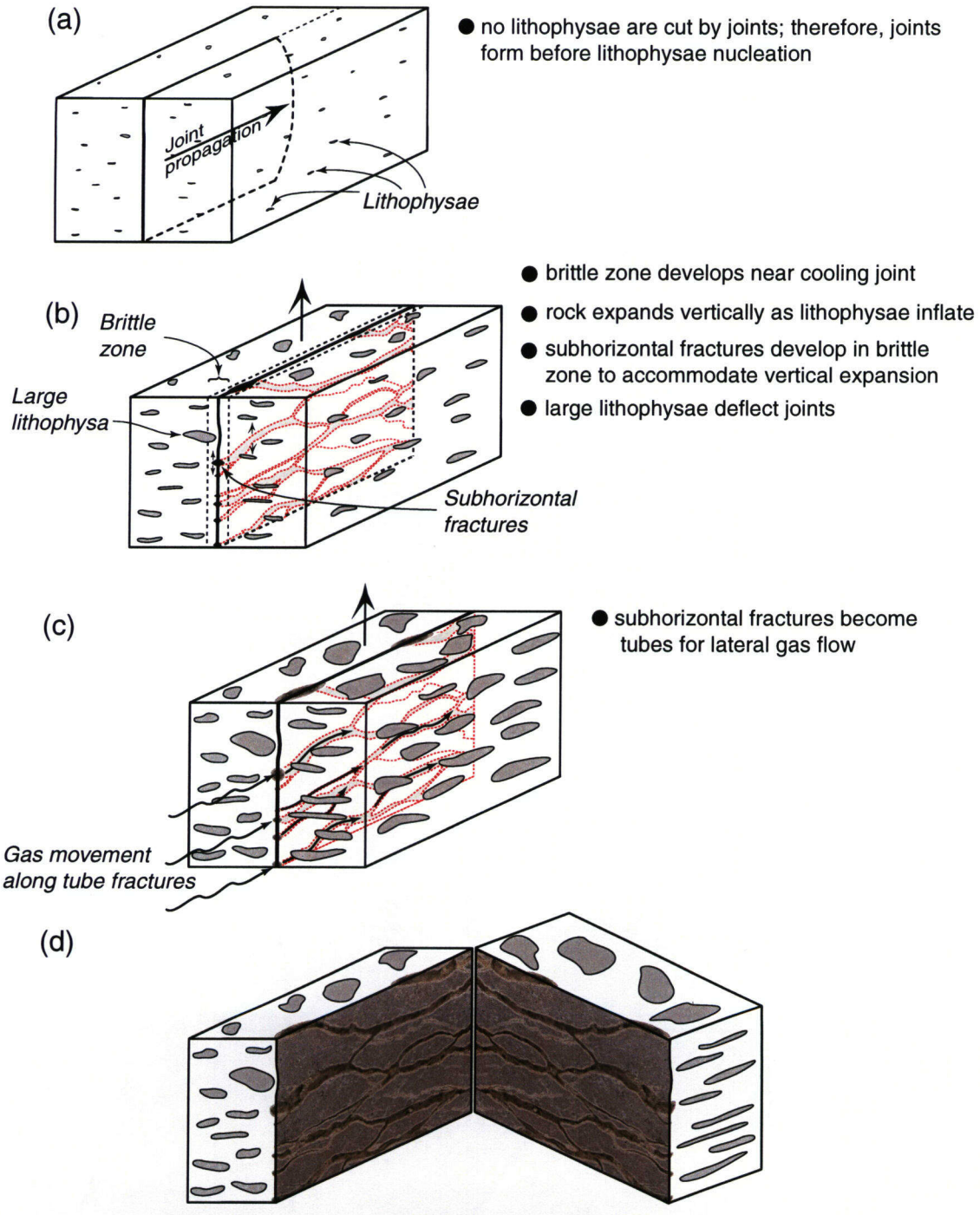

Figure 4-6. Sequence of Formation of Cooling Joints with Tubes. (a) Contractional Joint Surface Propagates through Rock Prior to the Formation of Lithophysae. (b) Cooling Joint Causes Formation of Adjacent Brittle Zone, as the Rocks Expand Vertically with Formation of Lithophtsae Subhorizontal, Tube-Like Fractures Develop within the Brittle Zone. (c) Continued Degassing of the Rock Utilizes These Tubes for Gas Flow. (d) An Expanded View of a Cooling Joint to Show That the Two Sides Are Mirror Images of Each Other.

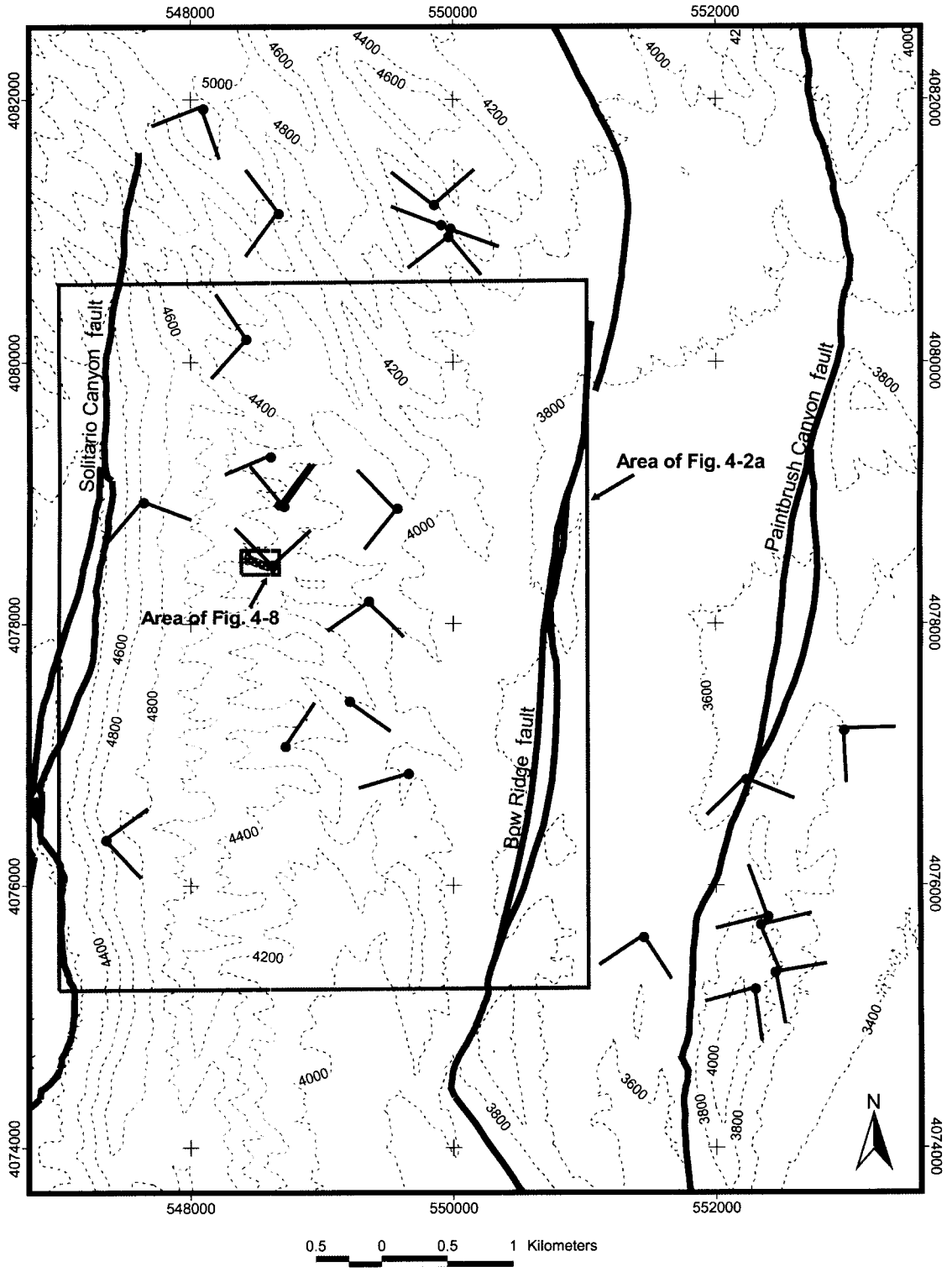

Figure 4-7. Map of Yucca Mountain to Fran Ridge (Modified from Day, et al., 1998b) Region Showing Strikes of Orthogonal Tube-Bearing Joints (Modified from Throckmorton and Verbeek, 1995), and the Locations of Figures 4-2a and 4-8. Dots on Joint Trend Tips are Station Locations.

Abundant vapor-phase silicates line the tube interiors and devitrification selvages commonly extend for half a tube diameter into the tuff matrix. In contrast, joint planes show only minor vapor-phase mineralization and very limited amounts of devitrification into the joint walls. These relationships are interpreted to indicate that the tubes formed as a brittle or semi-brittle response to vertical inflation of the tuff as a result of degassing. Tubes nucleated along the earlier formed fracture surfaces because these were localized zones of brittle behavior (Figure 4-6). Once formed, the tubes received the initial flush of hot gas, from which there was rapid vapor-phase precipitation. Further cooling permitted escape of the less saturated gas vertically along the fracture.

4.4.4.3 Fumarolic Association for Tube-Bearing Joints

Many ignimbrite deposits have early-formed joints (e.g., Sheridan, 1970; Hildreth, 1983; Keith, 1991), and near-orthogonal joints in ignimbrites have previously been recognized (Keith, 1991). Early-formed joints in the Valley of Ten Thousand Smokes and Bishop Tuff (Hildreth, 1983; Keith, 1991; Sheridan, 1970) are associated with fumarolic degassing and have obvious gas-escape features such as mineralized ridges at the top of the deposit and vapor-phase alteration of joint walls, which is present for the tube-bearing joints. These fumarolic joints have not been reported with tubes, but that may reflect that the joints have not been investigated in units with lithophysae (e.g., Sheridan, 1970; Hildreth, 1983; Keith, 1991). Fumarolic joints in these analog ignimbrite deposits form ridges that are underlain by single long joints or narrow swarms of joints (Figure 3a in Sheridan, 1970), which is consistent with the geometry of the tube-bearing joints at Yucca Mountain. These joints provide the vertical pathway for gas escape during tuff compaction and welding. Ridge lengths may be as little as tens of meters or may exceed 1 km, and the underlying joint swarms that feed the ridge have the same lateral persistence, which is again consistent with the tube-bearing joints at Yucca Mountain. Joints formed during the construction of fumarolic ridges are driven both by thermoelastic contraction as would be expected for simple cooling joints (Engelder and Fischer, 1996) and by elevated fluid pressure (Secor, 1968) due to degassing. Given that tube-bearing joints at Yucca Mountain are geometrically similar to fumarolic joints, are the oldest joints, and formed in a lithophysae-free matrix, the authors interpret them to have been very early gas escape pathways that may have served as the plumbing system for fumaroles at the surface.

4.4.4.4 Structural Geometry of Tube-Bearing Joints

A sample area of 20,787 m^2 with about 15 percent exposure (3,162 m^2) was examined on Live Yucca Ridge at Yucca Mountain to characterize the contribution of the orthogonal joint system to the total fracture network (Figures 4-7, 4-8). Both fracture traces and limits of exposed rocks were mapped so as to consider the influence of the distribution and quantity of rock exposure on trace data distribution. The sample area is about two orders of magnitude larger than that used for the cleared pavements, such as P100 (214 m^2; Figure 4-4a), which is within the new sample area (Figure 4-8).

A real-time kinematic differential Global Positioning System (Novatel®) with resolution of ±2 cm horizontal and ±10 cm vertical (2 sigma error) was used to map the topography of Live Yucca Ridge and to create a fracture trace map. Fracture positions were mapped using the Global Positioning System data collector's feature tagging option, where the position is tagged with a user-defined alphanumeric identifier. Fractures were tagged at their visible ends and at several

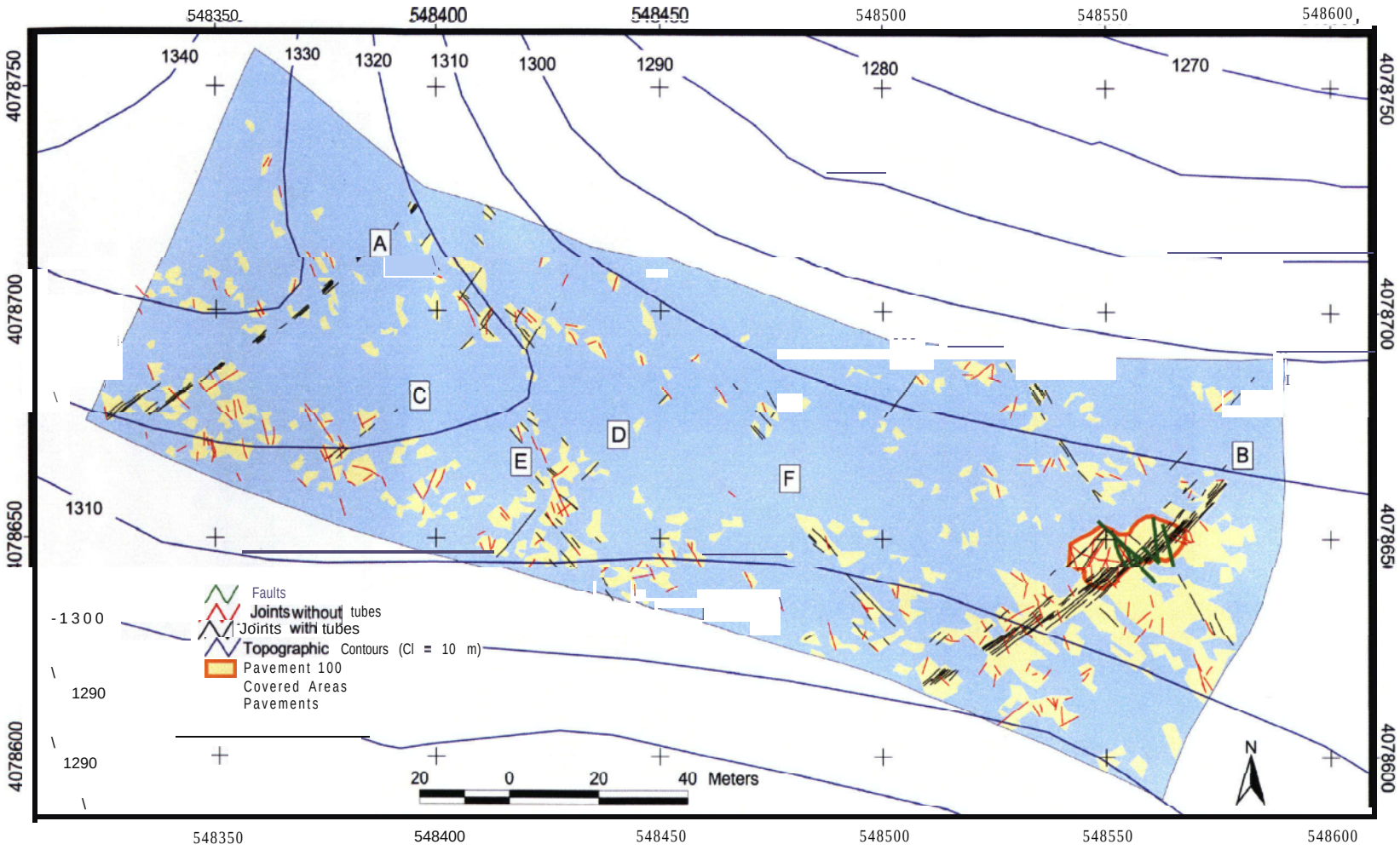

Figure 4-8. Fracture Trace Map at Live Yucca Ridge, Yucca Mountain, Showing Both Fracture Traces and Rock Exposure. Topographic Contour Interval Is 10 m, and Location Grid Is the Universal Transverse Mercator Zone 11 North American Datum of 1927 System. Letters in Rectangles Are Particular Locations Referred To in the Text.

intermediate points if they exceeded a few meters in size. Fractures were sequentially numbered and designated as either tube-bearing or lacking tubes. In addition, fracture orientations were input into the data collector. The tagged data points were then connected in a Geographic Information System to create a fracture-trace map. These data were downloaded to ArcView™ software to construct a map with a Geographic Information System database. Other field observations were measured and recorded using compasses, field notebooks, and cameras.

To facilitate useful, but efficient data collection over such a large sample area, the minimum recorded fracture trace length (cutoff length) was 2 m, and the minimum exposed area mapped was approximately equal to a circle with a diameter of 2 m. The truncation limit is an order of magnitude larger than the 0.2-m limit used to survey fracture traces on pavements such as P100 (Barton, et al., 1993). The reasons for using the larger truncation limit in this study were that both previous work and reconnaissance mapping performed during this study indicated that tube-bearing joints dominantly have tracelengths greater than 2 m, previous pavement work (Barton, et al., 1993) provided sample sets for the geometry of smaller fractures, and previous investigations at Yucca Mountain documented the tremendous increase in time necessary to document patterns for tracelengths of less than 1 m accurately (Sweetkind and Williams-Stroud, 1996).

The south side of Live Yucca Ridge is better exposed than the north, which is typical of the slopes of the east-west-trending ridges at Yucca Mountain. While P100 and the related swarm of northeast-trending, tube-bearing joints are in a relatively well-exposed portion of the ridge, visual inspection of the mapped locations of tube-bearing joints shows that their abundance does not correlate to areas of best exposure (Figure 4-8).

The true maximum length of tube-bearing joints is difficult to ascertain because their trace lengths are so long that they exceed the dimensions of even the largest exposures, and hence are censored (Epstein, 1954; Priest, 1993; Mauldon, et al., 2001). In a few cases, fracture traces were dug out between exposures to partially overcome the effects of censoring and determine maximum trace length. These traces are visible as black lines that are mostly not contained in regions of exposure in Figure 4-8. Even with these efforts, true fracture tips were seldom found for tube-bearing joints, and the authors are restricted to saying that many tube-bearing joints have trace lengths exceeding 10 to 15 m. The two sets of tube-bearing joints have different distribution patterns. Northeast-trending joints are generally either grouped in narrow swarms [e.g., swarms (a) and (b) in Figure 4-8] or occur as a few joints in near alignment [(c) and (d) in Figure 4-8]. In contrast, northwest-trending tube-bearing joints occur in wider swarms and have traces that are more typically *en echelon* rather than co-linear [swarms (e) and (f) in Figure 4-8e,f]. Also, northwest-trending joints are less numerous (67 versus 126) than northeast-trending joints (Figures 4-8, 4-9b).

The two sets of swarms form an approximately rectilinear network of fracture traces (Figure 4-8) as described by Barton, et al. (1993). The orthogonal distance between the two well-developed northeast-trending joint swarms is about 150 m (Barton, et al., 1993); however, this value is probably an overestimate of the swarm spacing, because between the two well developed northeast-trending swarms are two poorly developed swarms, particularly around area C (Figure 4-8), yielding a minimum swarm spacing of about 50 m for the northeast-trending set. The northwest-trending swarms also have spacings of about 50 m.

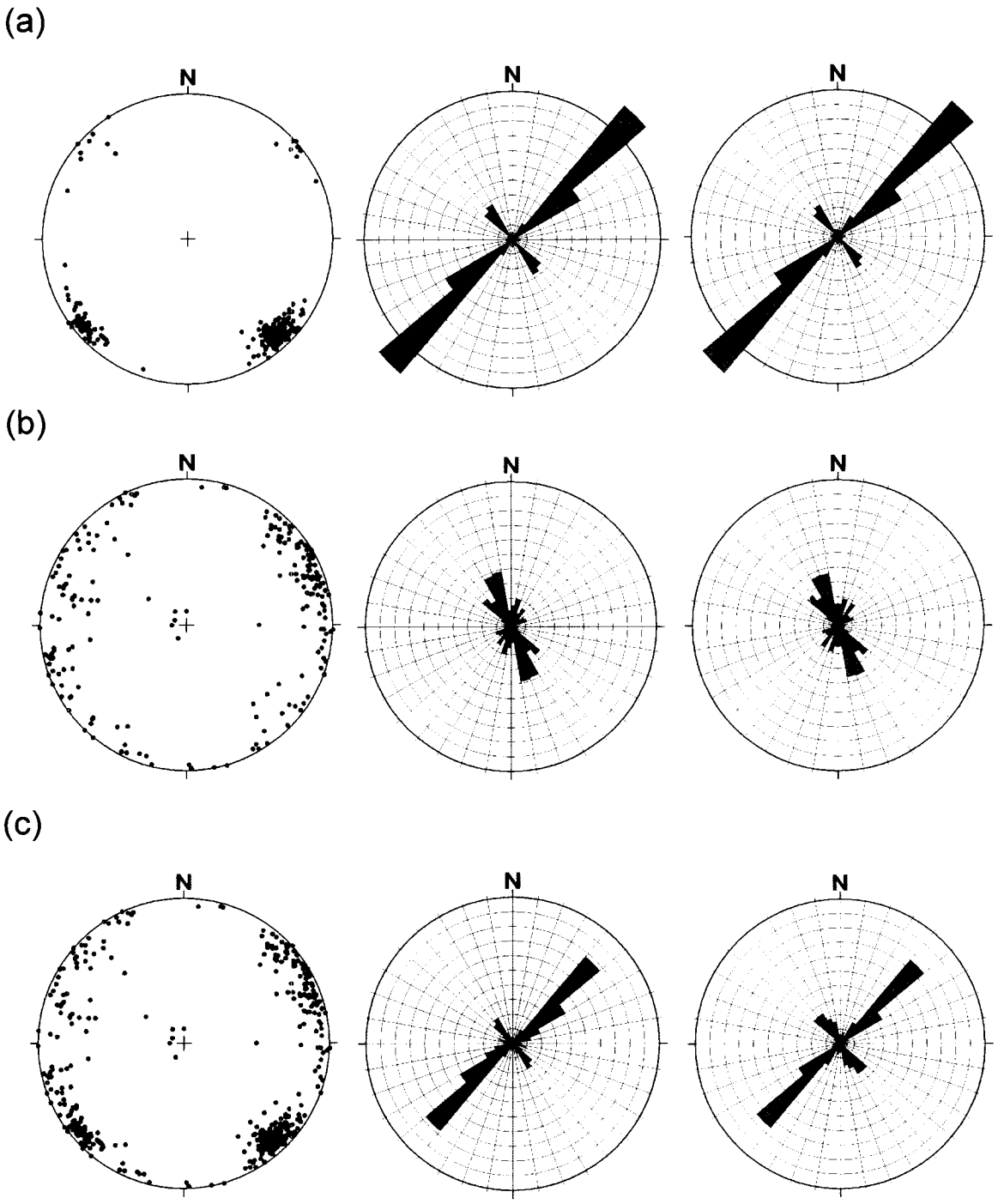

Figure 4-9. Orientation Data for Joints on Live Yucca Ridge. Left Column: Lower Hemisphere, Equal Area Plot of Poles to Joints. Middle Column: Unweighted Rose Diagram of Joint Traces. Plot Radius = 20 Percent. Right Column: Length-Weighted Rose Diagram of Joint Traces. Plot Radius = 20 Percent. (a) Tube-Bearing Joints; Number of Joints = 272; Cumulative Trace Length = 1,069 m. (b) Joints without Tubes; Number of Joints = 214; Cumulative Trace Length = 737 m. (c) All Joints; Number of Joints = 486; Cumulative Trace Length = 1,806 m.

Tube-bearing joints have a greater cumulative trace length with a narrower orientation spectrum than joints without tubes (Figures 4-8, 4-9). Even given the presence of censoring, field observations demonstrate that traces of tube-bearing joints, particularly northeast-trending ones, are longer than the traces of joints without tubes and that tube-bearing joints are more numerous. Thus, the swarms of tube-bearing joints provide a rectilinear framework to the fracture network, while joints without tubes enhance fracture network connectivity.

4.4.4.5 Possible Stress Sources for Control of Tube-Bearing Joint Orientations

Because the Tiva Canyon Tuff was deposited in a region undergoing east-west extension (Zoback, et al., 1981; Sawyer, et al., 1994; Morris, et al., 1996), and assuming that the orthogonal joints are Mode I extension fractures, they might be expected to strike north and east. However, across much of the Yucca Mountain region, the two tube-bearing sets strike northeast and northwest (Figures 4-4, 4-7, 4-8, 4-9). Thus, at least one additional stress component other than the remote regional stresses must have been operating to perturb the stress field and the joint orientations from the regional stress state. Such stress perturbation might result from cooling-related effects such as differential compaction or lateral temperature gradients, caldera evacuation during eruption, or active normal faulting due to regional stresses or related to the caldera evacuation and ignimbrite deposition.

Given that thicker tuff deposits remain hotter for longer periods and compact more than thin deposits because of their higher total heat capacity (e.g., Riehle, et al., 1995), distinguishing between joint formation due to stress perturbations by differential compaction or lateral temperature gradients (e.g., Lachenbruch, 1962) would be difficult. For an orthogonal system of fumarolic ridges in the Valley of Ten Thousand Smokes, Alaska (Keith, 1991), differential compaction was interpreted to cause one set of fumarolic ridges in the cooling tuff. As the ignimbrite deposit cooled, tuff in the valley center compacted more than the margins, creating tensional structures parallel to these margins. In the case of a basin, the depocenter compacts more (Sheridan, 1970). For the Tiva Canyon Tuff at Yucca Mountain, if the depocenter of a northwest-trending basin existed just north of the study area, the steepest compaction and temperature gradient would be along the short axis of the basin. Therefore, the greatest tension would be oriented northeast-southwest and would possibly generate northwest-trending joints.

The eruption of the ignimbrite that formed the Tiva Canyon Tuff involved a large caldera collapse that ejected about 1,000 km^3 of material from a site located within 50 km of the present study area (Byers, et al., 1976; Sawyer, et al., 1994). Such a collapse would have perturbed the regional stress field directly, and possibly could have triggered movement on nearby normal faults (e.g., Nostro, et al., 1998). Volcanic eruptions with less than 1 percent of this eruption volume have been interpreted to be causally linked to earthquakes on normal faults in regions with active extension (e.g., Abe, 1992; Nostro, et al., 1998, and references cited within). The timespan of this link is typically 1 to 10 years between the two events, but the time could be much shorter for a larger event.

The major normal faults at the Yucca Mountain region were active within the 100,000 years before and during the million years after the deposition of the Tiva Canyon Tuff in response to regional extension in the central Basin and Range province (Christiansen, et al., 1977; Sawyer, et al., 1994; Day, et al., 1998a; Fridrich, 1999). Thus, regional tectonic stresses with or

without perturbation from the aftermath of caldera formation could have reasonably triggered normal faulting during cooling of the tuff. If one or more of the normal faults in the area slipped, the regional stress field would be locally perturbed, which could explain an orthogonal joint geometry that did not match horizontal stress directions for the regional stress field alone (e.g., Crider and Pollard, 1998; Katterhorn, et al., 2000).

The occurrence of orthogonal joints above and within the proposed repository affects shallow groundwater infiltration and represents potential weaknesses that could strongly influence the stability of waste emplacement drifts. Existing data are not sufficient to model the distribution of orthogonal joints within and above the proposed repository. The role of differential compaction and thermal gradients cannot be tested, owing to the paucity of data about tuff thickness, possible basin geometry, and lateral temperature variations during cooling. Analytical models have been developed for modeling stress perturbation around small volume eruptive columns, but not for stress field perturbation effects of very large volume (approximately 1,000 km^3) eruptions. The available data for the orientation and distribution of tube-bearing joints, for normal fault geometry, and for possible regional stress conditions during the Miocene at Yucca Mountain, do allow workers to test whether interacting normal faults could locally perturb the regional stress field sufficiently to account for the formation of the fumarolic tube-bearing joint swarms.

4.4.5 Normal Faulting and Perturbation of Regional Stress Field

Dunne, et al. (2001) tested the proposition that active faulting during cooling of the Tiva Canyon Tuff could have locally perturbed the stress field to produce orthogonal joint systems with orientations different from those expected from the Miocene regional stress field. A three-dimensional, boundary-element method computer code (Thomas, 1993) was used by Dunne, et al. (2001) to calculate the stress and deformation fields around discontinuities in an elastic medium.

4.4.5.1 Model Configuration

Dunne, et al. (2001) modeled three major faults near the fracture-map study area: the Solitario Canyon fault, the Paintbrush Canyon fault, and the northern segment of the Bow Ridge fault (Figure 4-10). Because interest is in very-near-surface phenomena, only the upper (planar) portions of the faults were modeled. Each fault is modeled as a planar rectangular discontinuity, subdivided into as many as 324 rectangular elements. The modeled Solitario Canyon fault strikes north, dips 75° west, and has a trace length of 16 km. The modeled Paintbrush Canyon fault has parallel strike and dip and is slightly longer, at 19 km. The modeled northern segment of the Bow Ridge fault strikes 010° and dips 60° west. It has a trace length of 6 km. All three faults intersect the free surface of the model and extend 6 km down dip. The model fault geometries are simplified from the observed for numerical efficiency, so focus is on the generalized effects of stress perturbation by faulting, rather than local effects of bends and steps in the fault traces.

The faults are imbedded in a homogeneous elastic half-space, with standard crustal rheology (Poisson's ratio = 0.25, shear modulus = 30 GPa). Although cooling Tiva Canyon Tuff is expected to be significantly less stiff, it represents only a small volume of the crustal section. In addition, model trials with order-of-magnitude variations in shear modulus show significant

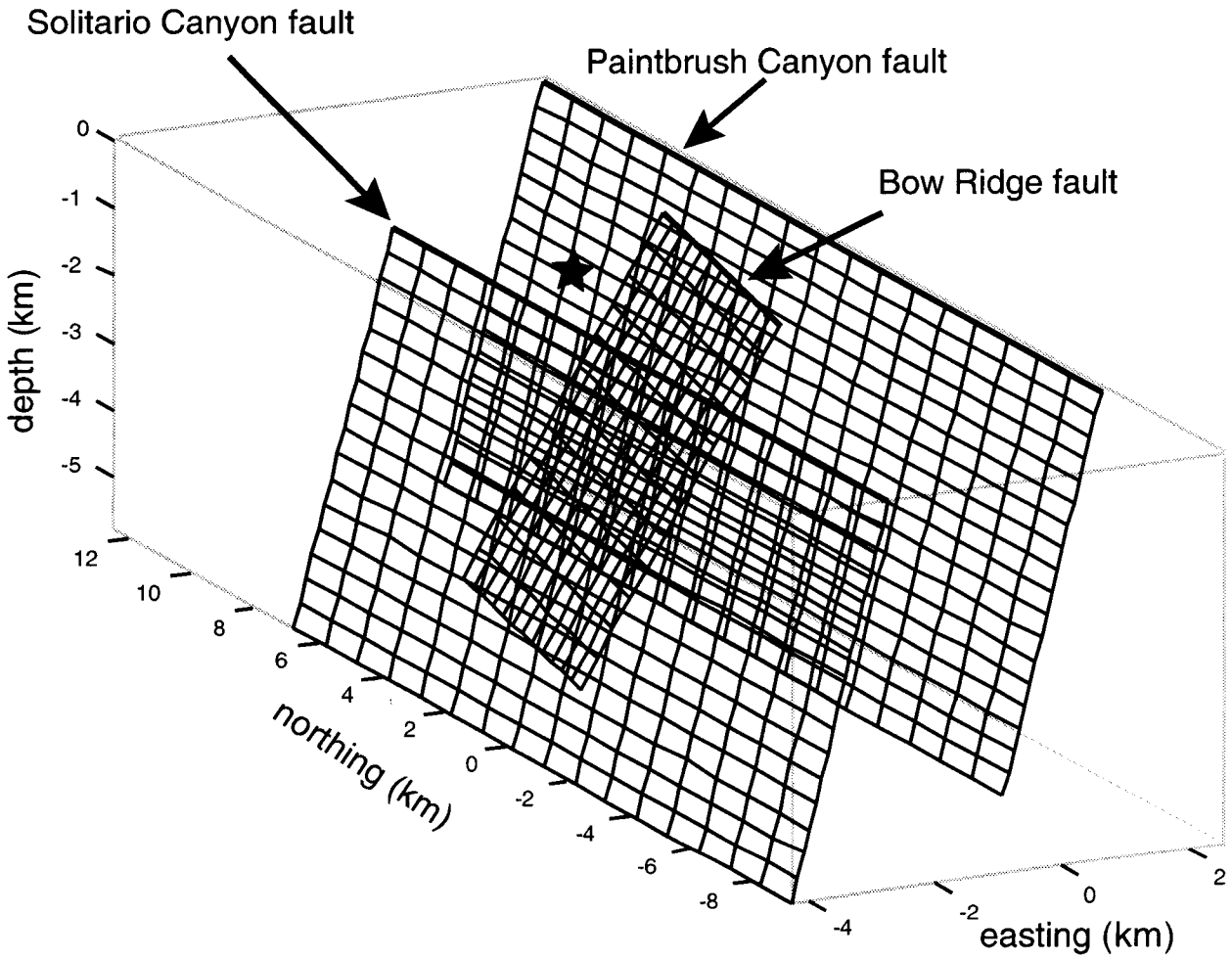

Figure 4-10. Three-Dimensional Perspective View of Modeled Faults, View to the Northeast. Star Is on the Surface and Marks the Location of Live Yucca Ridge. Origin of Coordinate System Corresponds to Universal Transverse Mercator 550000, 4075000 (Dunne, et al., 2001).

changes in fault slip, but no changes relative to each other in the orientation of the local stress directions. Frictional resistance to slip is not modeled, but the effect of linearly increasing lithostatic (confining) stress with depth is included.

Although direct measurements of the stress state in the Miocene are not available, deformation is assumed to have occurred in a normal-faulting stress regime, with maximum principal compressive stress (σ_1) vertical, intermediate principal compressive stress (σ_2) north-south, and minimum principal compressive stress (σ_3) east-west. This assumption is consistent with geologic estimates of Miocene stress state as interpreted by Zoback, et al. (1981). The authors test magnitudes for S_h (minimum horizontal compressive stress) and S_H (maximum horizontal compressive stress) in the range of modern measurements at Yucca Mountain. Stock, et al. (1985) give estimates for principal stresses, corrected for fluid pressure (Ferrill, et al., 1999b), at 1 km depth as: S_V = 21 MPa (approximately lithostatic), S_H = 17 MPa (or 4 MPa less than lithostatic), and S_h = 11 MPa (or 10 MPa less than lithostatic).

Results for two model trials are evaluated here. In the first, fault slip is modeled as driven by 10 MPa east-west tension only. This boundary condition mimics an S_h of 10 MPa less than lithostatic load in the east-west direction, such that $S_h < S_H = S_V$, and $S_H = S_V$ = the lithostatic stress. In the second trial, the north-south horizontal stress is reduced (by 8 MPa), such that S_h + 10 MPa = S_H + 8 MPa = S_V. In this case, fault slip is modeled as driven by an east-west tension of 10 MPa and a north-south tension of 8 MPa. This boundary condition mimics an S_h of 10 MPa less than lithostatic load in the east-west direction and an S_h of 8 MPa less than lithostatic load in the north-south direction.

4.4.5.2 Model Results and Interpretation

With these boundary conditions, the three modeled faults slip simultaneously, with maximum dip-slip at the free surface and approximately at the center of the fault trace. Slip distribution along each fault is approximately elliptical, modified by interaction among the three faults. The modeled segment of the Bow Ridge fault also shows a small component of left-lateral slip. The mean dip-slip on each fault is slightly more than 1 m. The modeled situation corresponds to a cluster of moderate-sized [moment magnitude (Mw) ~6] earthquakes, such as is common in western North America. Representative of this model would be (i) the 1993 Klammath Falls, Oregon, earthquakes (Braunmiller, et al., 1995); (ii) the Ridgecrest, California, sequence (Hauksson, et al., 1995); or (iii) the much larger Dixie Valley-Fairview Peak, Nevada, sequence (Doser, 1986).

Vertical tensile fractures are expected to form perpendicular to the least horizontal stress (S_h). Figure 4-11a shows modeled orientations of S_h and expected fracture orientations for trial 1 (east-west only driving stress). A dominant north-south fracture pattern, perpendicular to the regional S_h, is seen away from faults and outside the region of fault overlap. In the region of overlap, local perturbation of the stress orientations, and consequent rotation of predicted fracture orientations, is observed. The joint orientation normal to the predicted direction for the minimum horizontal stress compares favorably with the pattern of one of the sets of joint orientations recorded by Throckmorton and Verbeek (1995) (Figure 4-7). A northeast-trending set is predicted in the central block where the major clusters of tube-bearing joints occur (Figures 4-7, 4-8, 4-11b), and a north-south-trending set is predicted and found in the footwall of the Paintbrush Canyon fault. The strike of the modeled fracture orientations is not as

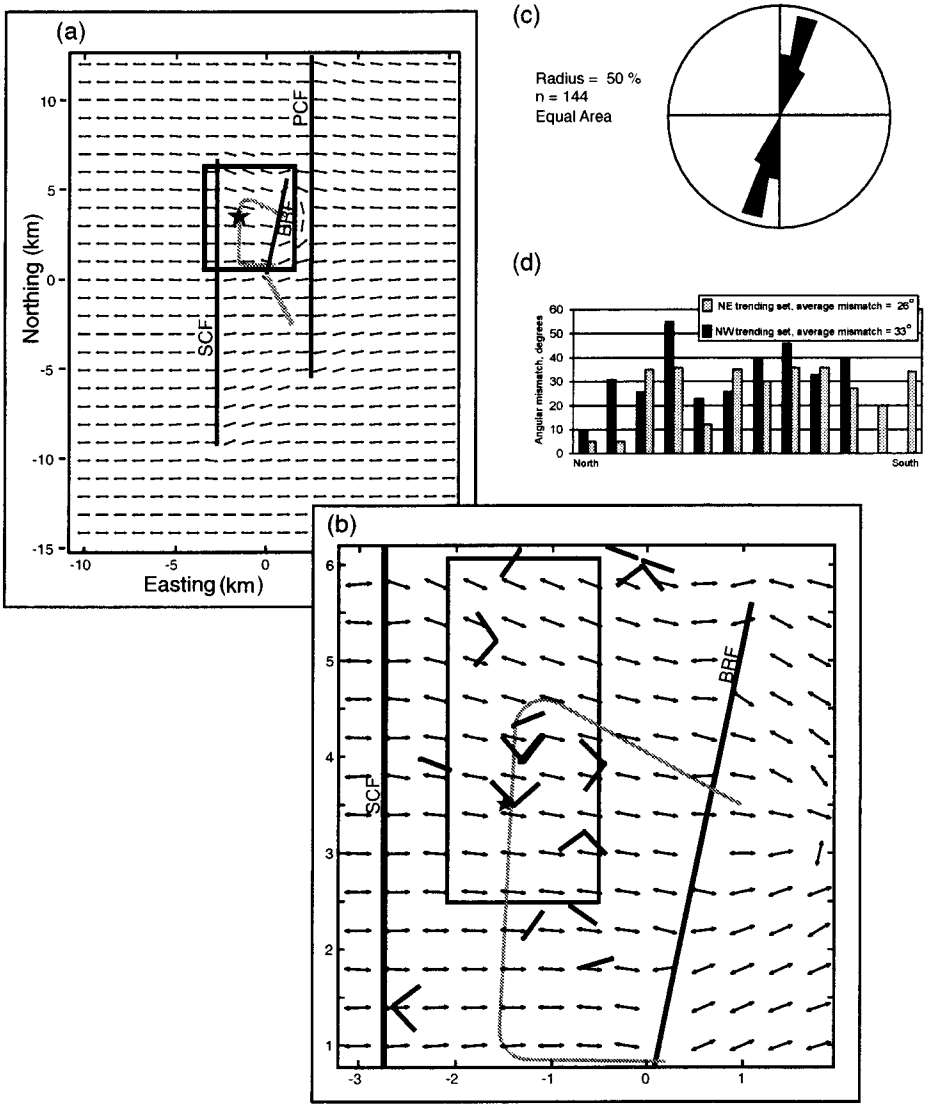

Figure 4-11. Modeled Stress Trajectories for the Case of East-West Tension = 10 MPa. Results for 100-m Depth. First-Formed Joints Would Form Perpendicular to Arrows. (a) Regional View. Arrows Show Direction of Minimum Horizontal Compressive Stress, S_h. Perturbation Is Observed in the Overlap Zone between the Faults. SCF = Solitario Canyon Fault. BRF = Bow Ridge Fault. PCF = Paintbrush Canyon Fault. Heavy Grey Line Shows Southern Segment of BRF, Not Modeled. Light Grey Line is Approximate Location of the Exploratory Studies Facility. Star Locates Live Yucca Ridge. Coordinate System as in Figure 4-10. Box Outlines Area of B. (b) Details of the Stress Perturbation in the Region around Live Yucca Ridge. Heavy Lines Are Observed Joint Populations (Throckmorton and Verbeek, 1995). Deflection of S_h in between Solitario Canyon Fault and Bow Ridge Fault Is Greatest North of the Exploratory Studies Facility. Box Indicates Data Plotted in C. (c) Rose Diagrams of Expected First-Formed Joint Orientations in the Vicinity of Live Yucca Ridge. Range Is from 000° to 030°. Plot Radius = 50 percent. (d) Angular Mismatch between Modeled Stress Trajectories and Joint Populations on and near Live Yucca Ridge (Dunne, et al., 2001).

easterly as the observed joints in the central block with a spread of orientations between 000° and 030° (Figure 4-11c).

In trial 2, north-south reduction in the lithostatic load and the match between modeled fractures and observed orientations of northeast-trending joints are improved (Figure 4-12). The stress perturbation in the footwalls of both the modeled Solitario Canyon and Paintbrush Canyon faults is greater than in trial 1. The modeled fracture orientations in the vicinity of the study area on Live Yucca Ridge are a close match to the present-day joint trends with a range of 026° to 066° and a mode between 045° and 050°.

Model results show that slip on faults can generate local stress perturbations that are consistent with orientations of northeast-trending joints observed at Yucca Mountain. Thus, active faulting synchronous with the eruption of the Tiva Canyon Tuff is a plausible mechanism for the control of the orientation and distribution of northeast-trending tube-bearing joints within the tuff.

4.4.6 Formation of Northwest-Trending Joint Swarms

Assuming that the northeast-trending set of tube-bearing joints in the Tiva Canyon Tuff was formed during volcanic degassing and active normal faulting, what was the mechanism that formed the second orthogonal set with the necessary 90° rotation of the horizontal stress directions? The likely possibilities are a regional-scale rotation of stress directions, changes in displacement behavior of the normal faults, and more local-scale rotation due to formation of the first-formed northeast-trending joints. Any of these mechanisms could have been aided by differential compaction in the postulated northwest-trending basin.

Considering regional-scale rotation, the central Basin and Range in which Yucca Mountain lies experienced east-west extension prior to 10 million years ago (Zoback, et al., 1981). Previous work (Zoback, et al., 1981; Wernicke, 1992; Axen, et al., 1993) does not indicate that a change occurred in regional principal strain directions and, hence, regional principal stress directions during this east-west extension. Consequently, the possibility of a regional-scale rotation of tectonic stresses is discounted.

Considering displacement behavior on the normal faults, horizontal stress directions might switch if fault-slip directions changed significantly or if different faults or parts of faults slipped sequentially. Although it is conceivable that changes in fault-slip direction during a slip event or sequential slip on different faults or parts of faults could produce both the northwest- and northeast-trending tube-bearing joints, diagnostic evidence for these scenarios is lacking for the joint system under investigation. This possibility cannot be discounted.

The possibility of a locally controlled rotation due to an additional perturbation of the stress field by the formation of the northeast-trending joints remains. A geometric support for this possibility is the fact that the northeast-trending joint swarms are better developed than the northwest-trending swarms in terms of joint size and abundance within swarms. The better development of the older set is a typical feature of orthogonal joint systems formed by local stress release (Hancock, 1985; Caputo, 1995; Bai, et al., 2001).

The case for local control of the rotation of the stress directions is analogous to the formation of stratal-bound layer-normal joints forming in response to remote tension (Hobbs, 1967;

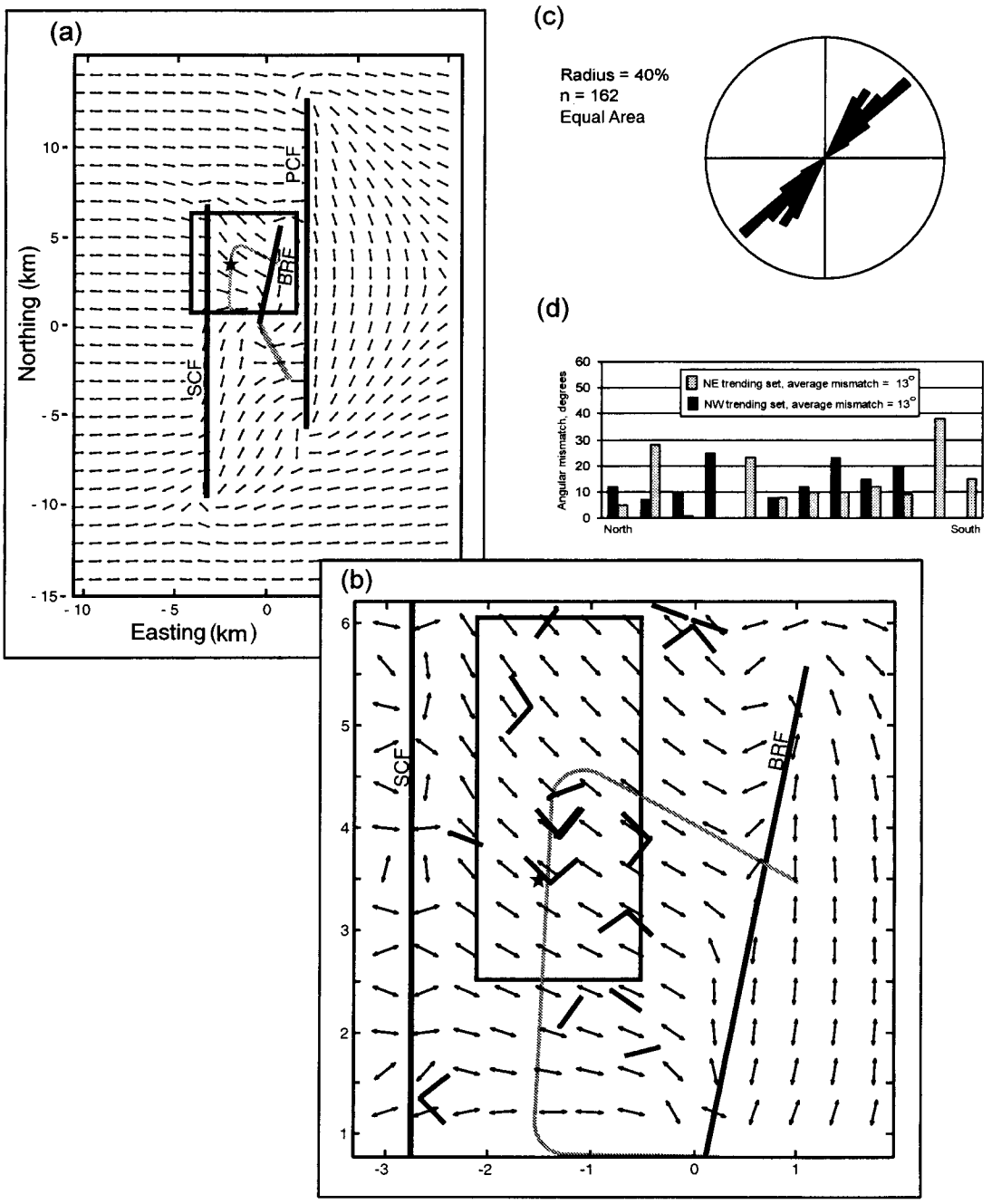

Figure 4-12. Modeled Stress Trajectories for the Case of East-West Tension = 10 MPa and North-South Tension = 8 MPa. Model Results for 100 m Depth. First-Formed Joints Would Form Perpendicular to Arrows. All Symbols as in Figure 4-11. (a) Regional View. Greater Deflection Is Observed in the Footwall of Both the Solitario Canyon Fault and Paintbrush Canyon Fault. (b) Details of the Stress Perturbation in the Region around Live Yucca Ridge. (c) Rose Diagrams of Expected First-Formed Joint Orientations in the Vicinity of Live Yucca Ridge. Range Is from 026° to 066° with a Mode Between 045° and 050°. (d) Angular Mismatch between Modeled Stress Trajectories and Joint Populations on and near Live Yucca Ridge (Dunne, et al., 2001).

Gross, et al., 1995). In this case, joint formation perturbs the stress field by causing a stress drop or shadow. Recent work by Bai, et al. (2001) shows that when joint spacing of the older joint set is <1.7 times the thickness of the layer containing the joints, and when S_h/S_H is >0.2, the horizontal stress directions in the rock mass between the first-formed joints swap. Given an interpreted penetration depth for the northeast-trending joints of 20 to 30 m, which is the thickness of the upper lithophysal unit, and a swarm spacing of about 50 m, the spacing to thickness ratio in the Tiva Canyon Tuff is 2.5 to 1.6, and is about the critical threshold of 1.7 for stress swapping when the ratio of horizontal stresses is >0.2, which seems likely in this case. Thus, a second perturbation of the stress field in the vicinity of Live Yucca Ridge by the formation of swarms of northeast-trending tube-bearing joints is a possible mechanism for rotating the horizontal stress directions to allow the formation of northwest-trending joints.

Care should be taken in applying this analogy to orthogonal swarm formation at Yucca Mountain. The Bai, et al. (2001) analysis was performed on natural fracture networks of individual joints with spacings on the order of centimeters to meters, whereas the Yucca Mountain case considers swarms of joints on the scale of tens of meters. The analogous case relies on uplift and erosion to achieve near-surface conditions for formation of the cross joints, whereas at Yucca Mountain the process occurs quite close to the ground surface after minimal burial. Also, while joint formation at Yucca Mountain was partially driven externally by thermoelastic contraction due to cooling, the joint formation was also internally driven by fluid pressure generated by volcanic gases, which differs from the analogy. Still, the analogy does offer an explanation. Future numerical modeling will explore the possibility of extrapolating this explanation to the larger-scale case of joint swarms partially driven by internal fluid pressure. Such an analysis would be applicable to sedimentary rocks with elevated fluid pressures in either the case of joints formed contemporaneously with fault displacements or in the absence of such displacement. In fact, the fluid-driven case may offer an explanation for some cases of joint swarm development, which is a widely recognized phenomenon (e.g., Hancock, 1985; Pollard and Aydin, 1988; Odling, et al., 1999).

4.4.7 Discussion

4.4.7.1 Cooling Joints Without Tubes

Cooling joints are ubiquitous features in moderately to densely welded ignimbrite deposits (e.g., Smith, 1960; Ross and Smith, 1961; Cas and Wright, 1987). They form in response to tensional stress induced by thermal contraction during cooling (Lachenbruch, 1962; DeGraff and Aydin, 1987; Engelder and Fischer, 1996) and are not associated with other deformation features such as tubes or lithophysae (Enlows, 1955; Ross and Smith, 1961; Sheridan, 1970; Cas and Wright, 1987). Cooling joints are pseudo-columnar, smooth or curviplanar; lack bleached walls; occur in a variety of orientations; and vary in length between 1 to 15 m. They also occur in tuffs with fumarolic joints and terminate against those early-formed joints (e.g., Sheridan, 1970).

By analogy with other welded ignimbrite deposits, abundant cooling joints should be expected in the rock volumes between early-formed fumarolic joints at Yucca Mountain (e.g., Sheridan, 1970). The characteristics of ignimbrite cooling joints appear identical to the criteria used by previous workers to identify tectonic joints at Yucca Mountain (Morgan, 1984; Barton, et al., 1993, 1984; Barton and Larsen, 1985; Carr, 1992; Sweetkind, et al., 1995a,b; Throckmorton

and Verbeek, 1995; Albin, et al., 1997; Eatman, et al., 1997; Mongano, et al., 1999). Given the morphological similarities and the reasonable expectation that the tube-bearing joints are not the only cooling joints in the tuff, it is believed that many joints previously interpreted as tectonic joints at Yucca Mountain are likely cooling joints. Distinguishing between the origins of these morphologically similar joints may require detailed studies of the different deuteric facies within the Tiva Canyon Tuff (cf. Buesch, et al., 1996), because cooling joints should exhibit a correlation with degree of degassing, welding, and devitrification processes.

4.4.7.2 Implications for Other Tuffs With Tube-Bearing Joints at Yucca Mountain

The focus of this report is on jointing in the upper lithophysal zone of the crystal-poor member of the Tiva Canyon Tuff. The observations, interpretations, and conclusions, however, have direct relevance to fracturing in other parts of the Tiva Canyon and Topopah Springs Tuffs. The best data set available for evaluating the distribution and characteristics of fractures within Yucca Mountain are the scan line and full-periphery mapping data from the Exploratory Studies Facility and Enhanced Characterization of the Repository Block tunnels (Mongano, et al., 1999; CRWMS M&O, 2000b).

Although tubular structures may not have been described for locations other than Yucca Mountain, they are relatively common in lithophysal units of both the Tiva Canyon and Topopah Springs Tuffs of the Paintbrush Group sampled in the underground Exploratory Studies Facility and Enhanced Characterization of the Repository Block tunnels at Yucca Mountain. The interpretation of very early origin (within days or weeks after pyroclastic deposition) for joints with tubular structures also applies to other cooling units of the Paintbrush Group, suggesting that many of the joints in these units previously interpreted to have tectonic origins may, in fact, have cooling origins.

During fracture data collection from the Exploratory Studies Facility and Enhanced Characterization of the Repository Block, cooling joints were identified based on the presence of tubular structures, and, in the absence of tubular structures, on the basis of length greater than 5 m, smooth surfaces, presence of vapor-phase mineralization, vapor-phase margin, and undulatory surfaces. Tubular structures are generally associated with cooling joints in lithophysal units. Small-diameter tubes or no tubes on large, smooth planar or undulatory joints, and evidence of vapor-phase mineralization or alteration are typical of less lithophysal or lithophysae-barren cooling units. Orientation data from cooling joints classified according to these criteria reveal that cooling joints through both the Tiva Canyon and Topopah Springs welded tuffs dominantly have northwest strikes. A secondary northeast-trending population is also present in the data.

The approximately 1-km long intensely fractured zone along the north-south main drift of the Exploratory Studies Facility is overwhelmingly dominated by northwest-trending joints. The dominant cooling joint orientation at the northern end of the intensely fractured zone is northwest, and cooling joint orientations gradually transition to west northwest-east southeast to the south. Mongano, et al. (1999) illustrated that the intensely fractured zone corresponds to a large displacement gradient along the Ghost Dance fault. This correspondence between cooling joints and displacement gradient on the Ghost Dance fault implies that the Ghost Dance fault slipped during cooling of the Topopah Springs Tuff.

4.4.7.3 Potential Significance of Orthogonal Joint Swarms for Assessment of Yucca Mountain Flow, Transport, and Rock Stability

The data and interpretations presented in this section (Section 4.4) provide new input for infiltration modeling and allow new models of fracturing at Yucca Mountain. These new inputs and models have very broad relevance in the Yucca Mountain repository program. The results of fracture mapping presented in Section 4.4.4.4 provide key input for development of valid area-average infiltration fracture porosity for the upper lithophysal zone of the crystal poor member of the Tiva Canyon Tuff. In Section 4.13, these mapping results are analyzed with published fracture data to determine fracture apertures and fracture porosities at the bedrock/cover interface. The results of this analysis show that fracture apertures and fracture porosities at the bedrock/cover interface are considerably larger than values previously used by Flint, et al. (1996a) in infiltration analysis.

In all DOE site description documents (e.g., CRWMS M&O, 2000a), fracture characterization was focused on the volume of tuff between the Bow Ridge and Solitario Canyon faults. Site characterization included documentation of tens of thousands of fractures encountered by the Exploratory Studies Facility and Enhanced Characterization of the Repository Block. These data provide the best available data set for analyses of fracture-dependent processes such as rock fall, groundwater percolation, and seepage at the repository level. These data, however, are limited to the sampled tunnel paths. Although from near or along the margin of the proposed waste emplacement volume, these data are not from within the actual rock volume planned for waste emplacement. For example, planned emplacement drifts were reoriented by DOE to presumably increase drift stability, based on dominant rock mass joint orientation and rock block size and frequency considerations. These analyses have taken fracture data from subsurface excavations at face value (CRWMS M&O, 2000b), implicitly assuming that fracture network characteristics from the Exploratory Studies Facility and Enhanced Characterization of the Repository Block are representative of fractures throughout the proposed repository volume within each lithostratigraphic unit (Ferrill, et al., 2000a). The DOE has not yet provided a technical basis for this extrapolation of fracture data from the Exploratory Studies Facility and Enhanced Characterization of the Repository Block throughout the emplacement area.

In the absence of direct characterization of fractures in each emplacement area, data from underground excavations and boreholes, and surface mapping at the ground surface must be extrapolated or interpolated through the proposed emplacement volume(s) and surrounding rock for use in process modeling. The fracture network in the tuffs of Yucca Mountain includes fractures of very early origin, during degassing and cooling of the ignimbrites, tectonic joints and faults, unloading joints, and perhaps excavation-induced fractures. Unloading joints associated with weathering at the ground surface are absent at repository depths. Therefore, the only natural fractures of concern for repository performance are of volcanogenic and tectonic origins. Understanding the origin of fractures is the key to interpreting fracture distribution and characteristics throughout the proposed waste emplacement areas. As an example, consider the intensely fractured zone along the main drift of the Exploratory Studies Facility. Presently, data from the Exploratory Studies Facility and Enhanced Characterization of the Repository Block are assumed to be representative of the primary repository emplacement block. DOE contractors, however, have shown that the intensely fractured zone corresponds to a large displacement gradient on the Ghost Dance fault. If this large displacement gradient is the cause of the intensely fractured zone as implied by Mongano, et al. (1999), then the

Exploratory Studies Facility data may not be representative of fractures throughout the primary emplacement area. The DOE has not provided an interpretation of the areal distribution of the intensely fractured zone.

The DOE is now considering a range of designs and operational modes for the proposed high-level waste repository at Yucca Mountain (CRWMS M&O, 2001). These alternative plans include designs with expanded emplacement areas beyond the single primary emplacement area (between Solitario Canyon and Ghost Dance faults) generally assumed in site characterization and modeling to date. Given the potential local structural control on fracturing within fault blocks, fault and fracture orientation and intensity data collected from the Exploratory Studies Facility and Enhanced Characterization of the Repository Block are unlikely to be representative of other potential emplacement areas under consideration.

In summary, fracture intensity and orientation are important inputs to repository design, especially with respect to rockfall. Improved knowledge of these variables from the Exploratory Studies Facility and Enhanced Characterization of the Repository Block has already resulted in a design modification of the repository. Although the Exploratory Studies Facility and Enhanced Characterization of the Repository Block sampling provides the best available fracture dataset for the proposed waste emplacement interval, the actual rock volume(s) in which the proposed repository would be placed is essentially unsampled and therefore uncharacterized. The analysis presented here is an attempt to assess potential geologic controls on the pattern and areal distribution of early jointing in the welded tuffs of Yucca Mountain. The analysis focuses on processes that were likely to be active during cooling and degassing of the ignimbrites. In Section 4.6, tectonic controls are considered on fracturing within fault blocks that may have started during cooling of the ignimbrites and that may have continued, under different conditions, to the present. Fracture data from tunnels and boreholes at Yucca Mountain cannot simply be assumed to be representative of fracturing throughout the proposed emplacement areas. In the absence of direct characterization of the potential emplacement areas, consideration of volcanogenic and tectonic controls on fracturing is critical for interpolating and extrapolating of fracture data from limited sampling through the proposed emplacement areas. To date, the DOE has not presented a defensible rationale for extrapolating fracture into the proposed emplacement volumes.

4.4.8 Conclusions

1. The oldest joints in the Tiva Canyon Tuff at Yucca Mountain are tube-bearing and consist of two orthogonal sets. They were previously interpreted to be related to tuff degassing and dilation during cooling. Given that such processes likely occurred within 1 month of tuff deposition, the entire orthogonal joint system formed within the same timeframe.

2. The preferred interpretation for the formation history of tube-bearing joints is

   - Initial ignimbrite eruption of the Tiva Canyon Tuff and collapse of the Claim Canyon caldera.

   - Deposition of the ignimbrite over topography that may have included a shallow, northwest-trending basin.

- Development of a perturbed stress field due to (i) thermal gradient, (ii) differential compaction, (iii) caldera collapse, and (iv) faulting.

- Slip on the Solitario Canyon, Bow Ridge, and Paintbrush Canyon faults, triggered by caldera collapse and increased vertical loading associated with newly deposited ignimbrite sheet that perturbed the regional stress field in the vicinity of Yucca Mountain, is a strong candidate model for the perturbation of the stress field.

- Formation of the northeast-trending joints in response to gas pressure with orientation controlled by the perturbed stress field.

- Formation of the northwest-trending joints controlled by a stress swap due to the presence of the extensive northeast-trending joint swarms and possibly aided by differential compaction across the northwest-trending basin.

- Tube formation on both joint sets during degassing and lithophysae formation in the upper Tiva Canyon Tuff.

Modeling of fault-controlled stress field perturbation does not completely exclude other possible contributions to stress field perturbation due to either an absence of appropriate data or limitation in available modeling techniques. For example, with appropriate data, the roles of differential compaction and thermal gradients could have been explicitly assessed. Similarly, a better understanding of the role of caldera collapse in perturbing stress fields and triggering fault motions might have provided a sufficient basis for a quantitative analysis of this possibility. Nonetheless, it is believed that this contribution represents a useful first attempt to relate the roles of caldera collapse, tuff deposition, tuff cooling, fault behavior, and joint development to explain the origin of a joint network with an interesting formation history. This interpretation also illustrates that a series of stress sources acting at a variety of scales, timespans, and magnitudes can combine to produce an apparently simple orthogonal fracture geometry.

3. Because previous work had identified the tube-bearing joints as the cooling joints, this new interpretation necessitates that some joints previously identified as having a tectonic origin be reidentified as cooling joints that lack tubes and that formed in response to thermoelastic contraction. Morphologically, these cooling joints and the tectonic joints are quite similar, and detailed studies of the different deuteric facies within the Tiva Canyon Tuff might be needed to distinguish them.

4. Conclusions regarding very early development of joints with tubular structures, and the possibility that some of the interpreted tectonic joints are actually contractional cooling joints, apply to joints with similar tubular structures throughout the Paintbrush Group. Strong orientation clustering of interpreted cooling joints, and common occurrence of northwest and northeast strike trends, indicate that stress-field perturbation was a recurrent process during the repeated deposition and cooling of the Paintbrush Group ignimbrites.

4.5 Sampling Biases

Characterization of fracture networks at Yucca Mountain is impaired by several important sampling biases that are common to fracture analyses. If left uncorrected, these sampling biases lead to underrepresentation of fracture intensity, porosity, permeability, and connectivity.

First, the lengths of the longest fractures in a population are often unconstrained because the ends of the fracture are obscured (blind). This bias can lead to underestimation of fracture connectivity.

Second, the orientation of a one-dimensional sampling line (e.g., borehole or detailed line survey scanline) or two-dimensional sampling surface (e.g., pavement, roadcut) inherently biases sampling against discontinuities parallel to the sampling line or surface, and in favor of sampling discontinuities at a high angle to the sampling line or surface. Mathematical corrections (Terzaghi, 1965) can partially compensate for this sampling bias.

Third, because measuring every fracture from microscale to megascale is impractical or impossible for large sample areas, fracture studies usually have a size (e.g., length) cutoff. Fractures smaller than a given dimension are not counted. Consequently, small fractures are underrepresented in fracture characterization. Exclusion of small fractures could lead to an underestimation of hydrologic properties such as porosity, permeability, and fracture connectivity in these units. Elimination of fractures less than 1 m also may modify fracture intensity interpretations near faults such as for the Ghost Dance fault in the Exploratory Studies Facility, where the 1-m cutoff for trace length leads to extremely variable fracture intensity estimates over a wide zone (Sweetkind, et al., 1997a,b).

Fracture data analyses in the upper lithophysal unit of the Tiva Canyon Tuff on Live Yucca Ridge illustrate the importance of sampling location and fracture trace length and directional sampling bias (Figures 4-8, 4-9, and 4-13). Analyses of Exploratory Studies Facility and Enhanced Characterization of the Repository Block data illustrate potential correction for directional sampling biases (Figure 4-14).

1. **Distribution Bias:** A strong bimodal distribution of fractures is apparent on Live Yucca Ridge (Figures 4-8, 4-9). This bimodel distribution is not well represented in P100 (Figure 4-13a,b). Although a subset of the Live Yucca Ridge map area (Figure 4-8), P100, samples an area that is too small to be representative of fracturing at Live Yucca Ridge as a whole.

2. **Trace Length Bias:** Rose diagrams are not typically weighted by fracture length; they treat all fractures as equally important. Visual inspection of P100 (Figure 4-13a) gives a clear impression of dominant northeast-southwest fractures that are only partially captured by the rose diagram in Figure 4-13b. Plotting a length-weighted rose diagram (Figure 4-13c) emphasizes the importance of the northeast-southwest fractures. When considering vertical percolation pathways, and potential rockfall into a tunnel, for example, fracture size (in this case, length) is an important parameter.

3. **Directional or Orientation Bias:** A common approach to correcting for directional sampling bias is the Terzaghi (1965) method, which applies a correction for the angle

(a) Barton's Pavement 100

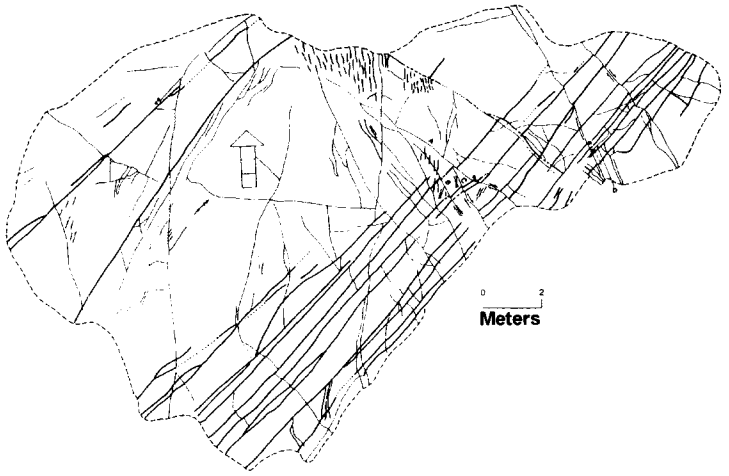

(b) Cooling Joints and Tectonic Joints

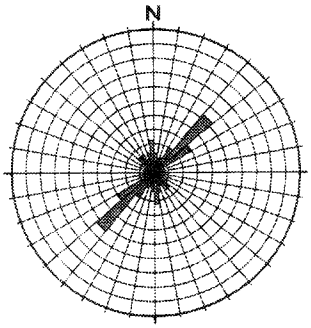

n = 226 (number of fractures)
Plot Radius = 20%

(c) Length Weighted Cooling Joints and Tectonic Joints

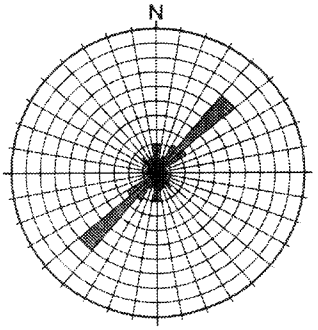

N = 542 m (cumulative fracture length)
Plot Radius = 20%

Figure 4-13. Summary of Cooling and Tectonic Joints on Pavement 100. (a) Map of Pavement 100 on Live Yucca Ridge (After Barton, et al., 1993). (b) Rose Diagram of Fractures in Pavement 100. (c) Length-Weighted Rose Diagram of Fractures in Pavement 100.

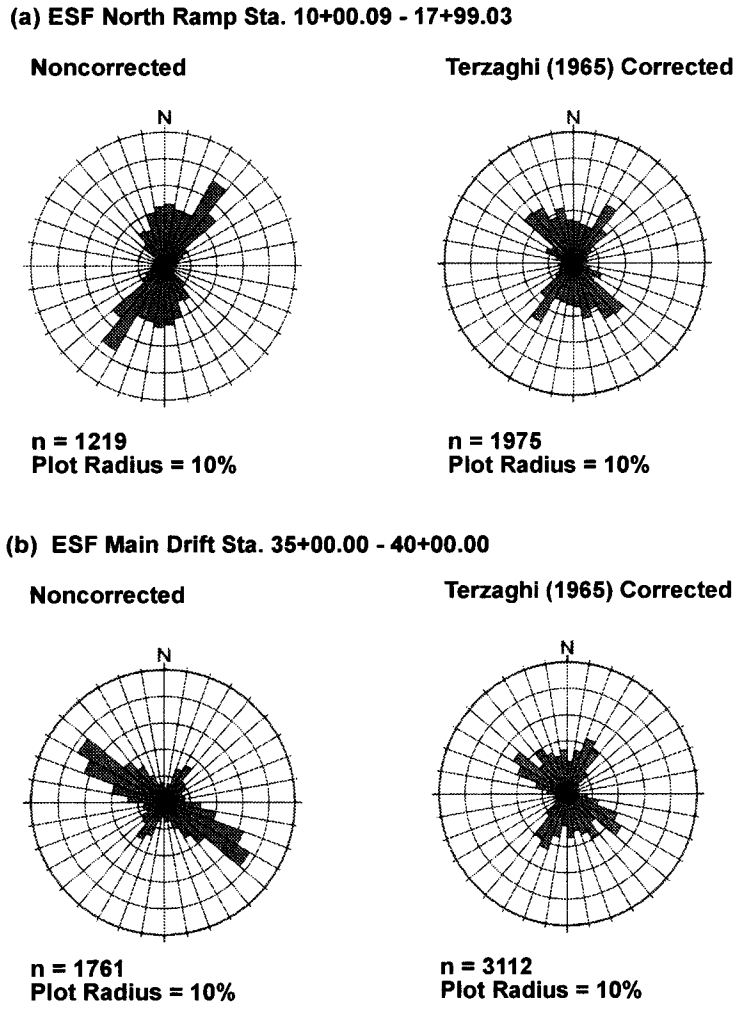

Figure 4-14. Examples of Uncorrected and Terzaghi (1965)-Corrected Fracture Data from Detailed Line Survey Data Collected in the Exploratory Studies Facility at Yucca Mountain. Raw Data from Exploratory Studies Facility Detailed Line Survey Data Were Collected by the Bureau of Reclamation and U.S. Geological Survey (Exploratory Studies Facility Data Transmitted from DOE to CNWRA, August 1998: DOE Document Tracking Numbers GS960708314224.008, .101, .011, .014, .003, .008, .010, .012, .020, .021, .022, .023, .024, .025, .026, and .028; Technical Data Information Form Numbers 305556, 305554, 305624, 306645, 306017, 306284, 306298, 306299, 306509, 306510, 306511, 306512, 306513, 306514, 306515, 306517). The Files Used in (a) Represent the Midpoints of the North Ramp, (b) Main Drift, and (c) South Ramp of the Exploratory Studies Facility. Rose Diagrams Were Constructed Using StereoNet, Version 3.0, for Windows Software. The Raw Data Were Terzaghi (1965)-Corrected to Compensate for Directional Sampling Bias. (a) The North Ramp between Stations 10+00.09 and 17+99.03 Traversed the Pah Canyon Tuff, Pre-Pah Canyon Tuff, Topopah Spring Crystal-Rich Vitric Zone, Topopah Spring Crystal-Rich Nonlithophysal Zone, Topopah Spring Crystal-Rich Lithophysal Zone Units into the Topopah Spring Crystal-Poor Upper Lithophysal Zone Unit. (b) The Main Drift from Stations 35+00.00 to 40+00.00 Is Entirely in the Topopah Spring Crystal-Poor Upper Lithophysal Zone.

(c) ESF South Ramp Sta. 65+00.00 - 70+00.00

Noncorrected

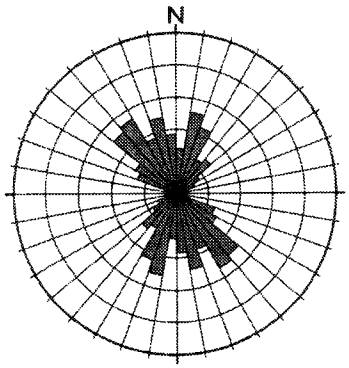

n = 448
Plot Radius = 10%

Terzaghi (1965) Corrected

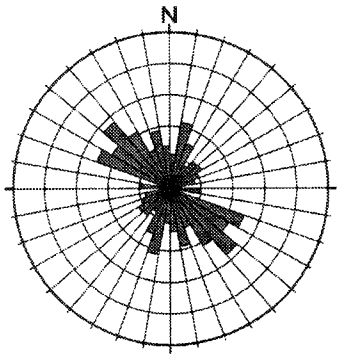

n = 639
Plot Radius = 10%

(d) ESF All Sta. 00+61.70 - 78+77.00

Noncorrected

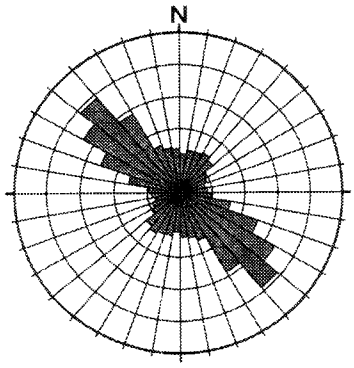

n = 17812
Plot Radius = 10%

Terzaghi (1965) Corrected

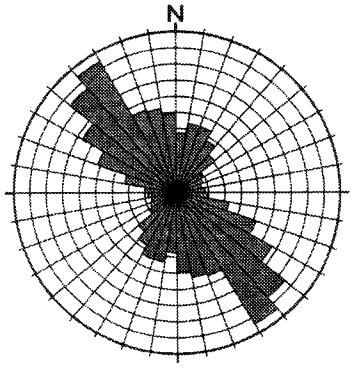

n = 28199
Plot Radius = 40%

Figure 4-14 (continued). (c) The Middle Section of the South Ramp Encounters Topopah Spring Crystal-Rich Lithophysal Zone, Topopah Spring Crystal-Rich Nonlithophysal Zone, Topopah Spring Crystal-Rich Vitric Zone, Pre-Pah Canyon Tuff, Tiva Canyon Crystal-Poor Vitric Zone, Tiva Canyon Crystal-Poor Lower Nonlithophysal Zone, and Topopah Spring Crystal-Poor Upper Lithophysal Zone Units from Stations 65+00.00 to 70+00.00. (d) Terzaghi (1965) Correction of Detailed Line Survey Data from the Entire Exploratory Studies Facility at Yucca Mountain. Note that the Rose Diagrams of Uncorrected and Terzaghi (1965)-Corrected Fracture Orientations for the Entire Exploratory Studies Facility Are Similar Due To the Combination of Data from Nearly Orthogonal Scanlines (Approximately East-West Ramps and North-South Main Drift). The Combination of all the Detailed Line Survey Data, However, Suppresses Important Local Variability Related to Lithology and Structural Position.

between the scanline and the pole to each sampled fracture. The frequency of each fracture is given by a Terzaghi factor:

$$T_f = \frac{1}{\cos\theta} \tag{4-1}$$

where θ is the angle between the normal to the fracture and the scanline. In the examples shown in Figure 4-14, the Terzaghi (1965) correction was truncated for $T_f > 4$ (i.e., for $\theta \geq 75°$, fractures are assigned a frequency of 4). This correction accounts, in part, for underrepresented fractures that intersect the scanline at low acute angles.

In addition to sampling biases, fracture characterization based on existing studies is impaired because fracture data were collected from different sources including boreholes, pavements, and the Exploratory Studies Facility, and different information was collected from each of the three sets of studies. The only observations consistent to all data sets are orientation and lithology (Sweetkind and Williams-Stroud, 1996).

4.6 Local Controls on Fracturing and Small-Scale Faulting

Yucca Mountain consists of a thick accumulation of volcanic tuff deposited on an irregular surface of eroded and deformed Paleozoic and Precambrian basement composed of highly faulted and folded sedimentary and metasedimentary rocks. These tuffs were erupted from a series of Middle to Late Miocene (15 to 9 million years ago) calderas that collectively form what has been defined as the southwestern Nevada volcanic field (see Sawyer, et al., 1994, for the most recent regional stratigraphy of the Miocene volcanic rocks in the Yucca Mountain region). Rocks of the Paintbrush Group, principally ash flows of the Topopah Spring Tuff (12.8 million years ago) and Tiva Canyon Tuff (12.7 million years ago) make up the main surface exposures of Yucca Mountain. The Paintbrush Group Tuffs rest on a sequence of older tuffs, including the Prow Pass and Bullfrog members of the Crater Flat Group. Younger tuffs related to the Timber Mountain Group are locally exposed at Yucca Mountain in topographic lows between large block-bounding faults. This observation, along with evidence for growth faults in the Paintbrush rocks in Solitario Canyon (Carr, 1990; Day, et al., 1998b), suggests that faulting and tuff deposition were synchronous at Yucca Mountain.

The majority of faults at Yucca Mountain are either north-trending normal faults or northwest-trending dextral strike-slip faults. The larger faults in these two orientations bound the fault blocks that underlie the study area. These two sets of faults are interpreted to be coeval, based on mutual terminations and secondary structures between them such as pull-apart basins (Day, et al., 1998b). Some northwest-trending faults are dominantly normal faults, accommodating extension in relay ramps between overlapping normal faults (Ferrill, et al., 1999a). Only four reverse faults with north-south or northeast-southwest strikes have been identified, but they are potentially key features for constraining the kinematic history of the region (Day, et al., 1998b). Based on Cl-36 data from the Exploratory Studies Facility, one of these, the Diabolus Ridge fault, has been interpreted to be an important infiltration and percolation pathway (Levy, et al., 1997). Much of the detailed fieldwork to study faults in the central block focused on the Ghost Dance and Sundance faults, which are close to the subsurface trace of the Exploratory Studies Facility (Spengler, et al., 1994; Potter, et al., 1996).

Yucca Mountain itself consists of a sequence of north to north-northeast-trending fault-bounded ridges crossed by occasional northwest-trending dextral strike-slip faults. Faults dip almost uniformly to the west and separate blocks of gentle to moderate east-dipping tuff strata. From north to south, both fault displacement and stratal tilt increases, indicating progressively greater extension of the Crater Flat basin southward. This pattern is most profound on the west flank of Yucca Mountain, which is defined by a series of left-stepping and north-trending *en echelon* faults (Day, et al., 1998a; Ferrill, et al., 1999a). The southward increase in fault offset is coupled with greater block rotation, both horizontal and vertical (Scott, 1990). Work by the U.S. Geological Survey (Hudson, et al., 1994; Minor, et al., 1997) suggests that this pattern of faulting, along with rotated paleomagnetic direction in the tuffs, resulted from a discrete period of extension followed by a discrete period of dextral shear, akin to an oroclinal bending model. More recent reanalysis of these data suggests an alternative explanation. The north-to-south displacement gradient and rotation of fault blocks is simply a result of increased rollover deformation in the hanging wall above a listric Bare Mountain fault (Stamatakos and Ferrill, 1998).

En echelon faulting defines the western edge of Yucca Crest and the fault line escarpment that follows the west-dipping Solitario Canyon, Iron Ridge, and Stagecoach Road faults (Day, et al., 1998a). The geometry of faults and ridges defines a scallop trend, composed of linear north-trending fault segments connected by discrete curvilinear northwest-trending fault segments. For example, the ends of the north-trending curvilinear Iron Ridge fault bend to the northwest near its overlap with both the Stagecoach Road and Solitario Canyon faults. Yucca Mountain also contains numerous swarms of small northwest-trending faults that connect the large north-trending faults. One example is at West Ridge, which is cut by numerous small faults that connect segments of the Windy Wash and Fatigue Wash faults. This geometry strongly suggests that the entire Yucca Mountain fault system is an *en echelon* branching fault system (Ferrill, et al., 1999a), in which faulting on the large block-bounding fault triggers relatively widespread, but predictable, secondary faulting on connecting and linking faults. Linkage of the *en echelon* system is either by lateral propagation of curved fault tips or formation of connecting faults that breach the relay ramps (Figure 4-15; Day, et al., 1998a; Ferrill, et al., 1999a; Peacock and Sanderson, 1994; Trudgill and Cartwright, 1994). The western Yucca Mountain fault system contains examples of both linking mechanisms (Figures 4-15, 4-16, 4-17). More importantly, from this interpretation of *en echelon* faulting, it follows that locally developed faults and fractures were produced by local variations of the stress field, rather than dramatic swings of the regional extension direction (Throckmorton and Verbeek, 1995). Recent numerical modeling of stresses related to displacement on overlapping normal faults show that local perturbations of the stress field in the fault overlap zone are likely to lead to the development of faults and fractures in orientations oblique to the regional trend (Crider and Pollard, 1998).

This model for the evolution of an *en echelon* fault system has several potentially important implications for groundwater flow. Unfaulted relay ramps may provide important aquifer connectivity across faults (Figure 4-15d). Faulted relay ramps may provide local fault-controlled traps for perching of groundwater. Localized fracturing in relay ramps may locally enhance hydraulic conductivity (Figure 4-15d).

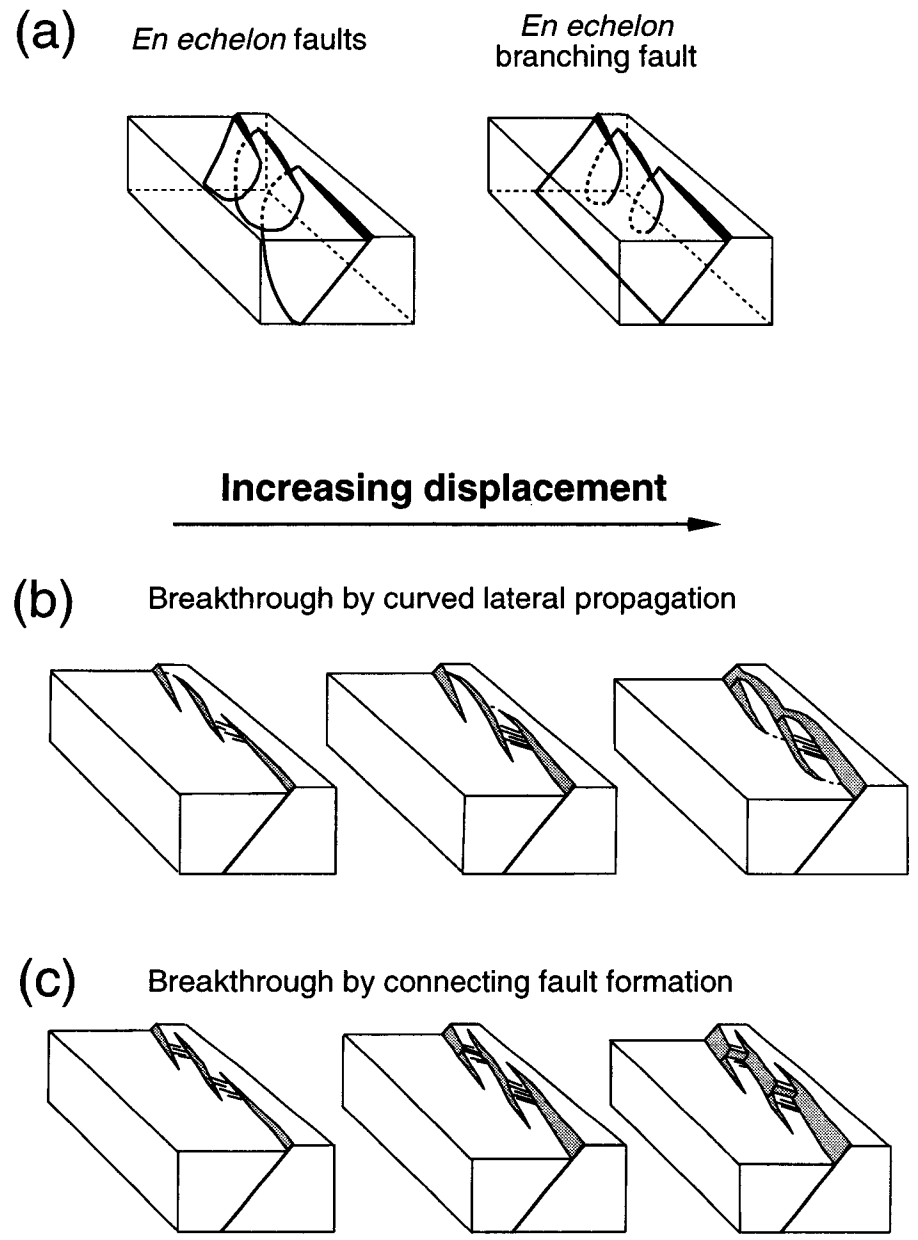

Figure 4-15. Block Diagrams Illustrating Geometry and Development of Corrugated Normal Faults. Figures Show (a) Topology of *En Echelon* Fault System and *En Echelon* Branching Fault, (b) Sequence of Evolution of *En Echelon* Normal Fault Array or *En Echelon* Branching Normal Fault Involving Linkage and Breakthrough by Lateral Propagation of Curved Fault Tips, and (c) Sequence of Evolution of *En Echelon* Normal Fault Array of *En Echelon* Branching Fault System Involving Linkage and Breakthrough by Connecting Fault Formation.

(d)

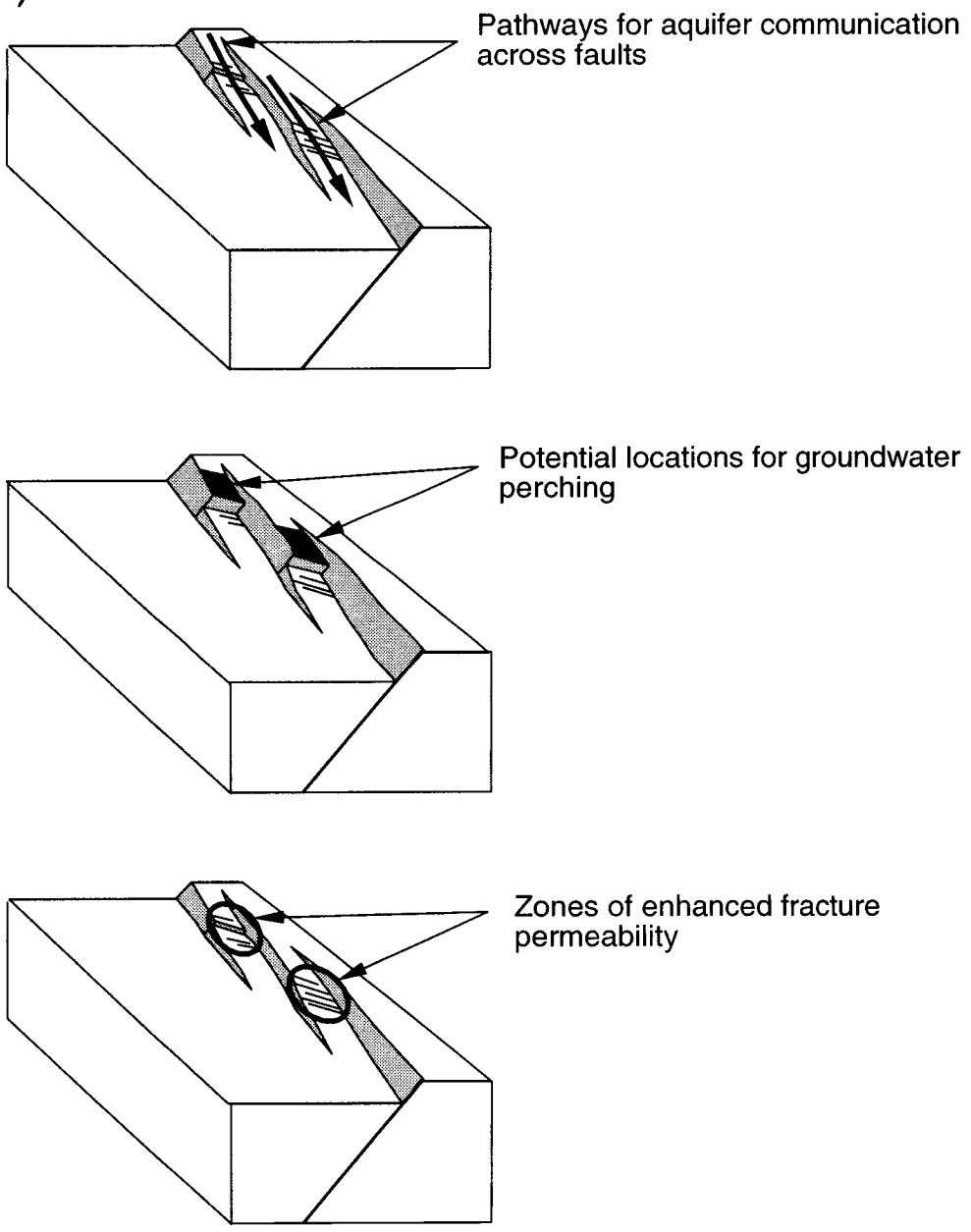

Figure 4-15 (continued). (d) Block Diagrams Illustrating Aspects of Fault Interaction and Fault-Block Geometry Important for Groundwater Flow and Perching

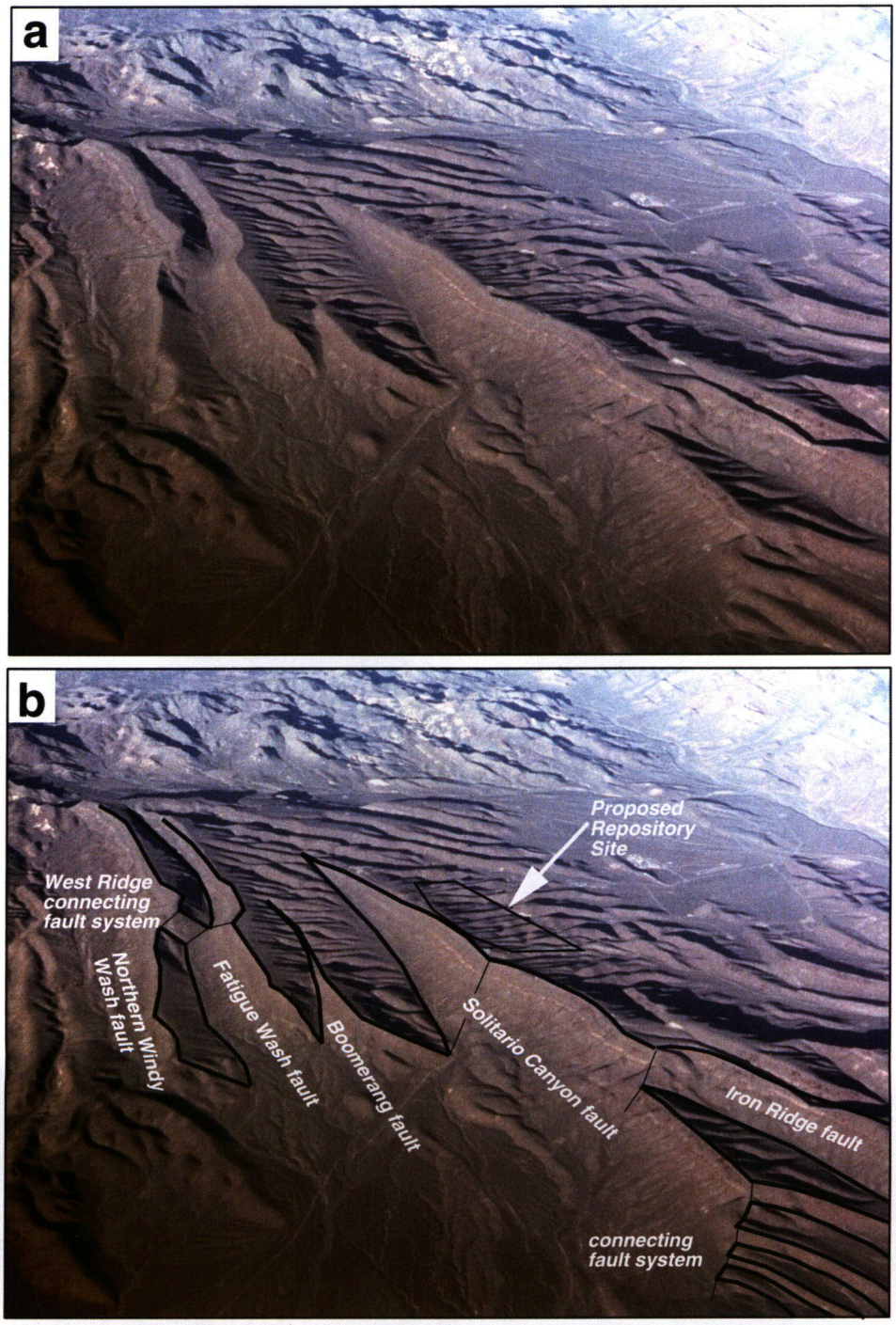

Figure 4-16. Aerial Photographs Showing the *En Echelon* Fault System that Bounds the Western Side of Yucca Mountain. (a) Unannotated and (b) Annotated Aerial Photographs (Looking Northeast) of Yucca Mountain, Nevada, Illustrate the Solitario Canyon-Iron Ridge Fault System and the Overall *En Echelon* Geometry of the Western Yucca Mountain Fault System. Width of the Field of View is Approximately 15 km.

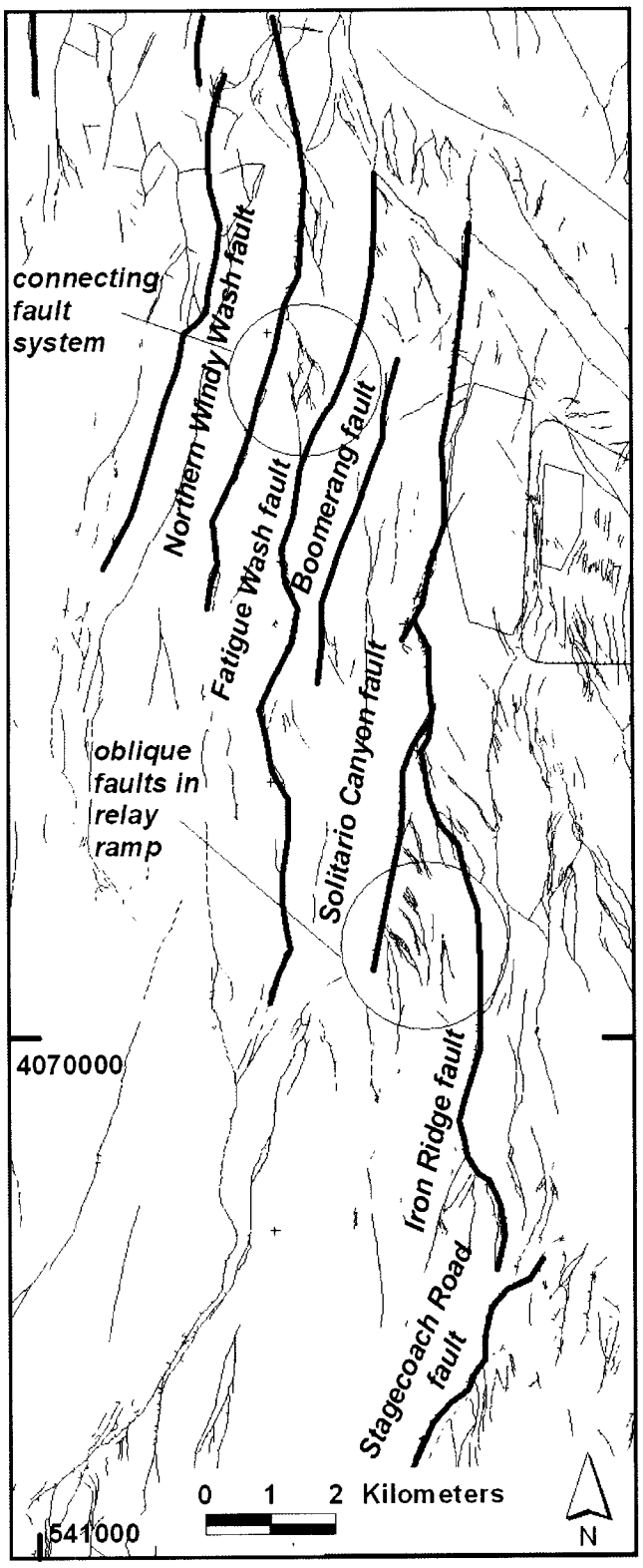

Figure 4-17. Map of Western Yucca Mountain Fault System (after Simonds, et al., 1995). The Map Illustrates Arrangement and Connection of Major Normal Faults (Bold Lines).

4.6.1 Displacement Gradient and Deformation in Normal Fault Systems

A simple method for estimating cutoff-parallel elongation (extension or contraction) related to fault displacement gradient is presented in the following sections (after Ferrill and Morris, 2001). The method is applicable to deformation associated with the hanging wall and footwall of individual faults, or relay ramps between overlapping faults. The method is based on readily measured parameters such as the orientation of hanging-wall and footwall cutoffs, fault dip, and fault displacement direction. This section considers examples of normal faulting from Yucca Mountain, Nevada, the proposed site for a high-level waste repository. Recent mapping of fault systems at Yucca Mountain has revealed the presence of several large breached relay ramps and indications that several smaller or more subtle relay structures may also be present. Fault-system architecture and displacement gradients on Yucca Mountain faults are generally consistent with patterns of deformation predicted by CNWRA's geometric model. These results indicate that some localized faulting is controlled by fault displacement gradients and interaction, rather than simply the regional stress field.

4.6.2 Conceptual Framework

Relay ramps in brittle rocks transfer displacement between overlapping normal faults by vertical axis rotation (accommodating horizontal heave gradients on faults) and tilting (accommodating vertical throw gradients on the faults). A simple relay ramp can be simulated by making two parallel, overlapping cuts in a piece of paper, then extending the paper perpendicular to the cuts (e.g., Figure 4-18a). In the simple case in which the paper is extended perpendicular to the fault traces without tearing, fold hinges localize at the fault (cut) tips at the top and bottom of the relay ramp, and fault displacement follows a circular arc, initially vertical, and eventually horizontal. The ramp is hinged at the top and bottom and, to avoid tearing, the paper is not extended within the ramp.

Rock is widely recognized as being weak in extension under brittle deformation conditions. Unlike the paper relay ramp described above, extension localized in a rock relay ramp is likely to produce permanent deformation. In the case of true dip slip on two overlapping, ramp-bounding normal faults, the ramp is geometrically required to (i) rotate around a vertical axis, (ii) tilt, and (iii) extend parallel to hanging-wall and footwall cutoff lines. The magnitude of this cutoff-parallel extension is directly related to the displacement gradients on the ramp-bounding normal faults (Figures 4-18, 4-19). In the case of an initially horizontal surface (represented only by footwall cutoff, FB, and hanging-wall cutoff, HB) cut by a terminating and planar normal fault (see triangle FBH in Figure 4-19) with true dip slip, both the footwall and hanging-wall cutoff lines (see FB and HB in Figure 4-19) may experience extension.

Layer extension relates directly to the deflection of hanging-wall or footwall cutoff from the original horizontal position. Deflection of the cutoff lines is a function of fault displacement gradient. The anticipated cutoff-parallel extension in a relay ramp has both hanging-wall and footwall cutoff components and can be estimated from a knowledge of (i) the orientation of the ramp-bounding faults, (ii) the slip vector(s), and (iii) the orientations of the cutoff lines. This simplifies to knowing, for each bounding fault, the fault orientation, rakes of the hanging-wall and footwall cutoffs within the respective faults, and the rakes of the slip vectors within the faults.

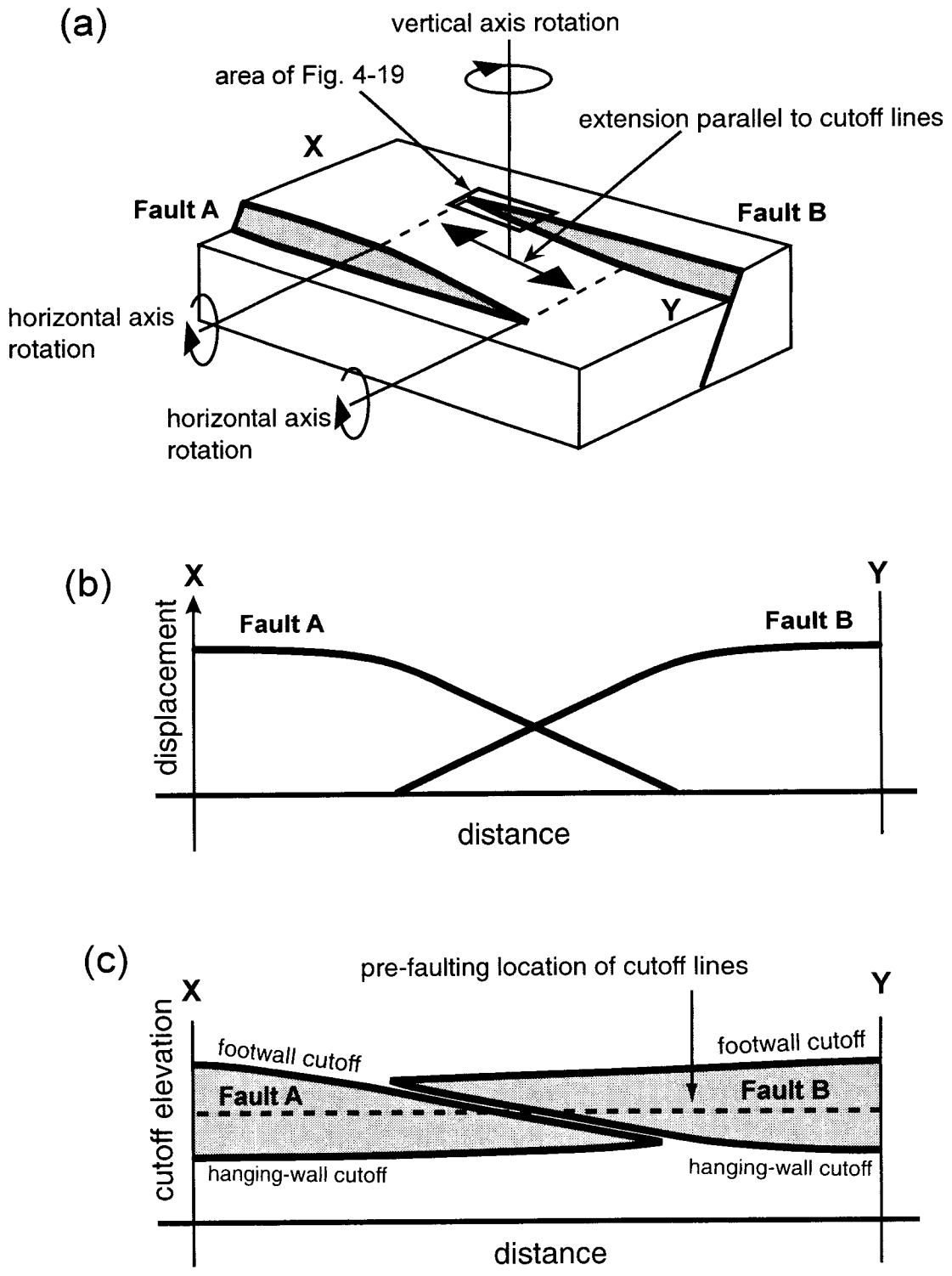

Figure 4-18. Displacement Transfer between Normal Fault Segments. (a) Schematic Block Diagrams Illustrating an Extensional Relay Ramp. (b) Distance Versus Displacement Diagram for the Profile XY in (a). (c) Distance Versus Fault-Cutoff Elevation for the Profile XY in (a).

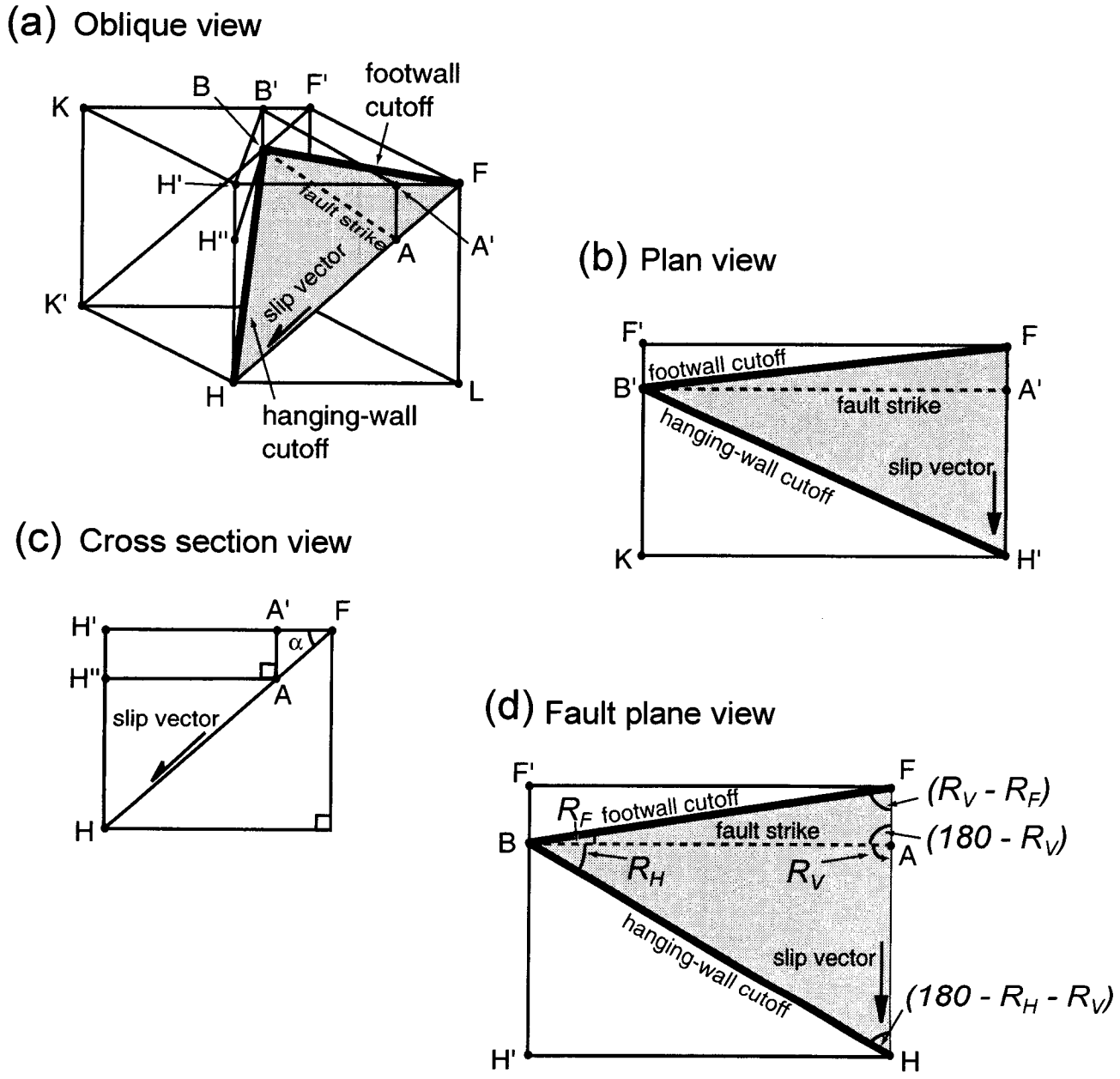

Figure 4-19. Diagrams of Geometric Elements Used for Fault Analysis. (a) Cut-Away Block Diagrams of a Fault Gap (Shaded Triangular Area) Near a Fault Tip (Point B) Illustrating the Geometric Elements Used in the Analysis Presented Here. Shaded Area Represents Fault Surface, Point A Lies within the Fault Surface at the Same Elevation as the Fault Tip Point B, Lines FB and HB Are Footwall and Hanging-Wall Cutoff Lines Respectively. (b) Plan View of Fault Termination Region. (c) Cross-Sectional View. (d) Fault Plane View. R_F = Acute Angle (Rake) of Footwall Cutoff, Measured As Shown and Counted As Negative in Figure 4-20b; R_H = Acute Angle (Rake) of Hanging-Wall Cutoff, Measured As Shown and Counted As Positive in Figure 4-20b; R_V = Rake of Slip Vector, Measured As Shown from the Strike Line Facing the Fault Slip Vector, May Have Values from 0° to 180° (See Also Figures 4-22d,e, 4-23a).

4.6.3 Geometric Analysis

In this section, equations allow estimation of cutoff-parallel elongation (positive = extension; negative = contraction) based on orientations of the fault, fault cutoff lines, and fault slip vector. These equations apply to hanging wall or footwall deformation associated with any normal or normal-oblique slip fault with a lateral displacement gradient. For simplicity, it is assumed that, prior to slip on the fault, the hanging-wall and footwall cutoff lines were coincident and horizontal and that the fault dip and slip direction do not change during progressive deformation. However, the geometrical relationships and the model can be applied to a fault of any orientation if the position and orientation of the pre-faulting cutoff line is known or can be assumed.

Ramp-parallel elongation [derivations provided in Ferrill and Morris (2001)] is described by

$$e_C = \frac{\sin(R_V)}{\sin(R_V \pm R_C)} - 1 \qquad (4\text{-}2)$$

where R_V is the rake of the fault's slip vector, R_C is the rake of the cutoff in the fault plane (Figure 4-19d; Appendix A in NRC, 1999a).

Equation (4-2) can be applied by appropriate choice of angle convention. Using these relationships, strain can be estimated from the fault dip (α) and the rake of the footwall and hanging-wall cutoffs in the fault plane. Figure 4-20 can be used to determine the cutoff-parallel elongation from the values of R_C. In the simple case of pure dip slip ($R_V = 90°$), all cutoff-parallel elongations are positive (i.e., extension, Figure 4-20). However, oblique slip can lead to zero or negative (shortening) cutoff-parallel strains.

In the case of the faults illustrated in Figure 4-18a, a right-lateral slip component will cause the ramp-bounding cutoff lines to experience less extension than in the simple dip-slip case, and it may experience contraction in cases of a major strike-slip component. Conversely, a left-lateral strike-slip component would cause greater cutoff-parallel extension than the simple dip-slip case.

4.6.4 Cutoff-Parallel Elongation

4.6.4.1 Hanging Wall Versus Footwall Deflection

Both footwall and hanging-wall cutoffs of a normal fault can be deflected away from their pre-faulting position. Excellent field examples of deflections of both footwall and hanging-wall cutoffs and various relay ramp geometries are exposed in the Volcanic Tableland north of Bishop, California (Figure 4-21). Here a welded unit of the 738 ± 3 thousand years old Bishop Tuff (Izett, et al., 1988) is cut by several hundred faults ranging in displacement from less than 1 m to more than 100 m (Bateman, 1965; Dawers, et al., 1993; Dawers and Anders, 1995; Willemse, et al., 1996; Willemse, 1997; Ferrill, et al., 1999a). The arid climate, relative youth, and resistance to weathering of the tuff result in remarkably well-exposed fault-line scarps that closely approximate the fault geometries (Figure 4-21). Although fault block geometries are well expressed by the topography, direct displacement direction indicators such as slickenlines are

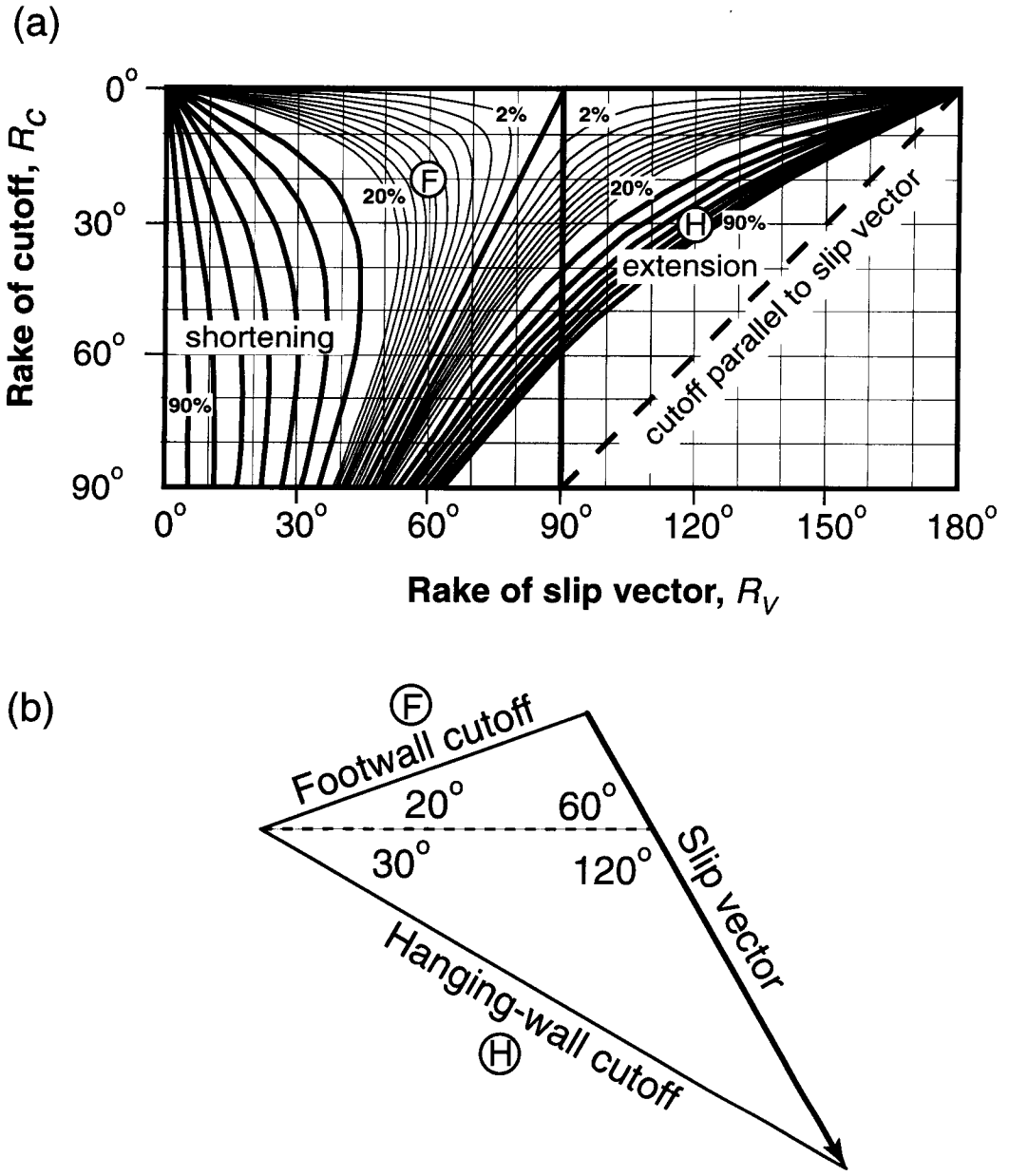

Figure 4-20. Graphical Solution to Eq. (4-2). (a) Graphical Solution to Eq. (4-2) Contoured with Respect to Percent Elongation. Strain Contours are in 10-Percent Increments (Heavy Solid Lines) for Values Greater Than 20 Percent, and 2-Percent Increments (Light Solid Lines) for Values of 20 Percent and Less. Shaded Areas Represent Extension (Positive Elongation), Unshaded Areas Represent Shortening (Negative Elongation). (b) Example of View. Perpendicular to a Fault Plane. Dashed Line Represents the Prefaulting Cutoff Line, Footwall and Hanging-Wall Cutoff Lines Are Labeled. The Footwall Cutoff Line Has a Rake of 20°, Its Strain State Is Given by (F) in (a). The Hanging-Wall Cutoff Has a Rake of 30° with a Slip Vector Rake of 120°, And Its Strain State Is Given by (H) in (a).

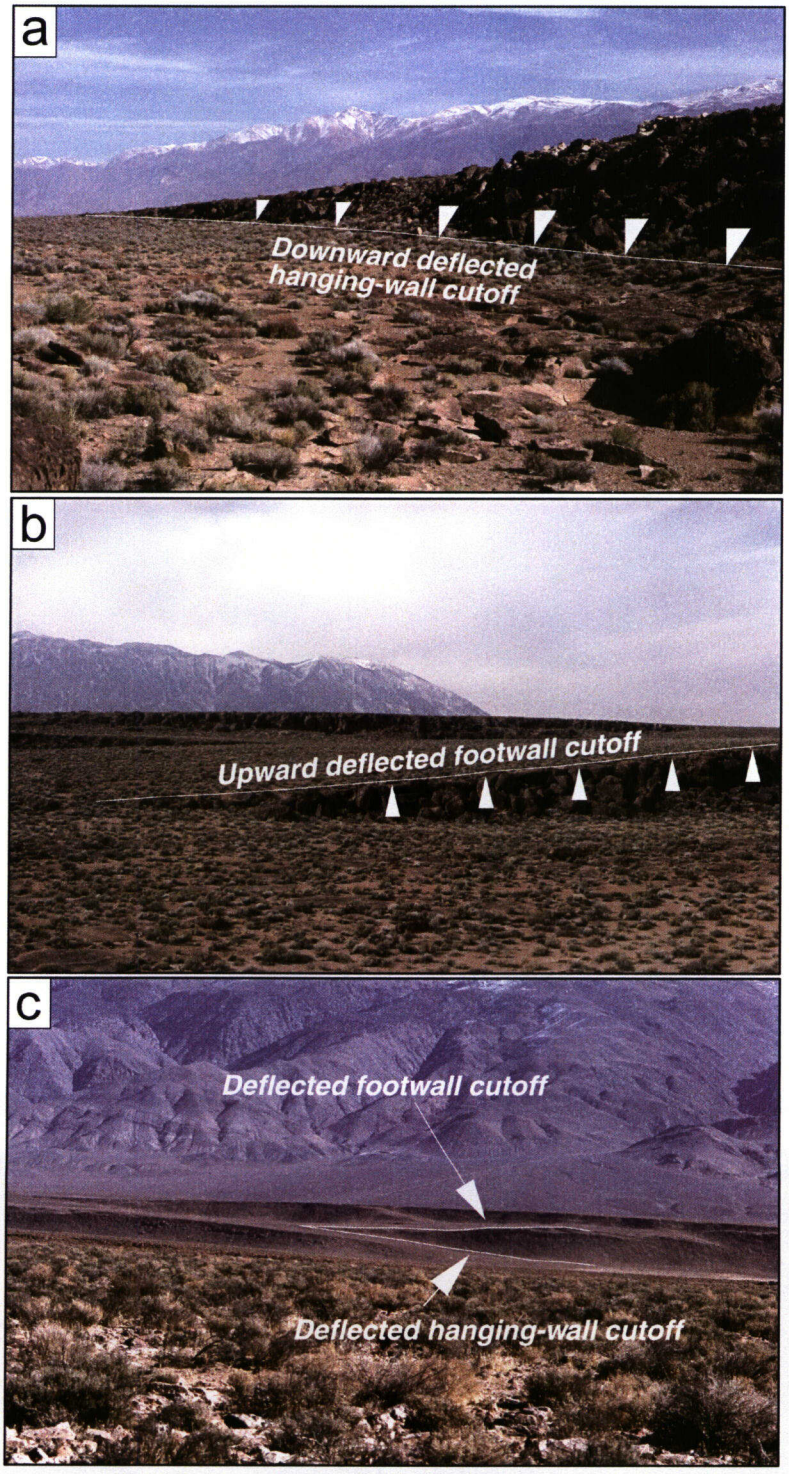

Figure 4-21. Field Photographs of Unfaulted and Breached Relay Ramps from the Volcanic Tableland, Owens Valley, California. Examples Include (a) Fault Gap Defined with Straight Footwall Cutoff and Deflected Hanging-Wall Cutoff, (b) Fault Gap Defined by Straight Hanging-Wall Cutoff and Deflected (Upwardly Bowed) Footwall Cutoff, and (c) Fault Gap Defined by Deflected Footwall and Hanging-Wall Cutoffs.

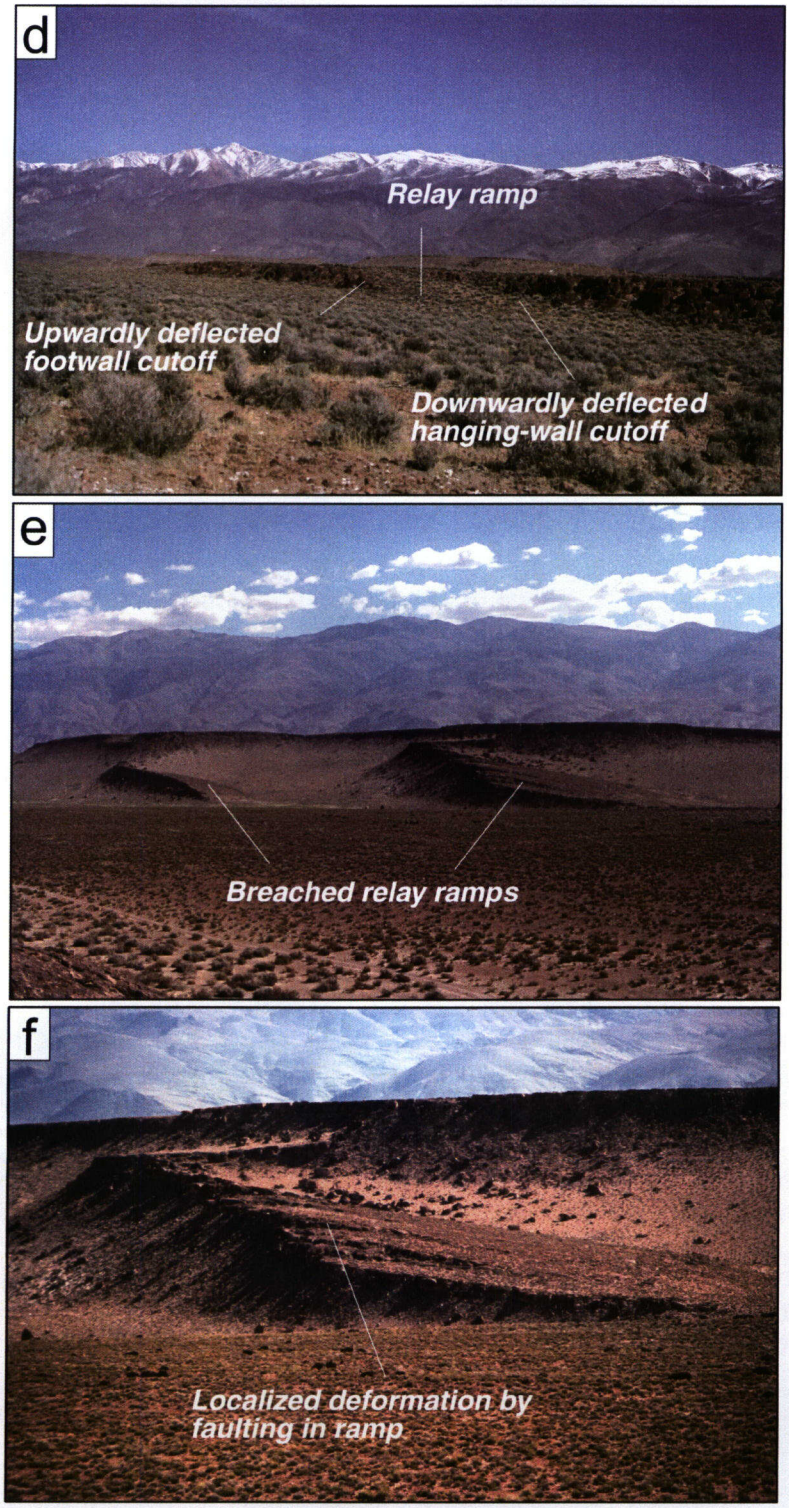

Figure 4-21 (continued). (d) Relay Ramp Bounded by Deflected Hanging-Wall and Footwall Cutoffs, (e) Breached Relay Ramps Bounded by Deflected Hanging-Wall and Footwall Cutoffs, and (f) Detail of Breached Relay Ramp Illustrating Small Displacement Faults (<5 m Displacements) Within Breached Ramp.

generally absent. These examples, however, serve to illustrate that footwall and hanging wall deflections can occur in a full range of relative proportions from hanging wall only to footwall only, and seemingly any combination of footwall and hanging wall deflection.

4.6.4.2 Hanging-Wall Versus Footwall Cutoff Elongation

Figure 4-22 illustrates six possible combinations of cutoff deflections and fault slip that lead to different patterns of strain partitioning between the hanging wall and footwall (also see Table 4-1). In each case illustrated in Figure 4-22, the faults dip 70° and the lateral gradient in fault gap (scarp) height is approximately the same. Fault displacement and total displacement gradients (measured in fault plane, parallel to slip vectors between hanging-wall and footwall cutoffs) are the same for Figures 4-22a, 4-22b, and 4-22c. Figures 4-22a and 4-22b differ only in whether the hanging wall or footwall deforms. In these two cases, the deflected cutoff lines extend more than 6 percent. In Figure 4-22c, both the hanging wall and footwall deform, and the resulting cutoff extensions are less than 2 percent, which is considerably less than strains in the end member (one block rigid) cases (Figure 4-22a,b). Oblique displacement on a fault (Figure 4-22d,e) may produce extension in one fault block and contraction of the opposing fault block. For the idealized relay ramp shown in Figure 4-22f, deflection of the hanging-wall and footwall cutoffs that bound the ramp produces cutoff extensions of less than 2 percent.

4.6.4.3 Effects of Oblique Slip

In the simple case of true dip-slip faulting, fault block extension is expected (Figure 4-23a,b) and partitioning of strain into the footwall versus the hanging wall depends on the deflection of the hanging wall and footwall. Oblique slip produces more or less extension than expected for dip slip and depends on fault dip and slip direction.

If a normal fault has oblique slip (i.e., the slip vector rake, R_V, of the fault is not 90°), then certain displacement gradient and slip vector configurations may produce strain reversals during slip accumulation. For example, the hanging wall of a fault that dips 60°, has a slip vector rake of 80°, and that laterally tips to the left (looking down the slip vector plunge; Figure 4-23c) will experience shortening followed by extension (Figure 4-23d). Shortening of the ramp occurs from the start of displacement until the cutoff line is perpendicular to the slip vector; and further displacement causes the hanging-wall cutoff to extend.

4.6.4.4 Relay Ramp Deformation

In the case of a relay ramp, the internal deformation should reflect deflection of the hanging-wall and footwall cutoffs that bound the ramp. Equal deflection of hanging-wall and footwall cutoffs (Figure 4-18) by dip slip produces uniform elongation across the width of the ramp and dip of the ramp in the fault-strike direction. Unequal deflection of hanging-wall and footwall cutoffs bounding a relay ramp would produce a deformation gradient across the ramp and is likely to produce tilting of the ramp toward the upthrown or downthrown side of the fault system.

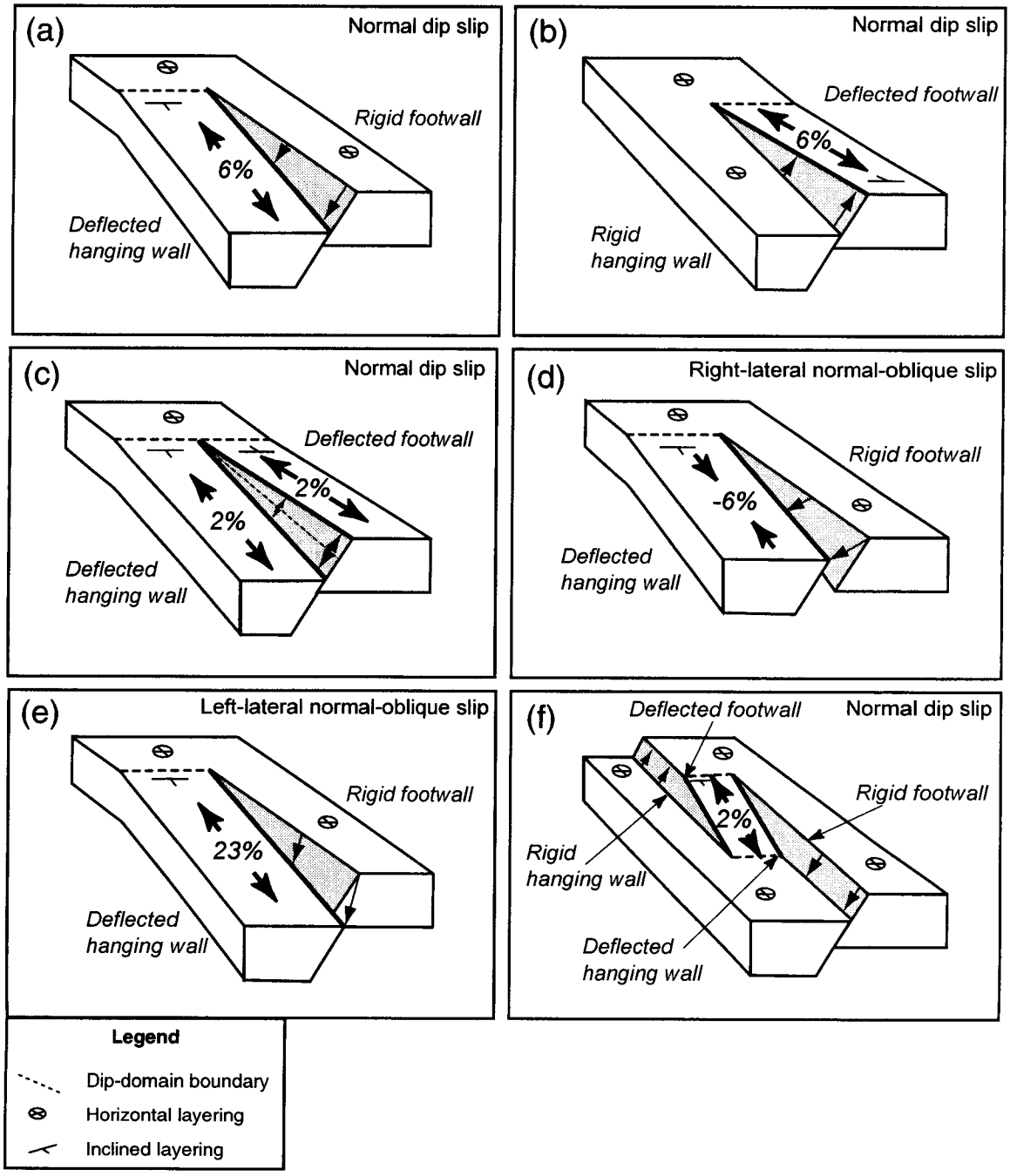

Figure 4-22. Block Diagrams Illustrating Different Patterns of Fault Displacement and Cutoff Line Deformation. Heavy Lines are Deformed Cutoffs. Solid Arrows in Fault Planes Indicate Displacement of Hanging-Wall Cutoff or Footwall Cutoff from Initial Position. (a) Rigid Footwall, Deforming Hanging Wall, Dip Slip. (b) Deforming Footwall, Rigid Hanging Wall, Dip Slip. (c) Deforming Footwall, Deforming Hanging Wall, Dip Slip. (d) Rigid Footwall, Deforming Hanging Wall, Contractional Oblique Slip. (e) Rigid Footwall, Deforming Hanging Wall, Extensional Oblique Slip. (f) Ideal Relay Ramp Bounded by Fault Tips with Dip Slip.

Table 4-1. Geometric Parameters and Calculated Elongations for Fault Displacement Gradients (Examples Illustrated in Figures 4-21 and 4-22)

Example*			Correlation to Figures†	Measured Angles, Degrees				Figure 4-20a Cutoff Rakes, Degrees		Figure 4-20b Extension, %	
#	FW	HW		α	δ_F	δ_H	R_v	R_F	R_H	e_{FW}	e_{HW}
1	rigid	def'd	Figures 4-21a, 4-22a	70	0	7	90	0	20	0	6
2	def'd	rigid	Figures 4-21b, 4-22b	70	7	0	90	-20	0	6	0
3	def'd	def'd	Figures 4-21c, 4-22c	70	4	4	90	-10	10	2	2
4	rigid	def'd	Figures 4-22d	70	0	7	70	0	20	0	-6
5	rigid	def'd	Figures 4-22e	70	0	7	110	0	20	0	23
6	def'd	def'd	Figures 4-21d, 4-22f	70	4	4	90	-10	10	2	2

Numbers rounded to nearest whole number.
* Note that FW and HW refer to cutoffs on opposing sides of a single fault gap in examples 1 to 5, and cutoffs on opposing sides of a relay ramp in Example 6.
† Figure 4-21 examples correlate in overall style (hanging wall versus footwall deflection) but not in detail (angles).

The typical distance-displacement graph (e.g., Figure 4-18b; Peacock and Sanderson, 1991; also see Figure 5 in Dawers and Anders, 1995; Cartwright and Mansfield, 1998) gives no indication of this strain partitioning. A better representation is given by a graph of distance versus cutoff elevation (e.g., Figure 4-18c; also see, Figure 4b in Dawers and Anders, 1995; Figure 6 in Huggins, et al., 1995).

4.6.5 Progressive Development of a Relay Ramp

The distribution and nature of strain within a relay ramp depend not only on the five geometric components (fault dip, fault shape, fault displacement gradients, orientation of slip vectors, and degree of footwall uplift versus hanging wall subsidence of the bounding faults), but also on the temporal evolution of the ramp. The CNWRA geometric model (discussed in Section 4.6.3) accounts for fault dip, displacement gradient, and slip vector, and because it is purely geometrical, can be applied to any segment of a cutoff line without *a priori* knowledge of faulting history. The roles of the above factors on cutoff elongation and their possible effects on relay ramp strain are discussed in Section 4.6.4. Here, the importance of the developmental history of the ramp in determining the overall strain present in a relay ramp is considered.

As discussed earlier, relay ramps transfer displacement between two overlapping normal faults by tilting, vertical axis rotation, and cutoff-parallel elongation. In an ideal relay ramp, the relay ramp accomplishes all of the displacement transfer and lateral displacement-gradient related deformation, and rock outside the relay ramp is displaced but not tilted or internally deformed related to the lateral fault displacement gradients (e.g., Figure 4-22f). The Daisyhill relay ramp (Figure 6 in Huggins, et al., 1995) is close to the ideal relay ramp geometry. The two bounding

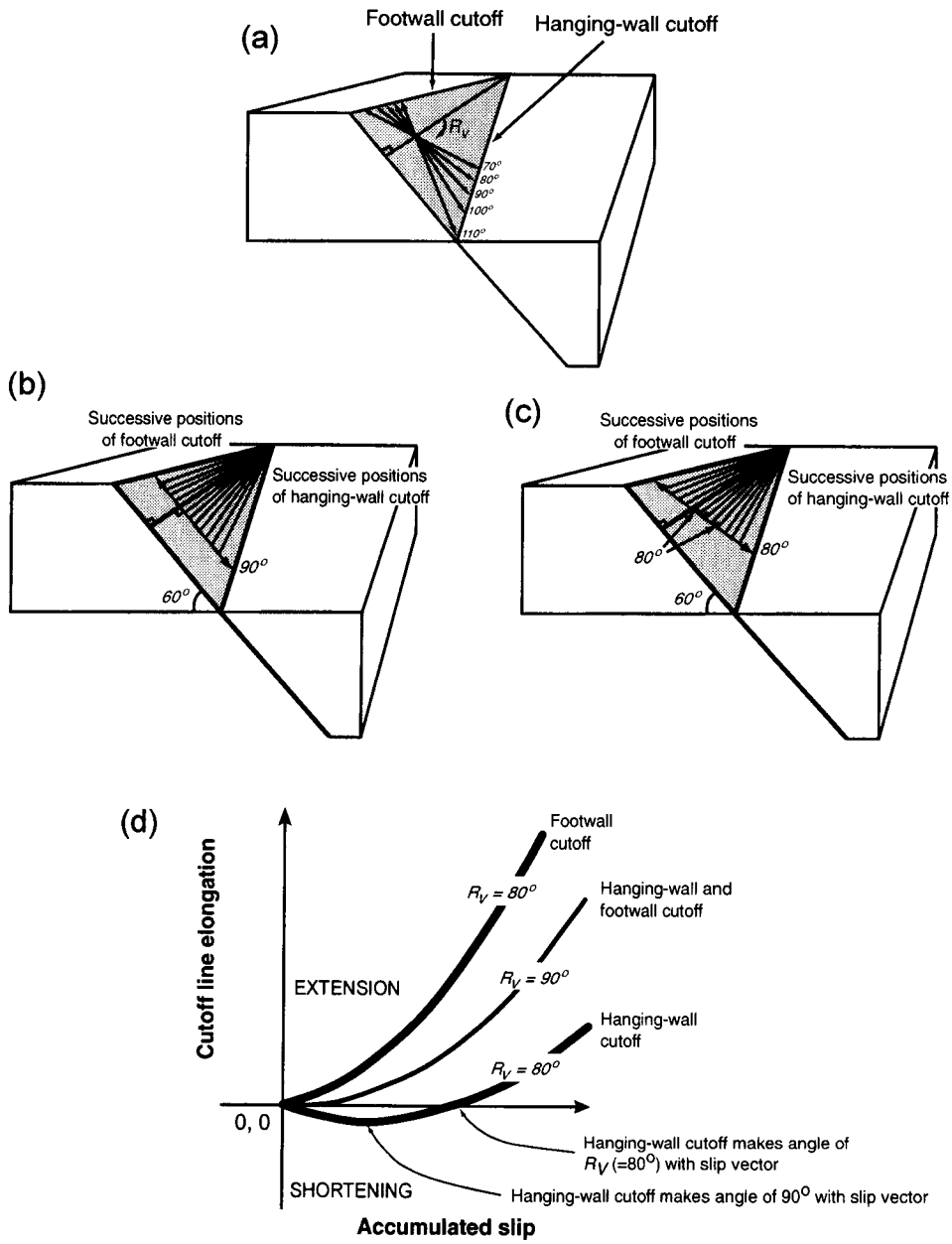

Figure 4-23. Effects of Slip Direction on Normal Faults. (a) Block Diagrams Illustrating the Opposing Influences of Oblique Slip on Hanging-Wall and Footwall Cutoffs. (b) Block Diagram Illustrating Displacement History of Hanging-Wall and Footwall Cutoffs Displaced along a Dip-Slip Vector (R_V = 90°). (c) Block Diagram Illustrating Displacement History of Corresponding Hanging-Wall and Footwall Cutoffs Displaced along a Slip Vector with an 80° Rake. (d) Graph of Cutoff Line Elongation Versus Cumulative Slip Illustrates the Progressive Elongation of Hanging-Wall and Footwall Cutoffs. Given the Sense of Oblique Slip, the Hanging-Wall Cutoff Undergoes Shortening during Early Displacement Until the Cutoff Line Reaches Perpendicularly with the Slip Vector, and Extension during Later Displacement. In Contrast, the Footwall Cutoff Experiences Extension throughout Its Deformation History.

faults overlap, but their displacement gradients are not exactly complementary, thus the ramp dips obliquely basinward. Footwall cutoffs and hanging-wall cutoffs of the two bounding faults have essentially the same elevations immediately adjacent to the ramp, and the ramp has transferred all the cumulative displacement imbalance between the two faults by means of its oblique dip (about 5°). Even in the ramp-bounding fault segments of the Daisyhill ramp, displacement gradients on the bounding faults are extremely low, on the order of 0.07. Cutoff-parallel extension is commensurately low, about 0.4 percent, and this level is consistent with the lack of mapped extension features in the ramp.

4.6.5.1 Alternative Deformation Paths

As is the case for many geologic structures, the final geometry of a structure is not necessarily indicative of a unique deformation path. In the case of a relay ramp, for example, the relay ramp has a geometry that is consistent with the displacement gradients on the two bounding faults. Faults may grow in a self-similar fashion (Figure 4-24a), whereby the displacement to length ratio is consistent early in the development of the faults, and fault tip displacement gradients are constant throughout the fault development until faults connect by relay ramp breaching. In this simple conceptual model, the overlap to separation ratio will continue to increase until the relay ramp is breached. However, along an alternative deformation path, the bounding faults may propagate to their overlapping configuration rapidly, early in their development. Arrested propagation, but continued displacement, leads to increasing displacement to length ratio (Figure 4-24b). In that case, the final overlap to separation ratio is produced early in the relay ramp development, then displacement produces increased tilting, vertical axis rotation, and internal deformation. A third possible case of relay ramp evolution may develop where fault tip propagation is arrested while the fault continues to accumulate displacement, which is then followed by a period of rapid fault tip propagation (Figure 4-24c). In this third case, the displacement to length ratio will decrease with time. Fault propagation may proceed by one or a combination of the processes illustrated in Figures 4-24b and 4-24c, which over time could produce the same geometry as self-similar propagation (Figure 4-24a). However, depending on the magnitudes of fault-cutoff parallel elongation generated by displacement gradients at the propagating fault tips, permanent deformation by faulting may develop in the displacement transfer zone. Therefore, faults developed within a relay ramp or displacement transfer system during its progressive development may have orientations oblique or perpendicular to the bounding faults, depending on the evolutionary history. Deformation path depends on position on the controlling faults, shape and displacement patterns of fault planes, and other factors such as lithology and deformation conditions (e.g., Huggins, et al. 1995).

4.6.5.2 Evolution of a Conceptualized Relay Ramp

The displacement gradient along a fault generally increases toward its tips (Figure 2 in Dawers, et al., 1993; Figure 11 in Scholz, et al., 1993; Figure 4 in Trudgill and Cartwright, 1994; Figure 5 in Dawers and Anders, 1995; Figure 3 in Huggins, et al., 1995; Figure 3 in Cartwright and Mansfield, 1998; Figure 2e in Ferrill, et al., 1999a; Figure 5 in Moore and Schultz, 1999). Thus, two fault tips propagating past each other will generate a deformation front characterized by steep dips that will sweep through the relay zone. Depending on the history of the ideal relay ramp geometry (Figures 4-21d, 4-22f, 4-25a,b,c,d), a dipping panel may develop that is initially oblique to the strike of the bounding faults (pre-overlap situation). The relay-ramp dip in

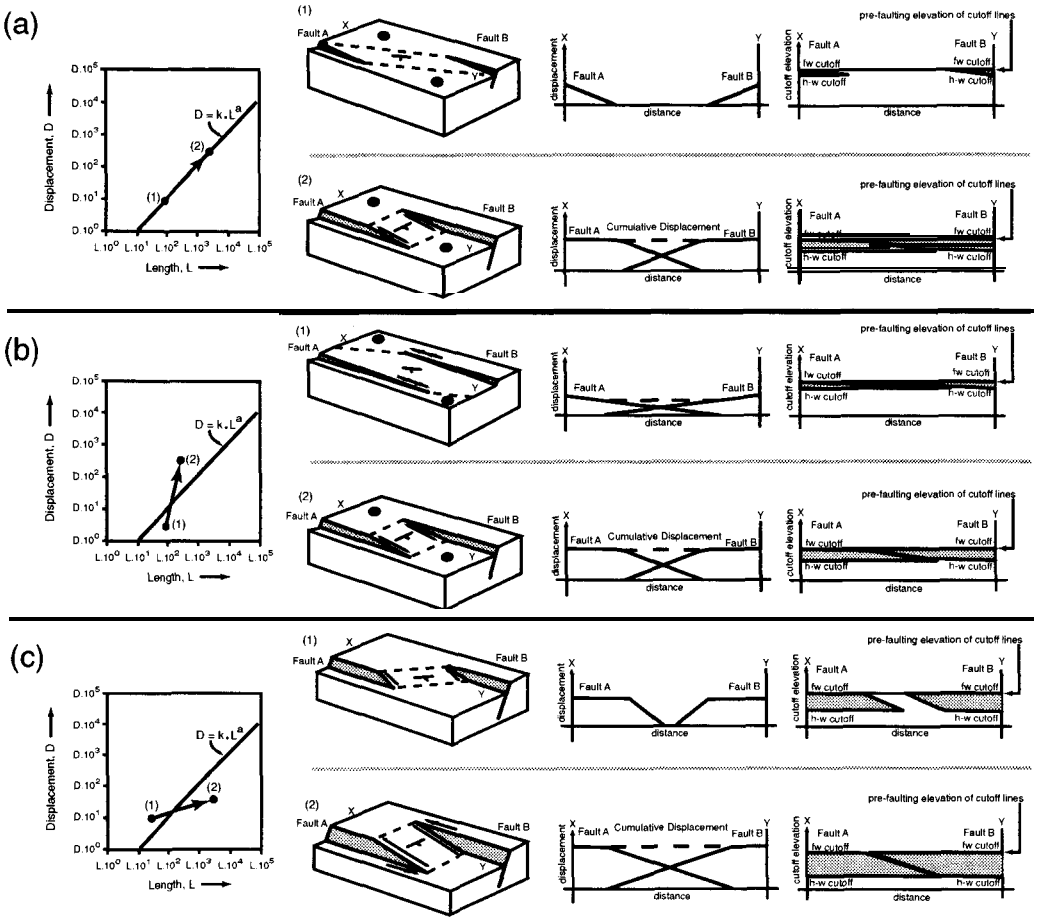

Figure 4-24. Block Diagrams Illustrating Influence of Fault Propagation and Displacement Gradient Development on the Function of Relay Ramps. (a) Self-Similar Fault Tip Propagation and No Change in Displacement Gradients with Time. (b) Rapid Fault Tip Propagation and Overlap Development Produces a Low Displacement Gradient Early in Fault Development. This Stage is Followed by Arrested Propagation and Displacement Accumulation, Producing an Increase in Displacement Gradient. (c) Arrested Fault Tip Propagation Produces a High Displacement Gradient That is Followed by a Period of Rapid Fault Tip Propagation and Decrease in Fault Tip Displacement Gradient. See Legend in Figure 4-22 for Explanation of Symbols. The Diagonal Lines on Graphs of Displacement (D) Versus Length (L) Represent Proportionality between the Two Parameters, Dependent on Constants k and a (see Dawers and Anders, 1995).

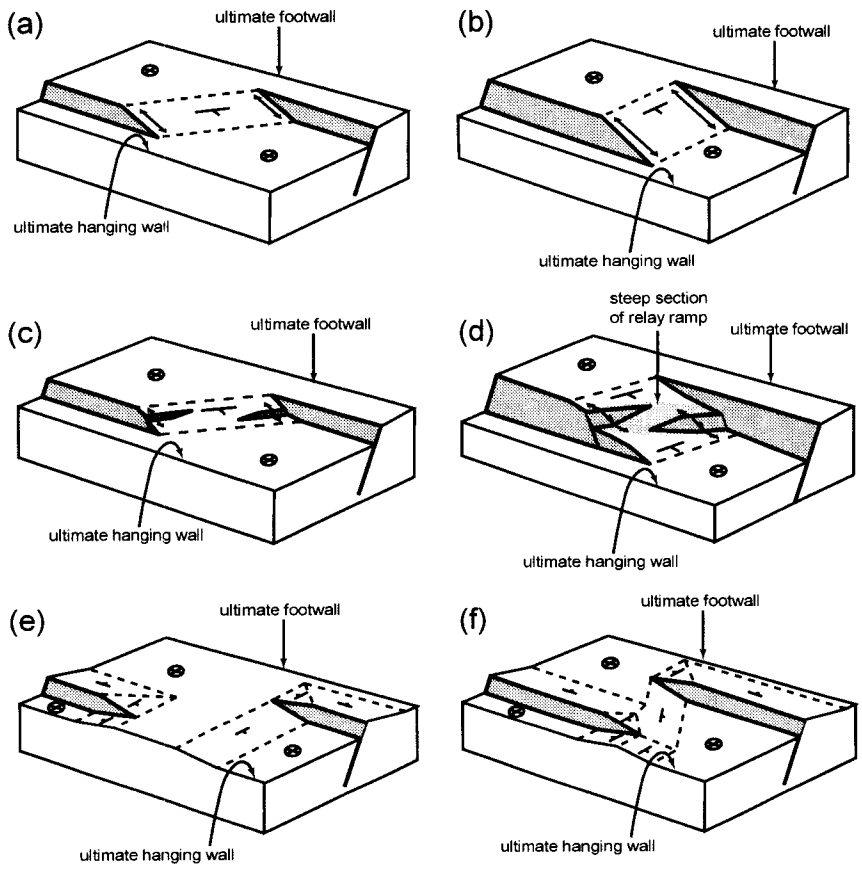

Figure 4-25. Block Diagrams Illustrating the Influence of Relative Footwall Uplift and Hanging Wall Subsidence on the Evolution of Deformation at Underlapping and Overlapping Fault Tips. (a) Pre-Overlap Situation with Ideal Relay Ramp Geometry. An Oblique Dip Panel Develops Linking the Tip Regions of the Bounding Faults. (b) Overlap Situation with Ideal Relay Ramp Geometry. The Dipping Panel Evolves to Geometry Where the Dip Direction is Parallel to the Bounding Fault Cutoffs. (c) Pre-Overlap Situation with Ideal Relay Ramp Geometry and Steep Displacement Gradients in the Tip Regions of the Bounding Faults. An Oblique Dip Panel Develops, Linking the Tip Regions of the Bounding Faults. In this Case, However, the Displacement Gradients that Produced Oblique Dip Panel Are Sufficient to Initiate Formation of Oblique Faults within the Relay Ramp Before the Bounding Faults Have Reached Overlap. (d) Overlap Situation with Ideal Relay Ramp Geometry and Steep Displacement Gradients in the Tip Regions of the Bounding Faults. The Bounding Faults Continue to Propagate and Extension Directions within the Ramp Region Rotate Closer to Parallelism with the Bounding Faults. This Extension, However, Can Be Accommodated by Oblique Slip on Faults Formed at an Earlier Stage in the Ramp's Evolution. This Leads to the Formation of an Oblique Steep Section of the Ramp, Which Contains a High Concentration of Faults and is Likely to Become the Locus of a Ramp-Breaching Fault System. (e) Pre-Overlap Situation Where the Ultimate Hanging Wall and Footwall Deform by Hanging Wall Subsidence and Footwall Uplift. (f) Overlap Situation Where the Ultimate Hanging Wall and Footwall Deform by Hanging Wall Subsidence and Footwall Uplift. See Legend in Figure 4-22 for Explanation of Symbols.

the ideal case evolves to parallelism with the strike of the bounding faults (Figure 4-25a,b) as fault overlap develops. The dip of this panel, and hence the extension it experiences, depends upon the displacement gradients and dips of the bounding faults. In cases where the bounding faults have steep displacement gradients near their tips, the obliquely dipping panel may experience sufficient extension to induce fracturing and faulting prior to full development of fault overlap (Figure 4-25c). As overlap continues to develop, and the ramp extension direction rotates into parallelism with the strike of the bounding faults, the early formed faults will continue to be well oriented to accommodate extension by oblique slip, obviating the need for new faults to form and suppressing steeper dips in the ramp as a whole (Figure 4-25d). Thus relay-ramp-breaching faults may be inherited from pre-overlap interaction between the principal bounding faults, and are likely to be oblique to the final ramp orientation.

In the ideal relay ramp, the ultimate footwall and hanging-wall cutoffs (cutoff segments that do not immediately bound the relay ramp) attain essentially uniform elevations, and the relay ramp transfers all displacement between the faults. Such structures are common in nature and are well documented as examples of relay ramps (e.g., Figure 4 in Dawers and Anders, 1995; Figure 6 in Huggins, et al., 1995). However, as illustrated in Section 4.6.4, the ultimate hanging-wall and footwall cutoffs may also be deflected, which modifies the pattern of dipping panels associated with the propagating tips of the bounding faults (Figure 4-25e,f).

4.6.6 Examples from Yucca Mountain, Nevada

4.6.6.1 Background

The Yucca Mountain fault system has been mapped in detail by Scott (1990), Simonds, et al. (1995), and Day, et al. (1998a,b). Extensional deformation has occurred in an evolving regional stress field, from east-west extension prior to 10 million years ago, to west northwest-east southeast extension after 10 million years ago (Zoback, et al., 1981; Morris, et al., 1996; Ferrill, et al., 1999b). Day, et al. (1998a) identified important relay structures at Yucca Mountain that consist of normal and oblique slip faults both within and cutting (breaching) relay ramps, curved fault tips bounding relay ramps, and right-lateral, strike-slip faults. Ferrill, et al. (1999a) interpreted several of the bends in major faults to be corrugations introduced by fault linkage resulting from the breaching of former relay ramp structures (see Figure 4-26a,b for relay structures at Yucca Mountain described in text).

In the context of the geometric models of fault block deformation presented here, there are numerous geometric structural relationships at Yucca Mountain that may indicate hanging wall, footwall, or relay ramp deformation related to fault displacement gradients. One prominent case is the West Ridge-connecting fault system that consists of several northwest-trending extensional faults that connect the Northern Windy Wash and Fatigue Wash faults across West Ridge (see Figure 4-26a,b, Position 1). Note the pronounced deflection of the fault cutoffs that define the edges of West Ridge where the connecting fault system cuts the ridge (Figure 4-26b).

Larger scale but more gentle fault-cutoff deflections are seen associated with the Boomerang Point and Solitario Canyon faults (Positions 2 and 3, Figure 4-26a,b). Although the dominant deflection appears to be in the hanging wall of each of these faults, the footwall of the Solitario Canyon fault is bowed upward in the proposed repository location along Yucca Crest. This

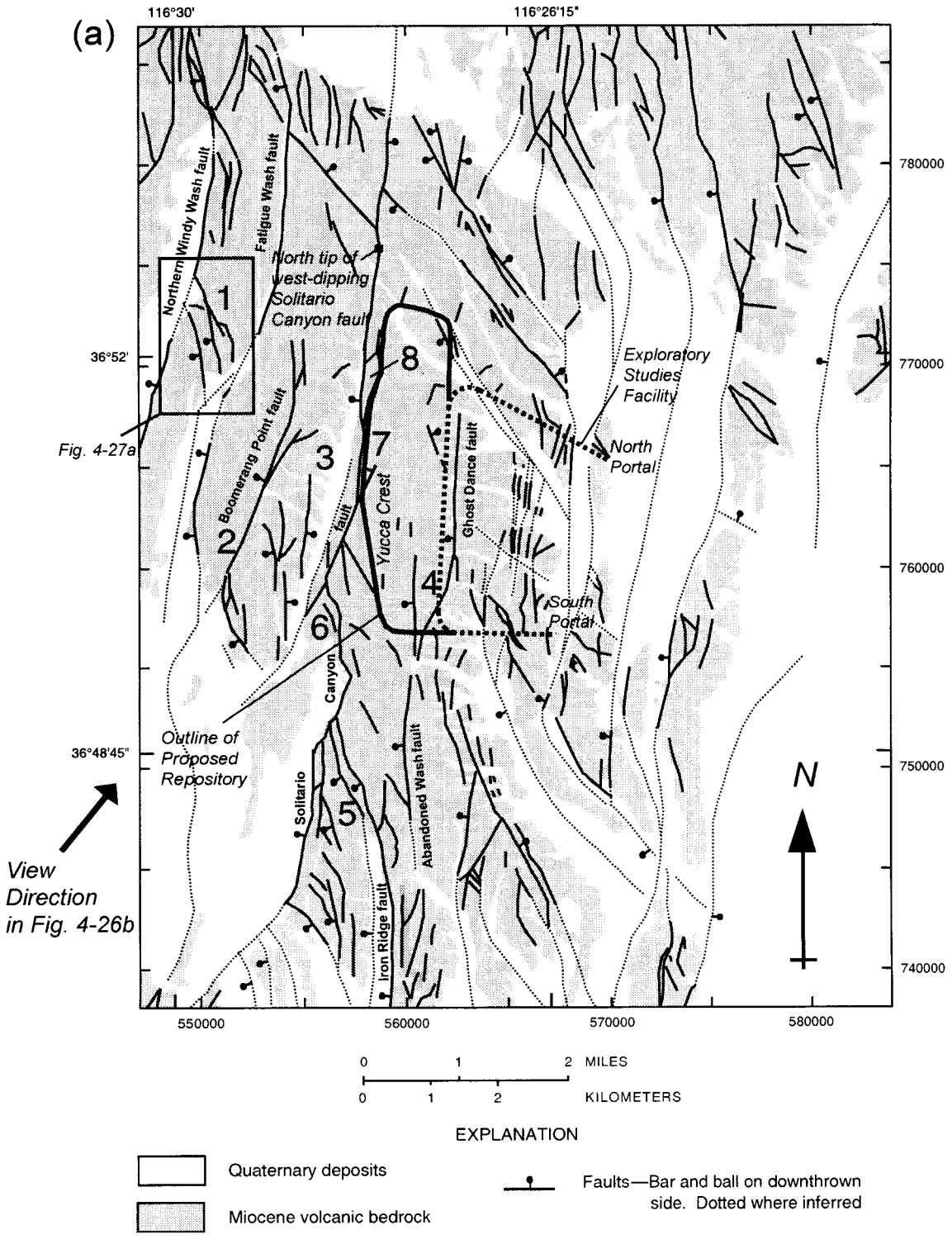

Figure 4-26. Map and Oblique View of Yucca Mountain Faults. (a) Map of Yucca Mountain Faults after Day, et al. (1998a). Annotations Indicate Positions of Potential Footwall, Hanging Wall, and Relay Ramp (Combined Hanging Wall and Footwall) Deformation.

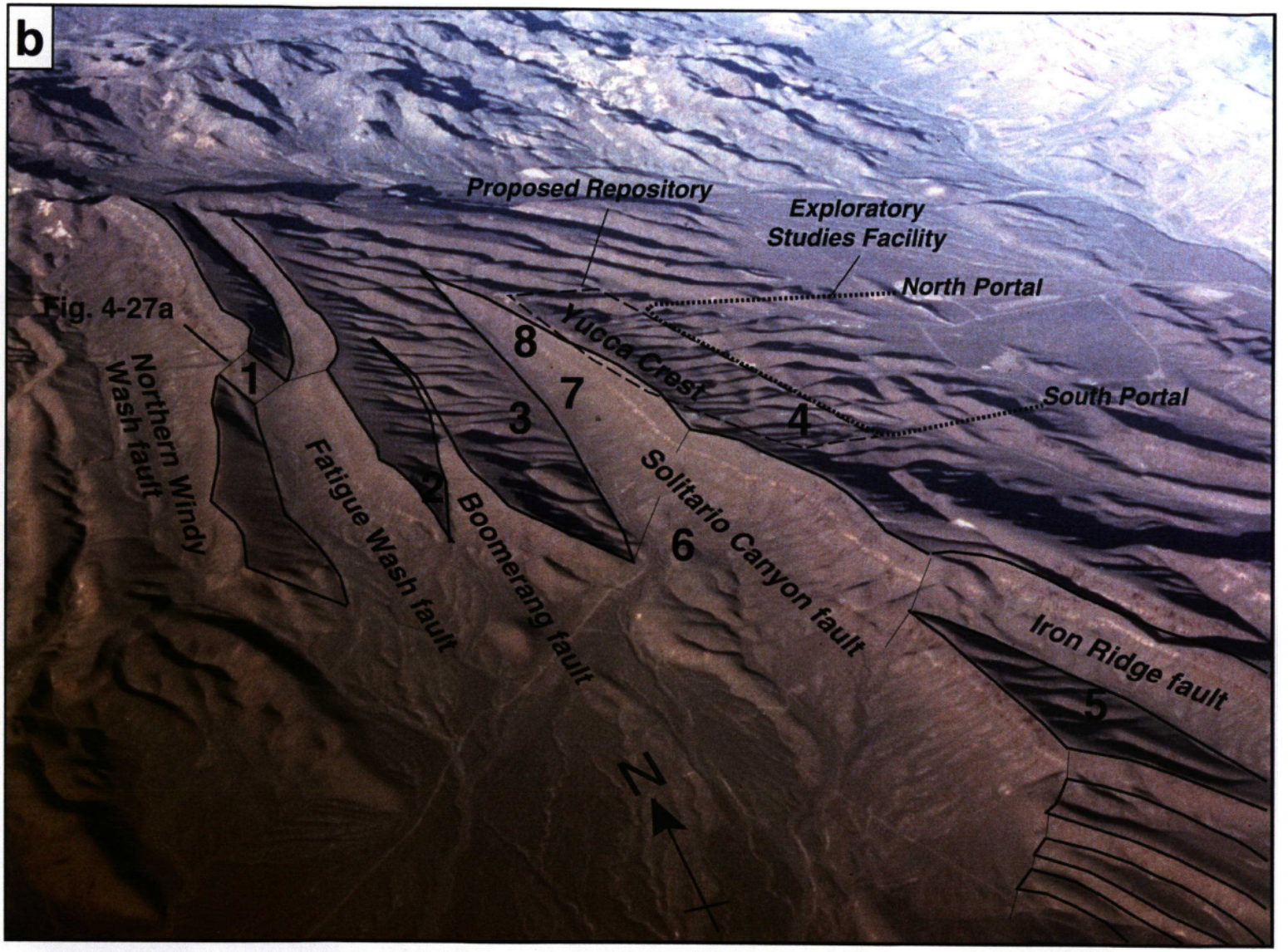

Figure 4-26 (continued). (b) Oblique Aerial Photograph Looking Northeastward across Western Yucca Mountain, Nevada. The Exploratory Studies Facility is a 7.8-km Long, 7.6-m Diameter Tunnel through Yucca Mountain.

footwall bowing can be seen in a three-dimensional structural horizon display (Figure 3a in Ferrill, et al., 1999b). Also within the proposed repository location is an apparent displacement transfer zone (breached relay ramp) between the Ghost Dance and Abandoned Wash faults (Position 4, Figure 4-26a,b).

At least four breached relay ramps along the Solitario Canyon fault (Figure 4-26a,b) are interpreted. The largest of these is the Solitario Canyon–Iron Ridge breached relay ramp (see Position 5, Figure 4-26a,b). This ramp contains numerous northwest-trending faults that, like the connecting fault system in West Ridge, are associated with pronounced deflection of the bounding cutoff lines (also see Figure 3 in Ferrill, et al., 1999a). The next potential breached relay ramp to the north, based on mapped fault relationships and a pronounced footwall corrugation is at Position 6 (Figure 4-26a,b). The authors interpret that the breakthrough of this ramp occurred by curved lateral fault propagation along the footwall trace, leaving the breached relay ramp attached to the hanging wall block. Two more potential breached relay ramps along the Solitario Canyon fault are associated with the two north-northeast-trending splays of the Solitario Canyon fault that extend into the footwall of the main fault, and the northern tip of the Solitario Canyon fault (Positions 7 and 8, Figure 4-26a,b). The two north-northeast-trending splays of the Solitario Canyon fault may be relict tips of original fault segments that have since been connected by the formation of connecting fault systems. Relict relay ramp segments in the footwall in this case would have corresponding breached ramp segments in the hanging wall.

4.6.6.2 West Ridge Connecting Fault System, Yucca Mountain, Nevada

Here the authors analyze the well-defined displacement transfer system between the Northern Windy Wash and Fatigue Wash faults (Position 1, Figure 4-26a,b). The displacement transfer system is a narrow fault system (~500 m wide) that transfers displacement between two faults that overlap for a distance of about 10 km. Although not a classical relay ramp occupying the complete overlap between two fault tips, the displacement transfer system may have initiated during an earlier stage of development with less overlap. Using the geometrical model outlined in this report, the strain in the ramp was estimated and compared with observed structures. The map of Day, et al. (1998a) is the primary data source (Figure 4-27a). Structure contours are drawn for the top of the vitric zone of the crystal-poor member of the Tiva Canyon Tuff. All strikes and dips are given using the right-hand rule, and an average fault dip of 70° is used based on measurements of Day, et al. (1998a). Fault throw versus distance, and cutoff elevation versus distance graphs (Figure 4-27b,c) were drawn using data extracted from the DOE Geologic Framework Model (CRWMS M&O, 1999) combined with data from the Day, et al. (1998a) map.

The Northern Windy Wash and Fatigue Wash faults have slightly different orientations (198/70 and 207/70, respectively). Structure contours reveal a northeast-southwest-trending, gently southeast-dipping homocline (037/09) with a strike oblique to both faults (Figure 4-27a). Between the two major faults is a rhomb-shaped panel trending approximately north-northwest-south-southeast that contains a system of relatively small, predominantly west-dipping extensional faults. This system of faults has displaced the otherwise homoclinal fault block down to the southwest (Day, et al., 1998a). The elevation of the top of the Tiva Canyon Tuff crystal-poor vitric zone northeast of this panel is consistently 152 m higher than

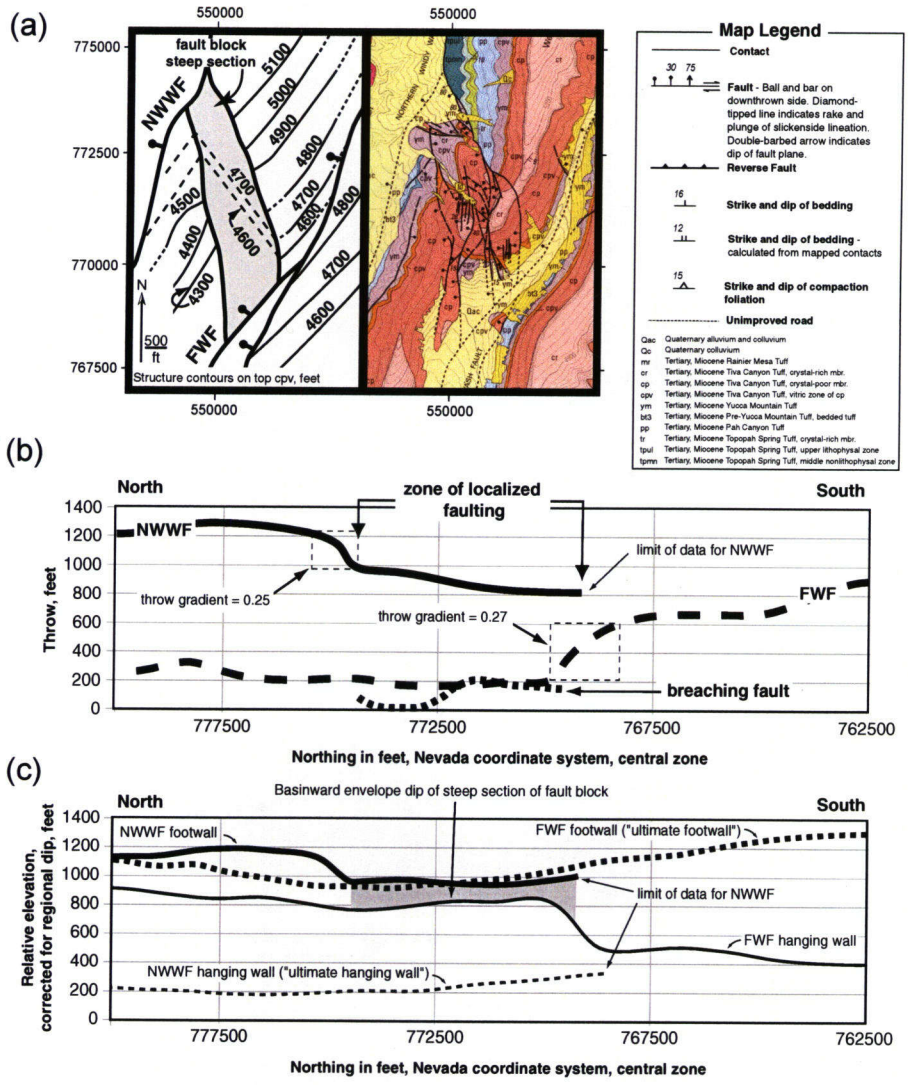

Figure 4-27. The Northern Windy Wash Fault–Fatigue Wash Fault Displacement Transfer System. (a) Extract from the Geologic Map of Day, et al. (1998b) (Right) with the Interpreted Structure Contours for the Top of Tiva Canyon Tuff Crystal-Poor Vitric Zone (Left). (b) Throw Versus Distance Graph for the Northern Windy Wash Fault, Fatigue Wash Fault, and the Breaching Faults. Note the Very High Throw Gradients on the Bounding Faults (Northern Windy Wash Fault and Fatigue Wash Fault) at the Margins of the Ramp Steep Section. These May Partially Represent Fossilized Fault Tip Throw Gradients for these Faults. These Gradients May Have Generated the High Strains within the Oblique Ramp Steep Section, Which, in Turn, Fixed the Location of the Ramp-Breaching Fault(s). (c) Fault Cutoff Elevation Versus Distance Graph for the Northern Windy Wash Fault and Fatigue Wash Fault. The North-to-South Component of the Regional Dip has been Removed by Rotation. The Ultimate Footwall and Hanging-Wall Cutoffs Follow the Same Trend through the Graph, Whereas the Cutoffs that Bound the Steep Section of the Fault Block Show Marked Deflections. The Mismatch in Elevation between the Ramp-Bounding Cutoffs Reflects the Oblique Basinward Dip of the Steep Section of the Fault Block (See Also Figure 6c in Huggins, et al., 1995).

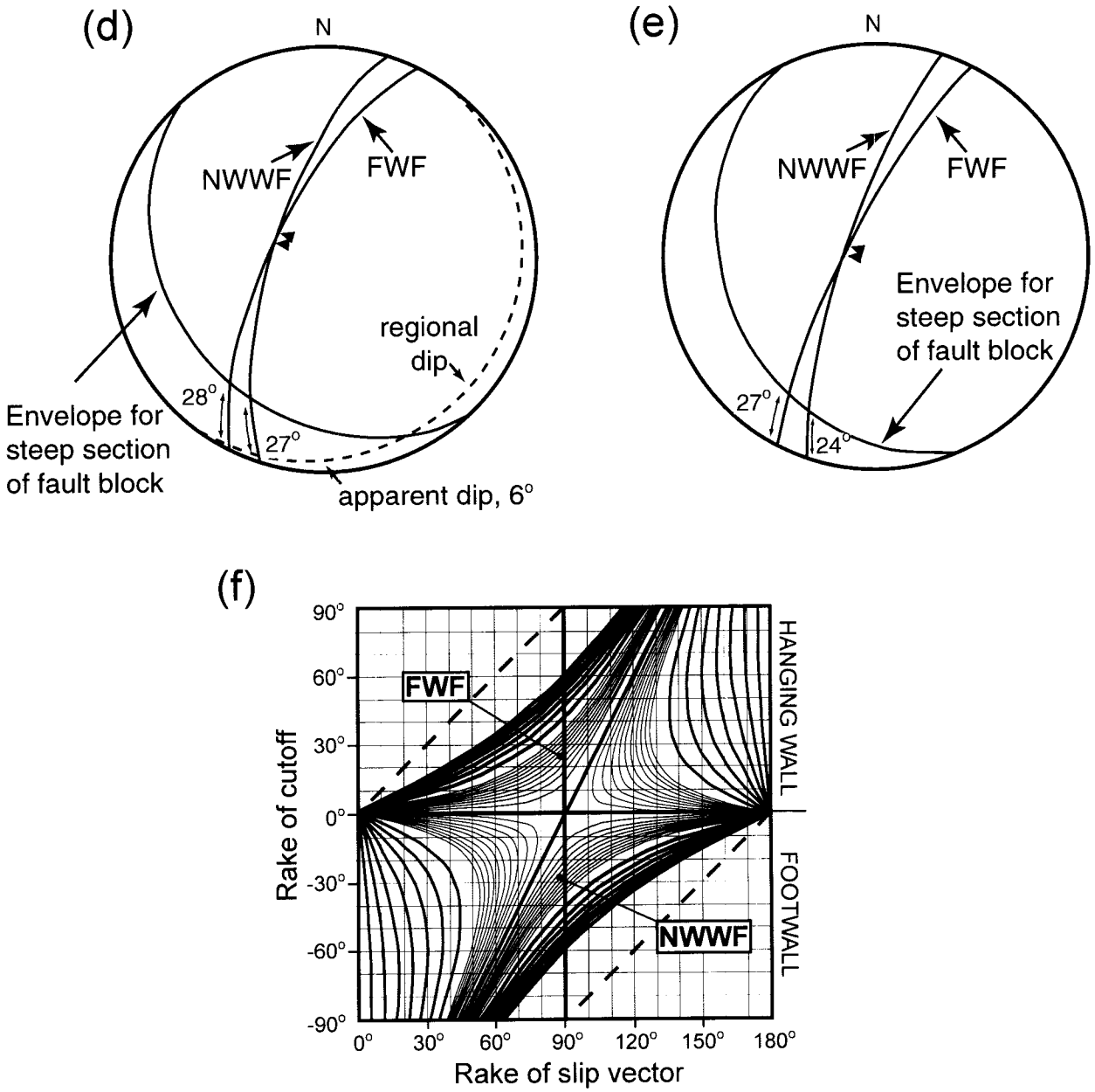

Figure 4-27 (continued). (d) Lower Hemisphere, Equal Area Projection of the Geometric Elements of the Fault-Block Steep Section in Present-Day Coordinates. (e) Lower Hemisphere, Equal Area Projection of the Geometric Elements of the Envelope of the Steep Section of the Fault Block, Corrected for the Regional Dip. (f) Reference Plot (Figure 4-20) to Show How the Bounding Cutoffs of the Ramp Steep Section Can Be Used to Determine Cutoff-Parallel Elongation. Fatigue Wash Fault—Hanging Wall-Cutoff Against the Fatigue Wash Fault. The Rake of the Slip Vector is 89° and the Rake of the Cutoff is 24°. This Yields an Elongation of 10 Percent. Northern Windy Wash Fault—Footwall Cutoff Against the Northern Windy Wash Fault. The Rake of the Slip Vector is 87°, and the Rake of the Cutoff is -27°. This Yields an Elongation of 10 Percent.

southwest of the panel (along bounding fault strike). This panel is referred to here as the steep section of the fault block.

Both the Northern Windy Wash and Fatigue Wash faults exhibit extremely steep throw gradients (0.25 for the Northern Windy Wash fault and 0.27 for the Fatigue Wash fault) at the steep section of the fault block. In the cutoff elevation graph shown in Figure 4-27c, the north-south component of the regional dip has been removed from the graph by rotating the graph 6° counterclockwise. Both bounding cutoff lines of the steep section of the fault block (Northern Windy Wash fault footwall and Fatigue Wash fault hanging wall) are strongly deflected, whereas the ultimate footwall and hanging wall show little deviation associated with the presence of the relay ramp (Figure 4-27c). This deflection pattern illustrates that all displacement transfer is accomplished in a narrow region, defined by the steep section of the fault block.

This displacement transfer system is interpreted to have evolved similarly to the sequence schematically illustrated by Figure 4-25c,d. The fault block steep section represents the location at which elongations were sufficient to produce faulting, and may reflect the geometry of an obliquely dipping panel prior to overlap of the two bounding faults. The elevation change across the steep section and its trend give an average orientation for an envelope surface representing layering in the section of 140/27. Using a stereonet (Figure 4-27d), the rake of the cutoff lines on the two bounding faults can be obtained: 28° in the Fatigue Wash fault and 27° in the Northern Windy Wash fault. Most of the slickenline measurements for the two bounding faults in the vicinity of this displacement transfer system indicate true dip-slip and therefore the rake of the slip vector is 90°. However, because the regional strike is oblique to the strikes of the bounding faults and the geometrical model depends on the angular difference between cutoffs in the fault plane, it is necessary to correct for the regional dip (Figure 4-27e). The corrected values of the rake of the envelope cutoff lines in the two bounding faults are 24° in the Fatigue Wash fault and 27° in the Northern Windy Wash fault. The corrected values for the rakes of the slip vectors are 89° in the Fatigue Wash fault and 87° in the Northern Windy Wash fault. The estimated extension of the envelope cutoff along the Fatigue Wash fault is 10 percent and along the Northern Windy Wash fault, 10 percent (Figure 4-27f). These extensions are sufficient to generate faulting in the development transfer zone.

4.6.6.3 Solitario Canyon Fault Footwall

Cutoff-parallel elongations are not confined to relay structures and are to be expected wherever there is a displacement gradient along a fault. Finite, cutoff-parallel elongations may be small, but the propagation of a fault tip and its associated deformation front may generate incremental and progressive elongations that are sufficient to fracture rock. Although footwall uplift along the larger faults at Yucca Mountain is not extreme, it is nevertheless present, including along Yucca Crest (Figure 4-26b). The footwall of the Solitario Canyon fault is bowed upward along Yucca Crest by 30.5 m along a strike distance of 6 km yielding an expected finite elongation of 0.006 percent. However, maximum footwall elevation gradients along the Solitario Canyon fault are of the order of 0.07, yielding a local elongation of approximately 0.02 percent. During propagation of the fault, similar steeper throw gradients would have swept through the footwall adjacent to the fault and therefore they influence a large rock volume. The footwall of the Solitario Canyon fault includes the entire proposed repository volume.

Maximum throw gradients along the Solitario Canyon fault are on the order of 0.24. The lack of major footwall deflection, associated with the large throw gradients, implies that much of the cutoff-parallel elongation that accompanied fault propagation was partitioned into the hanging wall of the fault. Therefore, the rocks in the hanging wall block, buried beneath alluvium in Solitario Canyon, likely exhibit higher fracture (fault or joint) densities than the footwall. Similar analyses can be made for all the major faults in the Yucca Mountain area.

Analyses of extension associated with displacement gradients on the largest normal faults at Yucca Mountain may in time help to explain fracture orientations (e.g., east-west and northwest-southeast) that are not consistent with the evolution of the regional stress field (see, for example, Crider and Pollard, 1998). In addition to influencing the orientations of tectonic fractures at Yucca Mountain, it is anticipated that relay ramps, and other deflected hanging wall and footwall blocks associated with lateral fault displacement gradients, are likely to be locations of enhanced fracture intensity. In the fractured welded tuff strata of Yucca Mountain, fracture intensity is a key factor that influences repository performance related issues such as (i) unsaturated and saturated zone water conductivity; (ii) the locations of fast pathways for infiltration, percolation, and flow; (iii) rock quality; and (iv) related tunnel stability.

4.6.6.4 Preliminary Analysis of Cutoff Elongations for Yucca Mountain Fault System

The method for estimating cutoff elongation described previously was applied to faults at Yucca Mountain. Fault cutoff lines for the proposed Repository host horizon were extracted from the Geologic Framework Model 3.1 (CRWMS M&O, 1999). These lines were then imported into 3DStress™ and examined in a simulated Miocene stress field (Figure 4-28), the time during which the faults were initiated. The computed slip vectors for (each small section of) the fault surfaces were used as input for the cutoff elongation model. Cutoff lines were calculated directly from the input data. Using the assumption that the tuff beds were initially horizontal, the elongation for each cutoff segment was calculated, and the cutoff line was colored according to the computed elongation (Figure 4-28). Areas of high extensional strain are predicted by the model at a number of locations, most notably (i) between the Northern Windy Wash and Fatigue Wash faults, (ii) between the Solitario Canyon and Iron Ridge faults, and (iii) the fault blocks between the Fatigue Wash and Solitario Canyon faults (Figure 4-28). This analysis is preliminary and should be continued using different stress fields and different initial tuff orientations. Strain magnitudes predicted by this model are sufficient to be manifest by fractures and faults. Predictions of the model should be field-checked because they represent a method by which fracture and small fault populations can be estimated in areas that have not been directly characterized.

4.6.7 Summary

All fault systems contain faults with lateral (along strike) displacement gradients. A geometrical model was developed for normal fault-block internal deformation related to fault displacement gradients that result in increasing fault cutoff-parallel extension with increasing normal fault displacement gradients (Ferrill and Morris, 2001). Oblique slip directions and convergent or divergent slip directions within a fault array may lead to reduced or enhanced local extension with respect to extension anticipated from an array of parallel dip-slip normal faults.

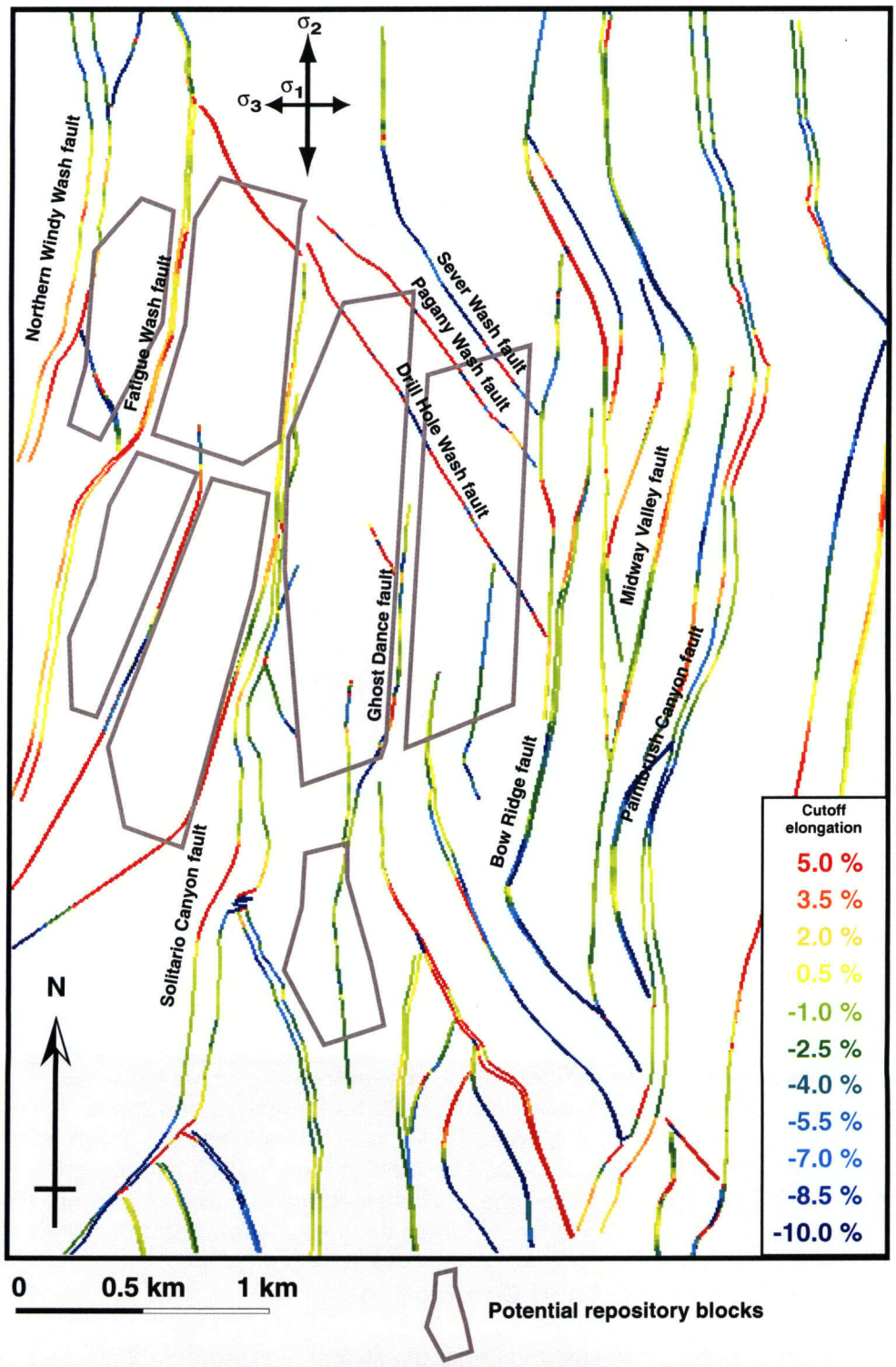

Figure 4-28. Fault Cutoff Elongations for Repository Host Horizon at Yucca Mountain Extracted from Geologic Framework Model 3.1 (CRWMS M&O, 1999). Effective Stresses Used are: σ_1 = Vertical, 20 MPa; σ_2 = Azimuth 180, 18 MPa; σ_3 = Azimuth 090, 10 MPa.

In the context of the geometric models of fault block deformation presented in this report, there are numerous structural relationships at Yucca Mountain, Nevada, that indicate localized deformation (e.g., zones of intense fracturing) related to fault displacement gradients. Deformation related to lateral fault displacement gradients may help to explain fracture orientations at Yucca Mountain that are not consistent with the evolution of the regional stress field. This analysis provides a conceptual basis for assessing the Yucca Mountain fracture framework, a key factor in the analysis of groundwater flow, tunnel stability, and possible future distributed deformation related to fault slip.

4.7 Contractional Faults at Yucca Mountain

Four reverse faults, with north-south or northeast-southwest strikes, have been identified and mapped at the surface at Yucca Mountain (Day, et al., 1998a,b). These faults occur in the upper part of the welded Tiva Canyon Tuff. Strike lengths have been mapped between 0.4 km and 1 km and displacements of tens of meters or less. Additional small-displacement reverse faults have been identified in the Exploratory Studies Facility and Enhanced Characterization of the Repository Block (Section 2.4 of this report). Although relatively few reverse faults have been identified at Yucca Mountain, they are potentially key features for constraining the kinematic history of faulting and fault block deformation within the mountain. These reverse faults also may be key infiltration and percolation pathways (Levy, et al., 1997). The reverse fault mapped within Diabolous Ridge (Figure 4-29a), which dips east-southeast, has been interpreted to be responsible for a bomb-pulse Cl-36 anomaly in the Exploratory Studies Facility. The other three reverse faults (Figure 4-29a), which dip east, are mapped in the vicinity of the South Portal of the Exploratory Studies Facility in Boundary Ridge (one fault) and Bow Ridge (two faults). Boundary Ridge is in the hanging wall of the Bow Ridge block bounding normal fault, and Bow Ridge is in the hanging wall of the Midway Valley block bounding normal fault. The reverse fault along the eastern edge of Boundary Ridge is depicted in cross section (Day, et al., 1998b) as gently dipping near the surface and steepening downward (Figure 4-29b).

Contractional structures in the pre-Tertiary strata in the Yucca Mountain region are easily understood in the context of tectonic evolution of the region, which experienced repeated contractional deformation prior to Tertiary time. The reverse faults mapped in the Tiva Canyon Tuff, however, are enigmatic in that there is no known regional east-west shortening event that could have produced the faults after tuff deposition (Zoback, et al., 1981; Morris, et al., 1996). Therefore, local structural interactions are considered to be the cause of the contractional faults in the Tiva Canyon Tuff. Here a model is presented that explains the origin of the reverse faults within an extensional fault system as a localized product of fault block impingement caused by fault shape and fault block rotation. This model is illustrated using a natural example from the Grabens area, south of Canyonlands National Park in southeast Utah (from Ferrill, et al., 2001).

4.7.1 Fault Block Impingement and Contraction

Slip of a rigid fault block along a broadly and continuously curved (listric) fault surface will produce fault block tilting, but may not require any additional deformation in proximity to the controlling fault. In contrast, slip of a rigid fault block above a listric normal fault that has a long, straight, steep segment encounters a space problem (geometric overlap) in the upper part of the hanging wall and footwall adjacent to the fault (Figure 4-30). This space problem does not

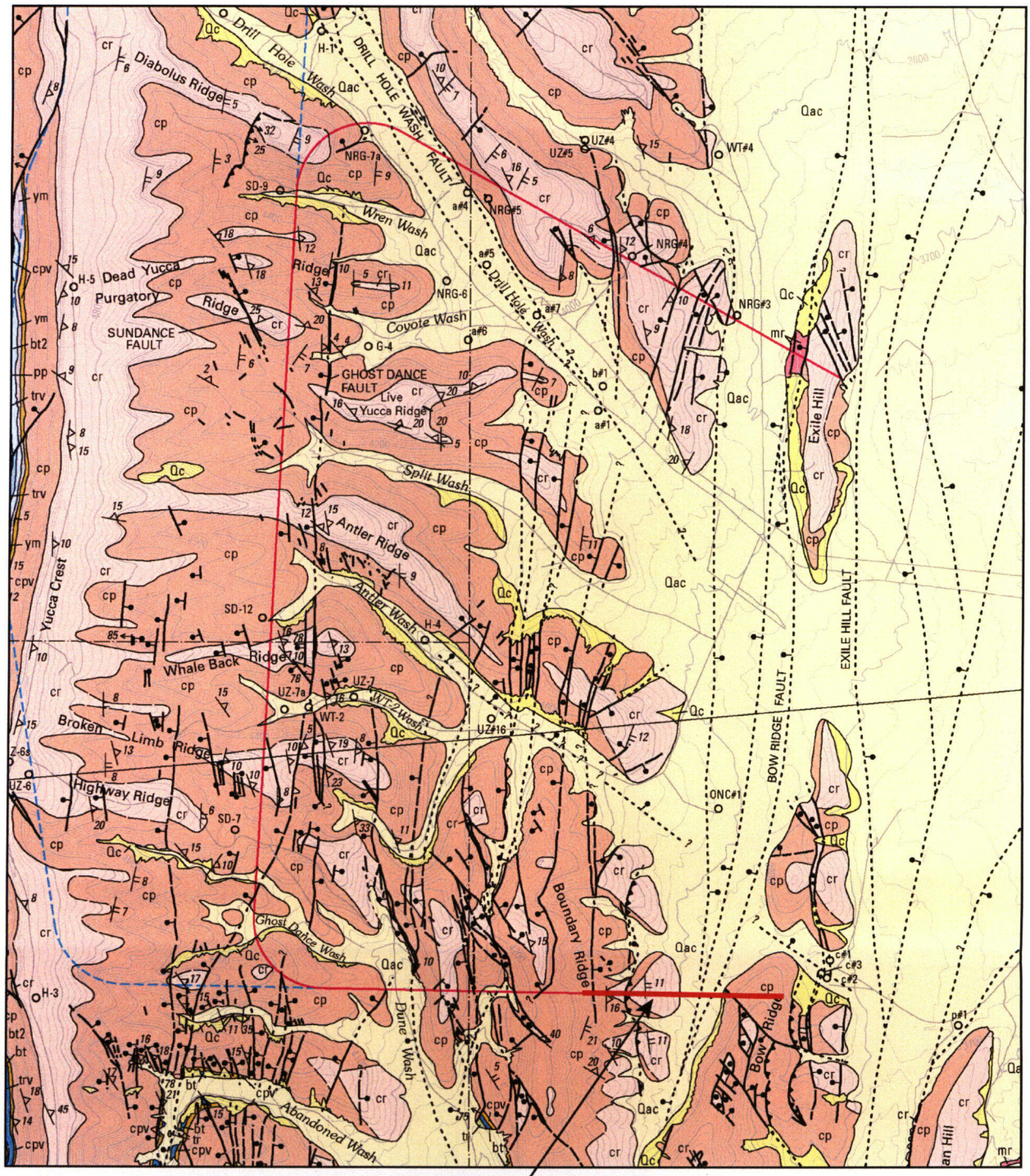

Figure 4-29. Local Contractional Faults at Yucca Mountain. (a) Geologic Map of Yucca Mountain, Nevada from Day, et al. (1998a) Shows Local Development of Contractional Faults

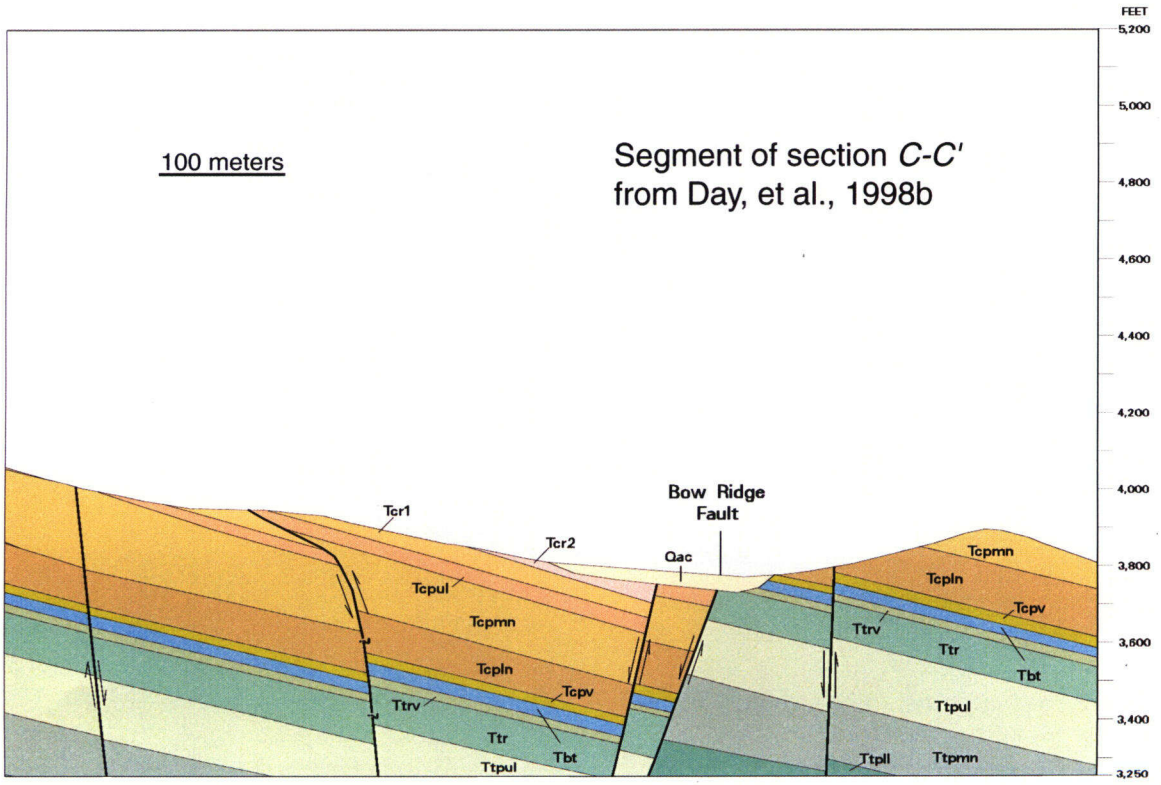

Figure 4-29 (continued). (b) Cross Section Illustrating a Reverse Fault in Profile (Day, et al., 1998b)

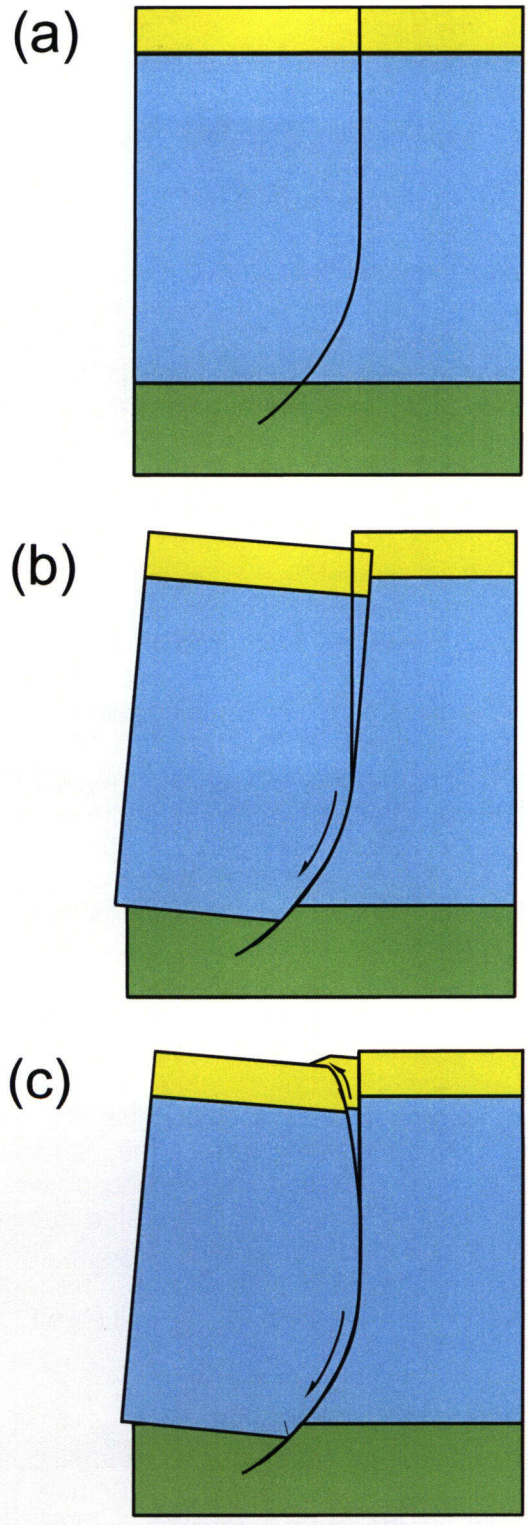

Figure 4-30. Schematic Illustration of Fault Block Impingement and Contraction

arise in geometric and kinematic models of nonrigid fault block deformation where fault blocks are assumed to deform by layer-parallel, inclined, or vertical shear (cf. Suppe, 1983; Dula, 1990; Ferrill and Morris, 1997; Morris and Ferrill, 1999). One mechanism for accommodating this space problem in a rigid block is by shortening and thickening layers adjacent to the fault, for example by thrust faulting in the hanging wall fault block where it impinges on the footwall (Figure 4-30).

4.7.2 Natural Analog—Bobby's Hole Fault (Utah)

The Grabens area is a region within and south of Canyonlands National Park that consists of an extensive network of valleys that are grabens and half grabens in Pennsylvanian and Permian sedimentary strata (McGill and Stromquist, 1979; Trudgill and Cartwright, 1994; Schultz and Moore, 1996; Cartwright and Mansfield, 1998; Moore and Schultz, 1999; McGill, et al., 2000). These structural basins formed in response to lateral unloading, caused by entrenchment and lateral erosion by the Colorado River in Cataract Canyon, and gliding down the gentle (~4°) regional dip to the west-northwest above the Pennsylvanian Paradox evaporites (McGill and Stromquist, 1979; Huntoon, et al., 1982; McGill, et al., 2000). Faults exposed at the surface are nearly vertical (e.g., McGill and Stromquist, 1979). Although Cartwright and Mansfield (1998) interpreted the faults as nearly vertical through the entire brittle plate, other workers have shown that the dip on at least some of the faults decreases from vertical at the surface to ~75° at a depth of 100 m, which persists to ~460 m depth (McGill, et al., 2000).

The Bobby's Hole fault is a near-vertical, northwest-dipping normal fault in the southeastern part of the Grabens area, south of Canyonlands National Park (Figure 4-31a). Hanging wall strata generally dip gently (4 to 15°) southeastward, toward the Bobby's Hole fault (Figure 4-31b). In a sandstone knob in the hanging wall (Figure 4-31) of the Bobby's Hole fault, layering adjacent to the fault dips to the northwest (5 to 37° northwest), synthetic to the Bobby's Hole fault (Figure 4-31b). A red sandstone layer in the hanging wall at this location is thickened and laterally contracted by two reverse faults. The contractional faults dip moderately (40 to 50° southeast) antithetic to the Bobby's Hole fault.

The reverse faults associated with the Bobby's Hole fault have the following characteristics; (i) restricted to hanging wall, (ii) only locally developed immediately adjacent to fault, (iii) adjacent to nearly vertical fault (with dip-parallel striations; Figure 4-31c) in antithetically dipping hanging wall block, and (iv) produce a synthetic dip panel in the hanging wall of the Bobby's Hole fault. The antithetic dip through most of the hanging wall is indicative of an upward steepening (listric) fault geometry. Based on these observations, the synthetic dip panel in the hanging wall of the Bobby's Hole fault is interpreted to be due to fault block impingement and contraction produced by slip on a listric Bobby's Hole fault, with a relatively long straight steep segment near the surface (Figure 4-32a). This fault block impingement and contraction locally produced reverse faults in the hanging wall (see Figure 4-32b).

4.7.3 Discussion

The principal condition that favors development of fault block impingement and contraction is the presence of a long steep section on a listric normal fault (Figure 4-30). Formation of a synthetic dip panel by hanging wall impingement is most likely to occur near the Earth's surface

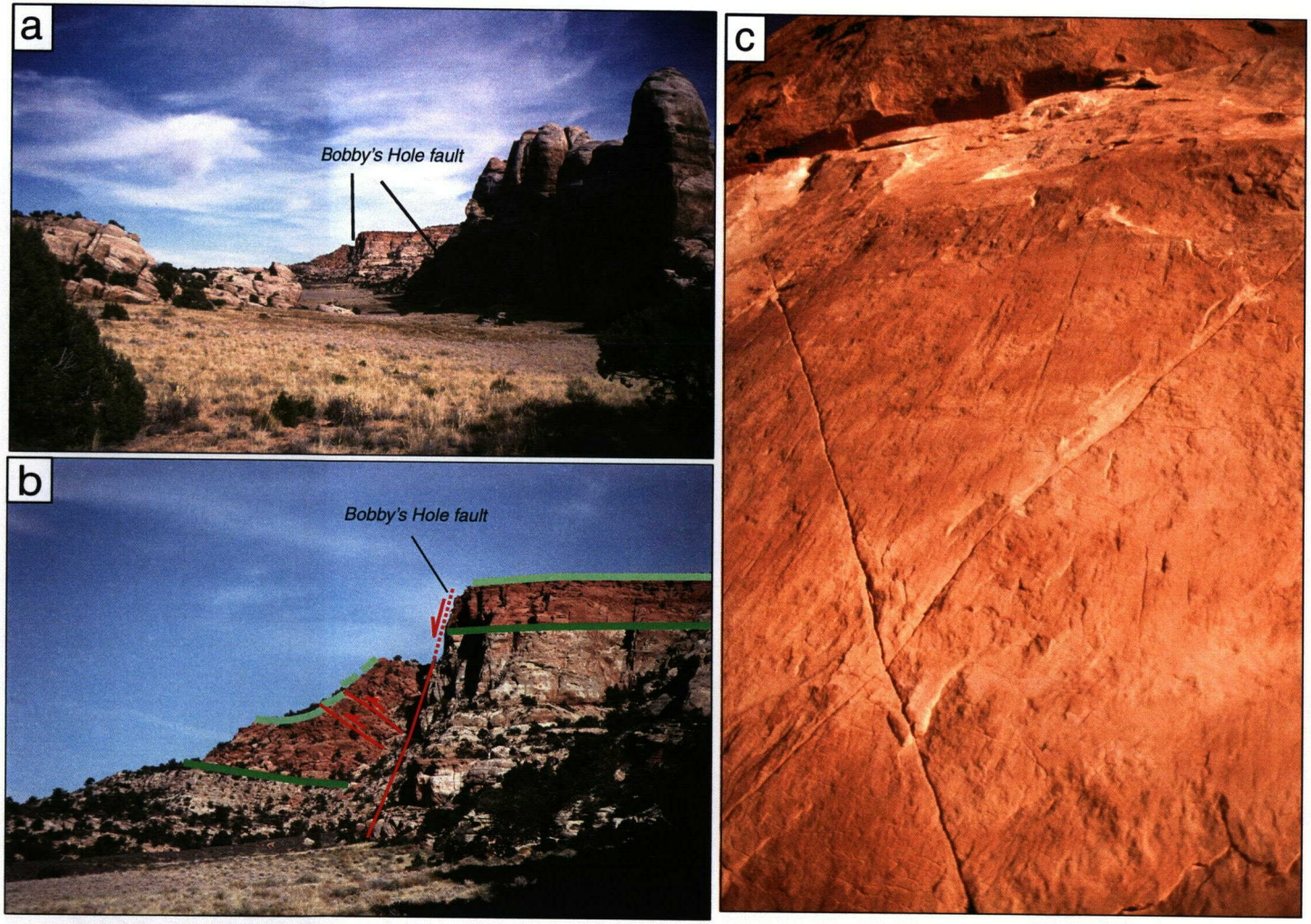

Figure 4-31. Field Photographs of Bobby's Hole Half Graben South of Canyonlands National Park, Utah. (a) View Looking Northeast along the Half Graben. Note Nearly Vertical Fault Scarp along Southeast Side of the Basin, and Southeast Dip of Strata in the Down-Dropped Hanging-Wall Strata. (b) Field Photograph of Localized Synthetic Dip Panel along the Bobby's Hole Fault. View is Looking Eastward, Oblique to the Fault. Red Lines Show Fault Traces, and Heavy Green Lines Show Bedding Traces. (c) Photograph of Grooves and Striations on Bobby's Hole Fault Surface.

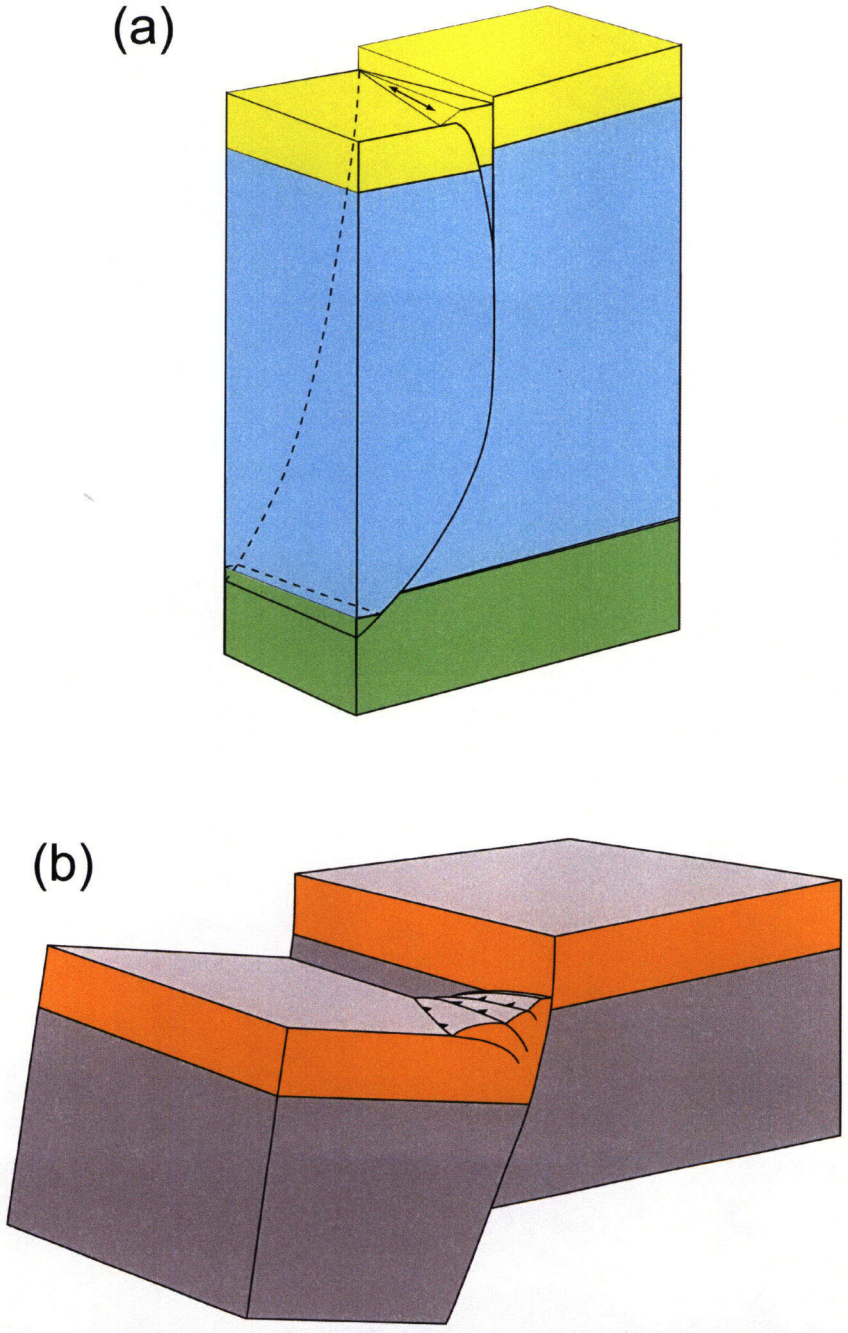

Figure 4-32. Schematic Diagrams of Contractional Elements of Normal Fault Systems. (a) Schematic Block Diagram Showing Hanging-Wall High Adjacent to Fault Where Hanging-Wall Impingement has Produced Lateral Shortening and Thickening of the Hanging Wall. Note that the Fault Changes Shape Laterally to a More Broadly Curved Fault Geometry for Which There is No Hanging-Wall Space Problem. Therefore, the Corresponding Hanging-Wall High Laterally Plunges and Diminishes. (b) Schematic Block Diagram Showing Contraction Faulting in the Hanging-Wall Impingement Zone. Shortening and Thickening of the Hanging Wall May Result in Locally Diminished Throw on the Normal Fault.

in well-lithified rocks where listric faults have very steep sections owing to low confining pressure.

In the case of Yucca Mountain, tuffs of the Tiva Canyon Formation were lithified at the ground surface. Yucca Mountain normal faults tend to be steep with dips commonly of 70° to 80°. The Bow Ridge fault has dips of 75° to 80° where it is exposed on the western edge of Bow Ridge (Simonds, et al. 1995), and the Midway Valley fault is represented as near vertical on cross sections drawn by Day, et al. (1998a). Fault blocks tend to dip gently, 5° to 10°, east or east-southeast. Fault shapes constructed using rule-based, cross-section construction methodology have produced faults with steep and relatively planar dips in the shallow section, and that curve relatively sharply at depths of around 6 km (Young, et al., 1991, 1992b). All these observations are consistent with the impingement model for the formation of small-displacement thrust/reverse faults in the hanging walls of steep normal faults. The faults in the South Portal area are interpreted as having formed by fault block impingement and contraction localized near the block bounding fault. In other words, the reverse faults in Boundary Ridge and Bow Ridge were produced by displacement on the Bow Ridge and Midway Valley block bounding faults. Differential fault block tilting (greater tilting of the hanging wall than the footwall) produced impingement of the hanging wall against the footwall, and contraction of the shallow part of the hanging wall—essentially chipping off the top of the hanging wall block adjacent to the normal faults.

4.8 Influence of Small Faults on Effective Permeability in Nonwelded Tuffs

The Paintbrush Tuff, nonwelded hydrologic unit comprises the stratigraphic interval from the top of the moderately to densely welded portion of the Topopah Spring Tuff to the base of the moderately to densely welded part of the Tiva Canyon Tuff (Moyer, et al., 1996). The Paintbrush Tuff, nonwelded hydrologic unit includes the basal nonwelded Tiva Canyon Tuff, Yucca Mountain Tuff, Pah Canyon Tuff, interstratified bedded tuff deposits, and the nonwelded top of the Topopah Springs Tuff (Moyer, et al., 1996). The Paintbrush Tuff, nonwelded hydrologic unit is assumed to have laterally homogeneous and isotropic matrix and fracture properties for purposes of unsaturated zone modeling (CRWMS M&O, 2000d). The DOE uses the Paintbrush Tuff, nonwelded unit as an analog for the Calico Hills Formation, in part because of the lack of hydrologic property data (especially fracture data) for the latter. DOE has divided the Calico Hills Formation into two zones, zeolitized and vitric, each of which is assumed to have laterally homogeneous and isotropic matrix and fracture properties. Modeling studies and geochemical data (e.g., Cl-36 data from the Exploratory Studies Facility) suggest that water may pass quickly through the Paintbrush Tuff, nonwelded unit along focused pathways (CRWMS M&O, 2000d; Illman and Hughson, 2001). These rocks at Yucca Mountain are cut by several large faults and numerous small faults, which may influence effective permeability and focus flow through the nonwelded units.

Faults at Yucca Mountain are primarily north-trending normal faults and northwest-trending dextral strike-slip faults (Morris, et al., 1996; Day, et al., 1998a,b; Ferrill, et al., 1999a; Ferrill and Morris, 2001). Small faults at Yucca Mountain are more numerous than large faults, following power-law relationships of abundance to displacement (Marrett, et al., 1998) or length (Marrett and Allmendinger, 1991; Cladouhos and Marrett, 1996). In addition to block bounding faults, there are numerous intrablock faults, which include fault splays, relict fault tips (Ferrill

and Morris 2001), connecting faults (Ferrill, et al., 1999a), and isolated intrablock faults (Day, et al,. 1998a). Major intrablock faults that cut through the main repository block include the north end of the Abandoned Wash fault, a north-northeast-trending fault connecting the Abandoned Wash and Ghostdance faults, a north-northeast-trending splay from Solitario Canyon fault, the Sundance fault, the Diabolous Ridge reverse fault, and a fault cutting the southeast end of Tonsil Ridge. These faults have displacements on the order of 5 m to >10 m. In addition, there are approximately 50 smaller faults with lengths of tens to hundreds of meters mapped in the Tiva Canyon Tuff within the proposed repository outline. Based on scaling predictions, there are expected to be at least tens of thousands of smaller faults with millimeter to meter displacements within Yucca Mountain.

A primary control on the permeability architecture of stratified rocks is the difference in permeability properties of sequential rock layers. If the stratigraphic sequence is undeformed, this vertical inhomogeneity and anisotropy will dominate. In faulted strata, however, such as those at Yucca Mountain, geologic structures, such as faults and fractures, exert three additional controls on conductivity and flow: (i) fault offsets alter the overall geometry of and communication between fault blocks (Allan, 1989; Ferrill and Morris, 2001), (ii) fault zones commonly form relatively impermeable barriers to cross-fault flow and permeable pathways for along-fault flow (Antonellini and Aydin, 1994; Caine, et al., 1996), (iii) relatively small faults and fractures lead to permeability anisotropy in fault blocks (Ferrill, et al., 2000b), and (iv) fault and fracture conductivity (and permeability anisotropy) may be influenced by the *in-situ* stress field (e.g., Evans, et al., 1997; Ferrill, et al., 1999b and references therein).

Several recent studies have focused on fault zone deformation processes and resulting effects on permeability in individual fault zones (e.g., Antonellini and Aydin, 1994; Caine, et al., 1996; Evans, et al., 1997; Ferrill, et al., 1999b). Fault zones in porous granular rock, such as nonwelded tuffs of the Paintbrush Tuff, nonwelded and Calico Hills Formation (Figure 4-33), may produce cataclastic grain-size reduction (Antonellini, et al., 1994), producing gouge zones, deformation bands, or deformation band swarms that have lower permeability and porosity than the host rock (e.g., Antonellini and Aydin, 1994; Caine, et al., 1996). In contrast, fault zone deformation in densely lithified rocks (e.g., crystalline rocks, welded tuff, and other rocks characterized by high intergranular strength) may tend to produce coarse-grained breccias and wide fault damage zones with enhanced permeability with respect to the host rock (Evans, et al., 1997; Section 2.4 of this report). With increasing displacement, a lower-permeability fault core may also develop within fault zones in densely lithified rocks (Section 2.4 of this report).

Intersecting and crossing conjugate normal fault networks, consisting of either permeability-reducing or permeability-enhancing faults, have an important influence on the bulk permeability of the host aquifer rock in the intersection region (Ferrill, et al., 2000b). Fault zone deformation mechanisms that result in either decreases or increases in fault zone permeability are likely to lead to development of permeability anisotropy approximated by a prolate (elongate) permeability ellipsoid in the intersection region of crossing conjugate normal faults. For example, consider the case where fault zone processes (e.g., grain-size reduction in cataclastic deformation bands in porous sandstone; Antonellini, et al., 1994) result in the reduction of fault zone permeability (Antonellini and Aydin, 1994) in otherwise isotropically permeable rock. Parallel impermeable faults produce a permeability anisotropy with permeability reduced in the direction perpendicular to the faults and unchanged in directions parallel to the faults. This permeability anisotropy produced by a parallel set of

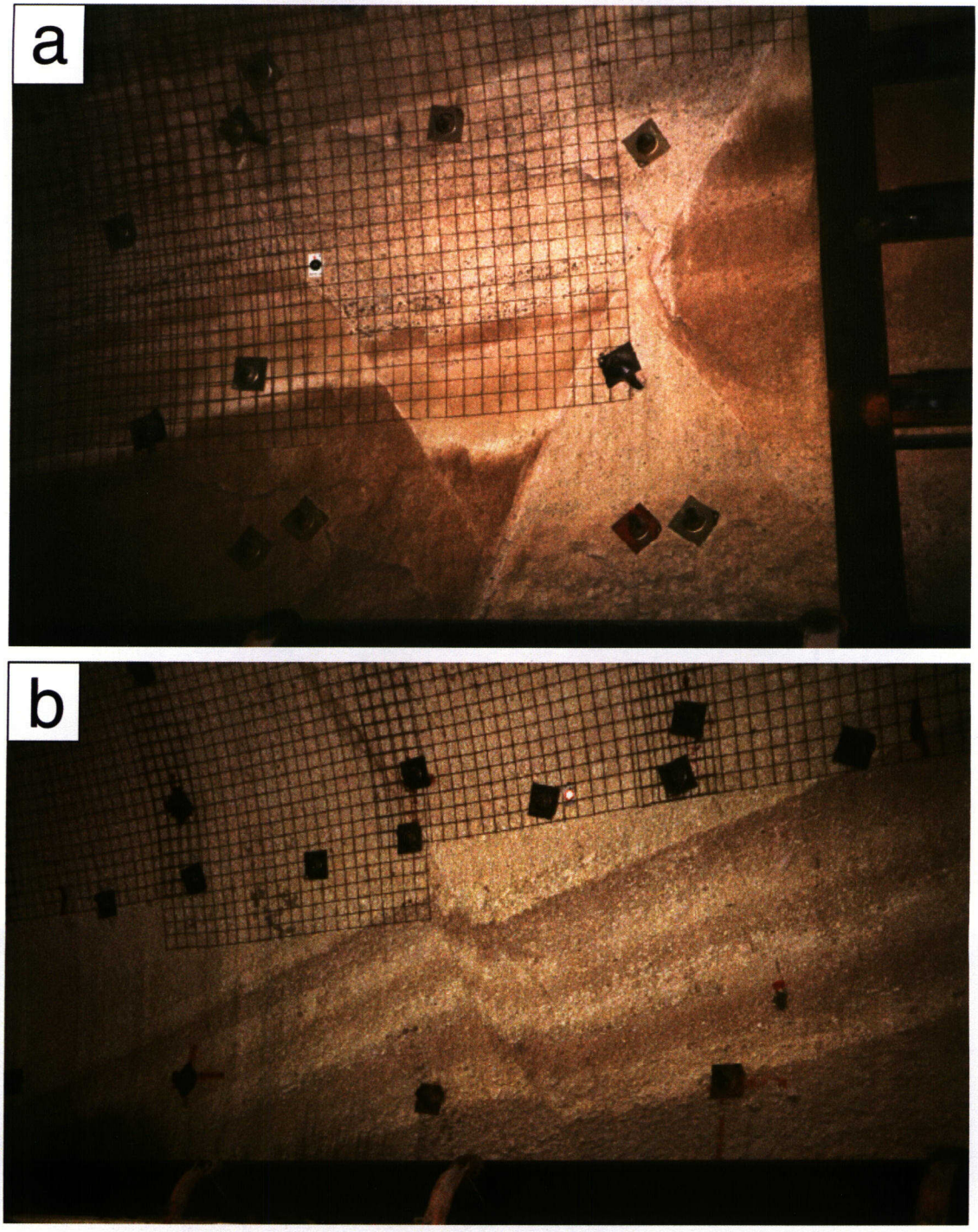

Figure 4-33. Crossing Normal Faults. (a–b) Photographs of Faults in Nonwelded Tuffs of the Paintbrush Tuff, Nonwelded along the North Ramp of the Exploratory Studies Facility.

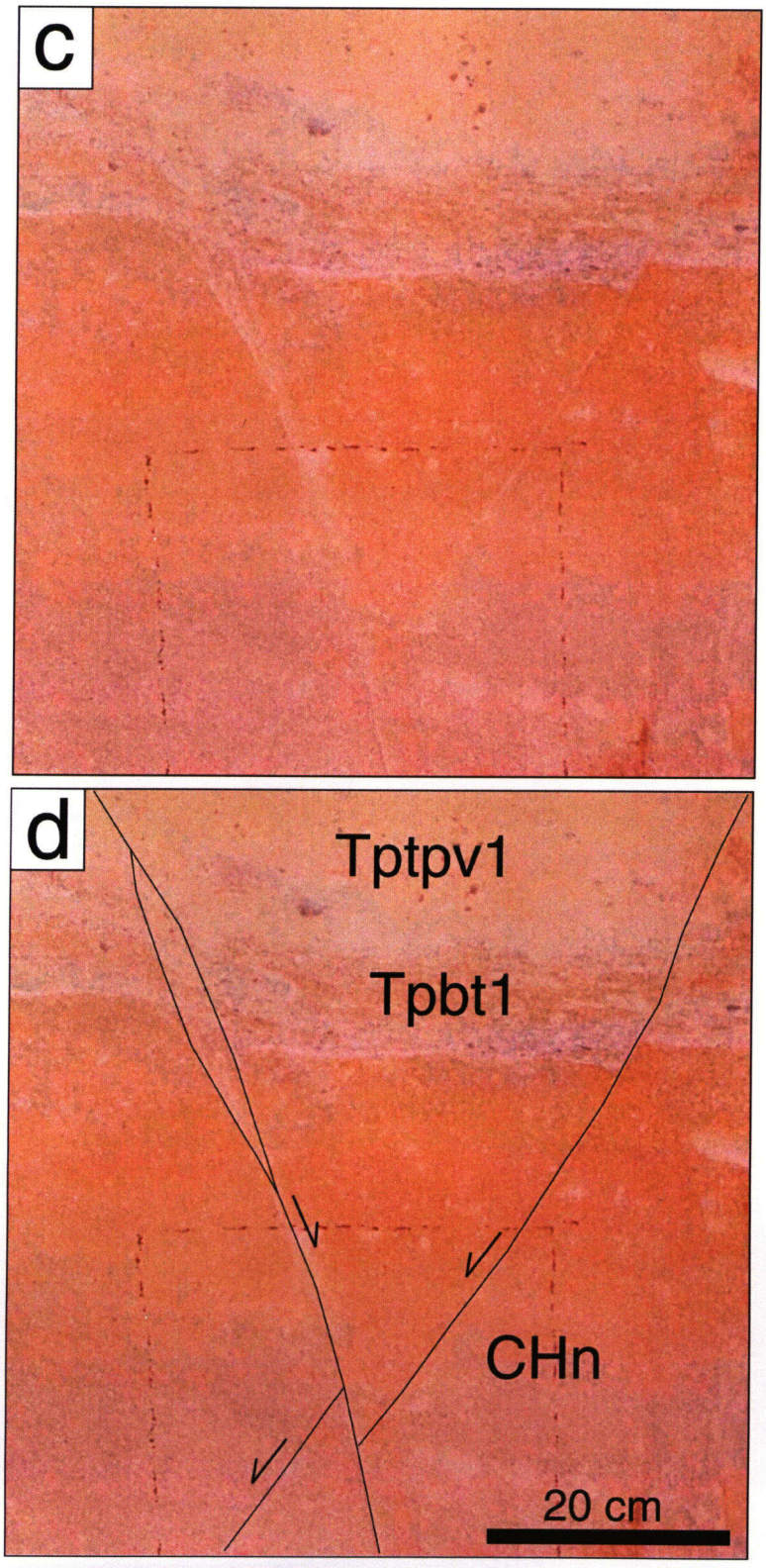

Figure 4-33 (continued). (c–d) Photographs of Faults in Nonwelded Calico Hills Tuff Exposed in the Busted Butte Test Facility.

permeability-reducing faults can be approximated by an oblate (flattened) permeability ellipsoid with minimum permeability in the direction perpendicular to the faults. Conjugate impermeable normal faults represent the intersection of two oblate permeability ellipsoids resulting in a linear permeability anisotropy approximated by a prolate permeability ellipsoid (Figure 4-34). The fault array produces barriers to lateral and vertical flow, except in the direction parallel to the fault intersection(s). Conversely, fault-related deformation processes (e.g., extension fracturing) that increase fault zone permeability result in locally enhanced permeability in directions parallel to the faults, and unchanged permeability perpendicular to the faults. Similar to the case of permeability-reducing faults, permeability anisotropy produced by a set of parallel permeability-enhancing faults can be approximated by an oblate permeability ellipsoid with minimum permeability in the direction perpendicular to the faults. Permeability anisotropy in the crossing fault region can be approximated by a prolate permeability ellipsoid with the direction of maximum permeability parallel to the fault intersection (Figure 4-34a,b).

Fault zones within the welded or nonwelded tuff units at Yucca Mountain may affect flow because of the effects of fault-related deformation on hydrological properties (Ofoegbu, et al., 2001). Faults through nonwelded tuffs would have lower porosity and saturated hydraulic conductivity. In the saturated zone, these changes create barriers to flow. The same deformational processes (cataclastic grain size and pore size reduction) that cause faults in nonwelded units to be barriers to flow, however, lead to changes in unsaturated zone hydraulic properties (especially enhanced capillarity) that enhance flow under most unsaturated conditions, thus creating preferential flow paths. If sufficiently continuous and numerous, small faults crossing nonwelded units increase the vertical flux and hasten vertical movement of water.

Faults that intersect the Paintbrush Tuff, nonwelded unit may be of particular importance to flow in the unsaturated zone because of the potential of such faults to capture and redirect lateral flow, resulting in focused vertical flow (Figures 4-33, 4-34). Lateral flow along the Paintbrush Tuff, nonwelded unit is expected considering the contrast in hydrologic properties between the Paintbrush Tuff, nonwelded unit and the underlying Topopah Springs Tuff. The evidence, however, suggests that lateral down-dip flow of water through the Paintbrush Tuff, nonwelded unit is limited to tens of meters before vertical breakthrough (CRWMS M&O, 1997). No perched water has been found, nor has any evidence of springs been found at exposed Paintbrush Tuff, nonwelded bedding contacts. Several hypotheses have been suggested for the lack of persistent lateral flow and ponding. Flow through fractures in the Paintbrush Tuff, nonwelded unit does not explain the lack of persistent lateral flow because matrix imbibition of the flowing in fractures is strong in the Paintbrush Tuff, nonwelded unit based on estimated hydrologic properties of the matrix and fractures (Flint, et al., 1996a,b). Laterally, the Paintbrush Tuff, nonwelded unit is a relatively uniform series of pyroclastic deposits with some local evidence of slight reworking (Moyer, et al., 1996). Primary lateral variations in the Paintbrush Tuff, nonwelded unit generally occur over large distances and thus cannot explain the lack of continuity of lateral flow.

Indirect evidence for the occurrence of elevated vertical flux in the vicinity of faults is provided by anomalous concentration of Cl-36 identified in matrix pore-water specimens collected from the Exploratory Studies Facility (CRWMS M&O, 1997; Fabryka-Martin, et al., 1998). Several matrix pore-water samples containing elevated Cl-36 values are spatially correlated with structural features such as faults or intensely fractured zones, either with the ground surface trace of the structural feature or the trace at depth. Some elevated Cl-36 values, however,

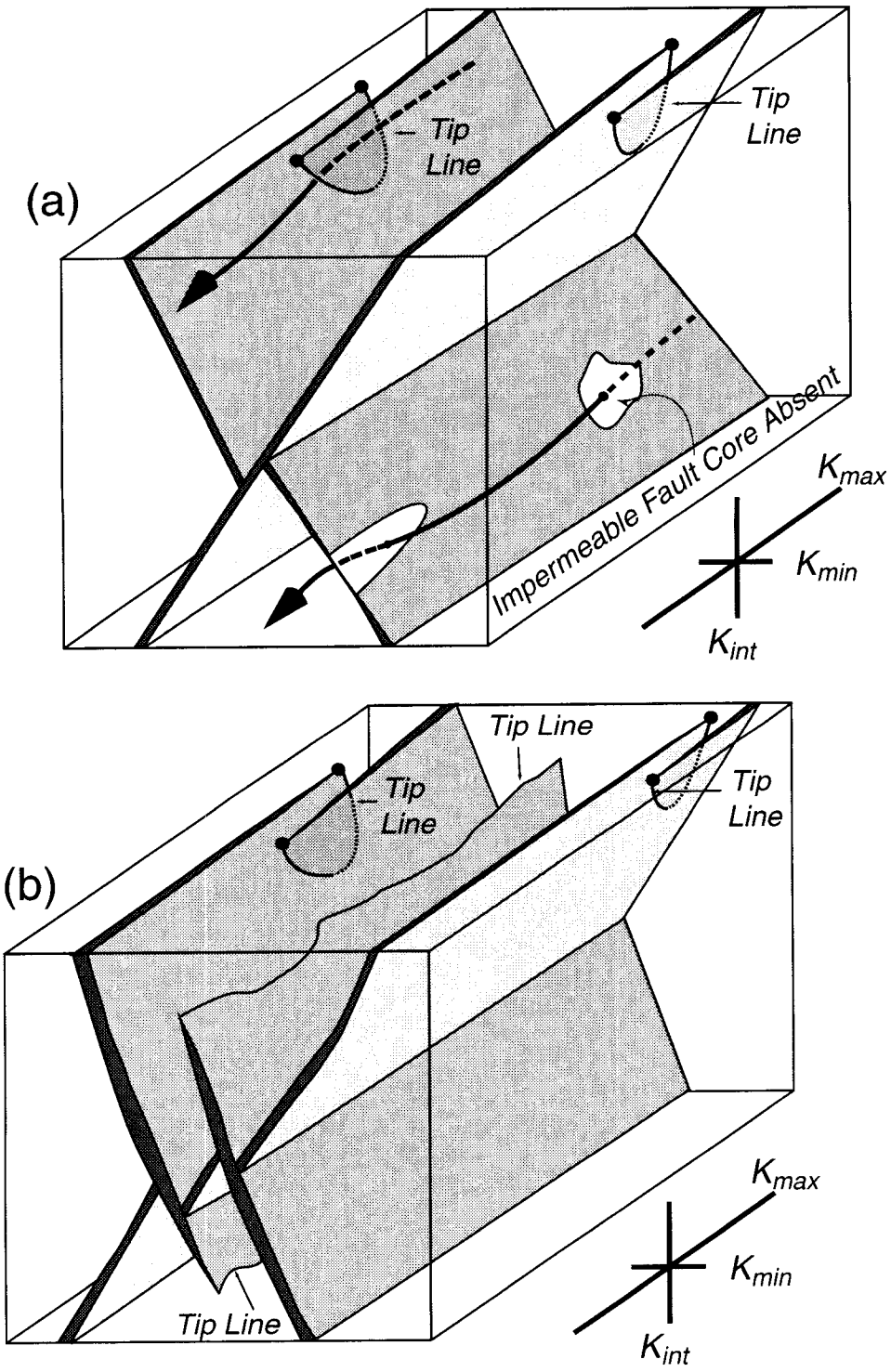

Figure 4-34. Schematic Diagram Illustrating Effects of Crossing Conjugate Normal Faults on Developing Permeability Anisotropy in Rock Where (a) Fault Zone Deformation Results in Permeability Decrease and (b) Where Fault Zone Deformation Produces Permeability Increase. K_{max}, K_{min}, and K_{int} Refer to Maximum, Minimum, and Intermediate Principal Permeabilities, Respectively.

show no such correlation. The occurrence of breakthrough of flow through the Paintbrush Tuff, nonwelded unit may be explained by considering that the unit is intersected by several faults, spaced on the order of tens of meters, with sufficient property contrast between the fault zone and the host rock to divert lateral flow and cause locally enhanced vertical flow. The authors believe that the correlation of Cl-36 values with faults would be improved by considering only faults that intersect the Paintbrush Tuff, nonwelded unit. Numerical-model results presented by Ofoegbu, et al. (2001) illustrate the potential effects of such faults on repository-level percolation flux.

4.9 Fracture and Fault Controls on Saturated Zone Permeability

A primary control on the permeability architecture of stratified rocks is the difference in permeability of sequential rock layers. If the stratigraphic sequence is undeformed, this vertical heterogeneity and anisotropy will dominate the permeability architecture. In faulted aquifers, however, such as those at Yucca Mountain, geologic structures (fault zones and fractures) exert four additional controls on subregional to regional and flow: (i) fault offsets alter the overall geometry of the aquifers and control aquifer communication between fault blocks (Allan, 1989), (ii) fault zones commonly form relatively impermeable barriers to cross-fault flow and permeable pathways for along-fault flow (Caine, et al., 1996), (iii) relatively small fracture and fault zones lead to permeability anisotropy in fault blocks, and (iv) fracture and fault zone conductivity and anisotropy may be influenced by the *in-situ* stress field (Barton, et al., 1995; Finkbeiner, et al., 1997; Ferrill, et al., 1995a,b, 1999b).

Fractures, including faults, impart a permeability characteristic to the rocks that may be measured at various scales. Fault zones commonly consist of a fault core, within which most of the displacement is accommodated, and a fault damage zone that consists of a network of subsidiary structures that bound the fault core (Caine, et al., 1996). Fault cores commonly have lower permeability than the protolith, because of grain size reduction and mineral precipitation. Fault damage zones commonly have enhanced permeability because of fracturing and faulting. Fault core and fault damage zone development is variable from fault to fault and along an individual fault (Caine, et al., 1996).

Fault zone architecture and related permeability structures may strongly control fluid flow into and out of the repository (Caine, et al., 1996). In many rock types, fault zones exhibiting grain-size reduction, and mineral precipitation generally contain core gouge zones with lower permeability and porosity than the adjacent protolith (Goddard and Evans, 1995; Caine, et al., 1996). These faults would form barriers to flow. In contrast, faults with coarse-grained breccias and wide fault damage zones containing numerous subsidiary structures that bound the fault core gouge may have greater permeability and porosity than the protolith, thereby enhancing fluid flow (Chester and Logan, 1986). These faults would act as conduits to fluid flow. Because faults commonly contain a less permeable core and a more permeable fault damage zone (Caine, et al., 1996), they have enhanced permeability parallel to the fault, but reduced permeability perpendicular to the fault. In the case of faults in welded tuff in the unsaturated zone at Yucca Mountain, fault cores probably have greater permeability than the protolith, but lower permeability than fault damage zones. Relatively fine-grained fault core material may be particularly important for water movement under low flux conditions, due to capillary forces.

Analysis of layer juxtaposition across faults and identification of fluid flow barriers and pathways is now routine practice in the oil industry (Allan, 1989). These analyses are key elements to assessing probability of fault-related trapping of hydrocarbons. Recently, fault zone deformation has been the subject of intensive investigation, with particular emphasis on fault zone permeability in sand and shale sequences, and implications for hydrocarbon migration and trapping (Yielding, et al., 1997, 1999; Alexander and Handschy, 1998). Consideration of aquifer and aquitard juxtaposition, fault zone deformation mechanisms in Yucca Mountain tuff aquifers, and the resulting influences on groundwater flow will be key elements for understanding groundwater flow and contaminant transport at Yucca Mountain.

The importance of fracture network characteristics differ considerably according to the flow regime under consideration. For example, narrow fracture apertures, and fine-grained fracture fillings comprise the percolation pathway under low unsaturated zone flow conditions. In contrast, large fracture apertures are important percolation pathways under high unsaturated zone flow conditions, such as caused by large precipitation events. Characteristics such as aperture distribution, including variation along fractures, and fracture intensity are also important in the percolation and near-drift unsaturated zone environments. Groundwater movement in the unsaturated zone may be relatively less sensitive to differences in fracture strike, due to the dominantly vertical gravity-driver flow in the unsaturated zone. In contrast, fracture strike is of relatively major importance for groundwater flow in the saturated zone, due to the dominantly lateral flow below the water table. Hydraulic properties and flow rates in the saturated zone are more directly dependent on fracture apertures than in the unsaturated zone.

Although many saturated zone flow modeling efforts have assumed homogeneous and isotropic permeability properties for aquifer strata, a mounting body of evidence indicates that aquifer permeability is strongly controlled by fault zones and fractures. Tectonic and structural features, such as fractures and fault zones exert a principal control on permeability and, therefore, influence groundwater flow. These effects occur over a large range of scale of observation from tens of square meters to thousands of square kilometers.

- At the regional scale (thousands of square kilometers), groundwater flow in the Yucca Mountain region flows from an area of recharge in higher altitude areas north of Yucca Mountain, to lower elevation areas of discharge in Amargosa Valley and ultimately the Death Valley pull-apart basin.

- At the subregional scale (tens to hundreds of square kilometers), large faults control the overall structural framework of Yucca Mountain and produce offset and tilting of aquifer strata and juxtapose different aquifers, allowing fluid communication between aquifers. In some cases, faults provide preferred pathways for groundwater flow. Furthermore, within strata in the Yucca Mountain area, fault zones and fractures produce the primary aquifer permeability. Fault and fracture permeability at the subregional scale can be addressed by dividing the subregion into domains represented by different permeability/conductivity tensors; some domains may represent specific fault zones.

- At the local scale (hundreds of square meters up to several square kilometers), individual faults and fracture swarms may dominate permeability or be fast flow paths, and intervening blocks of less fractured rock can be approximated by separate permeability tensors.

4.10 Influence of Stress on Permeability

Anisotropic permeability in fractured aquifers arises from the abundance and distribution of faults and fractures and permeability of associated damage zones (e.g., breccia). Although it is known that faulted and fractured aquifers commonly have anisotropic transmissivity (National Research Council, 1996), maps depicting regional-scale groundwater flow usually assume flow parallel to the gradient of the potentiometric surface. This simple assumption is true only if the transmissive properties of the aquifer are isotropic or if the major or minor semi-axis of the transmissivity tensor is everywhere parallel to the potentiometric gradient.

Recent studies, including one example from Yucca Mountain, have shown that faults favorably oriented for slip in the current stress field tend to be the most active groundwater flow pathways (Barton, et al., 1995; Finkbeiner, et al., 1997). This observation has been explained by increased small-scale fracturing and faulting in the vicinity of faults on the verge of shear failure (Barton, et al., 1995). The ability to recognize such faults allows us to identify the loci of increased fracturing.

A secondary, but measurable, influence on permeability is the effect of contemporary stress on reducing apertures of existing faults and fractures (Carlsson and Olsson, 1979; Barton, et al., 1995; Finkbeiner, et al., 1997). Faults and fractures perpendicular to the maximum principal stress are preferentially closed, thereby reducing permeability perpendicular to the maximum principal stress. Permeability perpendicular to the minimum principal compressive stress direction is relatively enhanced because lower resolved normal stress results in less fracture aperture reduction (e.g., Carlsson and Olsson, 1979).

4.11 Slip Tendency and Dilation Tendency

Stress analysis involves calculating resolved stresses on fault and fracture surfaces to analyze likelihood for slip or dilation in crustal stress fields.

Slip tendency analyses are applicable to planar discontinuities like faults, extension fractures, or layering (Morris, et al., 1996; Ferrill, et al., 1998). For faults and fractures, slip is likely to occur on a surface when the resolved shear stress, τ, on that surface equals or exceeds the frictional resistance to sliding. Frictional resistance is proportional to normal stress, σ_n, acting across that surface (Jaeger and Cook, 1979). The slip tendency, T_s, of a surface is the ratio of shear stress to normal stress acting on that surface (Morris, et al., 1996).

$$T_s = \tau / \sigma_n \tag{4-3}$$

As such, T_s depends solely on the stress field (stress tensor), and surface orientation. Whether or not a surface slips depends on its cohesive strength, if any, and the coefficient of static friction, μ. The coefficient of static friction, μ, is the value of T_s that causes slip on a cohesionless surface and is often referred to as the fault strength in earthquake focal mechanism analysis (Harmsen, 1994). Under most crustal conditions, faults with $T_s = 0.6$ are ideally oriented for slip (Byerlee, 1978). Slip-tendency analysis provides a way to assess which faults are near the ideal orientation for slip and which are the most likely to be associated with zones of increased fracture density and enhanced fracture permeability.

Dilation of fractures is largely controlled by the resolved normal stress, which is a function of lithostatic and tectonic stresses and fluid pressure. The normal stress that a fracture feels depends on the magnitude and direction of the principal stresses relative to the fracture plane. The ability of a fracture to dilate and transmit fluid is directly related to its aperture, which in turn is a function of the effective normal stress acting on it. The magnitude of the normal stress can be computed for surfaces of all orientations within a known or hypothesized stress field. This normal stress can be normalized by comparison with differential stress. The resulting dilation tendency, T_d for a surface is then defined as

$$T_d = (\sigma_1 - \sigma_n) / (\sigma_1 - \sigma_3) \quad (4\text{-}4)$$

where σ_1 is the maximum principal compressive stress, and σ_3 is the minimum principal compressive stress.

4.11.1 Bulk Transmissivity Anisotropy

A population of steep, aligned, relatively permeable faults and fractures cutting a less permeable rock mass will tend to orient the maximum directional transmissivity parallel to the structural grain. In the case of unequal horizontal stresses acting on a population of steep faults and fractures, faults that strikes parallel to the maximum horizontal compressive stress tend to open. Faults with strikes perpendicular to the maximum horizontal stress tend to close. Similarly, some faults in an anisotropic stress field will be more ideally oriented for slip and others for locking. Thus, even if fault and fracture orientation distribution is isotropic, transmissivity in the maximum horizontal stress direction can be enhanced, producing transmissivity anisotropy.

Because fault and fracture populations commonly exhibit preferred orientations and *in-situ* horizontal stresses are commonly unequal, both are likely to occur together in nature and lead to anisotropic transmissivity. For example, in cases where σ_3 is horizontal, vertical faults and fractures perpendicular to σ_3 have the highest dilation tendency and are likely to be more conductive than those in other orientations (Figure 4-35a). Faults and shear fractures are sensitive to the σ_1 direction and commonly form two conjugate sets intersecting at an acute angle (~60°) centered on σ_1 (Figure 4-35b,c). In normal fault regimes where σ_1 is vertical, two sets of opposite-dipping conjugate normal faults commonly develop (Figure 4-35b). In strike-slip fault regimes where σ_1 is horizontal, two sets of vertical conjugate strike-slip faults commonly develop (Figure 4-35c). In areas where σ_3 is horizontal, fault and fracture preferred orientations, and slip tendency and dilation tendency, all promote development of a net bulk transmissivity anisotropy with a maximum horizontal transmissivity perpendicular to σ_3 (Figure 4-35d). The interaction of aquifer transmissivity with faults and fractures can be field tested by aquifer pumping tests. The results can be used to determine the full transmissivity tensor and to compare the orientation of the principal components of this tensor with the maximum and minimum *in-situ* horizontal stress orientations and the distribution of faults and fractures.

4.11.2 Prediction of Anisotropic Transmissivity at Yucca Mountain

The pattern of faults and fractures in the Yucca Mountain region (Figure 4-36) resulted from deformation in a regional stress field that evolved from east-west extension before 10 million

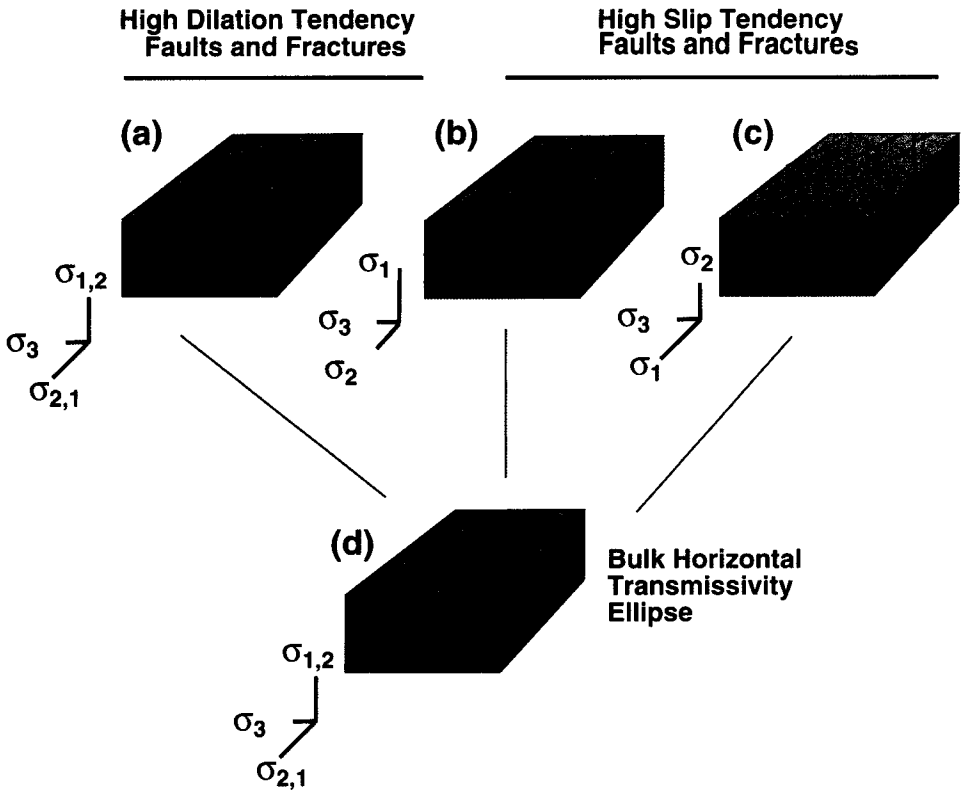

Figure 4-35. Conceptual Illustration of Effects of Faults with High Slip Tendency or High Dilation Tendency on Development of Anisotropic Permeability in Areas Such as the Yucca Mountain (Nevada) Region, Where the Minimum Principal Compressive Stress (σ_3) is Horizontal

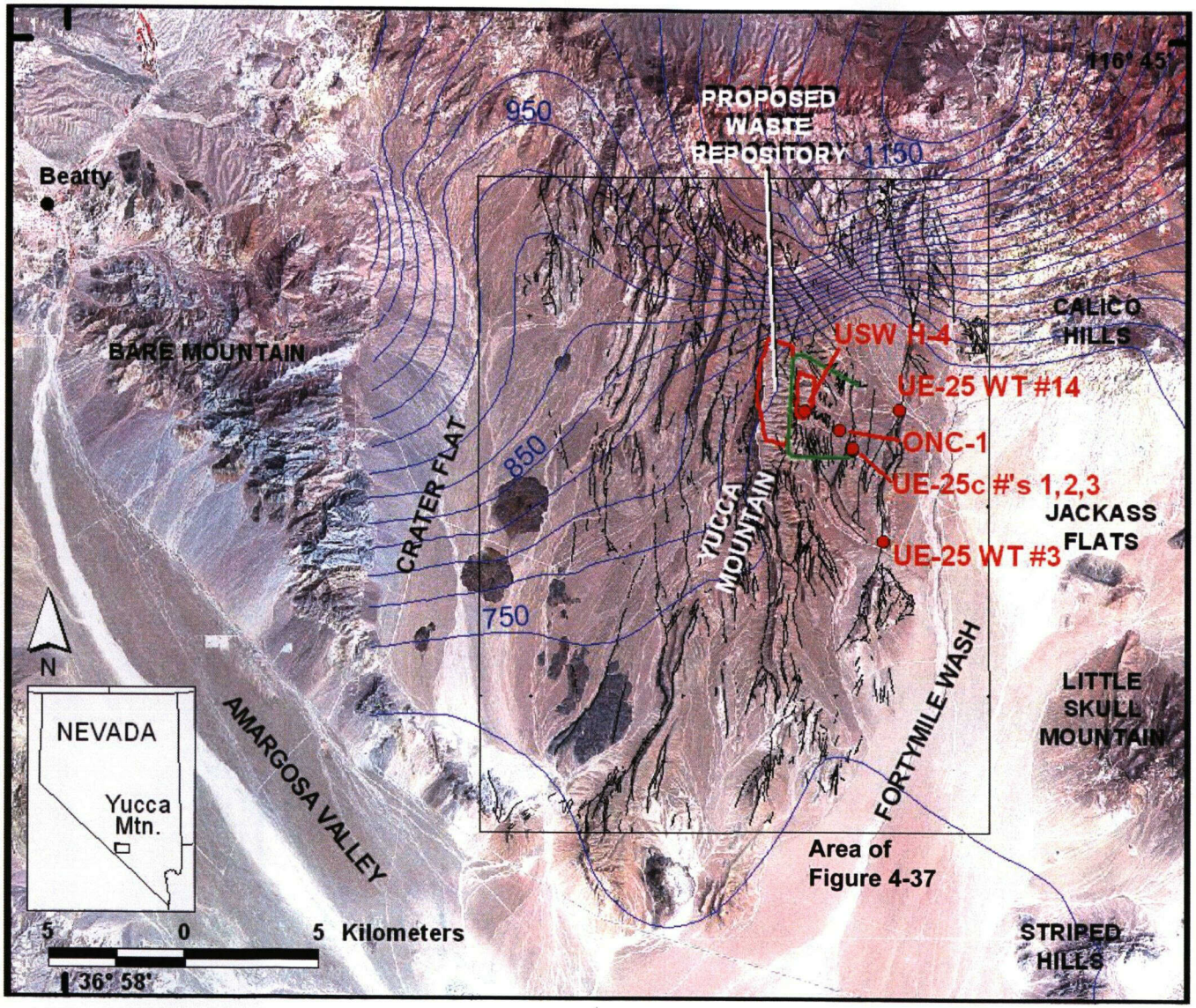

Figure 4-36. Thematic Mapper Scene of Yucca Mountain Region. Map Shows the Potential Repository Location: Wells (Red Dots), Faults (Irregular Black Lines), and Water Table Contours (Blue Lines). Water Table Contours are from Czarnecki, et al. (1997). Green Lines Show the Path of the Exploratory Studies Facility.

years ago to west-northwest to east-southeast extension after 10 million years ago (Zoback, et al., 1981), and from thermoelastic contraction during cooling of the ash-flow tuffs (Sweetkind and Williams-Stroud, 1996). The result is a dominant population of north-south to northeast-southwest-trending normal faults, a subordinate population of northwest-southeast-trending strike-slip faults, and a group of minor connecting faults and curved fault tips (Day, et al., 1998a; Ferrill, et al., 1999a). Fault growth by connection of overlapping fault segments produced irregular fault traces with cusps at fault intersections. Although faults at Yucca Mountain are related to several deformational episodes, some faults are unlikely to slip because of unfavorable orientations relative to the contemporary stress state.

Yucca Mountain lies within the western Basin and Range in a region characterized by both normal and strike-slip earthquakes. The regional occurrence of both normal and strike-slip earthquakes indicates that the maximum (σ_1) and intermediate (σ_2) principal compressive stresses have similar magnitudes (Zoback, 1992; Zoback, et al., 1992). The least principal compressive stress (σ_3) is approximately horizontal and trends west-northwest to east-southeast. Therefore, σ_3 is the odd axis of Krantz (1988) and has the most direct control on the pattern of fault-slip tendency. Stock, et al. (1985) estimate the following effective principal stresses (corrected for fluid pressure) at a depth of 1 km: σ_1 = vertical = 21 MPa, σ_2 = N25°–30°E = 17 MPa, and σ_3 = N60°–65°W = 11 MPa for the region.

4.11.3 Slip-Tendency Analysis of Yucca Mountain Faults

Slip-tendency analysis of Yucca Mountain faults was performed using the relative stress values of Stock, et al. (1985) given above, a three-dimensional fault model for western Yucca Mountain and the faults mapped by Simonds, et al. (1995) (Figure 4-37a). Maximum slip tendencies are experienced by faults that strike parallel to the north-northeast-trending maximum horizontal stress (025 to 030°; 028° in Figure 4-37a) and dip 55°. Slip tendencies are also near maximum (>0.3) for moderately to steeply dipping (40 to 65°), north-south to northeast-southwest (000 to 055) striking faults. Faults at 1-km depth have moderate slip tendencies relative to typical failure conditions. In contrast, at depths of earthquake rupture initiation (e.g., 5 to 15 km), stresses resolved on similarly oriented faults produce near-failure slip tendencies (Morris, et al., 1996). As described by Harmsen (1994), the pattern of slipped faults in the Little Skull Mountain (Figure 4-36) earthquake sequence is dominated by dip slip on southeast dipping normal faults and right-lateral strike-slip on vertical north-south-trending faults. This is the pattern predicted by slip-tendency analysis of the Yucca Mountain stress field, and it supports simultaneous activity of strike-slip and normal faults in this area (Morris, et al., 1996). Examination of Simonds, et al. (1995) reveals that nearly all faults with known or suspected late Quaternary displacement are in orientations of high-slip tendency (Figure 4-37a). Some noteworthy examples are the Northern and Southern Windy Wash, Fatigue Wash, Solitario Canyon, Iron Ridge, and Stagecoach Road faults. In contrast, the northwest-southeast-trending Pagany Wash, Sever Wash, and Yucca Wash faults are in low slip-tendency orientations (Figure 4-37a) and lack evidence of late Quaternary slip (Simonds, et al., 1995).

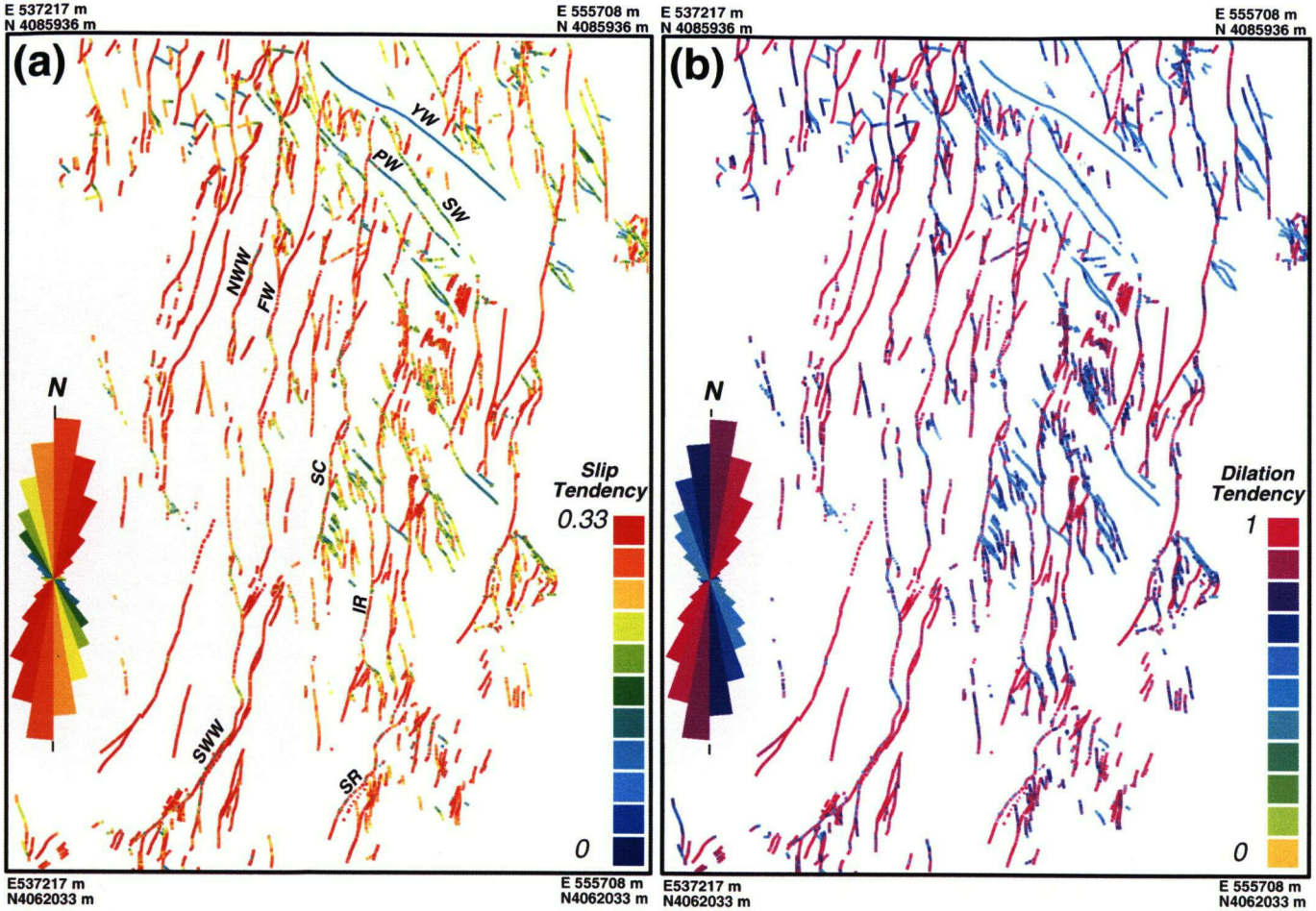

Figure 4-37. Slip- and Dilation-Tendency Maps of Yucca Mountain Faults. (a) Shows Slip-Tendency Map of Yucca Mountain Faults by Simonds, et al. (1995). Inset Rose Diagram Shows Cumulative Fault Length in 10-Degree Strike Azimuth Bins. Map and Rose Diagram are Colored According to Slip Tendency as Shown by Color Bar. Area as Shown in Figure 4-36. Named Faults Discussed in Text are Labeled on Map as NWW = Northern Windy Wash, SWW = Southern Windy Wash, FW = Fatigue Wash, SC = Solitario Canyon, IR = Iron Ridge, SR = Stagecoach Road, PW = Pagany Wash, SW = Sever Wash, and YW = Yucca Wash. (b) Dilation Tendency Map of Yucca Mountain Faults. Map and Rose Diagram are Colored According to Dilation Tendency as Shown by Color Bar.

4.11.4 Dilation-Tendency Analysis of Yucca Mountain Faults

Dilation-tendency analysis of faults and associated fractures at Yucca Mountain (e.g., Figure 4-37b) was performed assuming the same relative stresses and mapped faults used for slip-tendency analysis. The results show that maximum dilation tendencies are experienced by vertical faults and fractures that strike parallel to the maximum horizontal stress (025 to 030°; 028° in Figure 4-37b). Faults trending 028 ± 35° and dipping 65 to 90° have dilation tendencies of 0.8 or greater in the present stress field. Dilation-tendency analysis of faults at Yucca Mountain illustrates an abundance of steeply dipping north-northeast-trending faults that have high-dilation tendency.

4.12 Modification of Fractures

After a fracture forms, it may be modified or altered in some way that changes its original attributes. Modifications may occur immediately on fracturing or anytime thereafter. Evidence of modification may occur sporadically along a fracture, or only in certain locations underground, leading to occasional observations that are initially surprising. Modifications expected at Yucca Mountain include fracture-filling by minerals such as calcite and opal and/or rock fragments, brittle deformation of fracture walls by repeated faulting, vibratory ground motion or excavation methods, and hydrothermal alteration of fracture walls or fracture-fillings. When such modifications to a fracture or to fractures of particular origin are known to have occurred, important attributes of that fracture may be assumed because particular characteristics have been correlated with certain modifications (e.g., fracture-filling reduces hydraulic conductivity; hydrothermal alteration along fractures and/or within filled fractures reduces rock-mass strength and stiffness; armoring fracture walls by mineral precipitation or deposition of water-entrained particles may enhance hydraulic conductivity in the unsaturated zone at low flow rates in cases where the fracture is not completely filled). Therefore, an adequate investigation and explanation of modifications to fractures at Yucca Mountain that may affect characteristics of fractures that is consistent with field and laboratory observations and analog studies should be attempted by the DOE to help constrain the interpolation between and extrapolation beyond locally exposed fractures and faults that are abstracted into process level and performance assessment models (Evolution of the Near-Field Environment, Repository Design and Thermal-Mechanical Effects, and Radionuclide Transport Issue Resolution Status Reports).

Fracture characteristics are expected to change during the lifetime of a Yucca Mountain repository. Thermal, hydrologic, chemical, mechanical, seismic, and tectonic strain processes that are expected to occur are known to modify such fracture characteristics as aperture, strength, propagation, and arresting of new and existing fractures, and related hydrologic and rock-mechanical parameters. Therefore, an adequate investigation and explanation of current and future modifications to fractures at Yucca Mountain, is important to help constrain the parameters, assumed ranges, probability distributions and/or bounding assumptions of perturbed conditions that are abstracted into process and performance assessment models (Evolution of the Near-Field Environment, Repository Design and Thermal-Mechanical Effects, and Radionuclide Transport Issue Resolution Status Reports). This explanation of modification of fractures should be consistent with natural analogs, laboratory and empirical observations and forward modeling of fracture behavior.

4.13 Pavement Infiltration Analyses

Fractures, fracture zones, and fault zones provide the primary discontinuities (i.e., the structural framework) along which groundwater infiltration and percolation occurs in the unsaturated zone at Yucca Mountain. Bedrock exposures above the proposed repository site consist of welded tuffs of the upper lithophysal unit of the Tiva Canyon Tuff. The upper lithophysal zone of the crystal poor member of the Tiva Canyon Tuff is one of the primary (by area) units exposed above the proposed repository. Pavement mapping data from the upper lithophysal unit of the Tiva Canyon Tuff (Barton, et al., 1993; Figures 4-2a, 4-38,) and new surface mapping from above the repository site (Figure 4-8) were used to evaluate the fracture porosity estimates used by Flint, et al. (1996a) for infiltration modeling. Based on this analysis (as presented in the Section 4.13.2), fracture porosity estimates used by Flint, et al. (1996a) appear to underestimate fracture porosity in the upper lithophysal unit of the Tiva Canyon Tuff at the bedrock/overburden interface. The source of differences between fracture-porosity values of Flint, et al. (1996a) and new values presented here are likely the result of long-term weathering and erosional phenomena acting on fractures exposed at the ground surface. Fracture properties, particularly apertures of newly exposed fractures in boreholes used by Flint, et al. (1996a) are not representative of fractures exposed at the ground surface, sites of groundwater infiltration at Yucca Mountain.

4.13.1 Fractures in Tiva Canyon Tuff

Joints in the repository block at Yucca Mountain have been categorized into three groups according to age and genesis: (i) cooling joints (oldest), (ii) tectonic joints of (intermediate), and (iii) unloading joints (youngest) (Barton and Larsen, 1985; Barton and Hsieh, 1989; Barton, et al., 1993; Sweetkind, et al., 1995a,b; Throckmorton and Verbeek, 1995; Sweetkind and Williams-Stroud, 1996). Cooling joints are distinguishable because they have local degassing-related tubular structures (Figure 4-5a; Barton, et al., 1984, 1993), do not cut lithophysae (Figure 4-5a,d), have a smooth planar appearance (between tubular structures; Figure 4-5a,b,d), have surface areas in excess of 100 m^2, and predate other joints (based upon abutting relationships). Interpreted tectonic joints are distinguishable from the recognized cooling joints because they lack tubular structures, cut lithophysae, are not normally as smooth, are commonly smaller, and in many cases abut against cooling joints. Some tectonic joints, however, cut across cooling joints, which suggests that either the cooling joints were filled by minerals at the time of tectonic joint propagation or that the crossing tectonic joints originated as shear fractures. Finally, unloading joints occur near the surface; are subhorizontal, rough, and curviplanar; and generally terminate against cooling and tectonic joints. In addition to joints, approximately 50 faults were mapped in the Tiva Canyon Tuff above the proposed repository (Day, et al., 1998a), and a multitude of smaller (submap scale) faults are present.

Cooling joints in the Tiva Canyon Tuff occur as two orthogonal sets, trending northeast and northwest (Figures 4-8, 4-38). Detailed analyses of cleared pavements in the upper lithophysal unit of the Tiva Canyon Tuff by Barton, et al. (1993) demonstrated that cooling joints are not uniformly distributed but are instead locally organized in swarms (Figures 4-8, 4-38). Mapping of large joints (lengths >2 m) in the upper lithophysal unit of the Tiva Canyon Tuff on Live Yucca Ridge shows that cooling joints tend to be clustered into swarms (as wide as 5 to 10 m) that trend northeast and northwest (Figures 4-5c, 4-8, 4-39a,b). Swarm spacings are approximately 30 to 100 m. Cooling joint swarms consist of extensive planar smooth fractures

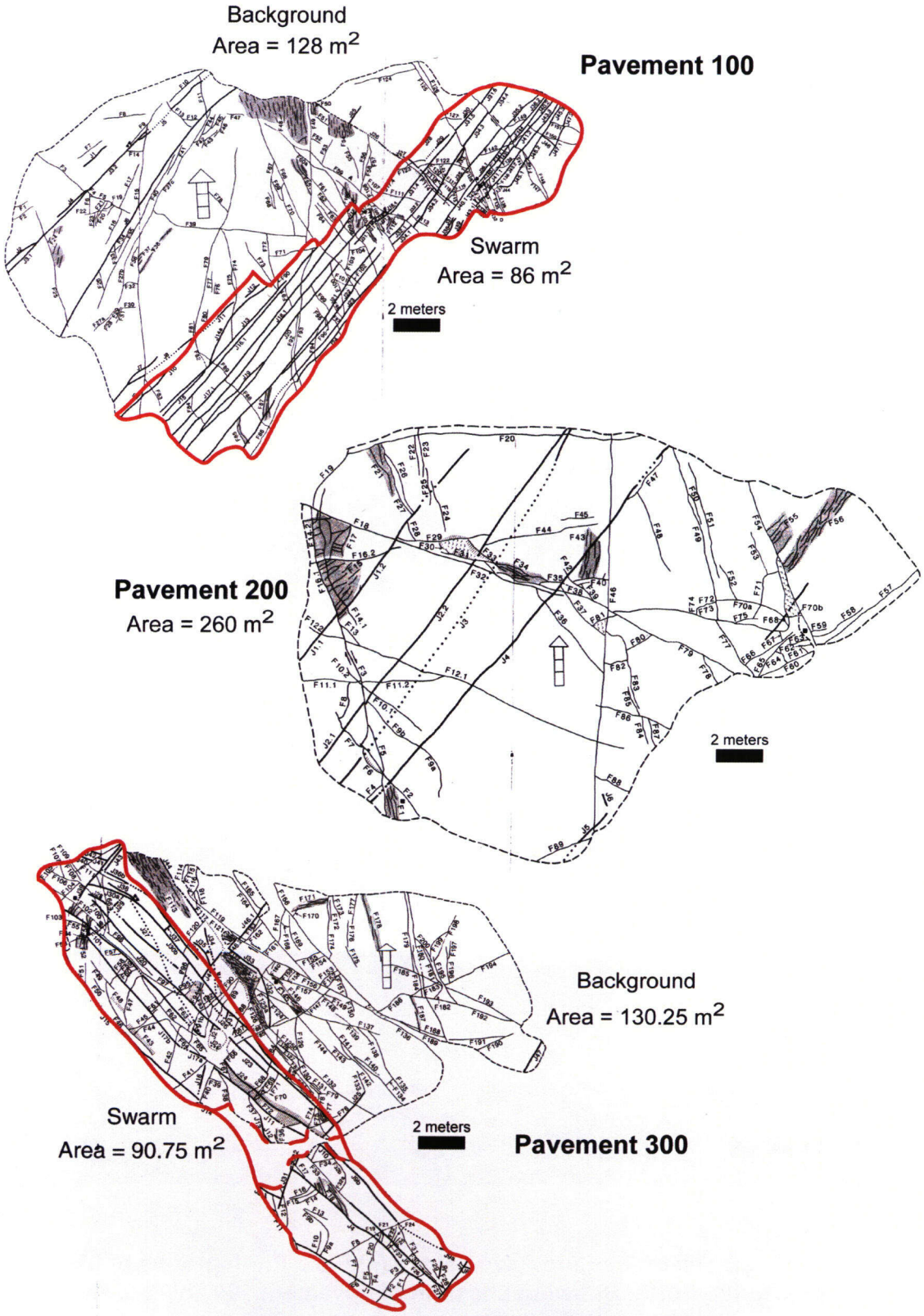

Figure 4-38. Maps of Pavements 100, 200, and 300 (from Barton, et al., 1993)

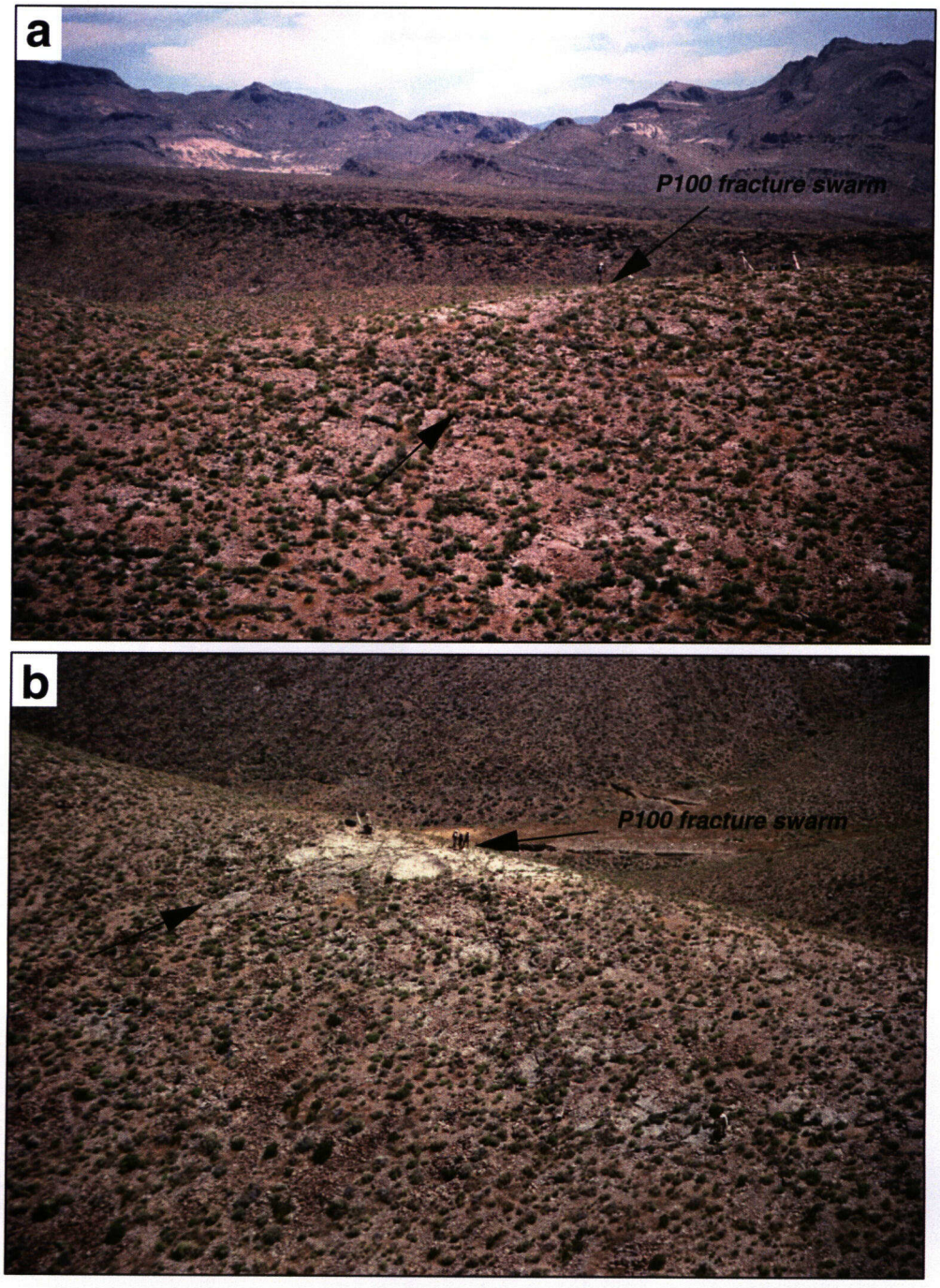

Figure 4-39. Photographs of Fracture Pavements. (a) Field Photographs of Live Yucca Ridge (View to the North) Showing Location of Pavement 100 and Vegetation Alignments, Many of Which are Localized along Fractures; and (b) Pavement 100 (View to the South) and Cooling Joint Swarm

occurring in sets of three to eight fractures, with joint spacings of about 25 cm and trace lengths typically 10 m. Individual cooling joint trace lengths exceed 25 m in some cases. Swarms span the entire thickness of the upper lithophysal unit of the Tiva Canyon Tuff and have observed lengths that exceed 100 m. True lateral extents of swarms remain unconstrained.

4.13.2 Input Parameters for Fracture Infiltration Modeling

Fracture aperture and related total fracture porosity are key parameters for modeling infiltration at Yucca Mountain. Local variations in fracture porosity at the bedrock overburden interface may cause localization of water pulses for deeper groundwater percolation in the unsaturated zone. Fracture apertures measured at depth from boreholes or from the Exploratory Studies Facility are likely to be altered because of local unloading and stress perturbation around boreholes and excavations. Previous infiltration modeling for Yucca Mountain relied on fracture aperture measurements gathered from boreholes (Flint, et al., 1996a). However, surface measurements of fracture aperture and related fracture parameters would be the ideal basis for surface infiltration modeling. Low confining stress and long-term surface weathering phenomena, such as frost wedging, root wedging, and slope creep, are likely to increase fracture apertures at the ground surface through time.

Mapping of cleared pavements in the upper lithophysal unit of the Tiva Canyon Tuff by Barton, et al. (1993) provides the most complete surface fracture data set for the upper lithophysal unit of the Tiva Canyon Tuff at Yucca Mountain. All fractures greater than 0.2 m in length were mapped with the intention of eliminating a multitude of smaller fractures, many of which may be localized weathering related features and too short to provide connected infiltration pathways. As input for the fracture infiltration modeling, surface porosity measurements are needed in the form of open aperture area as a proportion of total surface area (fracture porosity). The Barton, et al. (1993) data is the best available and most appropriate to evaluate surface infiltration porosity.

4.13.3 Swarm Versus Background

Fracture data (Barton, et al., 1993) from pavements 100, and 300 are subdivided into swarm and background as indicated in Figure 4-38. Pavement 200 contains no fracture swarms and is treated as all background. Total pavement areas are given by Barton, et al. (1993, page 6), and swarm areas for Pavements 100 and 300 were measured directly from the Barton, et al. (1993) pavement maps (Figure 4-38). Fractures with unmeasurable apertures were included in some aspects of the analysis [Table 4-2, datasets labeled all, and combined (2)] and excluded from others [Table 4-2, datasets labeled meas. and combined (3)]. Each of the subdivided data sets was used to calculate total fracture length (m), total fracture length per unit area of pavement (areal fracture density, m/m^2), individual open fracture area (m^2), and open fracture area per unit area of pavement (raw fracture porosity, m^2/m^2). These data were then collected into three categories: (i) swarm data, (ii) background data, and (iii) all data.

Table 4-2. Fracture Data from Yucca Mountain Pavements												
Data Set	Swarm				Background				All Data			
	N	AFD	NFA	FP	N	AFD	NFA	FP	N	AFD	NFA	FP
P100 all	129	3.11			99	1.89			228	2.38		
P100 meas.	116	2.97		0.0073	94	1.85		0.0102	210	2.30		0.0090
P200 all					105	1.42			105	1.42		
P200 meas.					97	1.38		0.0040	97	1.38		0.0040
P300 all	136	2.77			119	1.98			257	2.35		
P300 meas.	115	2.49		0.0077	109	1.81		0.0044	220	2.09		0.0058
COMBINED (1)	227	2.72		0.0075	300	1.60		0.0056	527	1.89		0.0061
COMBINED (2)	227	2.72	0.0032	0.0087	300	1.60	0.0030	0.0048	527	1.89	0.0031	0.0058
COMBINED (3)	267	3.23	0.0032	0.0096	323	1.68	0.0030	0.0050	590	2.01	0.0031	0.0062
Flint, et al. 1996a*										23.4	0.0001	0.0022

N Number of fractures measured
AFD Areal fracture density, m/m^2
NFA Normalized fracture area, m^2/m
FP Fracture porosity, m^2/m^2
all Areal fracture density calculated using all recorded fractures regardless of measurable aperture
meas. Areal fracture density calculated using only fractures with measured apertures
(1) Raw value for FP
(2) Smoothed value for fracture porosity using length of fractures with measured aperture
(3) Smoothed value for fracture porosity using total fracture length

* Flint, et al. (1996a) fracture densities were estimated from borehole core logs. The estimated fracture density of 7.8 fractures per meter was more than assumed for all three fracture classes considered in their work (apertures 0.0025, 0.00025, and 0.000025 m), apparently tripling the borehole-derived fracture density to 23.4.

4.13.4 Fracture Porosity

It is possible to calculate the open aperture area as a proportion of total surface area directly from the field data:

$$\frac{\Sigma[\text{aperture} \times \text{length}]}{\text{Pavement Area}} \qquad (4\text{-}5)$$

This calculation method is particularly sensitive to potential weaknesses in the data and is strongly influenced by a small number of long or large aperture fractures. In the case of the Pavement 100 data set, the raw porosity for the background area (0.0102 m^2/m^2) is greater than that for the swarm (0.0073 m^2/m^2). This results from the single large fracture with a length of 12.4 m and an aperture of 34.3 mm that was included in the background data. Barton, et al. (1993) point out that individual aperture values are likely to misrepresent the natural aperture pattern but that they can be used to generate an aperture probability distribution.

A statistically more representative aperture distribution can be obtained by using the data to generate a normalized probability function that describes the aperture distribution per unit of fracture length. Each of the combined data subsets (swarm, background, and all data) was binned according to aperture, using a bin size of 0.05 mm. This bin size was chosen because it is greater than the smallest measured fracture aperture (0.04 mm) and provides a high-resolution view of the data. Binned aperture (abscissa) was plotted against normalized cumulative frequency (number of fractures in a bin, divided by the total number of fractures in the data set) for each of the three subsets on a log/log plot (Figure 4-40). Summing the area beneath the resulting curve over the range of the aperture data yields the aperture area of a representative fracture 1 m long (normalized fracture area) for that data set (Table 4-2), following the general methodology of Newendorp (1975, pages 233–243).

Although surface weathering phenomena are likely to increase fracture apertures through time, these surficial processes are expected to have a less pronounced effect on number and lengths of fractures. Pavement preparation (Barton, et al., 1993) ensured that a comprehensive census of fractures was made and that the lengths of all fractures longer than 0.2 m were accurately measured. Areal fracture density was computed by summing the total fracture length within the area of consideration and dividing by the area. Multiplying this areal fracture density (m/m^2) by the normalized fracture area (m^2/m), gives an alternative, and probably more representative, fracture porosity (here referred to as the smoothed fracture porosity) than the raw fracture porosity [see combined data sets (2) and (3) in Table 4-2]. Because of the reliability of the fracture length data, areal fracture density can be calculated in two ways, one uses only the summed lengths of fractures with measured apertures; and the other uses the summed lengths of all fractures (Table 4-2). These alternative values are then used to compute two values for the smoothed fracture porosities for the combined data sets (Table 4-2).

A statistically more representative aperture distribution can be obtained by using the data to generate a normalized probability function that describes the aperture distribution per unit of fracture length. Each of the combined data subsets (swarm, background, and all data) was binned according to aperture, using a bin size of 0.05 mm. This bin size was chosen because it is greater than the smallest measured fracture aperture (0.04 mm) and provides a

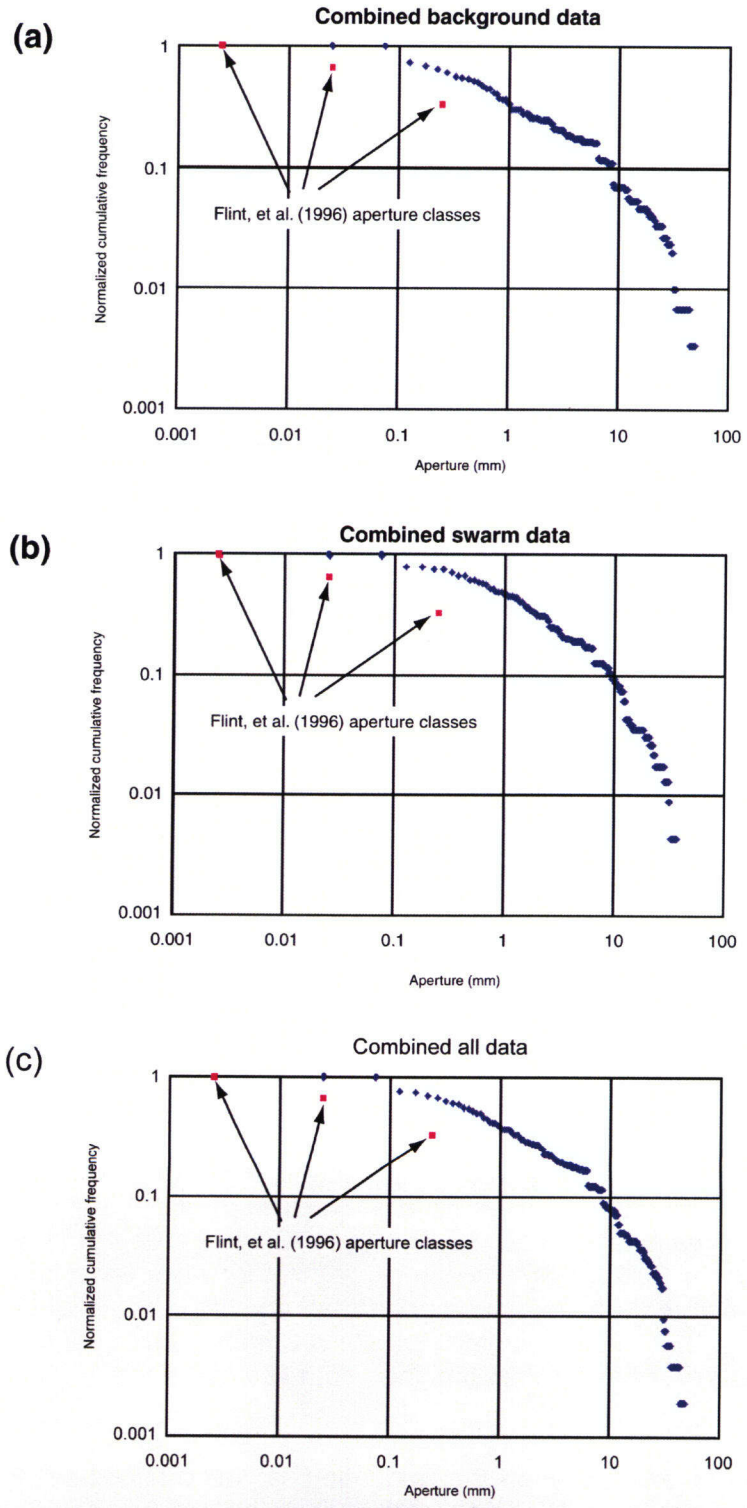

Figure 4-40. Plots Showing Normalized Cumulative Frequency of Fractures Versus Fracture Aperture. Fracture Data are Plotted for (a) Background, (b) Swarm, and (c) Combined Background and Swarm. Data are from Maps of Pavements 100, 200, and 300 (from Barton, et al., 1993).

high-resolution view of the data. Binned aperture (abscissa) was plotted against normalized cumulative frequency (number of fractures in a bin, divided by the total number of fractures in the data set) for each of the three subsets on a log/log plot (Figure 4-40). Summing the area beneath the resulting curve over the range of the aperture data yields the aperture area of a representative fracture 1 m long (normalized fracture area) for that data set (Table 4-2), following the general methodology of Newendorp (1975, pages 233–243).
Although surface weathering phenomena are likely to increase fracture apertures through time, these surficial processes are expected to have a less pronounced effect on number and lengths of fractures. Pavement preparation (Barton, et al., 1993) ensured that a comprehensive census of fractures was made and that the lengths of all fractures longer than 0.2 m were accurately measured. Areal fracture density was computed by summing the total fracture length within the area of consideration and dividing by the area. Multiplying this areal fracture density (m/m^2) by the normalized fracture area (m^2/m), gives an alternative, and probably more representative, fracture porosity (here referred to as the smoothed fracture porosity) than the raw fracture porosity [see combined data sets (2) and (3) in Table 4-2]. Because of the reliability of the fracture length data, areal fracture density can be calculated in two ways, one uses only the summed lengths of fractures with measured apertures; and the other uses the summed lengths of all fractures (Table 4-2). These alternative values are then used to compute two values for the smoothed fracture porosities for the combined data sets (Table 4-2).

4.13.5 Area-Average Infiltration Fracture Porosity

Mapping fractures of 2 m long and longer on Live Yucca Ridge (which encompasses Pavement 100) revealed that fracture swarms constitute 5 to 15 percent of the bedrock area (Figure 4-8). This area weighting can be used with fracture porosity estimates, from swarm versus background areas, to calculate an area-averaged fracture porosity at the bedrock/cover interface. For example, if swarms constitute 5 percent of the infiltration area using the combined data set (3), from Table 4-2, the area-averaged fracture porosity for the infiltration area would be 0.0047; whereas if swarms constitute 15 percent of the area, the area-averaged fracture porosity would be 0.0060.

4.13.6 Implications to Unsaturated Zone

Fracture apertures in upper lithophysal unit of the Tiva Canyon Tuff assumed by Flint, et al. (1996a) are in three size categories: 0.25, 0.025, and 0.0025 mm. In contrast, Barton, et al., (1993) report fracture apertures exposed in pavements in the upper lithophysal unit of the Tiva Canyon Tuff to range from 0.04 to 50.8 mm (Figure 4-40). Normalized fracture area (aperture area per unit length, m^2/m) calculated using the aperture distribution of Flint, et al. (1996a) is 0.0001, compared with the considerably larger values of 0.0031 and 0.0053 for the background and swarm data collected by Barton, et al. (1993).

Fracture porosity for upper lithophysal unit of the Tiva Canyon Tuff was estimated by Flint, et al. (1996a) to be 0.00222, based on borehole measurements (calculated by summing porosity contributions of 0.25, 0.025, and 0.0025 mm aperture fractures). Fracture porosities at the bedrock/cover interface range are approximately 0.017 for fracture swarms and 0.004 for background. Considering the areal proportions of swarm versus background the average fracture porosity in the upper lithophysal unit of the Tiva Canyon Tuff for larger areas is approximately 0.0047 to 0.0060.

The new estimates of fractures at the bedrock/cover interface show considerably larger fracture apertures and fracture porosities than values previously used by Flint, et al. (1996a) in infiltration modeling. The approach used in this analysis was to characterize the infiltration fracture porosity using the greatest strengths of the existing data and to provide statistically defensible values. To avoid overestimating the fracture porosity at the ground surface, the smoothed fracture porosity values were formulated. Nevertheless, significant inhomogeneities of fracture porosity occur at Yucca Mountain as large individual fractures and long fracture swarms. The occurrence of these features is not well-constrained, and the potential influence of such features on infiltration could and should be accounted for in future infiltration modeling.

4.14 Analyses of Enhanced Characterization of the Repository Block Data

Preliminary examination of raw data from the detailed line survey along the Enhanced Characterization of the Repository Block Cross Drift indicates both length and orientation sampling biases inherent to one- and two-dimensional sampling methods. The raw data indicate that fracture population consists of fractures in two dominant orientations at a high angle to the scanline (Figure 4-41a,b). Data with Terzaghi (1965) correction for scanline orientation bias indicate that fractures in the two dominant orientations are equally abundant. Because fractures oriented at a low angle to the scanline are undersampled (Figure 4-42a,b), fracture densities and orientation distributions derived from raw Enhanced Characterization of the Repository Block detailed line survey data (Mongano, et al., 1999) reflect sampling bias. Terzaghi (1965) corrections applied to fracture densities indicate that fracture densities derived from the raw Enhanced Characterization of the Repository Block detailed line survey data under represent the actual fracture densities in the rock mass (Figure 4-42b).

The main portion of the Enhanced Characterization of the Repository Block Cross Drift trends 229°, oblique to the north-south-trending, block-bounding normal faults in the Yucca Mountain region (Day, et al., 1998a). This orientation is favorable for the investigation of block-bounding and smaller scale faults. Of the 137 faults and shears intersected by the Enhanced Characterization of the Repository Block, 30 have displacements greater than 0.1 m (Mongano, et al., 1999). The faults encountered in the Enhanced Characterization of the Repository Block indicate variations in fault-damage-zone widths and spatial distribution, fault-zone textures, and fault-zone alteration (see discussion in Section 2.4). Faults and fault-damage zones exposed in the Enhanced Characterization of the Repository Block can be examined to provide technical bases for data and model justification and data and model uncertainties and verification.

4.15 Structure and Stratigraphy of the Alluvial Aquifer

One of the critical components in the evaluation of Yucca Mountain as a potential repository for safe disposal of high-level waste is groundwater flow in the saturated zone, from beneath the repository footprint to the critical group located 18 km down gradient toward the Amargosa Valley. Several important uncertainties remain unresolved in predicting the behavior of groundwater flow, including groundwater flow in the saturated alluvial or valley-fill aquifer down gradient from Yucca Mountain, near the 18-km compliance location designated in the EPA standards for Yucca Mountain, Nevada (40 CFR Part 197).

(a) ECRB Cross Drift Middle Nonlithophysal zone Sta. 10+15.04 - 14+42.28

Noncorrected

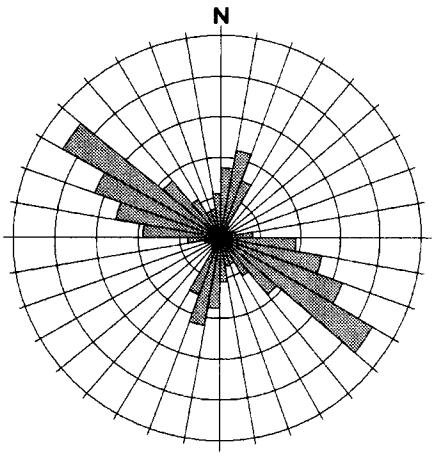

n = 930
Plot Radius = 10%

Terzaghi (1965) Corrected

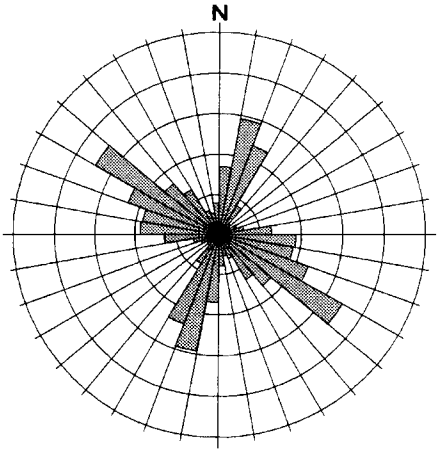

n = 1406
Plot Radius = 10%

(b) ECRB Cross Drift Straight Portion Sta. 03+27.25 - 23+20.70

Noncorrected

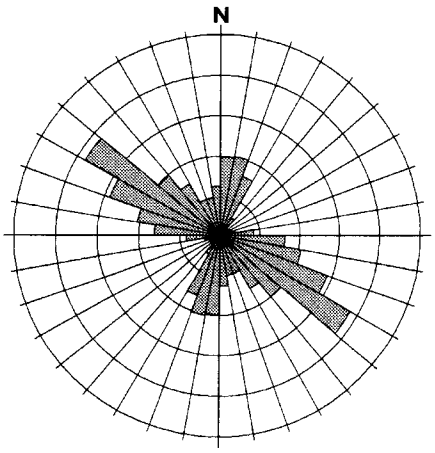

n = 1532
Plot Radius = 10%

Terzaghi (1965) Corrected

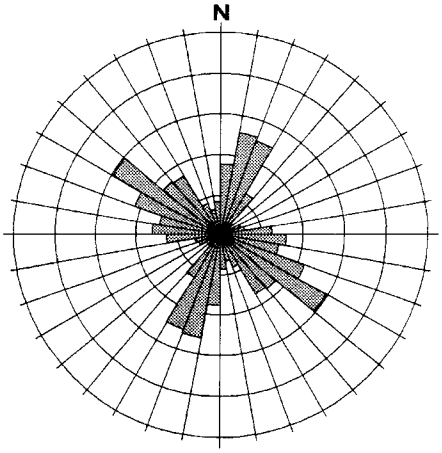

n = 2393
Plot Radius = 10%

Figure 4-41. Rose Diagrams Showing the Distribution of the Raw Fracture and Terzaghi (1965)-Corrected Data for the Enhanced Characterization of the Repository Block. (a) Shows the Middle Nonlithophysal Zone of the Topopah Spring Tuff and (b) Shows the Entire Enhanced Characterization of the Repository Block.

(a)

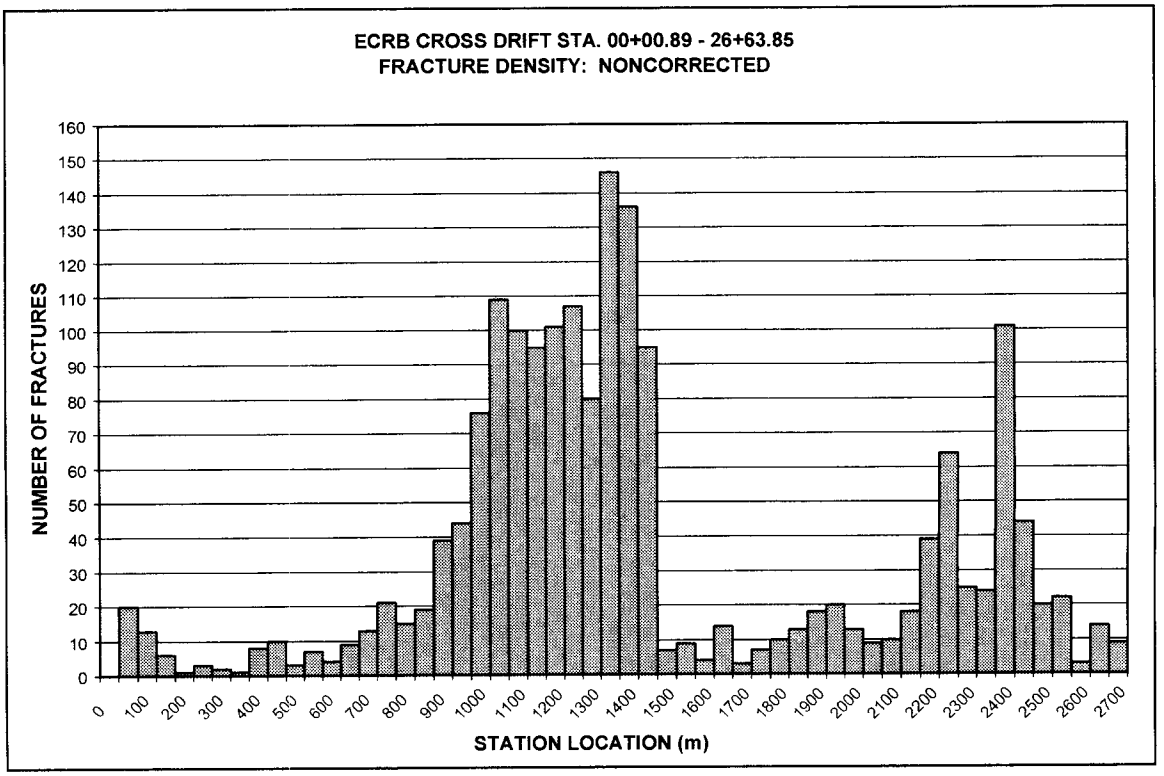

(b)

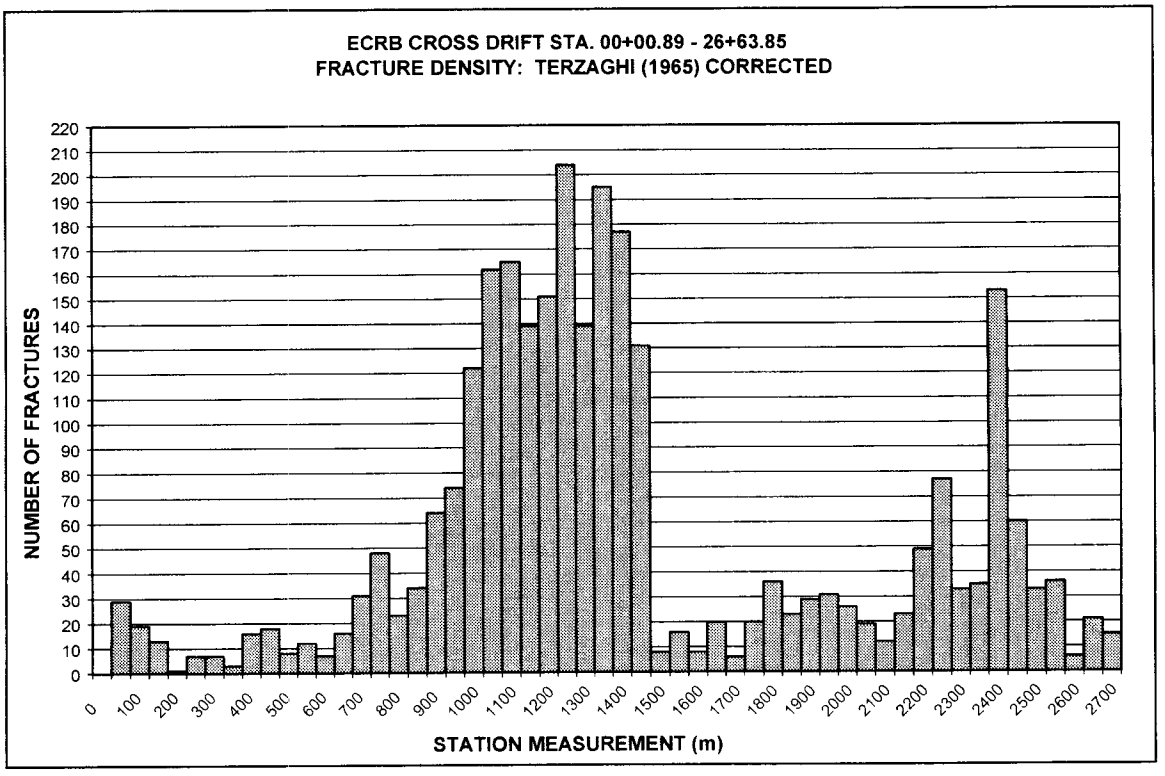

Figure 4-42. Frequency Diagrams of Fracture Density for the Enhanced Characterization of the Repository Block: (a) Raw Fracture Data and (b) Terzaghi (1965)-Corrected Data

As summarized in the Unsaturated and Saturated Flow Under Isothermal Conditions Issue Resolution Status Report (NRC, 1999b), site characterization data, principally from the Nye County drilling program, indicate that all flow paths crossing the 18-km boundary pass through at least some portion of the saturated valley-fill aquifer. Estimates of the distance any potential flow path might travel through alluvium remain an important uncertainty because migration of radionuclides is anticipated to be slowed in the alluvium. Geophysical data (gravity and electrical sounding) suggest that the valley-fill aquifer north of Amargosa Valley is thick. For example, a simple Bouguer anomaly map (Snyder and Carr, 1982) reveals a gravity low at Amargosa Valley that extends to the north-northwest across Fortymile Wash. This gravity low could be caused by a thick valley-fill aquifer beneath Fortymile Wash, extending at least 5 km north of U.S. Highway 95. Additionally, Oatfield and Czarnecki (1989) estimated that 5 km north of the town of Amargosa Valley, valley fill may be more than 1,000 m thick.

In current NRC performance assessment models, groundwater flow through the alluvium is one of the most critical factors to repository performance, with regard to production zone thickness, dilution at the wellhead, groundwater travel times, and attenuation of radionuclides by interaction with alluvium minerals (Jarzemba, et al., 1999). In the performance assessment models, the simplifying assumptions of homogeneity and isotropy have been applied to the valley-fill alluvium, but no investigations have been completed to evaluate the significance of these assumptions. Moreover, these simplifying assumptions ignore the observation that most natural sediments are heterogeneous, and that heterogeneities usually give rise to inhomogeneous and anisotopic hydraulic and sorptive properties.

The NRC Total-system Performance Assessment, Version 3.2 code assumes that effective porosity for alluvium follows a uniform distribution between 0.1 and 0.15 (Mohanty and McCartin, 1998). This range is based on crude estimates of specific yield provided by Walker and Eakin (1963). The Walker and Eakin (1963) values are not based on data from the valley-fill sediments south of Yucca Mountain but are instead based on estimates from other sites that these authors considered to be reasonable analogs. Total porosity measurements from near-surface valley-fill sediments (composed of varying quantities of sands and silts) located at the low-level radioactive waste site near Beatty, Nevada, range between 0.25 and 0.45 (Fischer, 1992). These measurements suggest values of effective porosity that appear to exceed estimates of Walker and Eakin (1963) (Farrell, et al., 2000). Because these sediments have undergone little compaction, however, the high-porosity values may not be representative of porosities in the valley-fill deposits below the water table south of Yucca Mountain.

Currently no site-specific data are available for effective porosity in alluvium units. The most recent DOE model of saturated zone flow and transport (CRWMS M&O, 2000c), therefore, relies on a range of effective porosity values estimated by Bedinger, et al. (1989) for alluvium within the southwest Basin and Range. For performance assessment, the effective porosity of alluvium is sampled stochastically from a truncated normal distribution, with a mean value of 0.18 and a standard deviation of 0.05 (CRWMS M&O, 2000c). In addition, geophysical data (e.g., Oatfield and Czarnecki, 1989), well logs (neutron, caliper, and resistivity in particular; see Nye County Early Warning Drilling Program, Phase 1–FY1999, Data Package), and drill cuttings indicate these deposits are composed of spatially varying thicknesses of sands, gravels, silts, clays, and cobbles. As a result, the hydrogeological properties of the valley-fill unit can be expected to show considerable spatial variability.

4.15.1 Alluvial Sedimentary Units of Fortymile Wash

To evaluate uncertainties associated with flow and transport of groundwater in the valley-fill aquifer, the Structural Deformation and Seismicity and Unsaturated and Saturated Flow under Isothermal Conditions Key Technical Issues initiated a joint project in 1998, as part of the Structural Effects on Groundwater Flow Working Group. The goal of the project was to refine concepts about structural and sedimentological controls on groundwater flow in the valley-fill aquifer. The work focused on investigations of valley-fill sediments exposed in Fortymile Wash, specifically to (i) delineate the sedimentary structure of the near-surface alluvium, (ii) determine if the near-surface alluvium can be used as an analog of the alluvium in the saturated zone, (iii) determine values for the hydraulic properties and the distribution of these hydraulic parameters within the alluvium, and (iv) develop a three-dimensional conceptual model of the stratigraphic and structural framework. The objective of this work is to develop a basis and technical expertise to evaluate DOE site characterization and analysis results. Several substantial outcrops of near-surface alluvium are exposed in the entrenched channel of Fortymile Wash. These exposures provide information on the types of sediment comprising the alluvium as well as sedimentary architecture. Because subsurface information about the alluvium in the saturated zone is limited and the collection of additional subsurface data is beyond the current scope of the project, the features observed in the near-surface alluvium are presently the best alternative analogs of the valley-fill material in the saturated zone.

Current work has focused on developing a hydrostratigraphic facies framework that can be used in hydrological modeling (Ressler, 2001). Future work will develop hydrological parameter distributions (permeability and conductivity) that can be used in conjunction with the facies results and geophysical profiles correlated with the facies with the geophysical logs of the Nye County Early Warning Drilling Project wells.

Complex pathways within the valley-fill aquifer are supported by detailed examination of the alluvial and fluvial sediments exposed in entrenched sections of Fortymile Wash. Work by Ressler (2001) indicates that a braided stream model best represents the depositional system of Fortymile Wash. The alluvium of Fortymile Wash consists of predominantly gravels and sands interpreted as braided stream deposits. Only minor deposits of sediment gravity flows were observed in the modern channel, but such deposits are more abundant on the transverse fans rimming Fortymile Wash. Ressler (2001) identified eight diagnostic lithofacies based on sediment grain size, sedimentary features, and sedimentary geometry. These eight lithofacies indicate a history of fluvial activity within a network of active braid channels and intervening bars, punctuated by deposits of larger magnitude, unchannelized flood flows. Laterally bounding the active channel zones were areas bypassed by active sedimentation (i.e., floodplains), reflected in the stratigraphic record by paleosols. Deposits of sediment gravity flows arise from the ridges rimming Fortymile Wash and interfinger with the deposits of Fortymile Wash along its margin.

Laboratory analyses indicate variations in hydraulic properties between several of the delineated facies. Results from Ressler (2001) show that the gravel-dominated facies have lower porosities and higher permeabilities than the sand-dominated facies. Hydraulic estimates for the different facies were developed from laboratory permeameter tests completed on samples of the alluvium, and from empirical relations based on the results of grain-size analyses completed on samples of the alluvium. Porosity estimates ranged from 0.21 to 0.42,

with the coarser grained samples having lower porosities than the finer grained samples. Permeability values within the valley-fill vary over at least three orders of magnitude. The least permeable lithofacies are the paleosols, which are commonly laterally extensive for hundreds of meters. The most permeable facies is horizontally stratified gravel and sand, which is also the volumetrically dominant facies observed in outcrop.

Ultimately, the conceptual model for the sedimentary structure of the valley-fill alluvium underlying Fortymile Wash will provide a basis for developing geostatistical descriptions of the distribution of hydrogeologic facies within the alluvium, which can be used to assess whether flow and transport models for the region appropriately account for the effects of the heterogeneous flow system, such as confinement of flow between lower permeability strata and channelization of flow in higher permeability zones within the alluvium.

4.15.2 Geophysical Investigation of Armargosa Valley Sinkhole

In addition to work on the architecture of sedimentary units that comprise the shallow alluvial sedimentary units of Fortymile Wash, staff working on the Structural Deformation and Seismicity Key Technical Issue are also investigating structural controls on groundwater flow along undetected voids and cavities within the alluvial groundwater system. These features could be washout or karst-like structures developed within the valley-fill aquifer or upper part of the regional carbonate aquifer system (Winograd and Thordarson, 1975) by groundwater flow along geologic structures, especially faults. Evidence for the existence of such features includes the large sinkhole exposed in the alluvial fan along the southern margin of Crater Flat (Figure 4-43) and the two large cavities encountered during drilling of the Felderhoff Federal 5-1 borehole (Carr, et al., 1995).

Geophysical investigations of the sinkhole were conducted in the spring of 2000. The sinkhole, located approximately 500 m north of Nye County Wells 1D and 1Dx (Figure 4-44), is roughly 10 m deep and 30 m across at its widest point. The sinkhole cuts Quaternary-Tertiary gravels and soils. Soil consists of a stage IV K horizon and a thick vesicular A horizon. These soils and alluvium rest unconformably on Ammonia Tanks and Rainier Mesa tuff units, Miocene basalt, and carbonate megabreccia deposits. One possibility is that the sinkhole resulted from dissolution of an underlying megabreccia layer or carbonate-dominated alluvial horizon from groundwater flow along faults. Carbonate-dominated cuttings were noted in the well log of Nye County well NC-EWDP-01DX between 60 to 65 feet. Stratigraphic data from Nye County Well NC-EWDP-01DX compared to NC-EWDP-01D indicate that a fault exists between the two wells.

Staff used a variety of geophysical techniques to image both shallow (less than 30 m) and moderate (30 to 300 m) subsurface depths. These techniques included ground magnetic surveying, transient electromagnetism, very low frequency electromagnetism, *Mise-à-la-masse* resistivity, self potential, magnetometric resistivity, electric resistivity tomography, and electromagnetic terrain tomography. Data analyses are ongoing, and results will be presented in future revisions of this report.

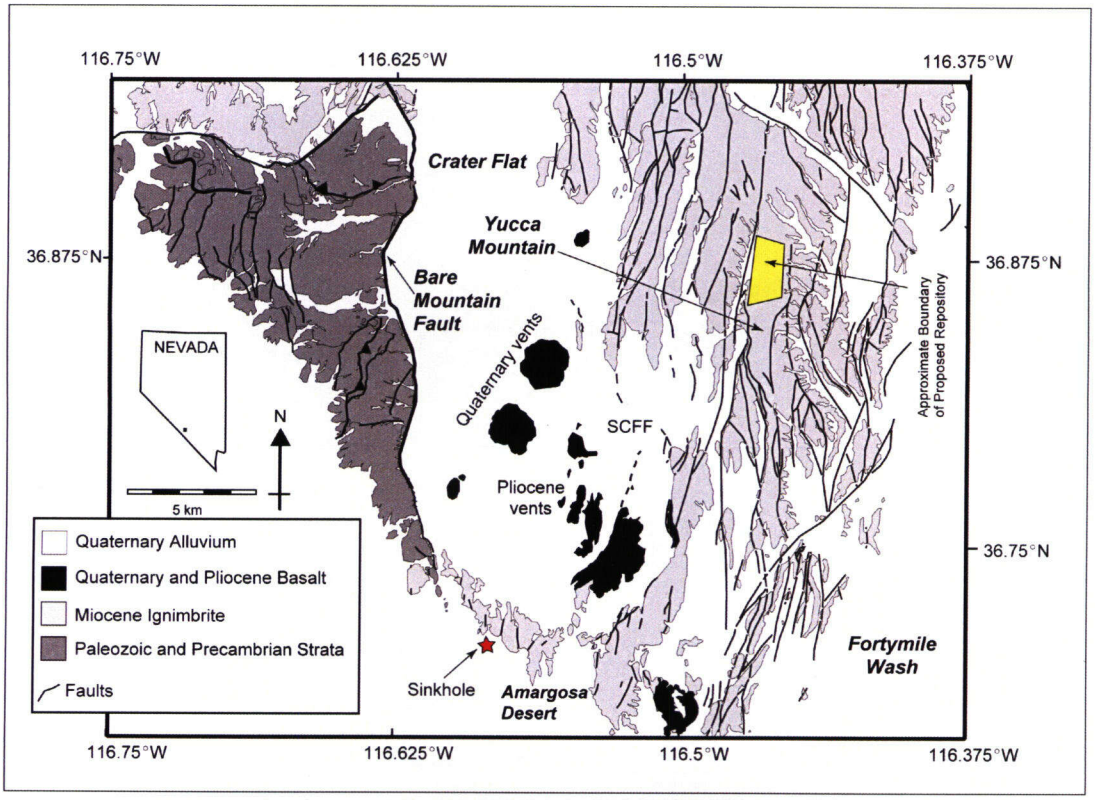

Figure 4-43. Generalized Geologic Map of the Yucca Mountain Region Showing the Location of the Sinkhole Relative to the Proposed High-Level Waste Repository. Fault and Lithologies are from Frizzell and Shulters (1990). Inset Shows a Field Photograph of the Sinkhole Looking Northeast.

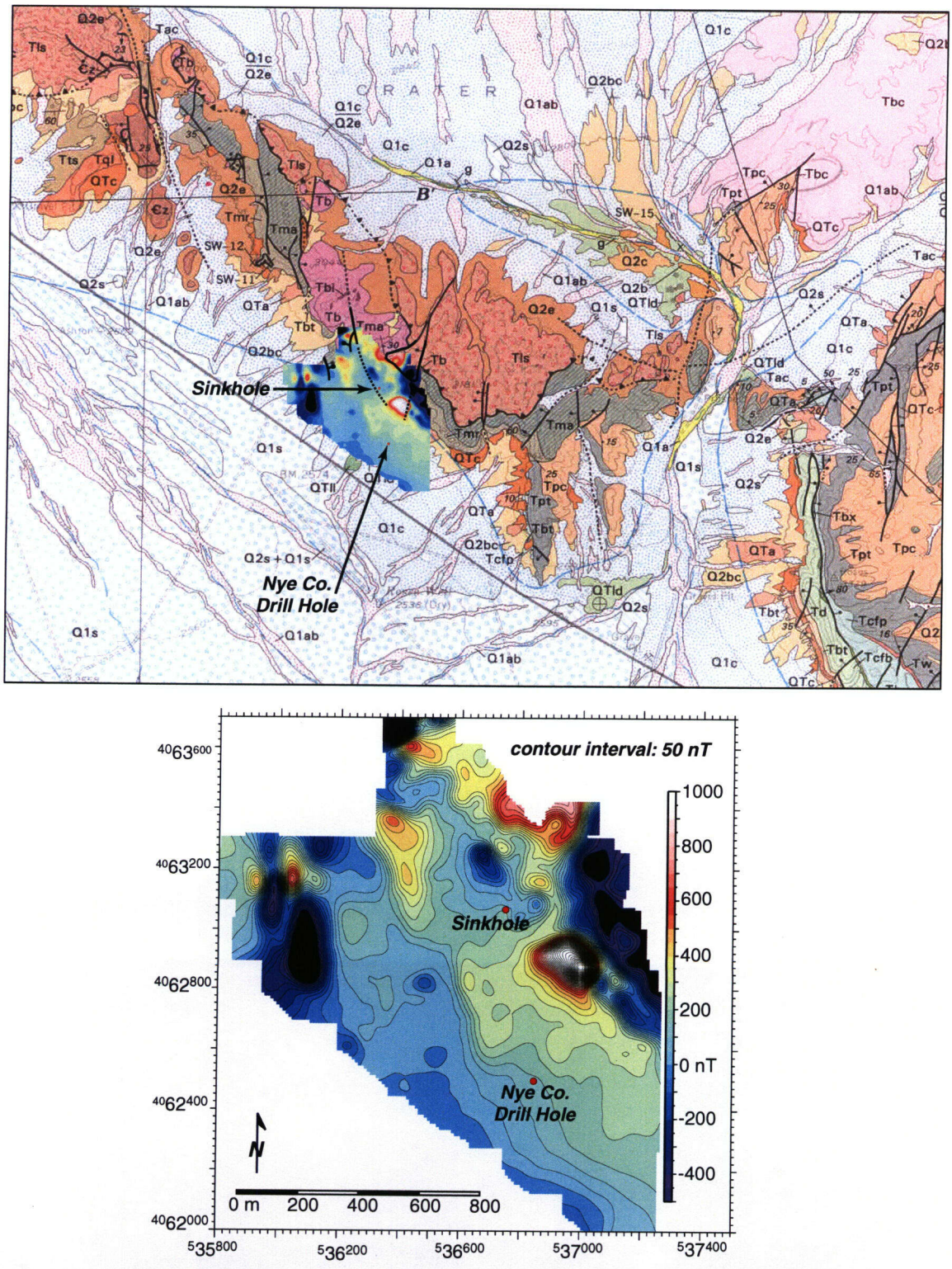

Figure 4-44. Ground Magnetic Map of the Area around the Sinkhole Overlain on the Geologic Map of Swadley and Carr (1987). Inset is an Enlargement of the Ground Magnetic Map. Inset Coordinates are Universal Transverse Mercator, Zone 11.

5 TECTONIC FRAMEWORK OF THE GEOLOGIC SETTING

Tectonic models of Yucca Mountain put geologic features, events, and processes in the site vicinity in the context of geological evolution of the Basin and Range geologic province. Tectonic model boundaries define the boundaries of the geologic setting of the repository. Also, tectonic models are tools that can be used to evaluate such attributes of the Yucca Mountain region as seismic sources, faulting probability, structural control of groundwater flow, magmatism, and long-term geologic stability of the natural and engineered systems. The tectonic framework of Yucca Mountain region refers to the mountain-basin scale of geologic features and processes relevant to repository design and performance. The tectonic framework of Yucca Mountain region overlaps and includes the structural framework of Yucca Mountain, which is discussed in the Fracturing and Structural Framework of the Geologic Setting (Section 4).

5.1 Viable Tectonic Models and Crustal Conditions

Tectonic models of the Yucca Mountain region depict large crustal features such as long faults (e.g., Solitario Canyon fault), extensive fracture systems, volcanoes, blocks of rock as big as mountain ranges, and basins such as Crater Flat, and additional evidence of strains caused by plate tectonics such as detachment faults and the progressive southerly vertical axis of rotation of fault blocks. No single explanation of these features and processes has been accepted by the geological community investigating Yucca Mountain. As a result of discussions held among geologists working on the Yucca Mountain project, five of the approximately one dozen published tectonic models are considered viable or working hypotheses. These are discussed in Section 5.1.2. The principal crustal condition of interest to seismotectonic hazard and volcanic hazard analysis is tectonic strain. Strain, as it affects seismotectonic hazards is also discussed in Section 5.1.2; strain in relation to volcanic hazard is discussed in the Igneous Activity Issue Resolution Status Report (NRC, 1999c).

Geological and geophysical investigations to characterize the Yucca Mountain site have been ongoing for two decades. In addition, the region has been the subject of detailed geological and geophysical investigations related to (i) weapons testing activities at the Nevada Test Site, (ii) academic research in the Basin and Range, and (iii) mineral and petroleum exploration. All of these efforts have provided the DOE (and subcontractors) and the NRC (and subcontractors) with a plethora of geological and geophysical data and interpretations.

The list following highlights those data and interpretations considered by staff as most pertinent to the development and evaluation of viable tectonic models.

5.1.1 Regional and Local Stratigraphic Elements

Regional and local stratigraphic elements to consider in tectonic models are

- Archean and Proterozoic rocks (Table E-1 in NRC, 1999a) that make up the basement in the Yucca Mountain region (Bowring and Karlstrom, 1990).
- Neoproterozoic, Paleozoic, and Mesozoic rocks (Table E-1 in NRC, 1999a) that constitute the bulk of the seismogenic crust in the Yucca Mountain region (Cornwall

and Kleinhample, 1961, 1964; Stewart, 1970; Cornwall, 1972; Monsen, 1983; Poole, et al., 1992, and references therein; Stevens, et al., 1991; Trexler, et al., 1996).

- Cenozoic sedimentary and igneous rocks that underlie most of the Quaternary basins (Table E-1 in NRC, 1999a) and make up Yucca Mountain itself (Ransome, et al., 1910; Byers, et al., 1976; Christiansen, et al., 1977; Vaniman and Crowe, 1981; Swadley, et al., 1984; Carr, et al., 1986a; Bradshaw and Smith, 1994; Sawyer, et al., 1994; Connor and Hill, 1995; Crowe, et al., 1995; Buesch, et al., 1996; Fleck, et al., 1996; Hill and Connor, 1996).

5.1.2 Regional and Local Tectonic Elements

Regional and local tectonic elements to consider in tectonic models are

- Paleozoic and Mesozoic tectonic features including the Mississippian Antler (Nilsen and Stewart, 1980; Burchfiel and Davis, 1972; Oldow, 1984), Permian Last Chance (Snow, 1992a), Permian Sonoma (Gabrielse, et al., 1983), and Mesozoic Sevier (Armstrong, 1968; Camilleri and Chamberlain, 1997) orogenies.

- Oligocene and older (Table E-2 in NRC, 1999a) extensional features (Wernicke, et al., 1987; Hodges and Walker, 1992; Axen, et al., 1993) including those presently exposed along the southwestern flank of Bare Mountain (Ferrill, et al., 1998).

- Neogene (Table E-2 in NRC, 1999a) tectonic features including (i) plate motions (Atwater, 1970; Dokka and Travis, 1990; Bohannon and Parsons, 1995; Dickenson, 1996), (ii) Walker Lane seismotectonics (Stewart, 1988; Hardyman and Oldow, 1991; Oldow, et al., 1994), (iii) Basin and Range detachment faulting (Anderson, 1971; Wright and Troxel, 1973; Stewart, 1978; Wernicke, 1981; Burchfiel, et al., 1982, 1987; Hamilton, 1987; Wernicke, et al., 1988; Maldonado, 1990), and (iv) Basin and Range core complexes (Davis and Coney, 1979).

5.1.3 Geometric Elements

Geometric elements to consider in tectonic models are

- Seismic reflection data (Majer, et al., 1997; Brocher, et al., 1993, 1996, 1998; Young, et al., 1992a).

- Gravity and aeromagnetic data (Snyder and Carr, 1982; Kane and Bracken, 1983; Langenheim, et al., 1991, 1993; Ponce, et al., 1992; Oliver and Fox, 1993; Langenheim and Ponce, 1995; Ponce and Oliver, 1995; Brocher, et al., 1996, 1998).

- Ground magnetic data (Brocher, et al., 1996; Connor, et al., 1997; Stamatakos, et al., 1997a).

- Geologic maps (Cornwall and Kleinhample, 1961; Nakata, et al., 1982; Scott and Bonk, 1984; Swadley and Parrish, 1988; Frizzel and Shulters, 1990; Maldonado, 1990; Monsen, et al., 1992; Faulds, et al., 1994; Simonds, et al., 1995; Day, et al., 1998a,b).

- Borehole data (Carr and Parrish, 1985; Carr, et al., 1986b, 1995).

- Structural cross sections (Scott and Bonk, 1984; Scott, 1990; Young, et al., 1992a,b; Ferrill, et al., 1996b; Fridrich, 1999).

5.1.4 Kinematic Elements

Kinematic elements to consider in tectonic models are

- Vertical-axis rotation markers from paleomagnetism (Gillett and van Alstine, 1982; Nelson and Jones, 1987; Rosenbaum, et al., 1991; Hudson, 1992; Gillett and Geissman, 1993; Holm, et al., 1993; Snow, et al., 1993; Zhang, et al., 1993; Hudson, et al., 1994, 1996; Sonder, et al., 1994; Ferrill, et al., 1995b; Stamatakos and Ferrill, 1996a, 1998; Fridrich, et al., 1999) and sedimentological markers (Snow and Prave, 1994).

- Exhumation and horizontal-axis tilting from radiogenic thermochronology studies (Noble, et al., 1989, 1991; Maldonado, 1990; Monsen, et al., 1992; Hoisch and Simpson, 1993; Sawyer, et al., 1994; Ferrill, et al., 1996b; Weiss, 1996; Hoisch, et al., 1997), calcite-twin deformation studies (Stamatakos and Ferrill, 1996a), conodont color alteration indices (Grow, et al., 1994), and paleomagnetic data (Stamatakos and Ferrill, 1996a, 1998).

- Three-dimensional motions from regional reconstructions based on palinspastic markers (Prave and Wright, 1986; Snow and Wernicke, 1989; Carr, 1990; Stevens, et al., 1991; Caskey and Schweickert, 1992; Snow, 1992a,b, 1994; Axen, et al., 1993; Serpa and Pavlis, 1996; Schweickert and Lahren, 1997).

- Fault displacement analyses (Wesnousky and Jones, 1994; Minor, 1995; Ofoegbu and Ferrill, 1995, 1998; Bruhn and Schultz, 1996; Ferrill, et al., 1996a, 1997, 1999a; Piety, 1995; Stamatakos, et al., 1997b; Marrett, et al., 1998).

- Remote sensing, geodetic, and Global Positioning System results (Gilmore, 1992; Savage, et al., 2001, 1998, 1994; Ferrill, et al., 1996b; Bennett, et al., 1997; Wernicke, et al., 1998; Pezzopane, et al., 1999).

- Stress analyses (Stock, et al., 1985, 1986; Stock and Healy, 1988; Zoback, 1992; Zoback, et al., 1992; Barton, et al., 1995; Bellier and Zoback, 1995; Morris, et al., 1996; Ferrill, et al., 1999b) or seismic moment analysis (Smith, et al., 1989; King, et al., 1994).

- Partitioning of strain (Lienkaemper, et al., 1997; Ferrill and Dunne, 1989; Dunne and Ferrill, 1995; Pezzopane, 1996; Ferrill, et al., 1996c, 1998; Morris, et al., 1996; Ferrill and Morris, 1997; Stamatakos, et al., 1997a; Ofoegbu and Ferrill, 1998; Marrett, et al., 1998; Wernicke, et al., 1998; Pezzopane, et al., 1999; Savage, et al., 2001, 1998)

5.1.5 Paleoseismic and Historical Seismic Elements

Paleoseismic and historical seismic elements to consider in tectonic models are

- Historic seismicity in the Yucca Mountain region, including the Little Skull Mountain earthquake (Arabasz and Julander, 1986; Harmsen, 1991, 1993, 1994; Rogers, et al., 1991; Smith and Arabasz, 1991; Harmsen and Bufe, 1992; Stover and Coffman, 1993; Meremonte, et al., 1995).

- Paleoseismic data from trenching studies along fault scarps and aerial photography analyses of surface deformation studies (Reheis, 1988, 1994; Anderson and Klinger, 1994; Menges, et al., 1995; Pezzopane, 1996; U.S. Geological Survey, 1996), including triggered and clustered seismicity (Anderson, et al., 1994; Bodin and Gomberg, 1994).

5.2 Role of Tectonic Models in Assessment of Data

Interpretations from the suite of viable tectonic models form the basis for investigators to assess the significant data, such as trenching results, in the large context of the site's faulting and seismic hazards. For example, trenching data alone provide useful information on age and amount of net separation of once contiguous horizons or other markers across a fault zone, but rarely provide enough information on actual fault displacement or fault zone kinematics. Additional information, including constraints from viable tectonic models, is needed to obtain a full picture of faulting and seismicity history. Constraints drawn from viable tectonic models help researchers assess other important considerations, including completeness and relative importance of the data to other measures of faulting and seismicity such as Global Positioning System strain rate measurements or the historic seismic record, development and importance of fractures, and development of site models such as the geologic framework models.

To highlight these points consider the following two examples:

- One of the five viable tectonic models proposed for the region is the Amargosa Desert fault of Schweickert and Lahren (1997). This model predicts cryptic strike-slip faulting under the proposed repository. This component of faulting, if it exists, would be poorly represented or completely overlooked by the trenching data results. Trenching techniques are, by themselves, limited to quantifying conspicuous expressions of mainly vertical fault displacement at the surface. Strike-slip faulting is difficult to quantify by trenching, especially if it is distributed, because the motion is horizontal and often results in subtle surface deformation. Even in cases where strike-slip faults are located and trenched, palinspastic markers are not available in the trench walls to allow investigators to gauge actual fault displacement. Other features, including offset stream channels, fold axes, or stratigraphic pinch-outs are necessary to fully describe such fault motion. Naturally, trenching techniques would be of no use in quantifying fault slip on a buried or cryptic strike-slip fault of the type proposed by Schweickert and Lahren (1997). The experts on the DOE probabilistic seismic hazard analysis (CRWMS M&O, 1998) included possible seismic sources based on the viable tectonics models, in addition to those quantified by the trenching data. The resulting seismic hazard curve for Yucca Mountain forecasts a greater seismic hazard than one would

predict if it the trenching data were used in isolation from all other geologic observations.

- Recent controversy regarding Global Positioning System strain-rate measurements (cf. Wernicke, et al., 1998; Savage, et al., 2001, 1998) also raised concerns regarding the applicability of the paleoseismic data to the generation of a reliable seismic hazard assessment. As discussed in this section of this report, recent confirmatory analyses by the Center for Nuclear Waste Regulatory Analyses (CNWRA) and the U.S. Geological Survey specifically designed to test the Wernicke, et al. (1998) results shows that the Global Positioning System readings are anomalous and not representative of actual crustal strain conditions that would lead to enhanced seismic activity at Yucca Mountain (e.g., Marrett, et al., 1998; Pezzopane.[2]) A critical part of those confirmatory analyses was the application of tectonic models to test the Global Positioning System strain rate results.

5.3 Viable Tectonic Models of Yucca Mountain Region

Review of the geologic literature by staff suggests that tectonic interpretations of the Yucca Mountain region can be organized into 11 tectonic models. Staff from the NRC, the CNWRA, the DOE, the U.S. Geological Survey, and the State of Nevada met in San Antonio on May 7–8, 1996, for an Appendix 7 meeting to discuss conceptual tectonic models. In this meeting, the 11 tectonic models proposed for the Yucca Mountain region were reviewed in the context of the most recent geological and geophysical data.

From discussions in the meetings, it was clear that 5 out of the 11 tectonic models were presently supported by the existing data (Appendix C-1 in NRC, 1999a). Although new data may promote one of the other six models currently considered not viable (Appendix C-2 in NRC, 1999a), the five models listed in Appendix C-1 (NRC, 1999a) form the bases for issue resolution at this time. In addition, there was no general consensus on which models are truly independent and which models may function as subsets of others. In a broader sense, these five models can be considered in two general categories of deformation. The first three models are dominantly related to extensional deformation, and the latter five are dominantly related to strike-slip deformation. Moreover, the five models are not mutually exclusive. Locally, extensional-dominated deformation (e.g., within Crater Flat) can exist within a larger region of trans-tensional deformation related to a pull-apart basin. The implications of the five viable models to repository performance subissues are summarized in Appendix C-3 (NRC, 1999a). All five viable tectonic models should be used to bound the impact of faulting, fracturing, and seismicity on repository performance.

The CRWMS M&O (1998) and O'Leary (U.S. Geological Survey, 1996) proposed a reclassification of the 11 tectonic models and suggested that the elastic-viscous model was the preferred or favored model. The CRWMS M&O (1998) and O'Leary (U.S. Geological Survey, 1996) organized tectonic models into three generic classes based on what O'Leary termed bulk mechanical behavior (U.S. Geological Survey, 1996, pages 8–51). These classes were simple, pure, and lateral shear. By simple shear, CRWMS M&O (1998) and O'Leary (U.S. Geological Survey, 1996) actually refer to models that evoke some form of detachment faulting (i.e., the

[2]Pezzopane. Oral Communication at Appendix 7 Meeting. March 2–3, 1999.

deep, intermediate, and shallow detachment models described in Appendices C-1 and C-2). By pure shear, CRWMS M&O (1998) and O'Leary (U.S. Geological Survey, 1996) refer to models that evoke horsts and graben fault block models like the planar fault block and domino fault block models (Stewart, 1978; Fridrich, 1999). By lateral shear, CRWMS M&O (1998) and O'Leary (U.S. Geological Survey, 1996) refer to strike-slip-dominated models like the Amargosa shear model of Schweickert and Lahren (1997). The caldera model of Carr (1982, 1984, 1988, 1990) and Carr, et al. (1986a) was considered as a fourth unique model. The synclinorium model of Robinson (1985) was not discussed (U.S. Geological Survey, 1996).

In summary, CRWMS M&O (1998) presents a favored model of planar, steeply-dipping faults. Fault blocks are considered to deform internally, and voids between fault blocks are allowed to be filled by a ductile (fluid) middle crust. The model is based on the boundary element modeling of Janssen (1995). In the model, the seismogenic crust is treated as a quasi-elastic layer resting on a viscous middle and lower crust. According to CRWMS M&O (1998), the model addresses the following important geological and geophysical considerations.

- Faulting and basaltic volcanism are episodic and coupled.
- The Crater Flat domain is essentially a half-graben with Yucca Mountain faults antithetic to the master Bare Mountain fault.
- The vertical-axis rotations from strike-slip faulting are a secondary phenomena, related to a discrete period of oroclinal bending.
- Faults are planar to the base of the seismogenic crust and dip between 30 and 60°. They are essentially linear cracks in which displacements are treated as stress perturbations.
- Stress conditions at the base of the crust control distribution of basaltic volcanism.
- Faulted blocks are in isostatic equilibrium.
- Elastic behavior of the crust (brittle and ductile) during an earthquake with relaxation creep in lower crust between earthquakes.
- Rollover into faults in Crater Flat, especially the Bare Mountain fault, is not a result of fault geometry but of elastic flexure of the hanging wall.

The CRWMS M&O (1998), following U.S. Geological Survey (1996) and Fridrich, et al. (1999), further subdivides the Crater Flat domain by a subdomain boundary simply referred to as the hinge line (Figure 8.6 in U.S. Geological Survey, 1996; Figure 3.3-1 in CRWMS M&O, 1998). The hinge line is defined as both a conceptual and physical feature. It apparently follows a subtle, but sudden, decline in average elevation of Yucca Mountain blocks—lower to the southeast (Fridrich, et al., 1999)—along a series of ridge terminations, aligned fault splays, Z-shaped bends in the ridge crests, and several small-magnitude aeromagnetic anomalies (U.S. Geological Survey, 1996). Northeast of the line, fault blocks with relatively high relief are juxtaposed across steeply dipping faults with relatively small displacements. Southwest of the hinge line, fault blocks are more strongly tilted and juxtaposed across faults with shallower dips and greater displacement (Scott and Bonk, 1984; Scott, 1990; Day, et al., 1998b).

U.S. Geological Survey (1996), CRWMS M&O (1998) and Fridrich, et al. (1999) consider the amount of clockwise vertical-axis rotations indicated by anomalous paleomagnetic declinations in the tuffs (Rosenbaum, et al., 1991; Hudson, et al., 1994) to be the most important indicator of the hinge line. Northeast of the line, clockwise vertical-axis rotations are limited to 20° or less. Southwest of the hinge line, vertical-axis rotations range between 20 and 45°. The vertical axis rotations are interpreted in terms of a discrete period of dextral, strike-slip strain following within about 1 million years of the major pulse of Crater Flat extension (Hudson, et al., 1996) or the result of concentrated strain along bending beams due to differential extension of southern Yucca Mountain (U.S. Geological Survey, 1996). Along with spatial and temporal variations in the amount of extension on faults, the significance of the paleomagnetic data is that the main locus of deformation in the Crater Flat domain has migrated to the southwest with time. The implication is that the hinge line effectively isolates Yucca Mountain in the northeast subdomain from active deformation in the southwest subdomain, thereby reducing the risk of future seismicity and volcanism at Yucca Mountain.

Several aspects of the hinge-line argument are inconsistent with the available geological and geophysical data. First, structural and gravity data define a diffuse eastern margin of the Crater Flat half graben well east of the ridges that comprise Yucca Mountain proper (Ferrill, et al., 1996b; Connor, et al., 2000). Within this half-graben, Yucca Mountain appears, in plan view, as bow-shaped, convex toward the east. Similar to many curvilinear structural features worldwide, curvature alone is not indicative of horizontal bending of a previously more linear feature (e.g., Stamatakos and Hirt, 1994), as supposed by the U.S. Geological Survey (1996) explanation. Numerous curved structural features are primary and simply reflect the interplay between local variations of the imposed deformation and lateral variations in crustal anisotropy (e.g., Marshak, 1988; Ferrill and Groshong, 1993).

Second, the interpretation that all faults change strike northwest and southwest of the hinge line is misleading. In northern Crater Flat, the northeast-trending faults are an extension of the radial pattern of faulting in the region immediately surrounding the Miocene Timber Mountain caldera. In southern Yucca Mountain, there are some northeast-trending faults, but many faults also have north-south strikes.

Third, the interpretation that anomalous paleomagnetic declinations necessarily signify vertical axis rotations related to oroclinal bending is overly simplistic (e.g., Gray and Stamatakos, 1997). The rigorous test of vertical-axis rotations resulting from oroclinal bending was defined in Schwartz and Van der Voo (1984). The test plots paleomagnetic declinations as a function of the orientation of structural trends. The assumption in an oroclinal bending model is that both prebending structures (in this case, normal faults) and corresponding paleomagnetic vectors will correlate if both were passively reoriented by vertical-axis rotations. A significant correlation between declination and strike with a slope of one implies bending of an originally linear feature (e.g., Van der Voo, et al., 1997). Significant correlations between declination and strike with a slope of less than one implies bending of an originally curved feature (e.g., Eldredge, et al., 1985).

Plots of the paleomagnetic declination versus strike of structural trends in Crater Flat and at Yucca Mountain based on available data do not support a simple orocline (vertical-axis rotation) model (Figure 2a in Stamatakos and Ferrill, 1998), especially when compared to regions in which oroclinal bending is well established (Figure 8 in Van der Voo, et al., 1997). The analysis of Stamatakos and Ferrill (1998) shows that the distribution of magnetic declinations recorded

in the Tiva Canyon Tuff (Rosenbaum, et al., 1991) at Crater Flat and Yucca Mountain is independent of structural trend.

An alternative explanation of the rotated paleomagnetic directions is that they resulted from differential displacement on listric normal faults (Figure 3a in Stamatakos and Ferrill, 1998). In this geometry, hanging walls rotate about a steeply inclined axis as displacement proceeds (Figure 3b in Stamatakos and Ferrill, 1998). Faults that are incorporated into the hanging walls of other faults may also rotate. Faults that form the ultimate footwall (not incorporated into a hanging wall of another fault) or faults that form after an initial period of extension may not necessarily be rotated (Figure 4c in Stamatakos and Ferrill, 1998). This situation appears to mimic that at southern Yucca Mountain (compare Figure 4c with Figures 1 and 2 in Stamatakos and Ferrill, 1998). In this interpretation, the increase in the amount of clockwise rotations indicated by the paleomagnetic declinations in southwestern Crater Flat result from lateral southward increases in displacement on Crater Flat faults, like the Solitario Canyon fault (e.g., Scott, 1990). Moreover, this interpretation is entirely consistent with the observation that the greatest amount of extension is in the southern part of Crater Flat (e.g., Scott, 1990; Ferrill, et al., 1996a; Stamatakos, et al., 1997b; Fridrich, 1999).

5.4 Comment on Snow and Wernicke (2000) Detachment Faulting Model

Snow and Wernicke (2000) reconstruct the Death Valley extensional belt to its pre-extensional state 36 million years ago. The proposed reconstruction fits together exposed fragments of a once-continuous Sevier-age fold and thrust belt dismembered by Tertiary extension of the Basin and Range. Key components in the reconstruction are palinspastic markers such as stratigraphic pinchouts and fault cutoffs, paleoflow directions, and paleomagnetic data. Bare Mountain, Nevada, which exposes two pre-Tertiary thrust faults within a thick section of Neoproterozic to late Paleozoic strata, has important features that bear on the validity of the Snow and Wernicke (2000) hypothesis. The implication of the Snow and Wernicke (2000) model is that there was substantial shallow-angle detachment faulting throughout the Yucca Mountain region in the late Miocene and even early Pliocene. Their model envisions east-west lateral displacements of large crustal blocks on the order of tens of kilometers and large vertical-axis rotations of these crustal blocks up to 90° or more. If correct, the Snow and Wernicke (2000) model calls into question several important assumptions (e.g., age and timing of faulting on the Bare Mountain fault) used to establish a framework for the tectonic setting used by experts of the probabilistic seismic hazard analysis.

5.4.1 Covariance of Thrust Faults and Paleoflow Data

Snow and Wernicke (2000) conclude that Bare Mountain rotated clockwise about a vertical axis nearly 90° between circa 16 and 10 million years ago (Figure 7 of Snow and Wernicke, 2000, pages 668–670). They cite the apparent covariance in orientations of thrust faults and paleoflow directions as evidence for the large vertical-axis rotation.

5.4.1.1 Thrust Faults

Snow and Wernicke (2000) interpret two pre-Tertiary thrust faults, the Panama thrust in southern Bare Mountain and the Meiklejohn Peak thrust in northeastern Bare Mountain, as part of their reconstructed fold and thrust belt. They draw the two pre-Tertiary thrust faults with

east-west strikes (Figure 3 of Snow and Wernicke, 2000, page 662) compared with their inferred north-south-trending and linear pre-extensional fold and thrust belt. According to the map of Monsen, et al. (1992), however, the Panama thrust actually strikes northeast-southwest and the Meiklejohn Peak thrust strike varies from northwest to east-northeast.

5.4.1.2 Paleoflow Data

Mean paleoflow directions from trough cross-beds in Neoproterozoic to Cambrian quartzites at Bare Mountain were interpreted to trend north compared to west trends of mean paleoflow directions in the same rock units exposed on nearby unrotated ranges (Snow and Prave, 1994). Nevertheless, paleoflow data for Bare Mountain exhibit a wide range of flow directions. As shown on Figure 3 of Snow and Prave (1994, page 171), azimuths of paleoflow directions from Bare Mountain are nearly evenly distributed between azimuth 330° and azimuth 120°. This type of broad and possibly bi-modal distribution is common in shallow marine and tidal depositional systems. As discussed in Potter and Pettijohn (1977), shallow marine sandstones may have paleoflow directions that are oriented offshore, oblique, and parallel to the paleoshoreline and paleoslope. In addition to questions about possible original variations in the orientation of sediment transport directions over such large distances, the authors conclude that such a broad distribution of directions does not provide a compelling basis for any interpretations of vertical-axis rotations.

5.4.2 Paleomagnetic Data

Permian-Triassic and Miocene magnetizations from Bare Mountain do not indicate any statistically significant vertical-axis rotations (Stamatakos, et al., 1998). Specifically, three distinct magnetizations at Bare Mountain were observed, all without significant vertical-axis rotations. These magnetizations are: (i) a dual-polarity Miocene primary or secondary magnetization in the 14 to 15 million years ago porphyry dikes (ages based on conventional Ar-40/Ar-39 dates from Weiss, 1996) carried by magnetite with relatively high unblocking temperatures (~560 to 580 °C); (ii) a dual-polarity Miocene or younger secondary magnetization (**H**-component magnetization) in the Ordovician carbonate rocks carried by hematite; and (iii) a dual-polarity Permian to Triassic secondary magnetization (**M**-component magnetization) carried by magnetite with relatively moderate unblocking temperatures (~420 to 480 °C) and intermediate coercivities (10 to 40 mT).

Snow and Wernicke (2000) dismiss these paleomagnetic results in favor of the paleoflow and fault-strike argument. They claim that the analysis of the paleomagnetism was flawed, arguing the age and significance of the **M**-component magnetization was incorrectly interpreted. Instead of the interpreted Permian-Triassic age, they conclude that the **M**-component magnetization was acquired in the late Miocene from hydrothermal alterations associated with movement along the nearby Fluorspar Canyon Detachment. Snow and Wernicke (2000) assert that the **M**-component magnetization was acquired just after significant clockwise rotation of Bare Mountain. Their assertion is based on proximity of the paleomagnetic sites to the Fluorspar Canyon Detachment, the dual polarity of the **M**-component magnetization compared to the dominant reversed polarity for Triassic-Permian magnetization elsewhere in southern Nevada, and an alternative structural plunge correction for Bare Mountain (east-southeast plunge instead of the northeast plunge) based on thermochronologic data from Hoisch, et al. (1997). The alternative east-southeast plunge correction aligns the **M**-component magnetization with

the Miocene reference direction. This reassessment of the paleomagnetic analysis is, however, incompatible with geological and geomagnetic evidence from Bare Mountain.

5.4.2.1 Remagnetization Related to Fluorspar Canyon Detachment

In spite of proximity to the Fluorspar Canyon detachment, carbonate rocks that carry the **M**-component magnetization are relatively unaltered compared to all other carbonate rocks at Bare Mountain. No evidence was found of hydrothermal alterations in the carbonate rocks bearing the **M**-component magnetizations. To the contrary, the rocks in the hanging wall of the Meiklejohn Peak thrust are the least altered rocks exposed at Bare Mountain. This observation is supported by paleothermometry data from calcite-twin geothermometry (Stamatakos and Ferrill, 1996b) and conodont color alteration indices (Grow, et al., 1994), which show these rocks record the lowest paleotemperatures of all rocks at Bare Mountain.

In addition, the timing argument proposed by Snow and Wernicke (2000) is incompatible with the age and orientation of the 14 to 15 million years ago porphyry dikes exposed in eastern Bare Mountain. Snow and Wernicke (2000) propose: (i) 90° clockwise vertical-axis rotation beginning at 16 million years ago; (ii) Fluorspar Canyon detachment faulting and acquisition of the **M**-component magnetization between 13 and 10 million years ago; and (iii) ~30°east-southeast tilting after remagnetization (i.e., after 13 to 10 million years ago).

The problem with this interpretation is that the14 to 15 million year old porphyry dikes in eastern Bare Mountain presently strike north-south and dip vertically. This orientation is consistent with known Miocene east-west extension (e.g., Zoback, et al., 1981). Thus, the authors contend that rotations of Bare Mountain about vertical or horizontal axes predates intrusion of the dikes. This assertion is based on the premise that the dikes were intruded vertically, perpendicular to the regional extension direction. The Snow and Wernicke (2000) proposed south-southeast tilt and 90° vertical-axis rotations require dikes with 60° dips to the north such that they were fortuitously tilted and rotated to their present north-south vertical positions by the later vertical- and horizontal-axis rotations.

Therefore, because rotation of eastern Bare Mountain occurred prior to 14 to 15 million years ago, a Miocene secondary magnetization acquired from hydrothermal fluids associated with 10 to 13 million years ago motion on the Fluorspar Canyon detachment could not record this earlier horizontal-axis tilting. The assertion by Snow and Wernicke (2000) that the **M**-component is a pre-tilting Miocene magnetization associated with movement on the Fluorspar Canyon detachment is thereby negated by the details of timing between dike intrusion, horizontal-axis rotation, and movement on the Fluorspar Canyon detachment.

5.4.2.2 Dual Polarity Magnetization

The argument by Snow and Wernicke (2000) that Permian-Triassic secondary magnetizations should all have reversed polarities is unfounded. In fact, dual polarity Permian-Triassic remagnetization should be expected. Unlike carbonate rocks in the central Appalachians, which were remagnetized during the approximately 30 million years ago long reversed-polarity Kiamen superchron, the Permian-Triassic secondary magnetizations in the Basin and Range were acquired at a time when the field was reversing at a rate comparable to average reversal-rate for the Tertiary (e.g., approximately 30 reversals in the last 20 million years of the

Permian according to Haag and Heller, 1991). More importantly, it is noted that the character of the **M**-component demagnetizations (i.e., moderate unblocking temperature and coercivity spectra) match those of other Permian-Triassic secondary magnetizations elsewhere in Nevada (e.g., Gillette and van Alstine, 1982). In addition, and in contrast to most localized hydro-chemical secondary magnetizations, the moderate unblocking temperatures are characteristic of Paleozoic orogen-scale remagnetizations of carbonate rocks worldwide (e.g., McCabe and Elmore, 1989; Stamatakos, et al., 1996; Van der Voo, et al., 1997).

5.4.2.3 North-Northeast Versus East-Southeast Structural Plunge

The east-southeast tilt for Bare Mountain inferred by Snow and Wernicke (2000) is based on a comparison of thermochronologic data from samples in the Bullfrog Hills to a spatially limited distribution of samples in the northwest corner of Bare Mountain (Figure 1 of Hoisch, et al., 1997, page 2816). The result is an interpretation of plunge from essentially a linear distribution of data. It is suggested that this limited two-dimensional survey of paleotemperatures is insufficient to defined adequately the three-dimensional structural correction for all of Bare Mountain, especially for the hanging wall anticline of the Meiklejohn Peak thrust.

The author's northeast plunge correction, which rotates the *in-situ* **M**-component magnetization to a Permian-Triassic direction, was determined from Pi-diagrams based on direct measurement of bedding around the Meiklejohn Peak fold plunge. Snow and Prave (1994, page 716) used an identical procedure (measurements of bedding around folds near the Panama thrust) to correct the paleoflow data from southern Bare Mountain.

The northeast structural plunge of Bare Mountain is, however, not limited to the hanging wall of the Meiklejohn Peak thrust. The overall map pattern of extensional structures exposed throughout most of Bare Mountain consists of north-dipping bedding and east-dipping extensional faults (see map of Monsen, et al., 1992). The resulting bedding-fault cutoff lines define the northeast structural plunge of extensional structures throughout most of the range (Ferrill, et al., 1998). Detailed measurements of extensional faults and bedding along the west flank of Bare Mountain define a structural plunge of 042/37 (Ferrill, et al., 1998), consistent with the 039/33 structural plunge determined from bedding measurements around contractional structures in the hanging wall of the Meiklejohn Peak thrust. This northeast structural plunge is in fact, consistent with the overall pattern of younging stratigraphy from southwest to northeast across the range, and lowest burial, metamorphic, and deformation temperatures in the northeast corner of the range (Stamatakos and Ferrill, 1996b).

Moreover, correction for an east-southeast tilt, as used by Snow and Wernicke (2000), restores the Meiklejohn Peak thrust to an orientation at odds with their correlative structures in the Last Chance thrust plate and equivalents in southern Nevada. Specifically, if the east-southeast tilt and later 90° vertical-axis rotation of Snow and Wernicke (2000) are assumed, then the fold axis of the Meiklejohn Peak hanging wall anticline corrects to approximately 345/30. This fold-axis orientation is not parallel to the pre-extension north-south fold and thrust belt envisioned by Snow and Wernicke (2000, Figure 7, pages 668–670).

5.4.3 Conclusions

The findings are reaffirmed that the **M**-component magnetization predates Basin and Range extension and that Bare Mountain has not been rotated clockwise 90° as suggested by the Snow and Wernicke (2000) reconstruction. As an alternative, it is suggested that one underlying assumption of the reconstruction—in which the original fold and thrust belt, with a single 400-km-long backfold, was neatly linear and narrowly confined—may be unduly simplistic, especially when compared to similar fold and thrusts belts around the world. A general feature of many fold and thrust belts is their along-strike sinuosity. Curvature in trends of contractional structures in fold and thrust belts is produced by lateral variations in thickness or mechanical behavior of precursor basin stratigraphy, lateral variation in displacement magnitude, and regional or temporal variation in shortening directions (e.g., Macedo and Marshak, 1999; Gray and Stamatakos, 1997; Ferrill and Groshong, 1993; Marshak and Wilkerson, 1992). Along-strike changes in structural trend of 45° or more are common over distances of tens to hundreds of kilometers. Thus, it is proposed the reconstruction by Snow and Wernicke (2000) be modified to permit original along-strike curvatures of the fold and thrust belt similar to those curvatures observed in the Appalachian, Idaho-Wyoming, Jura, Alpines, Carpathian, Sierra Madre Occidental, and numerous other fold and thrust belts around the world. This modification would preserve the regional correlation developed by Snow and Wernicke (2000) but remove the unsupported 90° vertical-axis rotation of Bare Mountain.

5.5 Summary of Staff Interpretation of Crater Flat Tectonics

The first-order structure of the Crater Flat-Bare Mountain region is the pronounced rollover of the Miocene tuffs into the Bare Mountain fault (Young, et al., 1992b; Ferrill, et al., 1996b). This rollover defines the shape of the Crater Flat half-graben, in which the deepest portion of the Crater Flat basin is adjacent to the Bare Mountain fault (e.g., Snyder and Carr, 1982; Ferrill, et al., 1996b). Rollover has long been recognized as the result of hanging wall deformation above a curved or listric fault (Groshong, 1990). The exact geometry of rollover and fault shape depends on the nature of deformation in the hanging wall (Dula, 1990), and the assumption that faulting is restorable because hanging wall volume is preserved during deformation.

The alternative proposed by O'Leary (U.S. Geological Survey, 1996) and more recently in Fridrich (1999) supposes that elastic flexure of the hanging wall causes the rollover geometry. The model does not consider surface geometry as a constraint to deformation kinematics. The ductile middle crust is allowed to fill voids in the subsurface where gaps open between fault blocks. Fault blocks can deform internally if space problems at the surface exist where fault blocks of different dip overlap. The potential mechanisms for internal block deformation, including increased fracturing, are not discussed. According to O'Leary (U.S. Geological Survey, 1996) and CRWMS M&O (1998), the model accounts for the observation that few, if any, historic earthquakes ruptured shallow-angle (detachment) normal faults, including the 1992 Little Skull Mountain earthquake, which appeared to have ruptured a steeply dipping fault near the base of the seismogenic crust.

The tectonic history of Crater Flat, including new modeling of existing geophysical data and the addition of new paleomagnetic data from Miocene basalt and megabreccia deposits in the hills just south of Crater Flat was recently completed (Stamatakos, et al., 1999). In that evaluation,

an alternative tectonic model was proposed that takes into account recent geophysical and geological data. The new model follows some of the general trends developed in Fridrich (1999) with regard to overall extension of Crater Flat Basin. The principal differences between the Fridrich (1999) version and the model proposed herein lies in interpretations of the details of the timing of deformation, the mechanism of hanging wall deformation, the listric versus planar style of faulting, the source of the magnetic anomalies in Crater Flat, and the explicit link developed between extension and vertical-axis rotations, as recorded by paleomagnetic vectors.

Paleomagnetic data and structural models indicate most of the post-15-million years before present extension of Crater Flat basin occurred during a geologically brief interval between 12 and 11 million years ago. Rapid extension of the basin is supported by several lines of evidence. First, rotation of the paleomagnetic directions reflects deformation of the hanging wall above the Bare Mountain fault. The pattern of hanging wall deformation arose from geometric conditions of the Bare Mountain fault in which horizontal extension of the Crater Flat basin was accomplished by southward increase in fault slip because of southward steepening of the Bare Mountain fault. Steeper portions of the fault require greater fault slip to accomplish the same net horizontal extension. Thus, the timing of the rotations constrains timing of the hanging wall deformation. Considering uncertainties in the radiometric dates of the tuffs, age of the remagnetization of the megabreccia in southern Crater Flat, and amounts of vertical axis rotations, the rapid pulse of deformation seems to have occurred roughly between 12 and 11 million years ago.

Second, geophysical modeling of the pattern of aeromagnetic anomalies in Crater Flat is best explained by a thick accumulation of Bullfrog Tuff in the central part of the basin and a wedge of Rainier Mesa Tuff deposited adjacent to the Bare Mountain fault. There is little geologic evidence to explain why the Bullfrog Tuff is so thick. One possibility is that the Bullfrog Tuff accumulated in a trough or basin developed by extensional faulting prior to or synchronous with the earliest eruptions of the southwest Nevada volcanic field. The thick accumulation of Rainier Mesa Tuff was deposited in a structural trough developed in a short period by rapid slip on the Bare Mountain fault between 12 and 11 million years ago.

Third, rapid deformation exposed a large Bare Mountain footwall block that quickly developed an overly steep and unstable topographic scarp. That scarp subsequently collapsed, at least three times, producing the large volumes of rock-avalanche megabreccia observed in Crater Flat (Carr and Parrish, 1985) and the Will Carr Hills. Collapses occurred during development of the structural trough, the first collapse sometime after deposition of the 12.7 ± 0.03 Tiva Canyon Tuff, the second collapse just prior to the deposition of the 11.6 ± 0.03 million years old Rainier Mesa Tuff, and the third, and most extensive collapse, shortly after eruption of the 11.1 ± 0.3 million years old basalt.

Given the structural and geophysical models for the Crater Flat basin, cumulative throw across the Bare Mountain fault for this period (12 to 11 million years ago) was 1 to 2 km. Thus, the slip rate during the most active period of deformation was approximately 1 to 2 mm/yr. This rate is comparable to rates derived for currently active normal fault systems. For example, Martinez, et al. (1998) record a modern-day, 5-mm/yr slip rate for the Wasatch fault based on Global Positioning System measurements. The 1 to 2-mm/yr rate is equivalent to the disputed rate proposed by Wernicke, et al. (1998) based on recent Global Positioning System data. What is notable for the Bare Mountain fault is that the pulse of high active rate persisted for

1 million years or less. Since 11 million years ago, it appears that the slip rate on Bare Mountain reduced one or two orders of magnitude. An average rate for the fault considering subsidence of southern Crater Flat and burial of the Little Cones is 0.06 mm/yr (Stamatakos, et al., 1997a). Paleoseismic estimates based on trenching data suggest a rate of less than 0.01 mm/yr (Klinger and Anderson, 1994). The implications of these different slip rates are discussed in the following paragraphs, evaluated in Section 3.2.5, and shown in Figure 3-2.

There are three important implications of these results to the current seismic hazard assessment for Yucca Mountain. First, the current seismic hazard assessment for Yucca Mountain (e.g., CRWMS M&O, 1998) assumes traditional planar-shaped domino-style faults. Estimates of M_{max} derived from empirical fault-scaling relationships (e.g., Wells and Coppersmith, 1994) consider fault planes that cut the entire thickness of the brittle crust (about 15 km in Nevada). In contrast, because this proposed structural model incorporates outer-arc extension of the hanging wall, faults observed at the surface do not necessarily cut through the entire seismogenic crust. Many faults lose displacement downward and terminate well above the base of the seimogenic crust. Hence, the effective area for fault rupture on faults that do not reach the base of the seismogenic crust is reduced. A seismic hazard assessment that incorporates faults assumed to cut the full crustal thickness may be conservative, or overly conservative.

Second, a structural link between the faults at Yucca Mountain and slip on the Bare Mountain fault is proposed. By inference, a large earthquake on the Bare Mountain fault could lead to significant coseismic or postseismic deformation at Yucca Mountain. The Bare Mountain fault is the master fault of the basin. Crater Flat basin, including Yucca Mountain, comprises the hanging wall. Faults at Yucca Mountain accommodate deformation of the hanging wall above the Bare Mountain fault. In this interpretation, the southward increase in fault slip simply reflects the change in dip on the Bare Mountain fault. As dip on the Bare Mountain fault steepens, it becomes less efficient at accommodating extension and thus requires more deformation of the hanging wall.

Third, the majority of displacement presently observed across the Bare Mountain fault occurred in the Middle to Late Miocene, from 12 to 11 million years ago. Since 11 million years before present, the average slip rate on the fault has remained low, probably near the 0.06 mm/yr average rate previously derived for the past 1 million years, based on progressive burial of the Little Cones (Stamatakos, et al., 1997a). Thus, the recently proposed slip rates of 1 to 2 mm/yr for the fault based on Global Positioning System results (Wernicke, et al., 1998) are either in error (e.g., Savage, et al., 2001, 1998) or represent a geologically recent spike of increased crustal strain (e.g., Connor, et al., 1999). There is simply not enough cumulative displacement across the fault remaining after the 12 to 11 million years before present pulse to allow for the 1 to 2 mm/yr rate to be long lived geologically (e.g., 10^4 to 10^6 years).

5.6 Crustal Conditions and Tectonic Strain

Crustal conditions characterize past, current, and predicted future stress and strain states and strain rates at the Yucca Mountain site and tectonic environs. Crustal conditions are critical to tectonic model development, fault slip, seismic motion, and development of fractures. Technical bases are primarily derived from consideration of the application of crustal conditions as tools to evaluate seismic sources, faulting probability, structural control of groundwater flow,

long-term evolution of natural and engineered barriers, and related structural deformation and seismicity issues.

Geologic stress components applicable to resolution of the Structural Deformation and Seismicity Key Technical Issues are lithostatic, hydrostatic, thermal, and seismotectonic stress. The present and predicted future states, including occurrence, distribution, and mechanisms of strain accommodation and how these strains affect the Yucca Mountain site and tectonic environs, form the primary bases for review methods and acceptance criteria for crustal conditions.

Stress states in rock may be (i) measured directly from fluid pressure, overcoring, borehole strain meters, and hydro/gas-fracturing in well bores; (ii) indirectly inferred from strain measurements, faults, fractures, overburden, dike orientations, and earthquake focal mechanisms; or (iii) abstracted from numerical and physical analog models. Stress states determined from local *in-situ* strain or stress measurements yield local values that are extrapolated over large volumes and may not reflect stress states at the larger scale. For example, upward scaling of locally determined stress and strain values may be affected by topography (Jaeger and Cook, 1979; Stock, et al., 1985; Stock and Healy, 1988), changes in lithology (Engelder, 1993; Crider and Pollard, 1998), or mechanical interactions between structures (Dupin, et al., 1993). As a result, regional stress fields determined from direct and indirect local strain or stress measurements require sampling in multiple and spatially distributed locations (Bellier and Zoback, 1995; Minor, 1995; Minor, et al., 1997).

Strain release in the upper crust may be local or regional in scale and induce a combination of seismic, microseismic, or aseismic responses. Seismic response results from significant displacement or rupture along discrete fault surfaces or fault zones and may result in regional or local uplift or subsidence or both, with present or subsequent effects on groundwater levels. Displacement along faults may introduce fast communication pathways between previously discrete fluid reservoirs or conduits or create or sever conduits between fluid systems or aquifers (Allan, 1989). Microseismic response may result from microcracking, formation, or growth of fractures or joints, or slip on small-scale faults. The introduction of new fractures or fracture sets may provide new fluid pathways that accelerate, retard, or redirect fluid flow (Finkbeiner, et al., 1997). Aseismic responses include positive or negative dilation of existing fractures or both, depending on fracture orientations relative to the stress field (Engelder, 1993). Preferential fracture dilation results in anisotropic changes in porosity and permeability (Ferrill, et al., 1999a). In every case, introducing fractures and faults reduces, to some degree, the bulk strength of coherent rock (Hoek and Brown, 1980).

Geologic strain rates and related seismic hazard risk analyses are commonly determined by comparing the length of palinspastically restored or retro-deformed cross sections with the present-day length along the same line of section, given the longevity of the regional deformation. One of the basic assumptions in this method, when applied to rocks deformed in the uppermost crust, is that all strain is accommodated by cross-sectional scale faulting.

Estimates of regional extension based on cross-sectional construction and restoration are minimum estimates of strain and do not account for the nonseismogenic strains accommodated by fractures, joints, small-scale faults, and microscale deformation (Wu, 1993; Dunne and Ferrill, 1995). Considering the contribution of fractures, small faults, dikes, and pressure

solution features, it seems improbable that the total strain of the Yucca Mountain region is accommodated by seismogenic rupture on fault surfaces.

Strain rates are inherently sensitive to errors in estimation and timing of cumulative slip on faults. Estimates of slip on individual faults or fault systems as determined from neo-tectonic features, including techniques such as trenching, stream offset mapping, and alluvial fan mapping, are considered minimum values (Reheis, 1988; Klinger and Anderson, 1994; Ferrill, et al., 1996a, 1997). Fault restoration models assume that deformation or slip rates are constant throughout the life of the developing structure. This assumption effectively smooths or averages crustal deformation to a constant or fixed strain rate and cannot account for the likely episodic nature of many crustal scale deformation events. An average rate will neither distinguish nor accurately model areas where quiescence is interspersed with periods of strain rates that are relatively high when compared to the averaged or smoothed strain rate. For the same reasons, Global Positioning System and other geodetic measurements of extension rates, gathered over the span of a few years or tens of years, represent only a small fraction of the life of crustal-scale structures and may not accurately reflect longer term rates of strain. Recent Global Positioning System and geodetic results from several locations, including the Yucca Mountain site, indicate possible anomalously high rates of strain (Wernicke, et al., 1998; Martinez, et al., 1998; CRWMS M&O, 1998) with varying degrees of confidence (Gilmore, 1992; Savage, et al., 1994).

Geodetic leveling surveys beginning in 1907 (Gilmore, 1992) indicate subsidence in at least southern Crater Flat, across the eastward dipping, normal-slip Bare Mountain fault zone. East of the Bare Mountain fault, survey results indicate a 20 to 100-mm drop in elevation over a period of 69 years (Gilmore, 1992), corresponding to throw rates well in excess of those measured from paleoseismic data (e.g., Anderson and Klinger, 1994). Slip rates on the Bare Mountain fault zone appear to increase southward concomitant with an increase in fault dip (Monsen, et al., 1992; Ferrill, et al., 1996a, 1997; Stamatakos, et al., 1997a). The change in slip rate and subsequent southward-increasing subsidence of Crater Flat is supported by studies of alluvial fan deposits along the eastern flank of Bare Mountain (Ferrill, et al., 1996a). Although the level-line results of Gilmore (1992) are not reflected in later surveys along a different line (U.S. Geological Survey, 1996), the earlier level-line surveys present additional uncertainty about the nature and rate of displacement on the Bare Mountain fault.

Although the U.S. Geological Survey (1996) reports no changes in elevation due to displacement on the Bare Mountain fault zone, its level-line survey does not cross the southern portion of the Bare Mountain fault zone. Instead, the survey deviates northward on the east side of the Bare Mountain fault (Benchmark S16, Figure 6-1 in CRWMS M&O, 1998) to cross Crater Flat to the northeast. The U.S. Geological Survey (1996) reports negative height changes in the 1980 to 1984 survey with respect to the 1915 survey (Gilmore, 1992). Considering the brief (4 years) time span of the level-line surveys (U.S. Geological Survey, 1996) and the deviation from the level line of the 1915 survey, sufficient evidence does not exist to negate the possibility of height change across the southern portion of the Bare Mountain fault.

Large slip rates exist within 50 to 100 km to the west and southwest of the Yucca Mountain site. Global Positioning System surveys indicate high slip rates on the Death Valley fault and Hunter Mountain fault systems within the Death Valley Shear Zone southwest of Yucca Mountain (Bennet, et al., 1997). Rates on the Death Valley fault alone are 3 to 5 mm/yr. If these rates

persist or increase over time, the potential exists for multiple $\mathbf{M}_w$ 6.5 to 7.5 seismic events in the next 10,000 years (Bennet, et al., 1997). Seismic activity to the east of the Yucca Mountain site at Little Skull Mountain resulted in measurable changes in elevation related to the 1992 Little Skull Mountain earthquake (**M**5.4) (Savage, et al., 1994; U.S. Geological Survey, 1996).

Wernicke, et al. (1998) propose crustal scale strain rates across Yucca Mountain that greatly exceed those inferred from the geologic record (Ferrill, et al., 1996a, 1997; Connor, et al., 1999; Marrett, et al. 1998). These results are important because they provide alternative estimates to significant structural deformation and seismicity and igneous activity performance parameters including (i) the frequency and magnitudes of earthquakes, (ii) recurrence rates of faulting, and (iii) probability of volcanism. Results from Wernicke, et al. (1998) suggest contemporary strain rates of 2 mm/yr across Yucca Mountain and Crater Flat, more than ten times the strain rate estimated from the geological record of faulting. Wernicke, et al. (1998) interpreted these anomalous rates to suggest an order of magnitude increase in seismic (including faulting) and volcanic hazards over the next 10 ka.

Savage, et al. (2001, 1998, 1994) evaluated crustal-scale strain rates using a geodetic strain network. The Savage, et al. (2001, 1998) survey consisted of a 13-station, 50-km aperture array, centered on Yucca Mountain, that encompassed the Global Positioning System baseline survey of Wernicke, et al. (1998). Savage, et al. (2001, 1998) surveyed the trilateration network in 1983, 1984, 1993, and 1998. Years 1983 and 1984 were completed with an electro-optical distance-measuring geodolite. The 1993 occupation was completed with Global Positioning System, and 14 lines were verified with geodolite (Savage, et al., 1994). Year 1998 was completed with Global Positioning System (Savage, et al., 2001, 1998). The Wernicke, et al. (1998) Global Positioning System survey consisted of five geodetic markers arrayed along a 14-km baseline from Bare Mountain to Jackass Flats. The ground-surface (rock) mounted stations were occupied annually from 1991 to 1997. The Little Skull Mountain earthquake (June 29, 1992, M = 5.4) occurred within the time-span of both surveys. The epicenter of the Little Skull Mountain earthquake was located approximately 8-km southeast of the easternmost station of the Wernicke, et al. (1998) baseline survey, and was encompassed by the trilateration network of Savage, et al. (2001, 1998, 1994). Coseismic offsets related to the Little Skull Mountain earthquake were calculated and removed from the results of Savage, et al. (2001, 1998). Wernicke, et al. (1998) quantified coseismic offset, but did not use the quantified values to correct the survey results (Savage, et al., 2001, 1998).

Wernicke, et al. (1998) reported strain rates of 50 ± 9 nanostrain/yr along the N65° west oriented baseline. Results from the Wernicke, et al. (1998) survey are not supported by the trilateration network of Savage, et al. (2001, 1998, 1994). Strain rates from trilateration surveys are reported in two dimensions. Savage, et al. (2001, 1998) report a strain rate of 5 ± 12 nanostrain/yr oriented N65° west. The results from Savage, et al. (2001, 1998) are an order of magnitude less than the rate reported by Wernicke, et al. (1998) and compare favorably with the rates inferred from the geologic record.

Pezzopane[3] used satellite radar interferometry to evaluate surface displacement related to the Little Skull Mountain earthquake. Preliminary results indicate as much as 25 ± 5 mm of subsidence related to the seismic event, with the area of subsidence including the upland

[3]Pezzopane. Oral Communication at Appendix 7 Meeting. March 2–3, 1999.

region of Little Skull Mountain. Modeling of displacement contours indicates predominately normal dip-slip on a northeast striking, steeply southeast-dipping planar fault. This places the structurally high Little Skull Mountain on the hanging wall of a normal fault. Based on the relationship of Little Skull Mountain to the interpreted fault orientation and displacement, Pezzopane, et al. (1999) interpret the fault as a tectonically minor component of the regional setting, related possibly to gravitational collapse of the Little Skull Mountain block. If correct, the interpretation of Pezzopane, et al. (1999) implies that either (i) the Little Skull Mountain earthquake is not related to an anomalous increase in strain rate as proposed by Wernicke, et al. (1998) or (ii) the interpreted anomalous increase in strain rate is incorrect.

Wernicke, et al. (1998) imply that the tenfold increase in strain rate determined from the Global Positioning System baseline survey results in a tenfold increase in hazard at Yucca Mountain. However, assessing an increase in hazard proportional to the increase in strain rate requires a series of suppositions that, at present, are not supported by the structural setting at Yucca Mountain or by conflicting assessments of crustal conditions (Pezzopane, et al., 1999; Savage, et al., 2001, 1998) or are not addressed in the current tectonic models (Savage, et al., 2001, 1998).

Suppositions that must be evaluated before seismic and volcanic hazards and hydrogeologic effects can be considered using Global Positioning System-determined strain rates are

1. That high strain rates must persist on time scales (10^3 to 10^4 yr) of duration sufficient to affect hazard estimates compared to estimates derived from the geologic record (10^5 to 10^6 yr)

2. That episodic strain accumulations must directly correlate with episodic volcanic eruptions or increased seismicity

3. The degree to which strain is partitioned between seismic, microseismic, and aseismic responses

4. The effects of partitioned strain on groundwater flow.

If the Yucca Mountain region is experiencing an episode of anomalous strain, it is difficult to assess or predict the future duration. If crustal strain is episodic, with bursts of rapid strain accumulation and release covering 10^3 to 10^4 yr between much longer periods of quiescence, average recurrence rates derived from the geologic record may not afford a reasonable measure of hazard over the next 10^3 to 10^4 yr.

It is unclear that episodic strain accumulations at Yucca Mountain directly correlate with episodic volcanic eruptions or increased seismicity. Wernicke, et al. (1998) suggest that anomalously high strain rates have been occurring in the Yucca Mountain region for the last 100 to 150 thousand years. However, this periodicity of strain has not resulted in a one order of magnitude increase in recurrence rate of volcanism or faulting. Clustered activity like the alignment of Quaternary volcanic cones in Crater Flat or the apparent clustered faulting at Yucca Mountain at 70 thousand years before present (Figure 1 in Savage, et al., 2001, 1998) are representative of the periodicity of crustal strain accumulation and release. The paucity of neotectonic features at Yucca Mountain indicates that the postulated high-strain episode is, at the scale of geologic time, newly begun. The relatively short timespan of the geodetic/Global

Positioning System/level-line surveys as conducted thus far is not sufficient to define such an episode. Continuation of the geodetic/Global Positioning System surveys should increase the degree of confidence in strain-rate assessment.

Crustal strain can be accommodated by seismic, microseismic, and aseismic processes. The current strain rates observed by Wernicke, et al. (1998), although high for geologically determined rates for the Basin and Range, may not be anomalous. Rather, the apparently high strain rate may be instead an average rate for the Quaternary across the Yucca Mountain region. In this case, total strain is partitioned between geological processes that contribute to hazard estimates (earthquakes and volcanoes) and those that do not (small faults, fractures, and other aseismic or microseismic deformation). Using fracture data from the Exploratory Studies Facility, regional fault observations, and a regional seismic catalogue to quantify extension rate, Marrett, et al. (1998) estimated extension rates for a variety of time and length scales. The estimates are in reasonable agreement, and range 5 to 20 nanostrain/yr, 2.5 to 10 times smaller than that predicted by the Global Positioning System measurements of Wernicke, et al. (1998), but 5 to 20 times greater than predicted by the paleoseismic record (Marrett, et al., 1998).

5.7 Geologic Framework Model, Version 3.1

The DOE Geologic Framework Model 3.1 is an update of Geologic Framework Model 3.0. The Geologic Framework Model 3.1 is the DOE stratigraphic and fault framework component of the DOE Integrated Site Model 3.0 shared by the following users: (i) unsaturated flow and transport, (ii) saturated zone flow and transport, (iii) near-field environment models, (iv) repository design, (v) mineralogy, and (vi) performance assessment.[4] The key technical issue groups will be relying on the stratigraphic and fault depictions for their assessments. The staff reviewed Geologic Framework Model 3.1 to evaluate its various uses by the DOE in site recommendation and licensing.

The staff tested and evaluated Geologic Framework Model 3.1, with the following objectives: (i) to determine the main differences between Geologic Framework Model 3.1 and Geologic Framework Model 3.0 and the rationales for the revision, (ii) to test and evaluate Geologic Framework Model 3.1 for accuracy in representing site stratigraphy and faults, (iii) to evaluate Geologic Framework Model 3.1 as part of evaluation of the Integrated Site Model 3.0, and (iv) to consider replacing the NRC EarthVision Geologic Framework Model with the Geologic Framework Model 3.1. Overall, the staff found Geologic Framework Model 3.1 adequate for the purposes of depicting faults, fault blocks, stratigraphic horizons, and the topographic surface at the scale of the repository site vicinity and providing a geologic framework for displaying and assessing the parameter distributions of other site characteristics. The testing and assessment procedures, results, and selected observations and limitations are presented in Appendix E (NRC, 1999a).

---

[4]M. Tynan. Personal Communication. 3D Modeling, Geologic Framework Model, DOE/NRC Quarterly Meeting. June 3–4, 1998.

6 REFERENCES

Abe, K. "Seismicity of the Caldera-Making Eruption of Mount Katmai, Alaska in 1912." *Bulletin of the Seismological Society of America.* Vol. 82, pp. 175–191. 1992.

Abrahamson, N.A. and W.J. Silva. "Empirical Response Spectral Attenuation Relations for Shallow Crustal Earthquakes." *Seismological Research Letters.* Vol. 68, No. 1. pp. 94–127. 1997.

Albin, A.L., W.L. Singleton, T.C. Moyer, A.C. Lee, R.C. Lung, G.L.W. Eatman, and D.L. Barr. "Geology of the Main Drift–Station 28+00 to 55+00, Exploratory Studies Facility, Yucca Mountain Project, Yucca Mountain, Nevada." *Summary Report by the U.S. Bureau of Reclamation to the DOE.* DTN GS970208314224.005. 1997.

Alexander, L.L. and J.W. Handschy. "Fluid Flow in a Faulted Reservoir System: Fault Trap Analysis for the Block 330 Field in Eugene Island, South Addition, Offshore Louisiana." *American Association of Petroleum Geologists Bulletin.* Vol. 82, No. 3. pp. 387–411. 1998.

Allan, U.S. "Model for Hydrocarbon Migration and Entrapment Within Faulted Structures." *American Association of Petroleum Geologists Bulletin.* Vol. 73, No. 7. pp. 803–811. 1989.

Anderson, J.G., J.N. Brune, J.N. Louie, Y. Zeng, M. Savage, G. Yu, Q. Chen, and D. dePolo. "Seismicity in the Western Great Basin Apparently Triggered by the Landers, California, Earthquake, 28 June 1992." *Bulletin of the Seismological Society of America.* Vol. 84. pp. 863–891. 1994.

Anderson, L.W. and R.E. Klinger. "Preliminary Evaluation of the Bare Mountain Fault Zone, Nye County, Nevada." Administrative Report in Support of Yucca Mountain Site Characterization Activity 8.3.1.17.4.3. Denver, Colorado: Bureau of Reclamation. 1994.

Anderson, R.E. "Thin-Skinned Distension in Tertiary Rocks of Southwestern Nevada." *Geological Society of America Bulletin.* Vol. 82. pp. 43–58. 1971.

Anna, L.O. "Preliminary Three-Dimensional Discrete Fracture Model of the Topopah Spring Tuff in the Exploratory Studies Facility, Yucca Mountain Area, Nye County, Nevada." U.S. Geological Survey Open-File Report 97-834. Lakewood, Colorado: U.S. Geological Survey. 1997.

Anna, L.O. and P. Wallman. "Characterizing the Fracture Network at Yucca Mountain, Nevada, Part 2: Numerical Simulation of Flow in a Three-Dimensional Discrete Fracture Network." *Fractured Reservoirs: Descriptions, Predictions, and Applications: Rocky Mountain Association of Geologists 1997 Guidebook.* T.E. Hoak, P.K. Blomquist, and A. Klawitter, eds. Denver, Colorado: Rocky Mountain Association of Geologists. pp. 199–208. 1997.

Antonellini, M. and A. Aydin. "Effect of Faulting on Fluid Flow in Porous Sandstones: Petrophysical Properties." *American Association of Petroleum Geologists Bulletin.* Vol. 78, No. 3. pp. 355–377. 1994.

Antonellini, M.A., A. Aydin, and D.D. Pollard. "Microstructure of Deformation Bands in Porous Sandstones at Arches National Park, Utah." *Journal of Structural Geology*. Vol. 16, No. 7. pp. 941–959. 1994.

Arabasz, W.J. and D.R. Julander. "Geometry of Seismically Active Faults and Crustal Deformation Within the Basin and Range Province, Northeastern Nevada." *Extensional Tectonics of the Southwestern United States: A Perspective on Processes and Kinematics*. L. Mayer, ed. *Geological Society of America Special Paper 208*. Boulder, Colorado: Geological Society of America. pp. 43–74. 1986.

Armstrong, R.L. "Sevier Orogenic Belt in Nevada and Utah." *Geological Society of America Bulletin*. Vol. 79. pp. 439–458. 1968.

Atwater, T. "Implications of Plate Tectonics for the Cenozoic Tectonic Evolution of Western North America." *Geological Society of America Bulletin*. Vol. 81. pp. 3,513–3,536. 1970.

Axen, G.J., W.J. Taylor, and J.M. Bartlet. "Space-Time Patterns and Tectonic Controls of Tertiary Extension and Magmatism in the Great Basin of the Western United States." *Geological Society of America Bulletin*. Vol. 105. pp. 56–76. 1993.

Bai, T., L. Maerten, M.R. Gross, and A. Aydin. "Orthogonal Cross Joints: Do They Imply a Regional Stress Rotation?" *Journal of Structural Geology*. Vol. 23, in review. 2001.

Banks, N.G. and R.P. Hoblitt. "Summary of Temperature Studies of 1980 Deposits." *The 1980 Eruptions of Mount St. Helens, Washington*. P.W. Lipman and D.R. Mullineaux, eds. *U.S. Geological Survey Professional Paper 1250*. Reston, Virginia: U.S. Geological Survey. pp. 295–314. 1981.

Barton, C.C. and P.A. Hsieh. "Physical and Hydrologic-Flow Properties of Fractures." Washington, DC: American Geophysical Union. 1989.

Barton, C.C. and E. Larsen. "Fractal Geometry of Two-Dimension Fracture Networks at Yucca Mountain." *Fundamentals of Rock Joints: Proceedings of the International Symposium on Fundamentals of Rock Joints*. O. Stephanson, ed. Sweden. *Bjorkliden*. pp. 77–84. 1985.

Barton, C.C., T.M. Howard, and E. Larsen. "Tubular Structures on the Faces of Cooling Joints—A New Volcanic Feature." *EOS, Transactions, American Geophysical Union*. Vol. 65, No. 1. p. F148. 1984.

Barton, C.C., E. Larsen, W.R. Page, and T.M. Howard. "Characterizing Fractured Rock for Fluid-Flow, Geomechanical, and Paleostress Modeling: Methods and Preliminary Results from Yucca Mountain, Nevada." U.S. Geological Survey Open-File Report 93-269. Denver, Colorado: U.S. Geological Survey. 1993.

Barton, C.C., M.D. Zoback, and D. Moos. "Fluid Flow Along Potentially Active Faults in Crystalline Rock." *Geology*. Vol. 23, No. 8. pp. 683–686. 1995.

Bateman, P.C. "Geology and Tungsten Mineralization of the Bishop District, California. USA." *U.S. Geological Survey Professional Paper 470*. Reston, Virginia: U.S. Geological Survey. 1965.

Bedinger, M.S., K.A. Sargent, W.H. Langer, F.B. Sherman, J.E. Reed, and B.T. Brad. "Studies of Geology and Hydrology in the Basin and Range Province, Southwestern United States, for Isolation of High-Level Radioactive Waste-Basis of Characterization and Evaluation." *Professional Paper 1370-A*. Denver, Colorado: U.S. Geological Survey. 1989.

Bellier, O. and M.L. Zoback. "Recent State of Stress Change in the Walker Lane Zone, Western Basin and Range Province, United States." *Tectonics*. Vol. 14. pp. 564–593. 1995.

Bennett, R.A., J.L. Davis, P. Elósegui, B.P. Wernicke, J.K. Snow, M.J. Abolins, M.A. House, G.L. Stirewalt, and D.A. Ferrill. "Global Positioning System Constraints on Fault Slip Rates in the Death Valley Region, California and Nevada." *Geophysical Research Letters*. Vol. 24. pp. 3,037–3,076. 1997.

Bernreuter, D.L., A.C. Boissonade, and C.M. Short. NUREG/CR–6606, "Investigations of Technique for the Development of Seismic Design Basis Using Probabilistic Seismic Hazard Analysis." Washington, DC: NRC. 1998.

Bierwirth, P.N. "Experimental Welding of Volcanic Ash." B.S. Honors Thesis. Australia: Monash University. 1982.

Bodin, G.E. and J. Gomberg. "Triggered Seismicity and Deformation Between Landers, California, and Little Skull Mountain, Nevada, Earthquakes." *Bulletin of the Seismological Society of America*. Vol. 84. pp. 835–843. 1994.

Bohannon, R.G and T. Parsons. "Tectonic Implications of Post-30 Ma Pacific and North American Relative Plate Motions." *Geological Society of America Bulletin*. Vol. 107. pp. 937–959. 1995.

Bonilla, M., R.K. Mark, and J.J. Lienkaemper. "Statistical Relations Among Earthquakes Magnitude, Surface Rupture Length and Surface Fault Displacement." *Bulletin of the Seismological Society of America*. Vol. 74, No. 2. pp. 379–2,411. 1984.

Bowring, S.A. and K.E. Karlstrom. "Growth and Stabilization of the Proterozoic Lithosphere in the Southwestern United States." *Geology*. Vol. 18. pp. 1,203–1,206. 1990.

Bradshaw, T.K. and E.I. Smith. "Polygenetic Quaternary Volcanism at Crater Flat, Nevada, *Journal of Volcanology and Geothermal Research*. Vol. 63. pp. 165–182. 1994.

Braunmiller, J., J. Nblek, B. Leitner, and A. Qamar. "The 1993 Klamath Falls, Oregon, Earthquake Sequence: Source Mechanisms from Regional Data." *Geophysical Research Letters*. Vol. 22. pp. 105–108. 1995.

Bredehoeft, J.D. "Fault Permeability Near Yucca Mountain." *Water Resources Research*. Vol. 33. pp. 2,459–2,463. 1997.

Brocher, T.M., M.D. Carr, K.F. Fox, and P.E. Hart. "Seismic Reflection Profiling Across Tertiary Extensional Structures in the Eastern Amargosa Desert, Basin and Range Quadrangle, Nevada." *Geological Society of America Bulletin.* Vol. 105. pp. 30–46. 1993.

Brocher, T.M., P.E. Hart, W.C. Hunter, and V.E. Langenheim. "Hybrid-Source Seismic Reflection Profiling Across Yucca Mountain, Nevada, Regional Lines 2 and 3." U.S. Geological Survey Open-File Report 96-02. Menlo Park, California: U.S. Geological Survey. 1996.

Brocher, T.M., W.C. Hunter, and V.E. Langenheim. "Implications of Seismic Reflection and Potential Field Geophysical Data on the Structure Frame Work of Yucca Mountain—Crater Flat Region, Nevada." *Geological Society of America Bulletin.* Vol. 110. pp. 947–971. 1998.

Bruhn, R.L. and R.A. Schultz. "Geometry and Slip Distribution in Normal Fault Systems: Implications for Mechanics and Fault-Related Hazards." *Journal of Geophysical Research.* Vol. 101. pp. 3,401–3,412. 1996.

Budnitz, R.J., G. Apostolakis, D.M. Boore, L.S. Cluff, K.J. Coppersmith, C.A. Cornell, and P.A. Morris. NUREG/CR–6372, UCRL–ID–122160 "Recommendations for Probabilistic Seismic Hazard Analysis: Guidance on Uncertainty and Use of Experts." Vol. 1. Livermore, California: Lawrence Livermore National Laboratory. 1997.

Buesch, D.C., R.W. Spengler, T.C. Moyer, and J.K. Gelsin. "Proposed Stratigraphic Nomenclature and Macroscopic Identification of Lithostratigraphic Units of the Paintbrush Group Exposed at Yucca Mountain, Nevada." U.S. Geological Survey Open-File Report 94-469. Denver, Colorado: U.S. Geological Survey. 1996.

Burchfiel, B.C. and G.A. Davis. "Structural Framework and Evolution of the Southern Part of the Cordilleran Orogeny, Western United States." *American Journal of Science.* Vol. 272. pp. 97–118. 1972.

Burchfiel, B.C., D.S. Cowen, and G.A. Davis. "Tectonic Overview of the Cordilleran Orogen in the Western United States." *The Cordilleran Orogen, Conterminous U.S.: The Geology of North America.* Vol. G-3. B.C. Burchfiel, P.W. Lipman, and M.L. Zoback, eds. Boulder, Colorado: Geological Society of America. pp. 407–479. 1982.

Burchfiel, B.C., K.V. Hodges, and L.H. Royden. "Geology of Panamint Valley-Saline Valley Pull-Apart System, California, Palinspastic Evidence for Low-Angle Geometry of a Neogene Range-Bounding Fault." *Journal of Geophysical Research.* Vol. 93. pp. 10,422–10,426. 1987.

Burkhard, M. "Calcite Twins, Their Geometry, Appearance and Significance As Stress—Strain Markers and Indicators of Tectonic Regime: A Review." *Journal of Structural Geology.* Vol. 15. pp. 351–368. 1993.

Bursik, M.I. and A.W. Woods. "The Dynamics and Thermodynamics of Large Ash Flows." *Bulletin of Volcanology.* Vol. 58. pp. 175–193. 1996.

Byerlee, J.D. "Friction of Rocks." *Pure and Applied Geophysics.* Vol. 116. pp. 615–626. 1978.

Byers, Jr., F.M., W.J. Carr, P.P. Orkild, W.D. Quinlivan, and K.A. Sargent. "Volcanic Suites and Related Cauldrons of the Timber Mountain-Oasis Valley Caldera Complex, Southern Nevada." *U.S. Geological Survey Professional Paper 919*. Reston, Virginia: U.S. Geological Survey. 1976.

Caine, J.S., J.P. Evans, and C.B. Forster. "Fault Zone Architecture and Permeability Structure." *Geology*. Vol. 24. pp. 1,025–1,028. 1996.

Camilleri, P.A. and K.R. Chamberlain. "Mesozoic Tectonics and Metamorphism in the Pequop Mountains and Wood Hills Region, Northeast Nevada: Implications for the Architecture and Evolution of the Sevier Orogen." *Geological Society of America Bulletin*. Vol. 109. pp. 74–94. 1997.

Caputo, R. "Evolution of Orthogonal Sets of Extension Joints." *Terra Nova*. Vol. 7. pp. 479–490. 1995.

Carlos, B.A., S.J. Chipera, D.L. Bish, and S.J. Craven. "Fracture-Lining Manganese Oxide Minerals in Silicic Tuff, Yucca Mountain, Nevada, U.S.A." *Chemical Geology*. Vol. 107. pp. 47–69. 1993.

Carlsson, A. and T. Olsson. "Hydraulic Conductivity and Its Stress Dependence." Proceedings of the 1979 Workshop Low-Flow, Low-Permeability Measurements in Largely Impermeable Rocks. Paris, France. pp. 249–259. 1979.

Carr, W.J.. "Volcano-Tectonic History of Crater Flat, Southwestern Nevada, As Suggested by New Evidence from Drill Hole USW-VH-1." U.S. Geological Survey Open-File Report 82-457. Denver, Colorado: U.S. Geological Survey. 1982.

———. "Regional Structural Setting of Yucca Mountain, Southwestern Nevada, and Late Cenozoic Rates of Tectonic Activity in Part of the Southwestern Great Basin, Nevada and California." U.S. Geological Survey Open-File Report 84-854. Denver, Colorado: U.S. Geological Survey. 1984.

———. "Volcano-Tectonic Setting of Yucca Mountain and Crater Flat, Southwestern Nevada in Geologic and Hydrologic Investigations of a Potential Nuclear Waste Disposal Site at Yucca Mountain, Southern Nevada." *U.S. Geological Survey Bulletin 1790*. M. Carr and J. Yount, eds. Denver, Colorado: U.S. Geological Survey. pp. 35–49. 1988.

———. "Styles of Extension in the Nevada Test Site Region, Southern Walker Lane Belt; An Integrated Volcano-Tectonic and Detachment Fault Model." *Geological Society of America Memoir 176*. Boulder, Colorado: Geological Society of America. pp. 283–303. 1990.

———. "Structures in Continuously Cored, Deep Drill Holes at Yucca Mountain, Nevada, with Notes on Calcite Occurrence." SAND91–7037. Albuquerque, New Mexico: Sandia National Laboratories. 1992.

Carr, W.J. and L.D. Parrish. "Geology of Drill Hole USW VH-2 and Structure of Crater Flat, Southwestern, Nevada." U.S. Geological Survey Open-File Report 85-475. Denver, Colorado: U.S. Geological Survey. 1985.

Carr, W.J., S.M. Keller, and J.A. Grow. "Lithologic and Geophysical Logs of Drill Holes Felderhoff Federal 5-1 and 25-1, Amargosa Desert, Nye County, Nevada." U.S. Geological Survey Open-File Report 95-115. Denver, Colorado: U.S. Geological Survey. 1995.

Carr, W.J., F.M. Byers, Jr., and P.P. Orkild. "Stratigraphy and Volcano-Tectonic Relations of Crater Flat Tuff and Some Older Volcanic Units, Nye County, Nevada." U.S. Geological Survey Professional Paper 1323. Reston, Virginia: U.S. Geological Survey. 1986a.

Carr, W.J., S.J. Wadell, G.S. Vick, J.M. Stock, S.A. Monsen, A.G. Harris, B.W. Cork, and F.M. Byers, Jr. "Geology of Drill Hole UE25p#1: A Test Hole into Pre-Tertiary Rocks Near Yucca Mountain, Southern Nevada." U.S. Geological Survey Open-File Report 86-175. Denver, Colorado: U.S. Geological Survey. 1986b.

Cartwright, J.A. and C.S. Mansfield. "Lateral Displacement Variation and Lateral Tip Geometry of Normal Faults in the Canyonlands National Park, Utah." *Journal of Structural Geology.* Vol. 20. pp. 3–19. 1998.

Cas, R.A.F. and J.V. Wright. *Volcanic Successions.* Winchester, Massachusetts: Unwin Hyman, Inc. 1987.

Caskey, S.J. and R.A. Schweickert. "Mesozoic Deformation in the Nevada Test Site and Vicinity: Implications for the Structural Framework of the Cordilleran Fold and Thrust Belt and Tertiary Extension North of Las Vegas Valley." *Tectonics.* Vol. 11. pp. 1,314–1,331. 1992.

Chekuri, V.S., S.W. Tyler, and J.W. Fordham. "The Role of Fracture Coatings on Water Imbibition into Unsaturated Tuff from Yucca Mountain." Nevada Agency for Nuclear Projects/Nuclear Waste Project Office NWPO-TR-024-95. Carson City, Nevada: Nevada Agency for Nuclear Projects. 1995.

Chester, F.M. and J.M. Logan. "Composite Planar Fabric of Gouge from the Punchbowl Fault, California." *Journal of Structural Geology.* Vol. 9. pp. 621–634. 1986.

Christiansen, R.L., P.W. Lipman, W.J. Carr, F.M. Byers, Jr., P.P. Orkild, and K.A. Sargent. "Timber Mountain-Oasis Valley Caldera Complex of Southern Nevada." *Geological Society of America Bulletin.* Vol. 88. pp. 943–959. 1977.

Cladouhos, T.T. and R. Marrett. "Are Fault Growth and Linkage Models Consistent with Power-Law Distribution of Fault Lengths?" *Journal of Structural Geology.* Vol. 18. pp. 281–293. 1996.

Connor, C.B. and B.E. Hill. "Three Nonhomogeneous Poisson Models for the Probability of Basaltic Volcanism: Application to the Yucca Mountain Region, Nevada." *Journal of Geophysical Research.* Vol. 100. pp. 10,107–10,125. 1995.

Connor, C.B., S. Lane-Magsino, J.A. Stamatakos, R.H. Martin, P.C. La Femina, B.H. Hill, and S. Lieber. "Magnetic Surveys Help Reassess Volcanic Hazards at Yucca Mountain, Nevada." *EOS, Transactions, American Geophysical Union.* Vol. 78, No. 73. pp. 77–78. 1997.

Connor, C.B., J.A. Stamatakos, D.A. Ferrill, and B.E. Hill. "Comment on Detecting Strain in the Yucca Mountain Area, Nevada." *Science*. Vol. 282. p. 1,007b. 1999.

Connor, C.B., J.A. Stamatakos, D.A. Ferrill, B.E. Hill, G.I. Ofoegbu, F.M. Conway, B. Sagar, and J. Trapp. "Geologic Factors Controlling Patterns of Small-Volume Basaltic Volcanism: Application to a Volcanic Hazard Assessment at Yucca Mountain, Nevada." *Journal of Geophysical Research*. Vol. 105. pp. 407–432. 2000.

Coppersmith, K.J. "Update on Data Related to Fault Displacement and Vibratory Ground Motion Hazard at Yucca Mountain for Use in EPRI Performance Assessment, in Yucca Mountain Total System Performance Assessment, Phase 3." J. Kessler and R. McGuire, eds. EPRI TR–107191 3055-02 Final Report. Palo Alto, California: Electric Power Research Institute. pp. 11-1 to 11-15. 1996.

Coppersmith, K.J. and R.R. Youngs. "Risk-Based Approach to High-Level Waste Repository Evaluation Plan 2." EPRI TR–100384 Interim Report. Golden, Colorado: Risk Engineering, Inc. 1992.

Cornell, C.A. "Engineering Seismic Risk Analysis." *Bulletin of Seismological Society of America*. Vol. 58. pp. 1,583–1,606. 1968.

Cornwall, H.R. and F.J. Kleinhampple. "Geology of the Bare Mountain Quadrangle." U.S. Geological Survey Quadrangle Map, GQ–157. Scale 1:62,500. 1961.

———. "Geology of the Bullfrog Quadrangle and Ore Deposits Related to the Bullfrog Hills Caldera, Nye County, Nevada and Inyo County, California." U.S. Geological Survey Professional Paper 454–J. Reston, Virginia: U.S. Geological Survey. 1964.

Cornwall, H.R. "Geology and Mineral Deposits of Nye County, Nevada." *Nevada Bureau of Mines and Geology Bulletin*. Vol. 77. Reno, Nevada: Nevada Bureau of Mines. 1972.

Crider, J.G. and D.D. Pollard. "Fault Linkage: Three-Dimensional Mechanical Interaction Between Echelon Normal Faults." *Journal of Geophysical Research*. Vol. 103, No. B10. pp. 24,373–24,391. 1998.

Crowe, B., F. Perry, J. Geissman, L. McFadden, S. Wells, M. Murrell, J. Poths, G.A. Valentine, L. Bowker, and K. Finnegan. "Status of Volcanism for the Yucca Mountain Site Characterization Project." Los Alamos National Laboratory Report 12908–MS. Los Alamos, New Mexico: Los Alamos National Laboratory. pp. 2-18 to 2-21. 1995.

CRWMS M&O. "Unsaturated Zone Flow Model Expert Elicitation Project." WBS 1.2.5.7. Las Vegas, Nevada: DOE. 1997.

———. "Probabilistic Seismic Hazard Analyses for Fault Displacement and Vibratory Ground Motion at Yucca Mountain, Nevada." WBS 1.2.3.2.8.3.6. Oakland, California: DOE. 1998.

———. "Geologic Framework Model (GFM3.1) Analysis Model Report." MDL–NBS–GS–000002. Revision 00 ICN 01. Las Vegas, Nevada: CRWMS M&O. 1999.

———. "Yucca Mountain Site Description." TDR–CRW–GS–000001. Revision 01 ICN 01. Las Vegas, Nevada: DOE. 2000a.

———. "Fracture Geometry Analysis for the Stratigraphic Units of the Repository Host Horizon." ANL–EBS–GE–000006. Revision 00. Las Vegas, Nevada: DOE. 2000b.

———. "Saturated Zone Flow and Transport Process Model Report." TDR–NBS–HS–000001. Revision 00. Las Vegas, Nevada: DOE. 2000c.

———. "Unsaturated Zone Flow and Transport Model Process Model Report." TDR–NBS–HS–000002. Revision 00. Las Vegas, Nevada: DOE. 2000d.

———. "Yucca Mountain Science and Engineering Report." DOE/RW–0539. Las Vegas, Nevada: DOE, Office of Civilian Radioactive Waste Management, Yucca Mountain Site Characterization Project. 2001.

Czarnecki. J.B., C.C. Faunt, C.W. Gable, and G.A. Zyvoloski. "Hydrogeology and Preliminary Three-Dimensional Finite-Element Groundwater Flow Model of the Site Saturate Zone, Yucca Mountain, Nevada." Yucca Mountain Project Milestone Report SP23NM3. Denver, Colorado: U.S. Geological Survey. 1997.

Davies, R.K., M. Crawford, W.F. Dula, Jr., M. Cole, and G. Dorn. "Outcrop Interpretation of Seismic-Scale Normal Faults in Southern Oregon: Description of Structural Styles and Evaluation of Subsurface Interpretation Methods." *The Leading Edge*. Vol. 16. pp. 1,135–1,141. 1997.

Davis, G.A. and P.J. Coney. "Geologic Development of the Metamorphic Core Complexes." *Geology*. Vol. 7. pp. 120–124. 1979.

Dawers, N.H. and M.H. Anders. "Displacement-Length Scaling and Fault Linkage." *Journal of Structural Geology*. Vol. 17. pp. 607–614. 1995.

Dawers, N.H., M.H. Anders, and C.H. Scholz. "Growth of Normal Faults: Displacement-Length Scaling." *Geology*. Vol. 21. pp. 1,107–1,110. 1993.

Day, W.C., R.P. Dickerson, C.J. Potter, D.S. Sweetkind, C.A. San Juan, R.M. Drake, II, and C.J. Fridrich. "Geologic Map of the Yucca Mountain Area, Nye County, Nevada." U.S. Geological Survey Geological Investigations Series, Map I–2627. Scale 1:24,000. 1998a.

Day, W.C., C.J. Potter, D.S. Sweetkind, R.P. Dickerson, and C.A. San Juan. "Bedrock Geologic Map of the Central Block Area, Yucca Mountain, Nye County, Nevada." U.S. Geological Survey Miscellaneous Investigations Series, Map I–2601. Scale 1:6,000. Denver, Colorado: U.S. Geological Survey. 1998b.

DeGraff, J.M. and A. Aydin. "Surface Morphology of Columnar Joints and Its Significance to Mechanics and Direction of Joint Growth." *Geological Society of America Bulletin*. Vol. 99. pp. 605–617. 1987.

dePolo, C.M., D.G. Clark, D.B. Slemmons, and A.R. Ramelli. "Historical Surface Faulting in the Basin and Range Province, Western North America, Implications for Fault Segmentation." *Journal of Structural Geology*. Vol. 13. pp. 123–126. 1991.

Dickenson, W.R. "Kinematics of Transrotational Tectonism in the California Transverse Ranges and Its Contribution to Cumulative Slip Along the San Andreas Transform Fault System." *Geological Society of America Special Paper 305*. Boulder, Colorado: Geological Society of America. 1996.

DOE. "Methodology to Assess Fault Displacement and Vibratory Ground Motion Hazards at Yucca Mountain." YM ITR–002–NP. Las Vegas, Nevada: DOE. 1997.

———. "Viability Assessment of a Repository at Yucca Mountain: Total System Performance Assessment, December 1998." Vol. 1. DOE/RW–0508. Las Vegas, Nevada: DOE, Office of the Civilian Radioactive Waste Management. 1998.

Dokka, R.K. and C.J. Travis. "Role of the Eastern California Shear Zone in Accommodating Pacific-North American Plate Motion." *Geophysical Research Letters*. Vol. 17. pp. 1,223–1,326. 1990.

Doser, D.D. and R.B. Smith. "An Assessment of the Source Parameters of Earthquakes in the Intermontane Region of the United States." *Bulletin of the Seismological Society of America*. Vol. 79. pp. 1,383–1,409. 1989.

Doser, D.I. "Earthquake Processes in the Rainbow Mountain–Fairview Peak–Dixie Valley, Nevada, Region, 1954–1959." *Journal of Geophysical Research*. Vol. 91. pp. 12,572–12,586. 1986.

Dula, Jr., W.F., "Geometric Models of Listric Normal Faults and Rollover Folds." *American Association of Petroleum Geologists Bulletin*. Vol. 75. pp. 1,609–1,625. 1990.

Dunne, W.M. and C.P. North. "Orthogonal Fracture Systems at the Limits of Thrusting: An Example from Southwestern Wales." *Journal of Structural Geology*. Vol. 12. pp. 207–215. 1990.

Dunne, W.M. and D.A. Ferrill. "Fractal Strain Distribution and Its Implications for Cross-Section Balancing, Discussion." *Journal of Structural Geology*. Vol. 17. pp. 757–760. 1995.

Dunne, W.M., D.A. Ferrill, J.G. Crider, B.E. Hill, P.C. La Femina, D.J. Waiting, A.P. Morris, and R. Fedors. "Orthogonal Jointing During Coeval Igneous Degassing and Normal Faulting, Yucca Mountain, Nevada." Letter Report to NRC (IM 01402.471.130). San Antonio, Texas: CNWRA. 2001.

Dupin, J.-M., W. Sassi, and J. Angelier. "Homogeneous Stress Hypothesis and Actual Fault Slip, A Distinct Element Analysis." *Journal of Structural Geology*. Vol. 15. pp. 1,033–1,043. 1993.

Eatman, G.L.W., Singleton, W.L., Moyer, T.C., Barr, D.L., Albin, A.L., Lung, R.C., and Beason, S.C. "Geology of the South Ramp—Station 55+00 to 78+77, Exploratory Studies Facility, Yucca Mountain Project, Yucca Mountain, Nevada." Milestone SPG42CM3. Denver, Colorado: U.S. Geological Survey. 1997.

Eldredge, S., V. Bachtadse, and R. Van der Voo. "Paleomagnetism and the Orocline Hypothesis." *Tectonophysics*. Vol. 119. pp. 153–179. 1985.

Engelder, T. "Stress Regimes in the Lithosphere, Princeton, New Jersey." Princeton, New Jersey: Princeton University Press. 1993.

Engelder, T. and M.P. Fischer. "Loading Configurations and Driving Mechanisms for Joints Based on the Griffith Energy-Balance Concept." *Tectonophysics*. Vol. 256. pp. 253–277. 1996.

Enlows, H.E. "Welded Tuffs of the Chiricahua National Monument, Arizona." *Geological Society of America Bulletin*. Vol. 66. pp. 1,215–1,246. 1955.

Epstein, B. "Truncated Life Tests in the Exponential Case: Annals of Mathematics and Statistics." Vol. 25. pp. 555. 1954.

Evans, J.P., C.B. Forster, and J.V. Goddard. "Permeability of Fault-Related Rocks, and Implications for Hydraulic Structure of Fault Zones." *Journal of Structural Geology*. Vol. 19. pp. 1,393–1,404. 1997.

Eyal, Y. and Z. Reches. "Tectonic Analysis of the Dead Sea Rift Region Since the Late Cretaceous Based on Mesostructures." *Tectonics*. Vol. 2. pp. 167–185. 1983.

Fabbri, O., P. Gaviglio, and J.-F. Gamond. "Diachronous Development of Master Joints of Different Orientations in Different Lithological Units Within the Same Fore-Arc Basin Deposits, Kyushu, Japan." *Journal of Structural Geology*. Vol. 23. pp. 239–246. 2001.

Fabryka-Martin, J.T., A.V. Wolfsberg, S.S. Levy, K. Campbell, P. Tseng, J.L. Roach, L.E. Wolfsberg. "Evaluation of Flow and Transport Models of Yucca Mountain, Based on Chlorine-36 Studies for FY98." Yucca Mountain Project Milestone Report SP33DDM4. Los Alamos, New Mexico: Los Alamos National Laboratory. 1998.

Faulds, J.E., J.W. Bell, D.L. Feuerbach, and A.R. Ramelli. "Geologic Map of the Crater Flat Area, Nevada." Nevada Bureau of Mines and Geology, Map 101. Scale 1:24,000. Reno, Nevada: Nevada Bureau of Mines and Geology, University of Nevada–Reno. 1994.

Farrell, D.A., J. Winterle, W.A. Illman, R.W. Fedors. "Review of Porosity Distributions in the Yucca Mountain Region." Letter Report to NRC (IM 01402.861.020). San Antonio, Texas: CNWRA. 2000.

Ferrill, D.A. "Calcite Twin Widths and Intensities as Metamorphic Indicators in Natural Low-Temperature Deformation of Limestone." *Journal of Structural Geology*. Vol. 13. pp. 667–675. 1991.

———. "Critical Re-Evaluation of Differential Stress Estimates from Calcite Twins in Coarse-Grained Limestone." *Tectonophysics*. Vol. 285. pp. 77–86. 1998.

Ferrill, D.A. and W.M. Dunne. "Cover Deformation Above a Blind Duplex, An Example from West Virginia, U.S.A." *Journal of Structural Geology*. Vol. 11. pp. 421–431. 1989.

Ferrill, D.A. and R.H. Groshong, Jr. "Kinematic Model for the Curvature of the Northern Subalpine Chain, France." *Journal of Structural Geology*. Vol. 15. pp. 523–541. 1993.

Ferrill, D.A. and A.P. Morris. "Geometric Considerations of Deformation Above Curved Normal Faults and Salt Evacuation Surfaces." *The Leading Edge*. Vol. 16. pp. 1,129–1,133. 1997.

Ferrill, D.A., S.R. Young, G.L. Stirewalt, A.P. Morris, and D.B. Henderson. "Tectonic Processes in the Central Basin and Range Region, NRC High-Level Radioactive Waste Research at Center for Nuclear Waste Regulatory Analyses, January–June 1994." B. Sagar, ed, CNWRA 94-01S. San Antonio, Texas: CNWRA. pp. 139–160. 1994.

Ferrill, D.A., D.B. Henderson, J.A. Stamatakos, K.H. Spivey, and A.P. Morris. "Tectonic Processes in the Central Basin and Range, NRC High-Level Radioactive Waste Research at CNWRA, January–June, 1995." B. Sagar, ed. CNWRA 95-01S. San Antonio, Texas: CNWRA. pp. 6.1–6.27. 1995a.

Ferrill, D.A., A.P. Morris, D.B. Henderson, and R.H. Martin. "Tectonic Processes in the Central Basin and Range Region, NRC High-Level Radioactive Waste Research at CNWRA, July–December 1994." B. Sagar, ed. CNWRA 95-01S. San Antonio, Texas: CNWRA. pp. 121–139. 1995b.

Ferrill, D.A., J.A. Stamatakos, S.M. Jones, B. Rahe, H.L. McKague, R.H. Martin, and A.P. Morris. "Quaternary Slip History of the Bare Mountain Fault (Nevada) from the Morphology and Distribution of Alluvial Fan Deposits." *Geology*. Vol. 24. pp. 559–562. 1996a.

Ferrill, D.A., G.L. Stirewalt, D.B. Henderson, J.A. Stamatakos, K.H. Spivey, and B.P. Wernicke. "Faulting in the Yucca Mountain Region, Critical Review and Analyses of Tectonic Data from the Central Basin and Range." NUREG/CR–6401. Washington, DC: NRC. 1996b.

Ferrill, D.A., J.A. Stamatakos, and A.P. Morris. "Structural Controls on Progressive Deformation of the Yucca Mountain (Nevada) Region." *Geological Society of America Abstracts with Programs*. Vol. 28. p. A–192. 1996c.

Ferrill, D.A., J.A. Stamatakos, and H.L. McKague. "Quaternary Slip History of the Bare Mountain Fault (Nevada) from the Morphology and Distribution of Alluvial Fan Deposits, REPLY." *Geology*. Vol. 25. p. 190. 1997.

Ferrill, D.A., A.P. Morris, S.M. Jones, and J.A. Stamatakos. "Extensional Layer-Parallel Shear and Normal Faulting." *Journal of Structural Geology*. Vol. 20. pp. 355–362. 1998.

Ferrill, D.A., J.A. Stamatakos, and D. Sims. "Normal Fault Corrugation: Implications for Growth and Seismicity of Active Normal Faults." *Journal of Structural Geology*. Vol. 21. pp. 1,027–1,038. 1999a.

Ferrill, D.A., J.R. Winterle, G. Wittmeyer, D. Sims, S. Colton, A. Armstrong, and A.P. Morris. "Stressed Rock Strains Groundwater at Yucca Mountain, Nevada." *GSA Today*. Vol. 9. pp. 1–8. 1999b.

Ferrill, D.A., W.M. Dunne, S. Hsiung, and A.P. Morris. "Review of AMR Entitled Fracture Geometry Analysis for the Stratigraphic Units of the Repository Host Horizon." Letter Report to NRC. San Antonio, Texas: CNWRA. 2000a.

Ferrill, D.A., A.P. Morris, J.A. Stamatakos, and D. Sims. "Crossing Conjugate Normal Faults." *American Association of Petroleum Geologists Bulletin*. Vol. 84, No. 10. pp. 1,543–1,559. 2000b.

Ferrill, D.A., A.P. Morris, D.W. Sims, D.J. Waiting, and S. Hasegawa. "Development of Synthetic Dip Adjacent to Normal Faults and Implications for Traps, Barriers, and Migration Pathways." American Association of Petroleum Geologists Annual Meeting (3-6 June 2001) Official Program. Vol. 10. p. A63. 2001.

Ferrill, D.A. and A.P. Morris. "Displacement Gradient and Deformation in Normal Fault Systems." *Journal of Structural Geology*. Vol. 23. pp. 619–638. 2001.

Finkbeiner, T., C.A. Barton, and M. Zoback. "Relationships Among In-Situ Stress, Fractures and Faults, and Fluid Flow, Monterey Formation, Santa Maria Basin, California." *American Association of Petroleum Geologists Bulletin*. Vol. 81. pp. 1,975–1,999. 1997.

Fischer, J.M. "Sediment Properties and Water Movement Through Shallow Unsaturated Alluvium at an Arid Site for Disposal of Low-Level Radioactive Waste Near Beatty, Nye County, Nevada." U.S. Geological Survey Water-Resources Investigations Report 92-4032. Reston, Virginia: U.S. Geological Survey. 1992.

Fleck, R.J., B.D. Turrin, D.A. Sawyer, R.G. Warren, D.E. Champion, M.R. Hudson, and S.A. Minor. "Age and Character of Basaltic Rocks of the Yucca Mountain Region, Southern Nevada." *Journal of Geophysical Research*. Vol. 101. pp. 8,205–8,227. 1996.

Flint, A.L., J.A. Hevesi, and L.E. Flint. "Conceptual and Numerical Model of Infiltration for the Yucca Mountain Area, Nevada." U.S. Geological Survey Water Resources Investigation Report, Milestone 3GUI623M. Denver, Colorado: U.S. Geological Survey. 1996a.

Flint, L.E., A.L. Flint, C.A. Rautmann, and J.D. Istok. "Physical and Hydrologic Properties of Rock Outcrop Samples at Yucca Mountain, Nevada." U.S. Geological Survey Open-File Report 95-280. 1996b.

Flint, L.E. and A.L. Flint. "Shallow Infiltration Processes at Yucca Mountain, Nevada–Neutron Logging Data 1984–93." U.S. Geological Survey Water-Resources Investigations Report 95-4035. Denver, Colorado: U.S. Geological Survey. 1995.

Fridrich, C.J. "Tectonic Evolution of the Crater Flat Basin, Yucca Mountain Region, Nevada, in Cenozoic Basins of the Death Valley Region." L. Wright and B. Troxel, eds. *Geological Society of American Special Paper 333*. Boulder, Colorado: Geological Society of America. pp. 169–196, 1999.

Fridrich, C.J., W.W. Dudley, Jr., and J.S. Stuckless. "Hydrogeologic Analysis of the Saturated-Zone Ground-Water System, Under Yucca Mountain, Nevada." *Journal of Hydrology*. Vol. 154. pp. 133–168. 1994.

Fridrich, C.J., J.W. Whitney, M.R. Hudson, and B.M. Crowe. "Late Cenozoic Extension, Vertical Axis Rotation, and Volcanism in the Crater Flat Basin, Southwest Nevada, in Cenozoic Basins of the Death Valley Region." L. Wright and B. Troxel, eds. *Geological Society of America Special Paper 333*. Boulder, Colorado: Geological Society of America. pp. 197–212. 1999.

Friedman, I., W. Long, and R.L. Smith. "Viscosity and Water Content of Rhyolite Glass." *Journal of Geophysical Research*. Vol. 68. pp. 6,522–6,535. 1963.

Frizzell, V.A., Jr. and J. Shulters. "Geologic Map of the Nevada Test Site, Southern Nevada." U.S. Geological Survey Miscellaneous Investigations Series, Map I–2046. Scale 1:100,000. Denver, Colorado: U.S. Geological Survey. 1990.

Gabrielse, H., W.S. Snyder, and J.H. Stewart. "Sonoma Orogeny and Permian to Triassic Tectonism in Western North America." *Geology*. Vol. 11. pp. 484–486. 1983.

Gay, N.C. and W.D. Ortlepp. "Anatomy of a Mining-Induced Fault Zone." *Geological Society of America Bulletin Part I*. Vol. 90. pp. 47–58. 1979.

Geldon, A.L., A.M.A. Umari, M.F. Fahy, J.D. Earle, J.M. Gemmell, and J. Darnell. "Results of Hydraulic and Conservative Tracer Tests in Miocene Tuffaceous Rocks at the C-Hole Complex, 1995 to 1997, Yucca Mountain, Nye County, Nevada." Milestone Report SP23PM3. Las Vegas, Nevada: U.S. Geological Survey. 1997.

Gillett, S.L. and J.W. Geissman. "Regional Late Paleozoic Remagnetization of Shallow-Water Carbonate Rocks in the Great Basin, The Usefulness of "Micro"-Fold Tests from Late Compaction Fabrics." *Application of Paleomagnetism to Sedimentary Geology, Society for Sedimentary Geology (SEPM) Special Publication 49*. pp. 129–147. 1993.

Gillett, S.L. and D.R. van Alstine. "Remagnetization and Tectonic Rotation of Upper Precambrian and Lower Paleozoic Strata from the Desert Range, Southern Nevada." *Journal of Geophysical Research*. Vol. 87. pp. 10,929–10,953. 1982.

Gilmore, T.D. "Geodetic Leveling Data Used to Define Historical Height Changes Between Tonopah Junction and Las Vegas, Nevada." U.S. Geological Survey Open-File Report 92-450. Menlo Park, California: U.S. Geological Survey. 1992.

Goddard, J.V. and J.P. Evans. "Chemical Changes and Fluid-Rock Interactions in Faults of Crystalline Thrust Sheets, Northwestern Wyoming, USA." *Journal of Structural Geology*. Vol. 17. pp. 533–547. 1995.

Gray, M.B., J.A. Stamatakos, D.A. Ferrill, and M.A. Evans. "Fault Behavior and Fault Zone Architecture for Miocene Volcanic Tuffs at Yucca Mountain, Nevada." *EOS, Transactions, American Geophysical Union*. Vol. 80, No. 46. p. F741. 1999.

Gray, M.B., J.A. Stamatakos, and D.A. Ferrill. Microstructural and Microtextural Analyses of Faulting at Yucca Mountain, Nevada." *EOS, Transactions, American Geophysical Union.* Vol. 79, No. 45. p. F823. 1998.

Gray, M.B. and J.A. Stamatakos. "A New Model for Evolution of Fold and Thrust Belt Curvature from Integrated Structural and Paleomagnetic Results Around the Pennsylvania Salient." *Geology.* Vol. 25. pp. 1,067–1,070. 1997.

Groshong, Jr., R.H. "Low-Temperature Deformation Mechanisms and Their Interpretation." *Geological Society of America Bulletin.* Vol. 100. pp. 1,329–1,360. 1988.

———. "Unique Determinations of Normal Fault Shape from Hanging-Wall Bed Geometry in Detached Half Grabens." *Eclogae Geologica Helvetica.* Vol. 83. pp. 455–471. 1990.

Gross, M.R., Fischer, M.P., Engelder, T., and Greenfield, R.J. "Factors Controlling Joint Spacing in Interbedded Sedimentary Rocks: Integrating Numerical Models with Field Observations from the Monterey Formation, U.S.A." Fractography: Fracture Topography as a Tool in Fracture Mechanics and Stress Analysis. M.S. Ameen, ed. *Geological Society of London Special Publication.* Vol. 92. pp. 215–233. 1995.

Grow, J.A., C.E. Barker, and A.G. Harris. "Oil and Gas Exploration Near Yucca Mountain, Southern Nevada." Proceedings of the Fifth Annual International Conference on High-Level Radioactive Waste Management. La Grange Park, Illinois: American Nuclear Society. pp. 1,298–1,315. 1994.

Gutenberg, B. and C.F. Richter. *Seismicity of the Earth.* Princeton, New Jersey: Princeton University Press. 1954.

Haag, M., and F. Heller. 1991. "Later Permian to Early Triassic Magnetostratigraphy." *Earth and Planetary Sciences Letters.* Vol. 107. pp. 24–54. 1991.

Hamilton, W.B. "Crustal Extension in the Basin and Range Province, Southwestern United States." *Continental Extensional Tectonics.* M.P. Coward, J.F. Dewey, and P.L. Hancock, eds. London, England: Geological Society Special Publications 28. pp. 155–176. 1987.

———. "Detachment Faulting in the Death Valley Region, California and Nevada, Geologic and Hydrologic Investigations of a Potential Nuclear Waste Disposal Site at Yucca Mountain, Southern Nevada." *U.S. Geological Survey Bulletin 1790.* M.D. Carr and J.C. Yount, eds. Denver, Colorado: U.S. Geological Survey. pp. 51–85. 1988.

Hancock, P.L. "Brittle Microtectonics: Principles and Practice." *Journal of Structural Geology.* Vol. 7. pp. 437–457. 1985.

Hardyman, R.F. and J.S. Oldow. "Tertiary Tectonic Framework and Cenozoic History of the Central Walker Lane, Nevada, Geology and Ore Deposits of the Great Basin." G.L. Raines, R.E. Lisle, R.W. Schafer, and W.H. Wilkinson, eds. Las Vegas, Nevada: Geological Society of Nevada Symposium Proceedings 1. pp. 279–301. 1991.

Harmsen, S.C. "Seismicity and Focal Mechanisms for the Southern Great Basin of Nevada and California in 1990." U.S. Geological Survey Open-File Report 91-367. 1991.

———. "Seismicity and Focal Mechanisms for the Southern Great Basin of Nevada and California in 1991." U.S. Geological Survey Open-File Report 92-340. 1993.

———. "The Little Skull Mountain, Nevada, Earthquake of 29 June 1992: Aftershock Focal Mechanisms and Tectonic Stress Field Implications." *Bulletin of the Seismological Society of America*. Vol. 84. pp. 1,484–1,505. 1994.

Harmsen, S.C. and C.G. Bufe. "Seismicity and Focal Mechanisms for the Southern Great Basin of Nevada and California, 1987 through 1989." U.S. Geological Survey Open-File Report 91-572. 1992.

Hauksson, E., K. Hutton, H. Kanamori, L. Jones, J. Mori, S. Hough, and G. Roquemore. "Preliminary Report on the 1995 Ridgecrest Earthquake Sequence in Eastern California." *Seismological Research Letters*. Vol. 66. pp. 54–60. 1995.

Henderson, D.B., D.A. Ferrill, and K.C. Clarke. "Mapping Geological Faults Using Image Processing Techniques Applied to Hill-Shaded Digital Elevation Models." Proceedings of the IEEE Southwest Symposium on Image Analysis. San Antonio, Texas. 1996.

Higgs, W.G., G.D. Williams, and C.M. Powell. "Evidence for Flexural Shear Folding Associated with Extensional Faults." *Geological Society of America Bulletin*. Vol. 103. pp. 710–717. 1991.

Hildreth, W. "The Compositionally Zoned Eruption of 1912 in the Valley of Ten Thousand Smokes, Katmai National Park, Alaska." *Journal of Volcanology and Geothermal Research*. Vol. 18. pp. 1–56. 1983.

Hill, B.E. and C.B. Connor. "Volcanic Systems of the Basin and Range, NRC High-Level Radioactive Waste Research at CNWRA, July–December, 1995." B. Sagar, ed. CNWRA 95–02S. San Antonio, Texas: CNWRA. pp. 5-1 to 5-21. 1996.

Hill, C.A., Y.V. Dublyansky, R.S. Harmon, and C.M. Schluter. "Overview of Calcite/Opal Deposits at or Near the Proposed High-Level Nuclear Waste Site, Yucca Mountain, Nevada, USA, Pedogenic, Hypogene, or Both?" *Environmental Geology*. Vol. 26. pp. 69–88. 1995.

Hobbs, D.W. "The Formation of Tension Joints in Sedimentary Rocks: An Explanation." *Geological Magazine*. Vol. 104. pp. 550–556. 1967.

Hodges, K.V. and J.D. Walker. "Extension in the Cretaceous Sevier Orogeny, North American Cordillera." *Geological Society of America Bulletin*. Vol. 104. pp. 560–569. 1992.

Hoek, E. and E.T. Brown. *Underground Excavations in Rock*. The Institution of Mining and Metallurgy. London, Hertford, England: Stephen Austin and Sons, Ltd. 1980.

Hoisch, T.D. and C. Simpson. "Rise and Tilt of Metamorphic Rocks in the Lower Plate of a Detachment Fault in the Funeral Mountains, Death Valley, California." *Journal of Geophysical Research.* Vol. 98. pp. 6,805–6,827. 1993.

Hoisch, T.D., M.T. Heizler, and R.E. Zartman. "Timing of Detachment Faulting in the Bullfrog Hills and Bare Mountain Area, Southwestern Nevada, Inferences From $^{40}Ar/^{39}Ar$, K-Ar, U-Pb, and Fission Track Thermochronology." *Journal of Geophysical Research.* Vol. 102, pp. 2,815–2,833. 1997.

Holm, D.K., J.W. Geissman, and B. Wernicke. "Tilt and Rotation of the Footwall of a Major Normal Fault System, Paleomagnetism of the Black Mountains, Death Valley Extended Terrain, California." *Geological Society of America Bulletin.* Vol. 105. pp. 1,373–1,387. 1993.

Hudson, M.R. "Paleomagnetic Data Bearing on the Origin of Arcuate Structures in the French Peak-Massachusetts Mountains Area of Southern Nevada." *Geological Society of America Bulletin.* Vol. 104. pp. 581–594. 1992.

Hudson, M.R., D.A. Sawyer, and R.G. Warren. "Paleomagnetism and Rotation Constraints for the Miocene Southwestern Nevada Volcanic Field." *Tectonics.* Vol. 13. pp. 258–277. 1994.

Hudson, M.R., S.A. Minor, and C.J. Fridrich. "The Distribution, Timing, and Character of Steep-Axis Rotations in a Broad Zone of Dextral Shear in Southwestern Nevada." *Geological Society of America Abstracts with Programs.* Vol. 28. p. A451. 1996.

Huggins, P., J. Watterson, J.J. Walsh, and C. Childs. "Relay Zone Geometry and Displacement Transfer Between Normal Faults Recorded in Coal-Mine Plans." *Journal of Structural Geology.* Vol. 17. pp. 1,741–1,755. 1995.

Hunter, R.L. and C.J. Mann. NUREG/CR–3354, SAND83–1342. "Techniques for Determining Probabilities of Events and Processes Affecting the Performance of Repositories." Washington, DC: NRC. 1990.

Huntoon, P.W., G.H. Billingsby, Jr., and W.J. Breed. "Geologic Map of Canyonlands National Park and Vicinity, Utah." Scale 1:62,500. Moab, Utah: The Canyonlands National History Association. 1982.

Illman, W. and D. Hughson. "Numerical Modeling of Unsaturated Flow in Thick Vadose Zones of Fractured Rocks." *EOS, Transactions, American Geophysical Union, Supplement.* Vol. 82, No. 20. 2001.

Izett, G.A., J.D. Obradovich, and H.H. Mehnert. "The Bishop Ash Bed (Middle Pleistocene) and Some Older (Pliocene and Pleistocene) Chemically and Mineralogically Similar Ash Beds in California, Nevada, and Utah." *United States Geological Survey Bulletin.* Vol. 1675. 1988.

Jaeger, J.C. and N.G.W. Cook. *Fundamentals of Rock Mechanics.* New York: Chapman and Hall. 1979.

Janssen, B. "Modelisation Numerique de L'extension de la Croute Terrestre Avec des Examples du Basin and Range, Etats-Unis." These de doctorat. Strasbourg, France: L'universite Louis-Pasteur de Strasbourg. 1995.

Jarzemba, M.S., R.B. Codell, L.M. Deere, J.R. Firth, C. Lui, S. Mohanty, K. Poor, J. Weldy, and V. Colten-Bradley. NUREG–1668. "NRC Sensitivity and Uncertainty Analyses for a Proposed HLW Repository at Yucca Mountain, Nevada, Using TPA 3.1: Results and Conclusions." Washington, DC: NRC. 1999.

Kane, M.F. and R.E. Bracken. "Aeromagnetic Map of Yucca Mountain and Surrounding Regions, Southwest Nevada." U.S. Geological Survey Open-File Report 83-616. Reston, Virginia: U.S. Geological Survey. 1983.

Katterhorn, S.A., A. Aydin, and D.D. Pollard. "Joints at High Angles to Normal Fault Strike: An Explanation Using 3-D Numerical Models in Fault-Perturbed Stress Fields." *Journal of Structural Geology*. Vol. 22. pp. 1–24. 2000.

Keith, T.E.C. "Fossil and Active Fumaroles in the 1912 Eruptive Deposits, Valley of Ten Thousand Smokes, Alaska." *Journal of Volcanology and Geothermal Research*. Vol. 45. pp. 227–254. 1991.

King, G.C.P., R.S. Stein, and J. Lin. "Static Stress Changes and Triggering of Earthquakes. *Bulletin of the Seismological Society of America*. Vol. 84. pp. 935–953. 1994.

Kirsch, G. "Die Theorie der Elastizitat und die Bedurfnisse der Festigheitslehre." *Zeitschrift des Vereines Deutscher Ingenieure*. Vol. 42. p. 797. 1898.

Klinger, R.E. and L.W. Anderson. "Topographic Profiles and their Implications for Late Quaternary Activity on the Bare Mountain Fault, Nye County, Nevada." *Geological Society of America Abstracts with Programs*. p. A63. 1994.

Krantz, R.W. "Multiple Fault Sets and Three-Dimensional Strain: Theory and Application. *Journal of Structural Geology*. Vol. 10, No. 3. pp. 225–237. 1988.

Lachenbruch, A.H. "Mechanics of Thermal Contraction Cracks and Ice-Wedge Polygons in Permafrost." *Geological Society of America Special Paper*. Vol. 70. 1962.

Langenheim, V.E. and D.A. Ponce. "Ground Magnetic Studies Along a Regional Seismic-Reflection Profile Across Bare Mountain, Crater Flat, and Yucca Mountain, Nevada." U.S. Geological Survey Open-File Report 95-834. Reston, Virginia: U.S. Geological Survey. 1995.

Langenheim, V.E., S.F. Carle, D.A. Ponce, and J.D. Phillips. "Revision of an Aeromagnetic Survey in the Lathrop Wells Area, Nevada." U.S. Geological Survey Open-File Report 91-46. Reston, Virginia: U.S. Geological Survey. 1991.

Langenheim, V.E., K.S. Kirchoff-Stein, and H.W. Oliver. "Geophysical Investigations of Buried Volcanic Centers Near Yucca Mountain, Nevada." Proceedings of the Third International Conference on High Level Radioactive Waste Management. La Grange Park, Illinois: American Nuclear Society. pp. 1,840–1,846. 1993.

La Pointe, P.R., and J.A. Hudson. "Characterization and Interpretation of Rock Mass Joint Patterns." *Geological Society of America Special Paper.* Vol. 199. 1985.

Levy, S.S., D.S. Sweetkind, D.S. Fabryka-Martin, P.R. Dixon, J.L. Roach, L.E. Wolfsberg, D. Elmore, and P. Sharma. "Investigations of Structural Controls and Mineralogic Associations of Chlorine-36 Fast Pathways in the Exploratory Studies Facility." Los Alamos Milestone SP2301M4. Los Alamos, New Mexico: Los Alamos National Laboratory. 1997.

Lienkaemper, J.J., S.K. Pezzopane, M.M. Clark, and M.J. Rymer. "Fault Fractures Formed in Association with the 1986 Chalfant Valley, California, Earthquake Sequence, Preliminary Report." *Bulletin of the Seismological Society of America.* Vol. 77, No. 1. pp. 297–305. 1997.

Lin, M., M.P. Hardy, and S.J. Bauer. "Fracture Analysis and Rock Quality Designation Estimation for the Yucca Mountain Site Characterization Project." SAND92–0449. Albuquerque, New Mexico: Sandia National Laboratories. 1993.

Lipman, P.W. and I. Friedman. "Interaction of Meteoric Water with Magma: An Oxygen-Isotope Study of Ash-Flow Sheets from Southern Nevada." *Geological Society of America Bulletin.* Vol. 86. pp. 695–702. 1975.

Lofgren, G. "Experimentally Produced Devitrification Textures in Natural Rhyolitic Glass." *Geological Society of America Bulletin.* Vol. 82. pp. 111–124. 1971.

Macedo, J. and S. Marshak. "Controls on the Geometry of Fold-Thrust Belt Salients." *Geological Society of America Bulletin.* Vol. 111. pp. 1,808–1,822. 1999.

Majer, E.L., M. Feighner, L. Johnson, K. Lee, T. Daley, E. Karageorgi, P. Parker, T. Smith, K. Williams, A. Romero, and T. McEvilly. "Milestone 0BB02—Results of Geophysical Surveys Along North-South and South Exploratory Studies Facility Alignment" and "Milestone 0BB03—Summary Report, Interpretations of Multiple Geophysical Surveys." Berkeley, California: Lawrence Berkeley National Laboratory. 1997.

Maldonado, F. "Structural Geology of the Upper Plate of the Bullfrog Hills Detachment Fault System, Southern Nevada." *Geological Society of America Bulletin.* Vol. 102. pp. 992–1,006. 1990.

Marrett, R.A. and R.W. Allmendinger. "Estimates of Strain Due to Brittle Faulting: Sampling of Fault Populations." *Journal of Structural Geology.* Vol. 13. pp. 735-738. 1991.

Marrett, R., J.A. Stamatakos, D.A. Ferrill, C.B. Connor, and B.E. Hill. "Extension Rate Estimates from Faults, Fracture Opening, and Earthquakes Near Yucca Mountain, Nevada." *EOS, Transactions, American Geophysical Union.* Vol. 80, No. 17. p. F203. 1998.

Marshak, S. "Kinematics of Orocline and Arc Formation in Thin-Skinned Orogens." *Tectonics.* Vol. 7. pp. 73–86. 1988.

Marshak, S. and M.S. Wilkerson. "Effects of Overburden Thickness on Thrust Belt Geometry and Development." *Tectonics.* Vol. 11. pp. 560–567. 1992.

Martel, S. "On the Paradox of Systematic, Contemporaneous, Orthogonal Opening-Mode Fractures." R. Nelson and S. Laubach, eds. *Rock Mechanics.* Rotterdam: Balkema. pp. 801–808. 1994.

Martinez, L.J., C.M. Meertens, and R.B. Smith. "Rapid Deformation Rates Along the Wasatch Fault Zone, Utah, From First GPS Measurements with Implication for Earthquake Hazard." *Geophysical Research Letters.* Vol. 25. pp. 567–570. 1998.

Mauldon, M., W.M. Dunne, and M.R. Rohrbaugh. "Circular Scanlines and Circular Windows: New Tools for Characterizing the Geometry of Fracture Traces." *Journal of Structural Geology.* Vol. 23. pp. 247–258. 2001.

Mayer, J.R. and J.M. Sharp, Jr. "Fracture Control of Regional Groundwater Flow in a Carbonate Aquifer in a Semi-Arid Region." *Geological Society of America Bulletin.* Vol. 110, No. 2. pp. 269–283. 1998.

McCabe, C. and D.R. Elmore. "The Occurrence and Origin of Late Paleozoic Remagnetization in the Sedimentary Rocks of North America." *Reviews of Geophysics.* Vol. 27. pp. 471–494. 1989.

McCalpin, J.P. *Paleoseismology.* San Diego, California: Academic Press. 1996.

McConnell, K.I., M.E. Blackford, and A.K. Ibrahim. NUREG–1451. "Staff Technical Position on Investigations to Identify Fault Displacement Hazards and Seismic Hazards at a Geologic Repository." Washington, DC: NRC. 1992.

McGill, G.E. and A.W. Stromquist. "The Grabens of Canyonlands National Park, Utah Geometry, Mechanics, and Kinematics." *Journal of Geophysical Research.* Vol. 84, No. B9. pp. 4,547–4,563. 1979.

McGill, G.E., R.A. Schultz, and J.M. Moore. "Fault Growth by Segment Linkage: An Explanation for Scatter in Maximum Displacement and Trace Length Data from the Canyonlands Grabens of Southeast Utah: Discussion." *Journal of Structural Geology.* Vol. 22. pp. 135–140. 2000.

McGuire, R.K. and W.J. Arabasz. "An Introduction to Probabilistic Seismic Hazard Analysis." *Geotechnical and Environmental Geophysics.* S.H. Ward, ed. Society of Exploration Geophysicists. pp. 333–353. 1990.

McKague, H.L., J.A. Stamatakos, and D.A. Ferrill. "Type I Faults in the Yucca Mountain Region." CNWRA 96-007. Revision 1. San Antonio, Texas: CNWRA. 1996.

Menges, C.W., J.W. Whitney, J.A. Coe, J.R. Wesling, F.H. Swan, E.M. Taylor, and D.J. Ponti. "Summary of Paleoseismic Investigations of the Paintbrush Canyon, Bow Ridge, and Stagecoach Road Faults of Eastern Yucca Mountain, Nye County, Nevada." U.S. Geological Survey Open-File Report 95-738. Denver, Colorado: U.S. Geological Survey. 1995.

Meremonte, M., J. Gomberg, and E. Cranswick. "Constraints on the 29 June 1992 Little Skull Mountain, Nevada, Earthquake Sequence Provided by Robust Hypocenter Estimate. *Bulletin of the Seismological Society.* Vol. 85. pp. 1,039–1,049. 1995.

Miller, T.F. "A Numerical Model of Volatile Behavior in Nonwelded Cooling Pyroclastic Deposits. *Journal of Geophysical Research.* Vol. 95. pp. 19,349–19,364. 1990.

Minor, S.A. "Superposed Local and Regional Paleostresses: Fault-Slip Analysis of Neogene Extensional Faulting Near Coeval Caldera Complexes, Yucca Flat, Nevada." *Journal of Geophysical Research.* Vol. 100. pp. 12,507–12,528. 1995.

Minor, S.A., M.R. Hudson, and C.J. Fridrich. "Fault-Slip Data, Paleomagnetic Data, and Paleostress Analyses Bearing on the Neogene Tectonic Evolution of Northern Crater Flat Basin, Nevada." U.S. Geological Survey Open File Report 97-285. Denver, Colorado: U.S. Geological Survey. 1997.

Mohanty, S. and T.J. McCartin. "Total-system Performance Assessment (TPA) Version 3.2 Code: Module Description User's Guide." San Antonio, Texas: CNWRA. 1998.

Mongano, G.S., W.L. Singleton, T.C. Moyer, S.C. Beason, G.L.W. Eatman, A.L. Algin, and R.C. Lung. "Geology of the Enhanced Characterization of the Repository Block Cross Drift—Exploratory Studies Facility, Yucca Mountain, Nevada." http://www.ymp.gov/timeline/site/spg42gm3_a/, 1999.

Monsen, S.A. "Structural Evolution and Metamorphic Petrology of the Precambrian–Cambrian Strata, Northwest Bare Mountain, Nevada." Master's thesis. University of California at Davis. Davis, California. 1983.

Monsen, S.A., M.D. Carr, M.C. Reheis, and P.A. Orkild. "Geologic Map of Bare Mountain, Nye County, Nevada." U.S. Geological Survey Miscellaneous Investigations Series, Map I–2201. Scale 1:24,000. 1992.

———. "Geologic Map of Bare Mountain, Nye County, Nevada." U.S. Geological Survey Open-File Report 90-25. Scale 1:24,000. 1990.

Montazer, P. and W.E. Wilson. "Conceptual Hydrologic Model of Flow in the Unsaturated Zone, Yucca Mountain, Nevada." Water Resources Investigations Report 84-4345. Lakewood, Colorado: U.S. Geological Survey. 1984.

Moore, J.M. and Schultz, R.A. "Processes of Faulting in Jointed Rocks of Canyonlands National Park, Utah." *Geological Society of America Bulletin.* Vol. 111. pp. 808–822. 1999.

Morgan, T.L. "Fracture Characterization in the Tiva Canyon Member, Paintbrush Tuff, Yucca Mountain." Master's thesis. Colorado State University. Fort Collins, Colorado. 1984.

Morris, A.P. and D.A. Ferrill. "Constant-Thickness Deformation Above Curved Normal Faults. *Journal of Structural Geology.* Vol. 21. pp. 67–83. 1999.

Morris, A.P., D.A. Ferrill, and D.B. Henderson. "Slip-Tendency Analysis and Fault Reactivation." *Geology.* Vol. 24. pp. 275–278. 1996.

Moyer, T.C., J.K. Geslin, and L.E. Flint. "Stratigraphic Relations and Hydrologic Properties of the Paintbrush Tuff Nonwelded Hydrologic Unit, Yucca Mountain, Nevada." United States Geological Survey Open-File Report 95-397. Denver, Colorado: U.S. Geological Survey. 1996.

Mozley, P.S. and L.B. Goodwin. "Patterns of Cementation Along a Cenozoic Normal Fault: A Record of Paleoflow Orientations. *Geology.* Vol. 23. pp. 539–542. 1995.

Nakata, J.K., C.M. Wentworth, and M.N. Machette. "Quaternary Fault Maps of the Basin and Range and Rio Grande Rift Provinces, Western United States." U.S. Geological Survey Open-File Report 82-579. Scale 1:2,500,000. Denver, Colorado: U.S. Geological Survey. 1982.

National Research Council, Commission of Physical Sciences, Mathematic, and Resources. *Probabilistic Seismic Hazard Analysis.* Washington, DC: National Academy Press. 1988.

———. *Rock Fractures and Fluid Flow.* Washington, DC: National Academy Press. 1996.

Nelson, M.R. and C.H. Jones. "Paleomagnetism and Crustal Rotations Along a Shear Zone, Las Vegas Range, Southern Nevada." *Tectonics.* Vol. 6. pp.13–33. 1987.

Newendorp, P.D. "Decision Analysis for Petroleum Exploration." Tulsa, Oklahoma: PennWell Books. 1975.

Nilsen, T.J. and J.H. Stewart. "The Antler Orogeny: Mid-Paleozoic Tectonism in Western North America." *Geology.* Vol. 8. pp. 298–302. 1980.

Noble, D.C., S.I. Weiss, and S.M. Green. "High-Salinity Fluid Inclusions Suggest that Miocene Gold Deposits of the Bare Mountain District, Nevada, Are related to a Large Buried Rare-Metal Rich Magmatic System." *Geological Society of America Abstracts with Programs 21.* Boulder, Colorado: Geological Society of America. p. A123. 1989.

Noble, D.C., S.I. Weiss, and E.H. McKee. "Magmatic and Hydrothermal Activity, Caldera Geology, and Regional Extension in the Western Part of the Southwestern Nevada Volcanic Field." *Geology and Ore Deposits of the Great Basin.* G.L. Raines, R.E. Lisle, R.W. Shafer and W.W. Wilkerson, eds. Reno, Nevada: Geological Society of Nevada. pp. 913–934. 1991.

Nostro, C., R.S. Stein, M. Cocco, M.E. Belardinelli and W. Marzocchi. "Two-Way Coupling Between Vesuvius Eruptions and Southern Apennine Earthquakes (Italy) by Elastic Stress Transfer." *Journal of Geophysical Research.* Vol. 103. pp. 24,487–24,504. 1998.

NRC. "Issue Resolution Status Report, Key Technical Issue: Repository Design and Thermal Mechanical Effects." Revision 3. Washington, DC: NRC, Division of Waste Management. 2000.

———. "Issue Resolution Status Report, Key Technical Issue: Structural Deformation and Seismicity." Revision 2. Washington, DC: NRC, Division of Waste Management. 1999a.

———. "Issue Resolution Status Report, Key Technical Issue: Unsaturated and Saturated Flow Under Isothermal Conditions." Revision 2. Washington, DC: NRC, Division of Waste Management. 1999b.

———. "Issue Resolution Status Report, Key Technical Issue: Igneous Activity." Revision 2. Washington, DC: NRC, Division of Waste Management. 1999c.

———. NUREG–0800. "Standard Review Plan for the Review of Safety Analysis Reports for Nuclear Power Plants." Washington, DC: NRC. 1997a.

———. "Identification and Characterization of Seismic Sources and Determination of Safe Shutdown Earthquake Ground Motion." Regulatory Guide 1.165, Washington, DC: NRC. 1997b.

Oatfield, W.J. and J.B. Czarnecki. "Hydrogeologic Inferences From Driller's Logs and From Gravity and Resistivity Surveys in the Amargosa Desert, Southern Nevada." U.S. Geological Survey Open-File Report 89-234. p. 296. 1989.

Odling, N.E., P. Gillespie, B. Bourgine, C. Castaing, J-P. Chiles, N.P. Christensen, E. Fillion, A. Genter, C. Olsen, L. Thrane, R. Trice, E. Aarseth, J.J. Walsh, and J. Watterson. "Variations in Fracture System Geometry and Their Implications for Fluid Flow in Fractured Hydrocarbon Reservoirs." *Petroleum Geoscience*. Vol. 5. pp. 373–384. 1999.

Ofoegbu, G.I. and D.A. Ferrill. "Mechanical Analyses of Listric Normal Faulting with Emphasis on Seismicity Assessment." *Tectonophysics*. Vol. 284. pp. 65–77. 1998.

———. "Mechanical Analyses of a Yucca Mountain Fault Model." Proceedings of the Topical Meeting on Methods of Seismic Hazards Evaluation, Focus '95. La Grange Park, Illinois: American Nuclear Society. pp. 115–124. 1996.

———. "Finite Element Modeling of Listric Normal Faulting." CNWRA 95-008. San Antonio, Texas: CNWRA. 1995.

Ofoegbu, G.I., S. Painter, R. Chen, R.W. Fedors, D.A. Ferrill. "Geomechanical and Thermal Effects on Moisture Flow at the Proposed Yucca Mountain Nuclear Waste Repository." *Nuclear Technology*. Vol. 134. pp. 241–262. 2001.

Oldow, J.S. "Spatial Variability in the Structure of the Roberts Mountain Allochthon, Western Nevada." *Geological Society of America Bulletin*. Vol. 95. pp. 174–185. 1984.

Oldow, J.S., G. Kohler, and R.A. Donelick. "Late Cenozoic Extensional Transfer in the Walker Lane Strike-Slip Belt, Nevada." *Geology*. Vol. 22. pp. 637–640. 1994.

Oliver, H.W. and K.F. Fox. "Structure of Crater Flat and Yucca Mountain, Southeastern Nevada, as Interpreted from Gravity Data." Proceedings of the Fourth Annual International Conference on High-Level Radioactive Waste Management, Las Vegas, Nevada. La Grange Park, Illinois: American Nuclear Society. pp. 1,812–1,817. 1993.

Olson, J.E. "Post-Compressional Relaxation and Orthogonal Fracture Pattern Development." Geological Society of America Abstracts with Programs. Vol. 28, No. 1. p. 56. 1996.

Paces, J.B., L.A. Neymark, B.D. Marshall, J.F. Whelan, and Z.E. Peterman. "Ages and Origins of Subsurface Secondary Minerals in the Exploratory Studies Facility." U.S. Geological Survey—Yucca Mountain Project Branch 1996 Milestone Report 3GQH450M. Denver, Colorado: U.S. Geological Survey. 1996.

Peacock, D.C.P. and D.J. Sanderson. "Displacements, Segment Linkage, and Relay Ramps in Normal Fault Zones. *Journal of Structural Geology*. Vol. 13. pp. 721–733. 1991.

———. "Geometry and Development of Relay Ramps in Normal Fault Systems." *American Association of Petroleum Geologists Bulletin*. Vol. 78. pp. 147–165. 1994.

Pezzopane, S.K. "Preliminary Table of Characteristics of Known and Suspected Quaternary Faults in the Yucca Mountain Region." U.S. Geological Survey Administrative Report. Denver, Colorado: U.S. Geological Survey. 1996.

Pezzopane, S.K., R.E. Carande, and K.D. Smith. "Preliminary Surface Displacement of the Little Skull Mountain Earthquake Measured by Satellite Radar Interferometry of the Yucca Mountain Region, Nevada." *EOS, Transactions, American Geophysical Union 80, Supplement*. p. S1. 1999.

Piety, L.A. "Compilation of Known and Suspected Quaternary Faults within 100 km of Yucca Mountain." U.S. Geological Survey Open File Report 94-112. Scale 1:250,000. Denver, Colorado: U.S. Geological Survey. 1995.

Ponce, D.A. and H.W. Oliver. "Gravity Investigations: Major Results of Geophysical Investigations at Yucca Mountain and Vicinity, Southern Nevada." U.S. Geological Survey Open-File Report 95-74. H.W. Oliver, D.A. Ponce, and W.C. Hunter, eds. Menlo Park, California: U.S. Geological Survey. 1995.

Ponce, D.A., S.B. Kohrn, and S. Waddell. "Gravity and Magnetic Data of Fortymile Wash, Nevada Test Site, Nevada." U.S. Geological Survey Open-File Report 92-343. Reston, Virginia: U.S. Geological Survey. 1992.

Poole, F.G., J.H. Stewart, A.P. Palmer, C.A. Sandberg, R.J. Madrid, R.J. Ross, Jr., L.F. Hintze, M.M. Miller, and C.T. Wrucke. "Latest Precambrian to Latest Devonian Time: Development of a Continental Margin." *The Cordilleran Orogen, Conterminous U.S.: The Geology of North America*. B.C. Burchfiel, P.W. Lipman, and M.L. Zoback, eds. Boulder, Colorado: Geological Society of America. Vol. G-3. pp. 407–479. 1992.

Pollard, D.D. and Aydin, A. "Progress in Understanding Jointing over the Past Century." *Geological Society of America Bulletin*. Vol. 100. pp. 1,181–1,204. 1988.

Potter, C.J., W.C. Day, D.S. Sweetkind, and R.P. Dickerson. "Fault Styles and Strain Accommodation in the Tiva Canyon Tuff, Yucca Mountain, Nevada." *EOS, Transactions, American Geophysical Union 77, Supplement.* p. S265. 1996.

Potter, P.E. and F.J. Pettijohn. *Paleocurrents and Basin Analysis.* New York: Springer-Verlag. 1977.

Prave, A.R. and L.A. Wright. "Isopach Patterns in the Lower Cambrian Zabriskie Quartzite: How Useful in Tectonic Reconstructions?" *Geology.* Vol. 14. pp. 251–254. 1986.

Priest, S.D. *Discontinuity Analysis for Rock Engineering.* New York, New York: Chapman & Hall. 1993.

Ragan, D.M. and M.F. Sheridan. "Compaction of the Bishop Tuff, California." *Geological Society of America Bulletin.* Vol. 83. pp. 95–106. 1972.

Rahe, B., D.A. Ferrill, and A.P. Morris. "Physical Analog Modeling of Pull-Apart Basin Evolution." *Tectonophysics.* Vol. 285. pp. 21–40. 1997.

Ransome, F.L., W.H. Emmons, and G.H. Gary. "Geology and Ore Deposits of the Bullfrog District, Nevada." *U.S. Geological Survey Bulletin.* Vol. 407. 1910.

Rawnsley, K.D., T. Rives, J.-P. Petit, S.R. Hencher, and A.C. Lumsden. "Joint Development in Perturbed Stress Fields Near Faults." *Journal of Structural Geology.* Vol. 20. pp. 1,641–1,661. 1992.

Reheis, M.C. "Preliminary Study of Quaternary Faulting on the East Side of Bare Mountain, Nye County, Nevada." Geologic and Hydrologic Investigations of a Potential Nuclear Waste Disposal Site at Yucca Mountain, Southern Nevada. M.D. Carr and J.C. Yount, eds. *U.S. Geological Bulletin.* Vol. 1790. pp. 103–112. 1988.

———. "Holocene Faulting Along the Central Fish Lake Valley Fault Zone, California and Nevada." *Geological Society of America, Cordilleran Section Meeting, Abstracts with Programs–1994.* Vol. 26. p. 83. 1994.

Reiter, L. *Earthquake Hazard Analysis, Issues and Insights.* New York, New York: Columbia University Press. 1990.

Ressler, T.R. "Preliminary Characterization of the Valley-Fill Aquifer in Fortymile Wash, Southwestern Nevada." Master's thesis. The University of Texas at Austin. Austin, Texas. 2001.

Riehle, J.R. "Calculated Compaction Profiles of Rhyolitic Ash-Flow Tuffs." *Geological Society of America Bulletin.* Vol. 84. pp. 2,193–2,216. 1973.

Riehle, J.R., Miller, T.F., and Baley, R.A. "Cooling, Degassing and Compaction of Rhyolitic Ash Flow Tuffs: A Computational Model." *Bulletin of Volcanology.* Vol. 57. pp. 319–336. 1995.

Ritzi, Jr., R.W. and R.H. Andolsek. "Relation Between Anisotropic Transmissivity and Azimuthal Resistivity Surveys in Shallow, Fractured, Carbonate Flow System." *Ground Water.* Vol. 30, No. 5. pp. 774–780. 1992.

Robinson, G.D. "Structure of Pre-Cenozoic Rocks in the Vicinity of Yucca Mountain, Nye County, Nevada—A Potential Nuclear-Waste Disposal Site." *U.S. Geological Survey Bulletin.* Vol. 1647. Denver, Colorado: U.S. Geological Survey. 1985.

Rogers, A.M., S.C. Harmsen, E.J. Corbett, K. Priestly, and D. dePolo. "The Seismicity of Nevada and Some Adjacent Parts of the Great Basin." *Neotectonics of North America.* D.B. Slemmons, E.R. Engdalhl, M.D. Zoback, and D.D. Blackwell, eds. Boulder, Colorado: Geological Society of America Bulletin. Vol. 1. pp. 153–184. 1991.

Rosenbaum, J.G. "Magnetic Grain-Size Variations Through an Ash Flow Sheet: Influence on Magnetic Properties and Implications for Cooling History." *Journal of Geophysical Research.* Vol. 98. pp. 11,715–11,727. 1993.

———. "Paleomagnetic Directional Dispersion Produced by Plastic Deformation in a Thick Miocene Welded Tuff, Southern Nevada: Implications for Welding Temperatures." *Journal of Geophysical Research.* Vol. 91. pp. 12,817–12,834. 1986.

Rosenbaum, J.G., M.R. Hudson, and R.B. Scott. "Paleomagnetic Constraints on the Geometry and Timing of Deformation at Yucca Mountain, Nevada." *Journal of Geophysical Research.* Vol. 96. pp. 1,963–1,979. 1991.

Ross, C.S. and R.L. Smith. "Ash-Flow Tuffs: Their Origin, Geologic Relations and Identification." *United States Geological Survey Professional Paper.* Vol. 366. 1961.

Rousseau, J.P., E.M. Kwicklis, and D.C. Gillis, eds. "Hydrology of the Unsaturated Zone, North Ramp Area of the Exploratory Studies Facility, Yucca Mountain, Nevada." Water Resources Investigations Report, Draft, Denver, Colorado: U.S. Geological Survey. 1996.

Savage, J.C., J.L. Svarc, and W.H. Prescott. "Strain Accumulation Near Yucca Mountain, Nevada, 1993–1998." *Journal of Geophysical Research.* Vol. 106, No. B8. pp. 16,483–16,488. 2001.

Savage, J.C., M. Lisowski, W.K. Gross, N.E. King, and J.L. Svarc. "Strain Accumulation Near Yucca Mountain, Nevada, 1983–1993." *Journal of Geophysical Research.* Vol. 99. pp. 18,103–18,107. 1994.

Savage, J.C., J.L. Svarc, and W.H. Prescott. "Strain Accumulation at Yucca Mountain, Nevada, 1983–1998." *EOS, Transactions, American Geophysical Union.* Vol. 79, No. 45. p. F203. 1998.

Sawyer, D.R., R.J. Fleck, M.A. Lanphere, R.G. Warren, D.E. Broxton, and M.R. Hudson. "Episodic Caldera Volcanism in the Miocene Southwestern Nevada Volcanic Field: Revised Stratigraphic Framework, $^{40}Ar/^{39}Ar$ Geochronology, and Implications for Magmatism and Extension." *Geological Society of America Bulletin.* Vol. 106. pp. 1,304–1,318. 1994.

Scholz, C.H., N.H. Dawers, J.-Z. Yu, and M.H. Anders. "Fault Growth and Fault Scaling Laws: Preliminary Results." *Journal of Geophysical Research.* Vol. 98. pp. 21,951–21,961. 1993.

Schwartz, D.B. and K.J. Coppersmith. "Fault Behavior and Characteristic Earthquakes: Examples from the Wasatch and San Andreas Faults." *Journal of Geophysical Research.* Vol. 89. pp. 5,681–5,698. 1984.

Schwartz, S.Y. and R. Van der Voo. "Paleomagnetic Study of Thrust-Sheet Rotation During Foreland Impingement in the Wyoming–Idaho Overthrust Belt." *Journal of Geophysical Research.* Vol. 89. pp. 10,077–10,086. 1984.

Schweickert, R.A. and M.M. Lahren. "Strike-Slip Fault System in Amargosa Valley and Yucca Mountain, Nevada." *Tectonophysics.* Vol. 272. pp. 25–41. 1997.

Scott, R.B. "Tectonic Setting of the Yucca Mountain Region, Southwest Nevada." *Geological Society of America Memoir.* Vol. 176. Boulder, Colorado: Geological Society of America. pp. 251–282. 1990.

Scott, R.B. and J. Bonk. "Preliminary Geologic Map of Yucca Mountain, Nye County, Nevada with Geologics." U.S. Geological Survey Open-File Report 84-494. Scale 1:12000. Denver, Colorado: U.S. Geological Survey. 1984.

Secor, D.T. "Mechanics of Natural Extension Fracturing at Depth in the Earth's Crust." Proceedings of Conference on Research in Tectonics, Ottawa 1968. A.J. Baer and D.K. Norris, eds. GSC Paper 68-52. pp. 3–48. 1968.

Seront, B., T.F. Wong, J.S. Caine, C.B Forster, and R.H. Bruhn. "Laboratory Characterization of Hydromechanical Properties of a Seismogenic Fault System." *Journal of Structural Geology.* Vol. 20. pp. 865–881. 1998.

Serpa, L. and T.L. Pavlis. "Three-Dimensional Model of the Late Cenozoic History of the Death Valley Region, Southeastern California." *Tectonics.* Vol. 15. pp. 1,113–1,128. 1996.

Sheridan, M.F. "Fumarolic Mounds and Ridges of the Bishop Tuff, California." *Geological Society of America Bulletin.* Vol. 81. pp. 851–868. 1970.

Sibson, R.H. "Fault Rocks and Fault Mechanisms." *Geological Society of London Journal.* Vol. 133. pp. 191–231. 1977.

Simonds, W.F., J.W. Whitney, K. Fox, A. Ramelli, J.C. Yount, M.D. Carr, C.D. Menges, R. Dickerson, and R.B. Scott. "Map of Fault Activity of the Yucca Mountain Area, Nye County, Nevada." U.S. Geological Survey Miscellaneous Investigations Series, Map I–2520. Scale 1:24,000. Denver, Colorado: U.S. Geological Survey. 1995.

Sims, D., D.A. Ferrill, and J.A. Stamatakos. "Role of Ductile Décollement in the Development of Pull-Apart Basins: Experimental Results and Natural Examples." *Journal of Structural Geology.* Vol. 21. pp. 533–554. 1999.

Slemmons, D.B. "Faults and Earthquake Magnitude." U.S. Army Corp of Engineers, Waterways Experiment Station, Miscellaneous Paper S-73-1, Report 6. 1977.

Smith, R.B. and W.J. Arabasz. "Seismicity of the Intermountain Seismic Belt. *Neotectonics of North America*. D.B. Slemmons, E.R. Engdalhl, M.D. Zoback, and D.D. Blackwell, eds, *Geological Society of America Bulletin*. Vol. 1. pp. 185–228. 1991.

Smith, R.L. "Zones and Zonal Variations in Welded Ash Flows." United States Geological Survey Professional Paper. Vol. 354-F. 1960.

Smith, R.B., W.C. Nagy, K.A. (Smith) Julander, J.J. Viveiros, C.A. Barker, and D.G. Gants. "Geophysical and Tectonic Framework of the Eastern Basin and Range–Colorado Plateau–Rocky Transition: Geophysical Framework of the Continental United States." *Geological Society of America Memoir 172*. L.C. Pakiser and W.D. Mooney, eds. Boulder, Colorado: Geological Society of America. 1989.

Snow, J.K. "Large-Magnitude Permian Shortening and Continental-Margin Tectonics in the Southern Cordillera." *Geological Society of America Bulletin*. Vol. 104. pp. 80–105. 1992a.

———. "Paleogeographic and Structural Significance of an Upper Mississippian Facies Boundary in Southern Nevada and East-Central California (Discussion)." *Geological Society of America Bulletin*. Vol. 104. pp. 1,067–1,071. 1992b.

———. "Mass Balance of Basin and Range Extension as a Tool for Geothermal Exploration." *Geothermal Resources Council Transactions*. Vol. 18. pp. 23–30. 1994.

Snow, J.K. and A.R. Prave. "Covariance of Structural and Stratigraphic Trends: Evidence for Anticlockwise Rotation within the Walker Lane Belt Death Valley Region, California and Nevada." *Tectonics*. Vol. 13. pp. 712–724. 1994.

Snow, J.K. and B.P. Wernicke. "Cenozoic Tectonism in the Central Basin and Range: Magnitude, Rate, and Distribution of Upper Crustal Strain." *American Journal of Science*. Vol. 300. pp. 659–719. 2000.

———. "Uniqueness of Geological Correlations: An Example From the Death Valley Extended Terrane." *Geological Society of America Bulletin*. Vol. 101. pp. 1,351–1,362. 1989.

Snow, J.K., J.W. Geissman, and B. Wernicke. "Paleomagnetic Data from Paleozoic Sedimentary Rocks and Permo-Triassic Intrusions, Death Valley Area, Southeast California, Implications for Mesozoic and Cenozoic Deformation." *EOS, Transactions, American Geophysical Union*. Vol. 74. p. F206. 1993.

Snyder, B.B. and W.J. Carr. "Preliminary Results of Gravity Investigations at Yucca Mountain and Vicinity, Southern Nye County, Nevada." U.S. Geological Survey Open-File Report 82-701. Denver, Colorado: U.S. Geological Survey. 1982.

Sonder, L.J., C.H. Jones, S.L. Salyards, and K.M. Murphy. "Vertical Axis Rotations in the Las Vegas Shear Zone, Southern Nevada: Paleomagnetic Constraints on Kinematics and Dynamics of Block Rotations." *Tectonics*. Vol. 13. pp. 769–788. 1994.

Spengler, R.W., C.A. Braun, L.G. Martin, and C.W. Weisenberg. "The Sundance Fault–A Newly Recognized Shear Zone at Yucca Mountain, Nevada." United States Geological Survey Open-File Report 94-49. Denver, Colorado: U.S. Geological Survey. 1994.

Stamatakos, J.A. and A.M. Hirt. "Paleomagnetic Considerations of the Development of the Pennsylvania Salient in the Central Appalachians." *Tectonophysics*. Vol. 231. pp. 237–255. 1994.

Stamatakos, J.A. and D.A. Ferrill. "Paleomagnetism of Ordovician Pogonip Group Carbonates in Southwestern Nevada: Implications for Tectonism of the Yucca Mountain Region." *EOS, Transactions, American Geophysical Union*. Vol. 77, No. 17. p. F173. 1996a.

———. "Tectonic Processes in the Central Basin and Range Region." NRC High-Level Radioactive Waste Research at CNWRA, July–December 1995. B. Sagar, ed. pp. 6-1 through 6-25. San Antonio, Texas: CNWRA. 1996b.

———. "Comment on Strike-Slip Fault System in Amargosa Valley and Yucca Mountain, Nevada by R.A. Schweickert and M.M. Lahren." *Tectonophysics*. Vol. 294. pp. 151–160. 1998.

Stamatakos, J.A., D.A. Ferrill, and K.H. Spivey. "Paleomagnetic Constraints on the Tectonic Evolution of Bare Mountain, Nevada." *Geological Society of America Bulletin*. Vol. 110. pp. 1,530–1,546. 1998.

Stamatakos, J.A., C.B. Connor, and R.H. Martin. "Quaternary Basin Evolution and Basaltic Volcanism of Crater Flat, Nevada, from Detailed Ground Magnetic Surveys of the Little Cones." *Journal of Geology*. Vol. 105. pp. 319–330. 1997a.

Stamatakos, J.A., P.S. Justus, D.A. Ferrill, R. Chen, and G.I. Ofoegbu. NUREG/CR–6513, No. 1, CNWRA 96-OIA. "Structural Deformation and Seismicity." NRC High-Level Radioactive Waste Program Annual Progress Report, Fiscal Year 1996. B. Sagar, ed. San Antonio, Texas: CNWRA. 1997b.

Stamatakos, J.A., A.M. Hirt, and W. Lowrie. "The Age and Timing of Folding in the Appalachians from Paleomagnetic Results." *Geological Society of America Bulletin*. Vol. 108. pp. 815–829. 1996.

Stamatakos, J.A., B.E. Hill, D.A. Ferrill, P.C. LaFemina, D. Sims, C.B. Connor, M.B. Gray, A.P. Morris, and C.M. Hall. "Composite 13-Ma Record of Extensional Faulting and Basin Growth of Crater Flat, Nevada." Letter Report to NRC. San Antonio, Texas: CNWRA. 1999.

Stauffer, M.R. and D.J. Gendzwill. "Fractures in the Northern Plains, Stream Patterns and Mid-Continent Stress Field." *Canadian Journal of Earth Science*. Vol. 24. pp. 1,086–1,097. 1987.

Stevens, C.H., P. Stone, and P. Belasky. "Paleogeographic and Structural Significance of an Upper Mississippian Facies Boundary in Southern Nevada and East-Central California." *Geological Society of America Bulletin*. Vol. 103. pp. 876–885. 1991.

Stewart, J.H. "Upper Precambrian and Lower Cambrian Strata in the Southern Great Basin, California and Nevada." *U.S. Geological Survey Professional Paper*. Vol. 620. Denver, Colorado: U.S. Geological Survey. 1970.

———. "Basin-Range Structure in Western North America, A Review." *Cenozoic Tectonic and Regional Geophysics of the Western Cordillera*. R.B. Smith and G.P. Eaton, eds. Boulder, Colorado: Geological Society of America Memoir. Vol. 152. pp. 1–31. 1978.

———. "Tectonic of the Walker Lane Belt, Western Great Basin–Mesozoic and Cenozoic Deformation in a Zone of Shear." *Metamorphism and Crustal Evolution of the Western United States*. W.G. Ernst, ed. Englewood Cliffs, New Jersey: Prentice-Hall, Inc. Vol. VII. pp. 684–713. 1988.

Stirewalt, G.L. and D.B. Henderson. "A Three-Dimensional Geological Framework Model for Yucca Mountain, Nevada, with Hydrologic Application, Report to Accompany 1995 Model Transfer to the U.S. Nuclear Regulatory Commission." CNWRA 94-023. San Antonio, Texas: CNWRA. 1995.

Stock, J.M. and J.H. Healy. "Stress Field at Yucca Mountain, Nevada, Geologic and Hydrologic Investigations of a Potential Nuclear Waste Disposal Site at Yucca Mountain, Southern Nevada." *U.S. Geological Survey Bulletin*. M.D. Carr and J.C. Yount, eds. Vol. 1790. pp. 87–94. 1988.

Stock, J.M., J.H. Healy, S.H. Hickman, and M.D. Zoback. "Hydraulic Fracturing Stress Measurements at Yucca Mountain, Nevada and Relationship to Regional Stress Fields. *Journal of Geophysical Research*. Vol. 90. pp. 8,691–8,706. 1985.

Stock, J.M., J.H. Healy, J. Soitek, and L. Mastin. "Report on Televiewer and Stress Measurements in Holes USW G-3 and UE-25pl, Yucca Mountain, Nye County, Nevada." U.S. Geological Survey Open-File Report 86-369. Washington, DC: U.S. Geological Survey. 1986.

Stothoff, S.A., D. Or, D.P. Groeneveld, and S.B. Jones. "The Effect of Vegetation on Infiltration in Shallow Soils Underlain by Fissured Bedrock." Letter Report to NRC. San Antonio, Texas: CNWRA. 1997.

Stover, C.W. and J.L. Coffman. "Seismicity of the United States, 1568–1989 (Revised)." U.S. Geological Survey Professional Paper 1527. Menlo Park, California: U.S. Geological Survey. 1993.

Stuckless, J.S., Z.E. Peterman, R.M. Forester, J.F. Whelan, D.T. Vaniman, B.D. Marshall, and E.M. Taylor. "Characterization of Fault-Filling Deposits in the Vicinity of Yucca Mountain, Nevada." Waste Management 1992 Conference Proceedings, Tucson, Arizona, March 1–5, 1992. Tucson, Arizona: Waste Management. pp. 929–935. 1992.

Suppe, J. "Geometry and Kinematics of Fault-Bend Folding." *American Journal of Science*. Vol. 283. pp. 684–721. 1983.

Swadley, W.C. and L.D. Parrish. "Surficial Geologic Map of the Bare Mountain Quadrangle, Nevada." U.S. Geological Survey Miscellaneous Investigations Series, Map I–1826. Scale 1:24,000. Denver, Colorado: U.S. Geological Survey. 1988.

Swadley, W.C and W.J. Carr. "Geologic Map of the Quaternary and Tertiary Deposits of the Big Dune Quadrangle, Nye County, Nevada, and Inyo County, California." U.S. Geological Survey Miscellaneous Investigations Series, Map I–1767. Denver, Colorado: U.S. Geological Survey. Scale 1:48,000. 1987.

Swadley, W.C., D.L. Hoover, and J.N. Rosholt. "Preliminary Report on Late Cenozoic Faulting and Stratigraphy in the Vicinity of Yucca Mountain, Nye County, Nevada." U.S. Geological Survey Open File Report 84-788. Denver, Colorado: U.S. Geological Survey. 1984.

Sweetkind, D.S. and S.C. Williams-Stroud. "Characteristics of Fracture at Yucca Mountain, Nevada: Synthesis Report." Denver, Colorado: U.S. Geological Survey. 1995a.

———. "Controls on the Genesis of Fracture Networks, Paintbrush Group, Yucca Mountain, Nevada." *EOS, Transactions, American Geophysical Union*. Vol. 76. p. F597. 1995b.

———. "Characteristics of Fractures at Yucca Mountain, Nevada: Synthesis Report." Administrative Report. Denver, Colorado: U.S. Geological Survey. 1996.

Sweetkind, D.S., E.R. Verbeek, J.K. Geslin, and T.C. Moyer. "Fracture Character of the Paintbrush Tuff Nonwelded Hydrologic Unit, Yucca Mountain, Nevada." Administrative Report. Denver, Colorado: U.S. Geological Survey. 1995a.

Sweetkind, D.S., E.R. Verbeek, F.R. Singer, F.M. Byers, Jr., and L.G. Martin. "Surface Fracture Network at Pavement 2001, Fran Ridge, Near Yucca Mountain, Nye County, Nevada." Administrative Report. Denver, Colorado: U.S. Geological Survey. 1995b.

Sweetkind, D.S., C.J. Potter, and E.R. Verbeek. "Interaction Between Faults and the Fracture Network at Yucca Mountain, Nevada." *EOS, Transactions, American Geophysical Union*. Vol. 77, No. 17. p. S266. 1996.

Sweetkind, D.S., L.O. Anna, S.C. Williams-Stroud, and J.A. Coe. "Characterizing the Fracture Network at Yucca Mountain, Nevada, Part 1: Integration of Field Data for Numerical Simulations, Fractured Reservoirs." *Characterization and Modeling Guidebook–1997*. T.E. Hoak, P.K. Blomquist, and A. Klawitter, eds. Denver, Colorado: Rocky Mountain Association of Geologists. pp. 185–196. 1997a.

Sweetkind, D.S., D.L. Barr, D.K. Polacsek, and L.O. Anna. "Administrative Report: Integrated Fracture Data in Support of Process Models, Yucca Mountain, Nevada." 1997 Milestone Report SPG32M3. Denver, Colorado: U.S. Geological Survey. 1997b.

Terzaghi, R. "Sources of Error in Joint Surveys." *Geotechnique*. Vol. 15. p. 287. 1965.

Thomas, A.L. "Poly3D: A Three-Dimensional, Polygonal Element, Displacement Discontinuity Boundary Element Computer Program with Applications to Fractures, Faults and Cavities in the Earth's Crust." Master's thesis. Stanford University. Stanford, California. 1993.

Throckmorton, C.K. and E.R. Verbeek. "Joint Networks in the Tiva Canyon and Topopah Spring Tuffs of the Paintbrush Group, Southwestern Nevada." U.S. Geological Survey Open-File Report 95-2. Denver, Colorado: U.S. Geological Survey. 1995.

Trexler, J.H., Jr., J.C. Cole, and P.H. Cashman. "Middle Devonian-Mississippian Stratigraphy On and Near the Nevada Test Site: Implications for Hydrocarbon Potential." *American Association of Petroleum Geologists.* Vol. 80. pp. 1,736–1,762. 1996.

Trudgill, B. and J. Cartwright. "Relay-Ramp Forms and Normal-Fault Linkages, Canyonlands National Park, Utah." *Geological Society of America Bulletin.* Vol. 106. pp. 1,143–1,157. 1994.

Twiss, R.J. and E.M. Moores. *Structural Geology.* New York, New York: W.H. Freeman and Company. 1992.

U.S. Geological Survey. "USGS Response to an Urban Earthquake–Northridge '94." U.S. Geological Survey Open File Report 96-0263. Denver, Colorado: U.S. Geological Survey. 1995.

———. "Seismotectonic Framework and Characterization of Faulting at Yucca Mountain, Nevada." J.W. Whitney, Report Coordinator. Denver, Colorado: U.S. Geological Survey. 1996.

Van der Voo, R., J.A. Stamatakos, and J.M. Parés. "Kinematic Constraints on Thrust-Belt Curvature from Syndeformational Magnetizations in the Lagos del Valle Syncline in the Cantabrian Arc, Spain." *Journal of Geophysical Research.* Vol. 102. pp. 10,105–10,119. 1997.

Vaniman, D.T. and B.M. Crowe. "Geology and Petrology of Basalts of Crater Flat: Applications to Volcanic Risk Assessment for the Nevada Nuclear Waste Storage Investigations. LANL–8845–MS. Los Alamos, New Mexico: Los Alamos National Laboratory. 1981.

Ver Steeg, K. "Jointing in Coal Beds of Ohio." *Economic Geology.* Vol. 37. pp. 503–509. 1942.

Walker, G.E. and T.E. Eakin. "Geology and Ground Water of Amargosa Desert, Nevada-California." Ground-Water Resources Reconnaissance Series Report 14. Nevada Department of Conservation and Natural Resources. 1963.

Wang, J.S.Y., P.J. Cook, R.C. Trautz, R. Salve, A.L. James, S. Finsterle, T.K. Tolunaga, R. Solbau, and J. Clyde. "Field Testing and Observation of Flow Paths in Niches, Phase I Status Report of the Drift Seepage Test and Niche Moisture Study." Yucca Mountain Project Milestone SPC314M4. Berkeley, California: Lawrence Berkeley National Laboratory. 1997.

Wang, J.S.Y., R.C. Trautz, P.J. Cook, S. Finsterle, A.L. James, J. Birkholzer, and C.F. Ahlers. "Testing and Modeling of Seepage into Drift Input of Exploratory Study Facility Seepage Test Results to Unsaturated Zone Models." Yucca Mountain Project Milestone SP33PLM4. Berkeley, California: Lawrence Berkeley National Laboratory. 1998.

Weichert, D.H. "Estimation of Earthquake Recurrence Parameters for Unequal Observations Periods for Different Magnitudes." *Bulletin of the Seismological Society of America*. Vol. 70. pp. 1,337–1,346. 1980.

Weiss, S.I. "Hydrothermal Activity, Epithermal Mineralization and Regional Extension in the Southwestern Nevada Volcanic Field." Ph.D. dissertation. University of Nevada at Reno. Reno, Nevada. 1996.

Wells, D.L. and K.J. Coppersmith. "New Empirical Relationships Among Magnitude, Rupture Length, Rupture Width, Rupture Area, and Surface Displacement." *Bulletin of the Seismological Society of America*. Vol. 84. pp. 974–1,002. 1994.

Wernicke, B.P. "Low-Angle Normal Faults in the Basin and Range Province: Nappe Tectonics in an Extending Orogen." *Nature*. Vol. 291. pp. 645–648. 1981.

———. "Cenozoic Extensional Tectonics of the Western Cordillera." *The Cordilleran Orogen, Conterminous U.S: The Geology of North America*. Vol. G-3. B.C. Burchfiel, P.W., Lipman, and M.L. Zoback, eds. Boulder, Colorado: Geological Society of America. pp. 553–581. 1992.

———. "Low-Angle Normal Faults and Seismicity—A Review." *Journal of Geophysical Research*. Vol. 100. pp. 20,159–20,174. 1995.

Wernicke, B.P., R.L. Christiansen, P.C. England, and L.J. Sonder. "Tectonomagmatic Evolution of Cenozoic Extension in the North American Cordillera." *Continental Extensional Tectonics*. M.P. Coward, J.F. Dewey, and P.L. Hancock, eds. London, England: Geological Society Special Publications. Vol. 28. pp. 203–221. 1987.

Wernicke, B.P., G.A. Axen, and J.K. Snow. "Basin and Range Extensional Tectonics at the Latitude of Las Vegas, Nevada." *Geological Society of America Bulletin*. Vol. 100. pp. 1,738–1,757. 1988.

Wernicke, B., J.L. Davis, R.A. Bennett, P. Elósegui, M.J.A. Bolins, R.J. Brady, M.A. House, N.A. Niemi, and J.K. Snow. "Anomalous Strain Accumulation in the Yucca Mountain Area, Nevada." *Science*. Vol. 279. pp. 2,096–2,100. 1998.

Wesnousky, S.G. and C.H. Jones. "Oblique Slip, Slip Partitioning, Spatial and Temporal Changes in the Regional Stress Field, and the Relative Strength of Active Faults in the Basin and Range, Western United States." *Geology*. Vol. 22. pp. 1,031–1,034. 1994.

Willemse, E.J.M. "Segmented Normal Faults: Correspondence Between Three-Dimensional Mechanical Models and Field Data." *Journal of Geophysical Research*. Vol. 102. pp. 675–692. 1997.

Willemse, E.J.M., D.D. Pollard, and A. Aydin. "Three-Dimensional Analyses of Slip Distributions on Normal Fault Arrays with Consequences for Fault Scaling." *Journal of Structural Geology*. Vol. 18. pp. 295–309. 1996.

Winograd, I.J. "Hydrogeology of Ash Flow Tuff: A Preliminary Statement." *Water Resources Research*. Vol. 7. pp. 994–1,006. 1971.

Winograd, I.J. and W. Thordarson. "Hydrogeologic and Hydrochemical Framework, South-Central Great Basin, Nevada-California, with Special Reference to the Nevada Test Site." U.S. Geological Survey Professional Paper 712-C. Denver, Colorado: U.S. Geological Survey. 1975.

Wittmeyer, G.W. and D.A. Ferrill. "Effect of Contemporary Regional Stress on the Anisotropy of Transmissivity in Fractured Rock Aquifers." *EOS, Transactions, American Geophysical Union*. Vol. 75, No. 44. p. F258. 1994.

Wittmeyer, G.W., W.M. Murphy, and D.A. Ferrill. "Regional Hydrologic Processes of the Death Valley Region." NRC High-Level Radioactive Waste Research at CNWRA, January–June 1994. B. Sagar, ed. San Antonio, Texas: CNWRA. pp. 189–212. 1994.

Wright, L.A. and B.W. Troxel. "Shallow-Fault Interpretations of Basin and Range Structure, Southwestern Great Basin." *Gravity and Tectonics*. K.A. de Jong and R. Scholten, eds. New York, New York: John Wiley and Sons. pp. 97–407. 1973.

Wu, S. "Fractal Strain Distribution and Its Implications for Cross-Section Balancing." *Journal of Structural Geology*. Vol. 15. pp. 1,497–1,507. 1993.

Yielding, G., B. Freeman, and D.T. Needham. "Quantitative Fault Seal Prediction." *American Association of Petroleum Geologists Bulletin*. Vol. 81, No. 6. pp. 897–917. 1997.

Yielding, G., J.A. Overland, and G. Byberg. "Characterization of Fault Zones for Reservoir Modeling: An Example from the Gullfaks Field, Northern North Sea." *American Association of Petroleum Geologists Bulletin*. Vol. 83, No. 6. pp. 925–951. 1999.

Young, S.R., A.P. Morris, and G.L Stirewalt." Preliminary Structural Interpretation of Reflection Seismic Line AV–1." CNWRA 92–024. San Antonio, Texas: CNWRA. 1992a.

Young, S.R., G.L. Stirewalt, and A.P. Morris. "Geometric Models of Faulting at Yucca Mountain." CNWRA 92-008. San Antonio, Texas: CNWRA. 1992b.

Young, S.R., A.P. Morris, and G.L. Stirewalt. "Geometric Analysis of Alternative Models of Faulting at Yucca Mountain, Nevada." Proceedings of the Fourth Annual International Conference on High-Level Radioactive Waste Management. La Grange Park, Illinois: American Nuclear Society. pp. 1,818–1,825. 1993.

Young, S.R., G.L. Stirewalt, and R.A. Ratliff. "Computer-Assisted Geometric and Kinematic Analysis of Subsurface Faulting in the Vicinity of Yucca Mountain, Nevada, Using Balanced Geologic Cross-Sections." Proceedings of the Second Annual International Conference on High-Level Radioactive Waste Management. La Grange Park, Illinois: American Nuclear Society. Vol. 1. pp. 248-259. 1991.

Youngs, R.R. and K.J. Coppersmith. "Implications of Fault Slip Rates and Earthquake Recurrence Models to Probabilistic Seismic Hazard Estimates." *Bulletin of the Seismological Society of America*. Vol. 75. pp. 939–964. 1985.

Zhang, X. and D.J. Sanderson. "Numerical Modeling of the Effects of Fault Slip on Fluid Flow Around Extensional Faults." *Journal of Structural Geology*. Vol. 18, No. 1. pp. 109–119. 1996.

Zhang, Y., S.L. Gillett, R.E. Karlin, and R.A. Schweickert. "Paleomagnetism of the Miocene Dikes in Bare Mountain, Southwestern Nevada, Implications for Regional Tectonics." *Geological Society of America, Cordilleran and Rocky Mountain Section Meetings, Abstracts with Programs*. Vol. 23, No. 5. p. A169. 1993.

Zoback, M.L. "First- and Second-Order Patterns of Stress in Lithosphere: The World Stress Map Project." *Journal of Geophysical Research*. Vol. 97, No. B8. pp. 11,703–11,728. 1992.

Zoback, M.L., R.E. Anderson, and G.A. Thompson. "Cainozoic Evolution of the State of Stress and Style of Tectonism of the Basin and Range Province of the Western United States." Philosophical Transactions of the Royal Society of London, London, England, Royal Society of London. Vol. A300. pp. 407–434. 1981.

Zoback, M.L. and 36 project participants. "World Stress Map Maximum Horizontal Stress Orientations." *Journal of Geophysical Research*. Vol. 97. pp. 11,703–11,728. 1992.